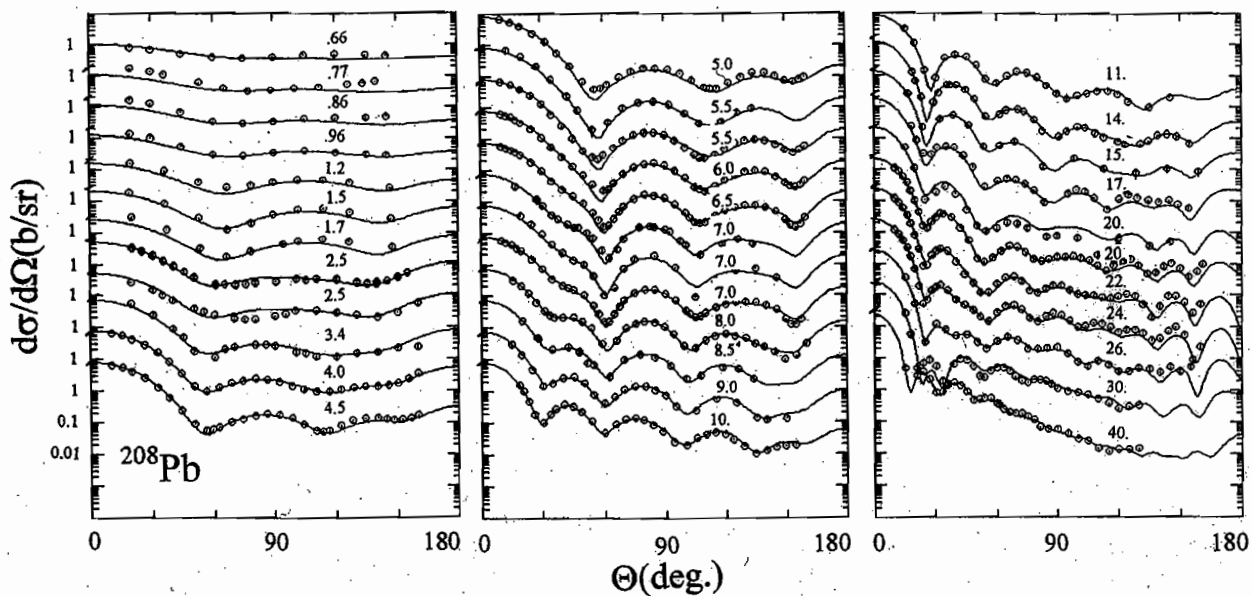


Remark on :-
The Neutron Spherical Optical-Model Absorption

Neutron Data and Measurement Series

Nuclear Engineering Division



About Argonne National Laboratory

Argonne is a U. S. Department of Energy laboratory managed by UChicago Argonne, LLC under contract DE-AC02-06CH11357. The Laboratory's main facility is outside of Chicago, at 9700 South Cass Avenue, Argonne, Illinois 60439. For information about Argonne see www.anl.gov.

Availability of This Report

This report is available, at no cost, at <http://www.osti.gov/bridge>. It is also available on paper to the U. S. Department of Energy and its contractors, for a processing fee, from :

U. S. Department of Energy
Office of Scientific and Technical Information
P. O. Box 62
Oak Ridge, TN 37831-0062
Phone (865) 576-6401
Fax (865) 576-5728
Reports@adonis.osti.gov.

Disclaimer

This report was prepared as an account of work sponsored by an agency of the United States Government. Neither the United States Government, nor any agency thereof, nor UChicago, LLC, nor any of their employees or officers, makes any warranty, expressed or implied, or assumes any legal liability or responsibility for the accuracy, completeness or usefulness of any information, apparatus, product or process disclosed, or represents that its use would not infringe privately owned rights. Reference herein to any specific commercial product, process or service by trade name, trademark, manufacturer, or otherwise, does not constitute or imply its endorsement, recommendation, or favoring by the United States Government or any agency thereof. The views and opinions of the document's author expressed herein do not necessarily state or reflect those of the United States Government of any agency thereof, or of Argonne National Laboratory or UChicago Argonne, LLC.

Remark on:-

The Neutron Spherical Optical Model Absorption

Nuclear Data and Measurement Series

by

Alan B. Smith

Nuclear Engineering Division, Argonne National Laboratory, and
The Physicist's Consultative, Ottawa, Illinois

August 10, 2007



UChicago
Argonne_{LLC}



A U.S. Department of Energy laboratory managed by UChicago Argonne, LLC

Table of Contents

Abstract	10
I. Introductory comment	10
II. Neutron Spherical Optical Model (SOM)	
II-A. Conventional SOM potential	11
II-B. A new additional SOM concept	13
III. Experimental data base	
III-A-1. Measured Pb-208 neutron total cross section	13
III-A-2. Measured Bi-209 neutron total cross section	14
III-B-1. Measured Pb-208 neutron elastic scattering cross sections	15
III-B-2. Measured Bi-209 neutron elastic scattering cross sections	16
III-C-1. Other Pb-208 and Bi-209 experimental results relevant to the present optical-model considerations	16
IV. SOM derivations	
IV-A. SOM baseline model	17
IV-B. Dispersion effects	19
IV-C. Iso-spin effects	21
V. Collective vibrational processes	21
VI. Absorption potential asymmetry	23
VII. Energy dependence of imaginary potential strength	26
VIII. A regional potential	27
References	28
Acknowledgements	31
Appendix A. Absorption asymmetry reference to Fermi energy	32
Appendix B. Dispersion in ²⁰⁹ Bi considerations	32
Appendix C. Neutron inelastic-scattering cross sections	33
Appendix D. Scattered-neutron polarizations	36

Appendix E. Effects of statistical level densities and dispersions	37
E-A. Compound nucleus and channel competition	37
E-B. Dispersion effects	39
IX. Tables	40
X. Figures	74

Nuclear Data and Measurement Series

Reports in the Argonne National Laboratory Nuclear Data and Measurement Series present results of studies in the field of microscopic nuclear data. The primary objective of the series is the dissemination of information in the comprehensive form required for nuclear technology applications. This series is devoted to a) measured microscopic nuclear parameters, b) experimental techniques and facilities employed in measurements, c) the analysis, correlation and interpretation of nuclear data, and d) the compilation and evaluation of nuclear data. Contributions to this Series are reviewed to assure technical competence and, unless otherwise stated, the contents can be formally referenced. This Series does not supplant formal journal publication, but it does provide the more extensive information required for technological applications (e.g., tabulated numerical data) in a timely manner.

Other Publications in the ANL/NDM Series

A listing of recent issues in this series is given below. Issues and/or titles prior to ANL/NDM-130 can be obtained from the National Technical Information Service, U. S. Department of Commerce, Technology Administration, Springfield, VA 22161, or by contacting the author of this report at the Nuclear Engineering Division, Argonne National Laboratory, 9700 South Cass Avenue, Argonne, IL 60439 (USA). In addition, the entire report series can be found on the Internet at the following URL:-

<<http://www.ne.anl.gov/capabilities/nd/reports/index.html>>,

including abstracts, complete reports, and associated computer programs.

- A. B. Smith and P. T. Guenther
Fast-neutron interaction with the fission product ^{103}Rh
ANL/NDM-130, September 1993
- A. B. Smith and P. T. Guenther
Fast-neutron scattering from vibrational Palladium nuclei
ANL/NDM-131, October 1993
- A. B. Smith
Neutron interaction with doubly magic ^{40}Ca
ANL/NDM-132, November 1993
- A. B. Smith
Neutron scattering at $Z=50$:- Tin
ANL/NDM-133, September 1994
- A. B. Smith, S. Chiba and J. W. Meadows
An evaluated neutronic data file for elemental Zirconium
ANL/NDM-134, September 1994
- A. B. Smith and S. Chiba
Neutron scattering from Uranium and Thorium
ANL/NDM-135, February 1995

- A. B. Smith
Neutron scattering and models:- Iron
ANL/NDM-136, August 1995
- A. B. Smith
Neutron scattering and models:- Silver
ANL/NDM-137, July 1996
- A. B. Smith and D. Schmidt
Neutron scattering and models:- Chromium
ANL/NDM-138 June 1996
- W. P. Poenitz and S. E. Aumeier
The simultaneous evaluation of the standards and other cross sections of
importance for technology
ANL/NDM-139, September 1997
- D. L. Smith and J. T. Daly
A compilation of information on the $^{31}\text{P}(p, \gamma)^{32}\text{S}$ reaction and properties of
excited levels in ^{32}S
ANL/NDM-140, November 2000
- A. B. Smith
Neutron scattering and models:- Titanium
ANL/NDM-141, July 1997
- A. B. Smith
Neutron scattering and models:- Molybdenum
ANL/NDM-142, July 1999
- R. E. Miller and D. L. Smith
Compilation of information on the $^{31}\text{P}(p, \gamma)^{33}\text{Cl}$ reaction and properties of
excited levels in ^{33}Cl
ANL/NDM-143, July 1997
- R. E. Miller and D. L. Smith
A compilation of information on the $^{31}\text{P}(p, \gamma)^{28}\text{Si}$ reaction and properties of
the excited levels in ^{28}Si
ANL/NDM-144, November 1997
- R. D. Lawson and A. B. Smith
ABAREX, a neutron spherical optical-statistical model code, A user's manual
ANL/NDM-145, June 1999
- R. T. Klann and W. P. Poenitz
Non-destructive assay of EBR-II blanket elements using resonance transmission
analysis
ANL/NDM-146, August 1998
- A. B. Smith
ELEMENTAL-ABAREX:- A user's manual
ANL/NDM-147, June 1999
- D. G. Naberejnev and D. L. Smith
A method to construct covariance files in ENDF/B formats for critical safety
applications
ANL/NDM-148, June 1999

- A. B. Smith
Neutrons and Antimony, physical measurements and interpretations
ANL/NDM-149, July 2000
- A. B. Smith and A. Fessler
Neutrons and Antimony, neutronic evaluations of ^{121}Sb and ^{123}Sb
ANL/NDM-150, July 2000
- A. B. Smith
Fast neutrons incident on Holmium
ANL/NDM-151, December 2000
- R. D. Lawson and A. B. Smith
Technical note, Dispersion contributions to neutron reactions
ANL/NDM-152, August 2001
- A. B. Smith
Fast-neutrons incident on Hafnium
ANL/NDM-153, June 2001
- D. L. Smith, Dimitri G. Naberejnev and L. A. Van Wormer
An approach for dealing with large errors
ANL/NDM-154, September 2001
- A. B. Smith
Fast-neutron scattering from elemental Rhenium
ANL/NDM-155, August 2003
- D. L. Smith
A demonstration of the lognormal distribution
ANL/NDM-156, July 2003
- A. B. Smith
Fast-neutrons incident on Gadolinium
ANL/NDM-157, April 2004
- D. L. Smith
A survey of experimental and evaluated fast-neutron Helium production data for
fusion applications
ANL/NDM-158, May 2004
- D. L. Smith
Covariance matrices for nuclear cross sections derived from nuclear model
calculations
ANL/NDM-159, January 2005
- A. B. Smith
Fast-neutrons incident on rotors, Tantalum
ANL/NDM-160, February 2005
- A. B. Smith
Neutron scattering from the standard ^{197}Au
ANL/NDM-161, June 2005
- F. Kondev
Evaluated Decay Data for ^{206}Tl
ANL/NDM-162, November 2006

A. B. Smith

Present work

ANL/NDM-163, August 2007

F. Kondev

Evaluated Decay Data for ^{246}Cm

ANL/NDM-164, November 2006

Remark on:-

THE NEUTRON SPHERICAL OPTICAL-MODEL ABSORPTION

by

Alan B. Smith^{a,b}

^aNuclear Engineering Division, Argonne National Laboratory

^bThe Physicists Consultive, Ottawa, IL.

Keywords:- The properties of the optical-statistical and coupled-channels models in the region of the doubly closed shell at $A = 208$ are examined with particular attention to the energy dependence of the imaginary potential. A new imaginary-potential shape is proposed.

Abstract

The energy-dependent behavior of the absorption term of the spherical neutron optical potential for doubly magic ^{208}Pb and the neighboring ^{209}Bi is examined. These considerations suggest a phenomenological model that results in an intuitively attractive energy dependence of the imaginary potential that provides a good description of the observed neutron cross sections and that is qualitatively consistent with theoretical concepts. At the same time it provides an alternative to some of the arbitrary assumptions involved in many conventional optical-model interpretations reported in the literature and reduces the number of the parameters of the model.

I. Introductory Comment

For many years the Pauli exclusion principle and other fundamental physical considerations have suggested that the optical-model absorption at low energies is primarily in the nuclear surface region, and extends into the target interior as the incident-particle energy increases (e.g. Hod63, Hod94, Elt61, Pau41, Gom59). The onset of the transition from primarily surface to volume absorption seems to occur at relatively low bombarding energies, e.g. at several tens of MeV or less. That is an energy region that is largely forbidden to charged-particle measurements by the coulomb barrier, and thus the wealth of experimental charged-particle scattering data is of only marginal value in defining the low-energy behavior of the optical-model potential. In addition, charged-particle measurements do not, as for neutrons, directly determine the total cross sections valued in model considerations. Recently the experimental knowledge of neutron total and scattering cross sections of ^{208}Pb and ^{209}Bi has appreciably improved and thus quantitative neutron-model assessments in the context of these two nuclides are more attractive. The large majority of target nuclei are multi-isotopic and/or have collective

characteristics that preclude simple and unequivocal spherical optical-model interpretations. The situation is further complicated by the prevalence of partially resolved resonance structure at relative low energies (particularly for lighter-mass targets) that is inconsistent with the energy-average concept of the optical model (Fes58, FPW54, Hod63, Hod94). Also, knowledge of the energy dependence of the potential remains no more than qualitative (Lan62, Pas67, Hod63, Hod94, Per63). There is only one spherical $T = 0$ target nucleus, ^{40}Ca , for which there is a wide range of neutron scattering and total cross section data, and where the mass is heavy enough to permit the determination of the energy-averaged cross-section behavior at lower energies in a manner consistent with the concept of the optical model. Since for ^{40}Ca $T \equiv 0$, iso-spin effects can be ignored. The spherical neutron optical model of ^{40}Ca will be discussed by the author elsewhere. ^{208}Pb is doubly magic and reasonably spherical, though the nuclear asymmetry $\eta = (N-Z)/A$ is 0.212. This implies that iso-spin effects must be considered in making global comparisons with ^{208}Pb based optical models. The ^{208}Pb neutron total cross sections are now well known to 500+ MeV, and differential elastic scattering is reasonably known from the discrete resonance region to ≈ 40 MeV. However, there remains a wealth of detailed compound-nucleus resonance structure at energies below ≈ 5 MeV that must be averaged before comparing with optical-model values. ^{209}Bi is only one proton from the same doubly-closed shell and thus nearly spherical, with a nuclear asymmetry of 0.206 which is essentially identical to that of ^{208}Pb . The ^{209}Bi neutron total and elastic-scattering experimental database is more extensive than that of ^{208}Pb , probably due to readily available measurement samples. Its measured total cross sections extend in detail to well above 500 MeV. Elastic-scattering measurements with results of good quality are available to ≈ 25 MeV, and, at very small scattering angles, to hundreds of MeV. These ^{208}Pb and ^{209}Bi experimental neutron databases are outlined below.

II. Neutron Spherical Optical Model (SOM)

In the beginning, a simple spherical optical-statistical model (Fes58, FPW54, Hod63, Hod94, Wol51) giving a reasonable description of the fast neutron interaction with ^{208}Pb and ^{209}Bi is sought as a basis for further investigating physical properties exhibited in the fast-neutron interaction with these nuclei. The ^{208}Pb target should be spherical to a rather high order due to its doubly-closed shell structure. ^{209}Bi should also be essentially spherical as it consists of a $f_{7/2}$ proton added to the doubly-closed-shell core. From this SOM basis more detailed physical aspects of the neutron interaction can be explored. This initial foundation should be soundly based upon the physically observed processes which, at lower energies, are primarily fast-neutron total and scattering cross sections.

II-A. Conventional SOM Potential

The present considerations are extensions of the conventional spherical surface-absorption neutron optical model. Therefore, it is important that this underlying foundation be clearly established, particularly as there are an unfortunate number of misstatements and outright errors in the literature, spread over approximately half a century.

The underlying potential form used here is (Hod63, Hod94, OR82, Elt61, Rap82, GPT68):-

$$V(r) = U f(r_u) + iW_v f(r_{wv}) + iW_s g(r_{ws}) + U_{so} (h/\mu\pi c)^2 (1/r_{so}) d/dr_{so} [f_{so}(r_{so})] \underline{\sigma} \cdot \underline{l}, \quad (\text{II-A-1})$$

Where U = real-potential depth, W_v = the volume-imaginary depth, W_s = the surface-imaginary depth, and U_{so} = the spin-orbit depth. $f(r_i)$ is taken to be the Saxon-Woods form

$$f(r_i) = 1/[1 + \exp((r_i - R_i)/a_i)] \quad (\text{II-A-2})$$

and $g(r)$ to be the Saxon-Woods-derivative form

$$g(r_i) = -4 b_w d/dr[(1 + \exp((r - R_w)/b_w))^{-1}], \quad (\text{II-A-3})$$

or thus

$$g(r_i) = 4 \exp((r - R_w)/b_w)/(1 + \exp((r - R_w)/b_w))^2. \quad (\text{II-A-4})$$

where r_U = reduced real radius, a_U = real diffuseness, the real radius $R_U = r_U A^{1/3}$ ($A \equiv$ target mass in AMU), the imaginary radius $R_w = r_w A^{1/3}$, where r_w = reduced imaginary radius, and b_w = the imaginary diffuseness. As will become clear in the following considerations, W_v is set identically to zero throughout the present considerations unless otherwise explicitly stated. The spin-orbit term is of the Thomas form and real (no imaginary spin-orbit component). Associated real and imaginary potential integrals-per-nucleon are (e.g. see Elt61, Ols+82, Hod63, Rap82),

$$J_U/A = (4/3) \pi (R_U^3/A) U [1 + ((\pi a_U)/R_U)^2] \quad (\text{II-A-5})$$

$$J_w/A = ((16 \pi R_w^2)/A) b_w W [1 + (1/3) ((\pi b_w)/R_w)^2]. \quad (\text{II-A-6})$$

The real and imaginary RMS radii are

$$\langle R_U^2 \rangle^{1/2} = [(3 R_U^2 + 7 \pi^2 a_U^2)/5]^{1/2} \quad (\text{II-A-7})$$

and

$$\langle R_w^2 \rangle^{1/2} = \{12 b R_w [1 + (\pi b/R_w)^2] (J_U^0/J_w^0)\}^{1/2}, \quad (\text{II-A-8})$$

where J_U^0 and J_w^0 are the values given by Eqs. II-A-5 and II-A-6 with $U = W \equiv 1$.

Comparisons with results obtained with appreciably different target masses should always consider iso-spin effects where $V = V_0 \pm \eta V_1$, $W = W_0 \pm \eta W_1$, ("+" for protons and "-" for neutrons) and $\eta \equiv (N-Z)/A$ (Lan62). However, the present considerations are limited to ^{208}Pb and ^{209}Bi targets which have essentially identical η values (i.e. 0.212 and 0.206, respectively). The above simple spherical model does not consider dispersion contributions which fundamentally couple real and imaginary potentials (Sat83, Lip66, Pas67, Fes58, JLM77), as discussed elsewhere in this note. The above formalism also

does not address collective effects and the associated deformations and direct interactions. Both ^{208}Pb and ^{209}Bi are known to have collective quadrupole vibrational states at relatively low energies (NDS). However, the respective deformation parameters, β_3 , are small so it is reasonable to initially ignore the neutron vibrational coupling, as in the context of the spherical optical model. Coupled-channels interpretations of the neutron interactions with the collective properties are discussed elsewhere in this note.

II-B. An Additional SOM Concept

The primary thrust of the present considerations is the introduction of an additional and novel model concept. Conventionally, the imaginary-potential diffuseness is taken to be symmetric about the imaginary radius R_W , as defined by Eqs. II-A-3 and II-A-4. The concept of an asymmetric imaginary diffuseness is introduced here, where "b_w" may have different values (b_{wi}) interior to and (b_{wo}) exterior to the imaginary radius R_W . This asymmetry of the surface absorption potential is here defined as

$$\text{ASYM} \equiv 1 + K \bullet E, \quad (\text{II-B-1})$$

where "K" is a constant and $b_{wi} = \text{ASYM} \bullet b_{wo}$. This concept provides for a progressive linear extension of the surface absorption into the interior of the nucleus with energy (i.e. a surface absorption growing linearly toward volume absorption with increasing energy). Eq. II-B-1 is a simple linear approximation of such an effect. Of course, more complex energy dependencies may be introduced. This transition in the shape of the surface absorption with "K" is illustrated by the relative distributions shown in Fig. II-B-1. The significance and implications of this concept are a primary thrust of these remarks. The concept replaces a minimum of four parameters associated with parameterizations using the conventional volume absorption potential (volume potential strength, radius, diffuseness, energy dependence of strengths and geometries and the threshold) with the single parameter "K". This is a prominent advantage in the use of an optical potential already overloaded with parameterization.

III. Experimental Data Base

III-A-1. Measured ^{208}Pb total cross sections.

An examination of National Nuclear Data Center (NNDC) files revealed a modest number of ^{208}Pb experimental neutron total-cross-section references (FG71, Day65, FC62, GM67, Far+65, Fin+93, Har99, Car+91 and Duk+67). Fortunately, several of these data sets are very large and, generally, all appear of good quality. Altogether there are a total of ≈ 19500 individual total cross-section values relevant to the present considerations. These results were combined into one large set and carefully culled by graphical inspection. At low energies resonance effects are reported with varying energy resolutions and energy scales leading to some discrepancies, but the average energy-dependent trends appear reasonably consistent. Only three individual values were felt to be erroneous and were abandoned. The remaining values were energy ordered and

averaged over 50 keV intervals below 0.5 MeV, over 100 keV intervals from 0.5 – 5.0 MeV and over 200 keV intervals at higher energies in order to provide averaged values reasonably consistent with the underlying concepts of the optical model. Resulting averaged cross-section values are illustrated in the four panels of **Fig. III-A-1-1**. The residual fluctuations resulting from the averaging of the gross resonance structure are evident below ≈ 5.0 MeV. These averaged measurements extend up to incident energies of ≈ 600 MeV. They are compared with the corresponding ENDF/B-VI values in **Fig. III-A-1-2**. The evaluation uses resonance parameters to represent the total cross sections below ≈ 1.0 MeV and a point-wise cross-section representation at higher energies. The evaluation is consistent with the present experimental averages up to the 150 MeV upper energy limit of the evaluation. Compound-nucleus resonance structure is clearly evident in the evaluation and it may persist in the energy-averaged total cross sections resulting in small fluctuations at lower energies. This may contribute to the systematic intermediate structure near 3 MeV suggested by several authors (e.g. Ols+82). In addition, at lower energies the measured total-cross-section magnitudes may be distorted by self-shielding effects. It is not always clear that these were given attention in the experimental measurements. They can result in serious distortions.

III-A-2. Measured ^{209}Bi total cross sections

The NNDC files were similarly searched for fast-neutron total cross sections of elemental bismuth (^{209}Bi). Nearly 20000 individual values were found, of which more than 14000 were relevant to the considerations of the present work. They extend from incident energies of ≈ 10 keV to a few GeV. With the majority of the values below several MeV the experimental resolution is often relatively good in order to define the structure in the unresolved resonance region. The respective references are ACQ53, Ang+71, BBP49, Bes+92, BPS58, CB67, CGB52, CHH55, Cie68, CW59, Das+90, Day65, DH53, Div68, DM58, Dri+73, Duk+67, Fin+93, FLM63, Fra88, Gib+56, Gio+78, GLM67, Goo62, GSW80, Gue+89, Gua+92, Har+72, HL55, HS77, HWH75, HL50, FG71, Maz+55, Kha56, KMM57, KVJ72, LR53, Man65, MEF55, Mil+52, ND53, Ort75, PBS60, SBN67, Sch+73, Sin+76, Smi+70, SW54, Tut+65 and WB55. With a very few exceptions, the measured values are relatively consistent. This is surprising, particularly in the lower-energy and fluctuating region where small changes in experimental resolutions and/or energy scale can lead to large differences. The experimental database was ordered by increasing energy and a very few obviously discrepant values removed as a result of graphical inspection. This culled result was then energy averaged to combine measured values and produce energy-averaged experimental total cross sections consistent with the physical concepts of the optical model. The energy-averaging increments were again:- i) 50 keV at incident energies of less than 0.5 MeV, ii) 100 keV for energies of 0.50 to 5.0 MeV, and iii) 200 keV at all higher energies. These averaged results are indicated by “+” symbols in the four panels of **Fig. III-A-2-1**. The four panels of **Fig. III-A-2-2** compare the present energy-averaged results with the ^{209}Bi ENDF/B-VI evaluated neutron total cross sections up to the 20 MeV upper limit of the evaluation. The agreement is very good. This is not surprising as, above the highly fluctuating region, the evaluation was constructed in the same manner as

used in the present work, from much the same data (Gue+89). Again, self-shielding effects may have distorted some of the experimental values at lower energies.

The above energy-averaged ^{209}Bi and ^{208}Pb total cross sections are remarkably alike as indicated by the percentage deviations between them as a function of energy shown in Fig. III-A-2-3. On the average the ^{209}Bi values are slightly larger than those of ^{208}Pb with energy, from a fractional percent at low energies to 1.5 – 2 percent at 600 MeV. Nuclear size effects suggest that the ^{209}Bi values should be about 0.3% larger than those of ^{208}Pb . The evident “ripples” above the low-energy resonance region have the character of statistical fluctuations. At very low energies there are larger fluctuations due to the persistent influence of incompletely averaged resonance structure. There remain some minor fluctuations in the energy averaged bismuth data near 3.0 MeV that may indicate intermediate structure as suggested in ref. Ols+82. The total cross sections are apparently not very sensitive to the quite different structure of the ^{208}Pb and ^{209}Bi targets.

III-B-1. Measured ^{208}Pb elastic-scattering cross sections.

The NNDC files contain sixteen references (AFD85, BKF72, Blo+03, Day71, Del+83, Dev80, Fin+84, Flo81, Fow66, GHS78, Hao+82, Han+85, KP74, Osb+04, Rap+78 and Rob+91) to fast-neutron elastic scattering from ^{208}Pb , relevant to the present considerations. They represent 82 differential distributions distributed between incident energies of ≈ 0.5 and 96.0 MeV. At some of the higher energies the angular coverage is minimal, with the results limited to very forward angles (e.g. less than 10–15 degrees). This is exclusively so above incident-neutron energies of ≈ 40 MeV (Osb+04). This high-energy behavior, combined with the scatter of the measured data, does not make for reasonable legendre polynomial and/or model fitting, and acceptable angle-integrated elastic-scattering cross sections. Thus, all such distributions were ignored and the ^{208}Pb model considerations limited to incident energies of ≤ 40 MeV, though the resulting potentials may extrapolate to higher energies. The measurements extend over nearly half a century, and often had quite different objectives. For example, Fowler (Fow66) reports a very nice set of high-resolution elastic distributions below 1.8 MeV, arranged to optimize resonance interpretations. In the same incident-energy region the measurements of Guenther et al. (GHS78) were directed toward the determination of the energy-averaged scattering cross sections more consistent with the concepts of the optical model. These goals are quite different, even conflicting, but they provide the majority of the differential elastic-scattering information in the fluctuating region below several MeV. Because of the fluctuations, the experimental differential-elastic cross sections at energies of ≤ 2 MeV were averaged over approximately 100 keV incident-energy intervals for the present model interpretations. Above ≈ 2 MeV the experimental differential-elastic distributions were treated individually as reported by the respective authors. These procedures resulted in thirty-five experimentally-based differential elastic-scattering distributions extending from incident energies of ≈ 0.6 to 40.0 MeV. They are illustrated by the data symbols in Fig. III-B-1-1. They represent most of the world’s knowledge of energy-averaged fast-neutron elastic scattering from ^{208}Pb above a few-tens of keV.

III-B-2. Measured ^{209}Bi Elastic-scattering Cross Sections

The NNDC files were also searched for fast-neutron experimental elastic-scattering cross sections of elemental bismuth (^{209}Bi). There are more than 100 reasonably acceptable and relevant differential distributions extending from ≈ 0.3 to 24.0 MeV incident energies, as cited in references AG85, AFD85, Bos+59, Bru+55, BWS56, CJ60, Das+90, Day65, Fin+91, Fer+77, GLM64, GSW80, Han+85, Hud+62, HWJ69, Kor+77, LGS87, Ols+82, Ols+87, Ray59, Smi+70, SW54, WB54, WB55, Wil+65, Tak+88, Tan+72 and Zaf+65. One reference (Smi+70) contains many distributions spread in energy between 0.3 and 1.5 MeV. These were averaged over ≈ 100 keV incident-energy intervals in order to reduce the number of values and to smooth the resonance fluctuations in this low-energy region. All of the elastic distributions were culled by graphical inspection and a few questionable ones removed. The rejections were generally based upon obvious qualitatively erroneous results and/or on the failure to fit the distribution in question with a rational legendre-polynomial expansion. At higher incident energies there are a number of the experimental distributions that do not provide sufficient definition for the higher-order polynomial fitting required for quantitative determination of angle-integrated elastic-scattering cross sections or for model determination. Therefore, these fragmentary higher-energy distributions were abandoned. The final result was 90 differential elastic-scattering distributions at incident energies between ≈ 0.3 and 24.0 MeV. These experimental results are illustrated in Fig. III-B-2-1 (two panels).

III-C. Other ^{208}Pb and ^{209}Bi experimental neutron results relevant to optical model considerations.

There is a considerable amount of measured data relevant to the inelastic neutron excitation of low-lying discrete levels in ^{208}Pb and ^{209}Bi , the latter primarily due to particle states built on the closed shells and the former to quadrupole collective excitations. This inelastic neutron scattering data is summarized in Appendix C. It is further discussed in Section V and Appendix C in the context of compound-nucleus and direct-collective excitation processes. There is also some experimental information about neutron polarization properties as outlined in Appendix D, though it is fragmentary and some of the accompanying elastic scattering distributions are questionable. In addition there are S_0 and S_1 strength functions deduced from low-energy resonance measurements (Mug+81, Mug06). This ancillary information will be discussed below in the context of the deduced optical and coupled-channels models, but is not used for model derivation via numerical parameter fitting.

IV. SOM Derivations

All of the SOMs considered in this section are by definition spherical and consist of real Saxon-Woods, imaginary Saxon-Woods-derivative, and Thomas spin-orbit

components as generically defined in **Section II-A**, above, unless explicitly otherwise specified. There are no volume absorption or imaginary spin-orbit contributions. All of the calculations included compound-nucleus contributions determined using the formalism of Moldauer (Mol80) that includes resonance width fluctuation and correlation corrections. Consideration is given to the excitation of discrete states up to ≈ 5.03 MeV for ^{208}Pb and up to ≈ 3.69 MeV for ^{209}Bi , using the excitation energies, spins and parities given in the Nuclear Data Sheets (NDS). Higher energy excitations are treated using the statistical model and parameters of Gilbert and Cameron (GC65), with the temperature optimized for best compound-nucleus results above the discrete levels, as discussed in **Appendix E**. The real spin-orbit potential parameters, fixed to those of Walter and Guss (WG65), are

$$\begin{aligned} V_{so} &= 5.767 - 0.015 \bullet E + 2.0 \bullet [(N-Z)/A] \\ r_{so} &= 1.103 \\ a_{so} &= 0.56. \end{aligned} \quad (\text{IV} - 1)$$

All of the SOM calculations used the most recent version of the code ABAREX (LS99, Smi05). This code is not relativistic, but comparisons with other codes using relativistic kinematics indicate the results are reliable up to incident energies of at least 100 MeV. (It is a pleasure to acknowledge the provision of test cases by Dr. P. G. Young.) Due to the fact that there are no comprehensive differential ^{208}Pb elastic-scattering distributions above ≈ 40 MeV, and for ^{209}Bi above ≈ 25 MeV, the model determinations are based on data extending to only 40 MeV and 25 MeV, respectively. The resulting models may or may not reasonably extrapolate to higher energies. All the fitting minimized the function

$$\chi^2 = (1/N) \sum_i \{(\sigma(\text{exp})_i - \sigma(\text{cal})_i) / \Delta\sigma(\text{exp})_i\}^2, \quad (\text{IV}-2)$$

where the sum is over the "N" experimental values, using a non-linear least-square fitting procedure (Cra+81). $\sigma(\text{exp})_i$ are the experimental cross sections, $\sigma(\text{cal})_i$ are their calculated counterparts, and $\Delta\sigma(\text{exp})_i$ are the experimental uncertainties. The experimental cross sections were limited to measured and/or averaged measured elastic-scattering and total cross sections. The elastic-scattering cross-section uncertainties were taken from the reported experimental measurements or, when dealing with averages of differential values or as necessary, as estimated by the author. Total cross sections were included in the fitting procedure at the energies of the differential elastic distributions as interpolated from the ordered and averaged total-cross-section databases of **Section III-A** or **III-B**. They were assigned various weights equivalent to those of one to 20 differential elastic-scattering values. After a number of preliminary manipulations a weight approximately equivalent to that of ten differential elastic values was accepted for each total cross section in all the fitting.

IV-A. SOM-Baseline Models.

As a starting point, SOM "Baseline" potentials were deduced from the above ^{208}Pb and ^{209}Bi elastic-scattering and total cross section data. The imaginary diffuseness of these potentials was assumed to be symmetric about the imaginary radius, i.e. "b_w" of

Eqs. II-A-1 to II-A-3 were identical inside and outside the imaginary radius. Thus $b_{\text{inside}} \equiv b_{\text{outside}}$, the K of Eq. II-B-1 $\equiv 0.0$ and $\text{ASYM} \equiv \text{unity}$ at all energies. These are then conventional, surface-absorption, neutron SOMs. The derivations of the six parameters (a_v , r_v , r_w , b_w , V , W) of the ^{208}Pb and ^{209}Bi models were independently pursued by progressively fitting the neutron differential scattering and total cross sections through the six steps, (i) six parameter fitting from which a_v was fixed, (ii) five parameter fitting fixing r_v , (iii) four parameter fitting fixing r_w , (iv) three parameter fitting fixing b_w , (v) two parameter fitting fixing the real strength V , and, finally, (vi) one parameter fitting giving the imaginary strength W . The entire fitting procedure was iterated three times to arrive at the final ^{208}Pb SOM Baseline parameters of **Table IV-A-1**, and those of ^{209}Bi as given in **Table IV-A-2**. These parameter sets give good descriptions of the measured ^{208}Pb total cross sections as illustrated in **Fig. IV-A-1** (upper panel), and of the ^{209}Bi total cross sections as illustrated in **Fig. IV-A-1** (lower panel). Above several MeV the SOM Baseline calculated ^{208}Pb total cross sections are in good agreement with the averages of the measured values. On the average, the agreement remains reasonable good at lower energies but fluctuations due to resonance structure persist even in the broad energy averages. The SOM Baseline description of the measured ^{208}Pb differential elastic scattering cross sections is generally good up to incident energies of ≈ 25 MeV, as illustrated in **Fig. III-B-1-1**. At higher energies and large scattering angles the calculated results are perhaps less suitable but this may reflect experimental problems in some cases. The ^{209}Bi Baseline SOM gives a very good description of the energy-averaged experimental total cross sections from several MeV up to at least 25 MeV, as illustrated in **Fig. IV-A-1** (lower panel). The same SOM potential gives a very good description of the experimental neutron differential elastic-scattering results from ≈ 0.3 to 25 MeV as illustrated in **Fig. III-B-2-1**. The real potential strengths of the ^{208}Pb and ^{209}Bi , measured in terms of volume-integrals-per-nucleon, are very similar as illustrated in **Fig. IV-A-2** (upper panel), with a marginally larger energy dependence of the ^{209}Bi values. The imaginary potential strengths differ in detail, possibly reflecting structure, resonance and collective differences between the two targets (see the lower panel of **Fig. IV-A-2**). These real and imaginary strengths are qualitatively consistent with those of a number of "global" SOM potentials reported in the literature. For example, the real strength (J_v) of the global potential reported by Rapaport (Rap82) is qualitatively similar to that of the present ^{208}Pb and ^{209}Bi SOMs (see **Fig. IV-A-1**) despite very different real-potential geometries. The agreement between the present and reference Rap82 imaginary-potential strengths is less satisfying but reference Rap82 makes the common assumption that the imaginary potential consists of volume and surface branches. Consideration of that assumption and an alternate concept is a major thrust of these remarks, particularly the considerations of **Section VI**. Though the present SOM derivations are based upon far more extensive ^{208}Pb and ^{209}Bi data, there is no firm evidence of a fermi-surface anomaly as described, for example, in ref. AFD85 for neutrons or in ref. MN81 for protons. This is particularly so for the real potential. It is less certain in the context of the imaginary potential as there is considerable fluctuation in the low-energy parameters deduced from fitting, in part due to resonance effects, and combinations of surface and volume potentials are often involved. This is particularly so in the case of ^{208}Pb where the resonance distortions are largest and the measurements sparse at low energies. Moreover, data sets from particular institutions frequently display systematic discrepancies from the

average energy-dependent trends suggesting experimental error. Indeed, some institutions have subsequently been critical of some of their own earlier work. The imaginary potentials of the present work extrapolate to zero values near the Fermi Energies as theoretically predicted from the Pauli principle. The present SOM potentials result in reasonable strength functions, particularly for ^{209}Bi where the lower-energy experimental data is less fluctuating. The present ^{209}Bi SOM potential leads to a S_0 strength function of $1.07 \pm \approx 0.2$ and a S_1 of $0.39 \pm \approx 0.2$ compared to the respective values of 0.65 ± 0.15 and 0.23 ± 0.05 deduced from resonance measurements (Mug06, Mug+81). The corresponding values for ^{208}Pb implied by the SOM potential are $S_0 = 0.52 \pm \approx 0.2$ and $S_1 = 0.40 \pm \approx 0.2$. The respective values following from discrete resonance measurements are uncertain due to the very few low-energy resonances in ^{208}Pb (Mug06). The discrete resonance situation is somewhat better in ^{207}Pb where $S_0 = 0.76 \pm 0.3$ and $S_1 = 0.45 \pm 0.07$ (Mug06, Mug+81).

IV-B. Dispersion Effects

It is well known that dispersion phenomena, reflecting causality, significantly impact upon optical-model considerations as they relate real and imaginary potentials (JLM77, Lan62, Sat83, Lip66, Pas67, Fes58). These effects can be expressed in the form,

$$J_V(E) = J_{\text{HF}}(E) + (P/\pi) \bullet \int [J_W(E')/(E-E')] dE' \quad (\text{IV-B-1})$$

where J_V is the strength of the real potential (in volume-integral-per-nucleon), J_{HF} that of the corresponding Hartree-Fock potential, and J_W the strength of the imaginary potential. "P" denotes the principle value of the integral, which is evaluated from $-\infty$ to $+\infty$. The integral of Eq. IV-B-1 can be broken into surface and volume components given by Eqs. IV-B-2 and IV-B-3, respectively

$$\Delta J_{\text{sur}}(E) = (P/\pi) \bullet \int [J_{\text{sur}}(E')/(E-E')] dE' \quad (\text{IV-B-2})$$

and

$$\Delta J_{\text{vol}}(E) = (P/\pi) \bullet \int [J_{\text{vol}}(E')/(E-E')] dE'. \quad (\text{IV-B-3})$$

With these equations, $J_V(E) = J_{\text{eff}}(E) + \Delta J_{\text{sur}}(E)$, where $J_{\text{eff}}(E) = J_{\text{HF}}(E) + \Delta J_{\text{vol}}(E)$, and $J_{\text{sur}}(E)$ and $J_{\text{vol}}(E)$ are surface- and volume-imaginary strengths, respectively. In the context of the present considerations, and with reasonable assumptions as to volume absorption, J_{HF} and ΔJ_{vol} are approximately linear functions of energy and are not distinguishable in experimental interpretations of the present type. The effect of Eqs. IV-B-2 and IV-B-3 is to add surface and volume components to the real potential that are some fractions of the imaginary surface and volume potentials. These contributions were calculated using the concepts and methods of Smith et al. (SGL86) and Lawson and

Smith (LS01). Such calculations require extensive energy extrapolations as the above integrals extend from $-\infty$ to $+\infty$ and the present ^{208}Pb potential of **Table IV-A-1** is not assured valid beyond ≈ 0 to 40 MeV, and that of the ^{209}Bi potential of **Table IV-A-2** beyond ≈ 0 to 25 MeV. The $\Delta J_{\text{sur}}(E)$ is a surface strength to be added to the real potential. It was assumed to have the same Saxon-Woods-Derivative shape and geometric parameters as the surface-imaginary absorption (**Section VI** deals with the asymmetric potential). It was further assumed that the $\Delta J_{\text{vol}}(E)$ retains the same Saxon-Woods geometries as the real potential over all energies. These are commonly used assumptions but they are just that - assumptions. Other portions of these remarks are directed toward the energy-dependent shape of the imaginary potential. It was further assumed that absorption was entirely a surface effect up to 35 MeV, following the present SOM parameters of **Table IV-A-1** and **Table IV-A-2**. It was then assumed to fall linearly to a zero value at 100 MeV. Concurrently, volume absorption was assumed to rise linearly from zero at 35 MeV to 100 MeV where it was given the strength of the surface absorption at 35 MeV. At higher energies the volume absorption was assumed to remain constant on to infinity. The imaginary potential was assumed to be zero at the Fermi Energy E_F , taken to be -6.0 MeV for ^{208}Pb and -5.87 MeV for ^{209}Bi (Tul05, LS99), and to have a quadratic energy dependence from E_F to zero laboratory energy. Finally, the entire imaginary potential was assumed to be symmetric about E_F . These assumptions and the calculational formalism for the evaluation of the dispersive integrals are described in detail by Lawson and Smith (LS01). The resulting ^{208}Pb surface dispersive component, $\Delta J_{\text{sur}}(E)$, and the total dispersive component, $\Delta J_{\text{sur}}(E) + \Delta J_{\text{vol}}(E)$, are illustrated as a function of energy in **Fig. IV-B-1**. The resulting fraction of the ^{208}Pb surface-imaginary potential that must be introduced into the real potential is give in **Fig. IV-B-2**. The corresponding fraction for ^{209}Bi is qualitatively similar to that for ^{208}Pb . These dispersive fractions fall from near unity at zero laboratory energy to several tenths at ≈ 30 to 40 MeV. The details of this behavior will vary to some extent with model parameters and the asymmetry discussed below. These fractions were introduced into the SOM fitting procedure and the entire model fitting processes repeated through three iterative cycles to obtain the ^{209}Pb and ^{209}Bi “dispersive optical model” (DOM) parameters given in **Table IV-B-1** and **Table IV-B-2**. These parameters give good descriptions of the measured neutron ^{208}Pb and ^{209}Bi strength functions and total cross sections as illustrated in **Fig. IV-B-3**. They are arguably superior to those obtained with the SOM (compare **Fig. IV-A-1** and **Fig. IV-B-3**). The ^{208}Pb and ^{209}Bi results obtained with the DOM potential of **Table IV-B-1** and **Table IV-B-2** are compared with the elastic-scattering data bases in **Fig. IV-B-4** and **Fig. IV-B-5** (two panels). The calculated results are in encouraging agreement with the measured values up to ≈ 20 MeV, at least as good as those obtained with SOM (compare **Figs. IV-B-4** and **IV-B-5**, and **Figs. III-B-1** and **III-B-2-1**). Above 20 MeV the DOM potential is arguably superior to the SOM, particularly at back angles, although the experimental data may, again, be doubtful, and far back-angle scattering is reported to be sensitive to the spin-orbit potential which was fixed in the present work. Interestingly, one study reported in the literature (AFD85), on pragmatic phenomenological grounds introduced a surface peaked component in the real potential. Such a property is simply a consequence of reasonable dispersion effects as illustrated in **Fig. IV-B-2**.

The strengths (J_i) of the SOM and DOM potentials of ^{208}Pb (Tables IV-A-1 and IV-B-1) and of ^{209}Bi (Tables IV-A-2 and IV-B-2) are in reasonable agreement (Fig. IV-B-6) and physically consistent. The low-energy behavior of these strengths is perhaps more consistent with the bound-energy behavior of the strengths (LGS87). The real diffusenesses differ by only $\approx 2\%$. The r_V of the DOM is smaller than that of the SOM and it is less energy dependent. This reflects the contribution of the surface fraction of Fig. IV-B-2, which adds a surface component to the real potential. The DOM real potential strength (J_V) is smaller and less energy dependent than that of the SOM, again reflecting the contribution of the dispersive fraction. The SOM and DOM imaginary potentials are remarkably similar in both strength and geometry. The two potentials lead to essentially the same σ_{total} values and modest differences in $d\sigma_{\text{el}}/d\Omega$ values; and even then only at large scattering angles and higher energies where the experimental values become increasingly uncertain. S_0 and S_1 strength functions calculated with the two potentials are similar but both tend to be somewhat larger than suggest by systematics in this mass region (Mug06, Mug+81). See Appendix B for further DOM discussion.

IV-C. Iso-spin Effects.

The real SOM and DOM neutron potential depths are believed to have an iso-spin dependence of the form $V = V_0 - V_1 \bullet \eta$, where $\eta = (N-Z)/A$ (Lan62, Hod63, Hod94, Per63). This implies an analogous expression for the strength in terms of volume-integral-per-nucleon of the form $J_V = J_{V0} - J_{V1} \bullet \eta$. In the present ^{208}Pb and ^{209}Bi cases, η are very similar, 0.212 and 0.206 respectively. The ratio V_1/V_0 (or J_{V1}/J_{V0}) cannot be determined from the present mono-isotopic considerations but is frequently taken to be ≈ 0.275 (e.g., Hod63, Hod94). With this estimate the above equations become

$$\begin{aligned} V &= V_0(1 \pm 0.275 \bullet \eta) \text{ and} & \text{Eq. IV-C-1} \\ J &= J_0(1 \pm 0.275 \bullet \eta), \end{aligned}$$

where "-" pertains to incident neutrons and "+" to incident protons. The V_0 and J_0 values are the quantities that should be compared in neutron interactions with various targets having different iso-spins (i.e. values of η). The present work implies for the ^{208}Pb SOM a $V_0 = 48.8416 - 0.1138 \bullet E$ (MeV) and a $J_0 = 438.346 - 3.0893 \bullet E$ (MeV-fm³), and for the ^{208}Pb DOM a $V_0 = 48.3803 - 0.09688 \bullet E$ and $J_0 = 417.243 - 3.7147 \bullet E$ (MeV-fm³). The corresponding ^{209}Bi SOM values are $V_0 = 47.3546 + 0.06206 \bullet E$ (MeV) and $J_0 = 448.087 - 4.2844 \bullet E$ (MeV-fm³) and the DOM values $V_0 = 48.2281 + 0.002152 \bullet E$ (MeV) and $J_0 = 422.48 - 5.3236 \bullet E$ (MeV-fm³).

V. Collective vibrational processes

^{208}Pb is a doubly-closed-shell collective octupole vibrator with a prominent 3–first-excited state at 2.614 MeV, a 5–second excited level at 3.197 MeV, and approximate ten additional negative parity states in the subsequent MeV of excitation energy (NDS). Inelastic neutron excitation of the first two of these excited states has been reasonably experimentally resolved. Higher energy excitations remain significant

but experimentally blur as the measurement resolution increasingly exceeds the level spacing. A number of the life times of these excited states are known (NDS), defining their character. The low energy excited structure of ^{209}Bi is not as clear as the lower excited levels appear to be particle states based upon the doubly-closed-shell core. There are many of these, the density of which exceeds the experimental neutron-scattering resolution, but for the inelastic excitation of the first two at 0.896 MeV ($f_{7/2}$) and 1.609 MeV ($i_{13/2}$) which has been reasonably experimentally determined. The inelastic excitation of these ^{209}Bi states is discussed in **Appendix C**. The present ^{208}Pb neutron data was interpreted in terms of a two-level vibrational coupled-channel model, coupling the 0^+ (g.s.) and 3^- (2.614 MeV) states together assuming octupole vibrations using a variety of β_3 values ranging from 0.0 to 0.30. The ^{208}Pb elastic scattering database defined above was refitted using the coupled-channels code ECIS (Ray96). The excitation was treated assuming compound-nuclear processes and the statistical model, as in the spherical interpretations, for higher energy excitations. The same iterative fitting procedure as used for the above spherical models was employed, progressively determining the six parameters of the real and imaginary potentials in the same manner through three cycles. The coupled-channels fitting did not include neutron total cross sections, but at various stages in the process comparisons were made with the experimentally determined total cross sections. There were five such sets of fits corresponding to the assumptions that i) $\beta_3 = 0$ (spherical case), ii) = 0.1, iii) = 0.15, iv) = 0.2 and v) = 0.3. These beta values reasonably extend over those reported in the literature (e.g. refs. AFD85 and NNDC). The resulting five potentials are given in **Tables V-1 to V-5**. The potentials of **Tables IV-A-1 and V-1** are reasonably consistent, as they should be, despite the fact that entirely different computational codes were used. All the five potentials of **Tables V-1 to V-5** gave qualitatively reasonable descriptions of the ^{208}Pb total cross sections, as illustrated by the panels of **Fig. V-1**. These comparisons suggest that the β_3 are ≈ 0.10 to 0.15 . Much larger beta values are clearly inappropriate. Values in this range are consistent with those reported in the literature from a variety of considerations (AFD85, NDS). From the comparisons of measured and calculated differential elastic scattering shown in **Figs. V-2 to V-6** one reaches the same conclusion, β_3 values are approximately 0.10 to 0.15. However, the effects of vibrations are small in the context of neutron total or elastic-scattering cross sections of ^{208}Pb and the simple spherical models (particularly with dispersion) qualitatively do as well.

The vibrational interaction will impact upon the calculation of the inelastic cross sections. This is illustrated by **Fig. V-7** where the inelastic excitation of the first 3^- 2.670 MeV level in ^{208}Pb is calculated with the potentials of **Tables V-1 to V-5**. The experimental results are far from definitive, but it is evident that one needs a β_3 of 0.10 to 0.15 to qualitatively account for the energy dependence of this first inelastic excitation function. Clearly $\beta_3 = 0$ is inappropriate, as are values of 0.20 or larger. Statistical-model temperatures will also have an impact on the calculated results, as outlined in **Appendix E**.

The above vibrational interpretations were extended to include the coupling of the 3.912 MeV (5^-) level in the modeling with a $\beta_3 = 0.125$. This fitting resulted in the parameters of **Table V-6**. The total cross section and elastic scattering results did not

appreciably change as indicated by **Figs. V-8 and V-9**. There is, however, an impact on the inelastic excitation of the second excited (3.912 MeV) level, as expected.

VI. Absorption Potential Asymmetry

The above SOM and DOM Baseline potentials assumed no asymmetry in the imaginary diffuseness b_w . Thus the "K" of Eq. II-B-1 was identically zero and the imaginary diffusenesses are symmetric about the imaginary radius (R_w) at all energies. There is no volume absorption. Asymmetric absorption is now considered where the "K" of Eq. II-B-1 can take values greater than zero resulting in the broadening of the surface absorption toward the nuclear interior (i.e. linearly shifting from surface toward volume absorption with incident energy). The "K" of Eq. II-B-1 was given the values 0.0 (i.e. as for the Baseline SOM and DOM), 0.05, 0.10, 0.15, 0.20, 0.25, 0.30, 0.35, 0.40 and 0.50 as representative values. Eq. II-B-1, of course, implies a linear energy dependence of the asymmetry. More complex energy dependencies may be warranted but the linear form is a reasonable first approximation. These assumed "K" values reasonably span the range from symmetric b_w values to volume absorption with increasing energies as illustrated in **Fig. II-B-1**. For example, a "K" of 0.3 will at 30 MeV result in $ASYM = 10$ which is approaching the conventional Saxon-Woods volume-absorption potential shape as illustrated in **Fig. II-B-1**, curve "10". At zero energy the $ASYM$ will remain the same symmetrical absorption form as the SOM and DOM take at all energies. What is represented is an absorption linearly shifting from surface to volume form with increasing energy. The dependence of this transition on energy is governed by the size of "K".

The six-parameter fitting of the ^{208}Pb data base of the SOM (**Section IV-A**) was repeated for the above "K" values. It rapidly became clear that the $ASYM$ (Eq. II-B-1) of the absorption had essentially no effect on the real-potential geometries resulting from the fitting. The resulting ten r_V values averaged to 1.2342 fms and the average of the ten a_V values was 0.6806 fms. These values differ from those of the ^{208}Pb SOM by only small percentages. Therefore the ^{208}Pb real potential radius and diffuseness were fixed to the average values resulting from the six-parameter fitting and the fitting repeated using four-parameter searches defining the imaginary radius (r_w) and diffuseness (a_w) and the real (V) and imaginary (W) potential depths. The resulting ^{208}Pb potentials are given in **Tables VI-1 to VI-10**. The corresponding real potential depths (V) and strengths (J_V) are insensitive to the $ASYM$ values of the absorption potential. The zero-energy magnitudes of the real strengths (**Table VI-11**) differ by only $\approx 0.1\%$ and their energy dependence by only $\approx 1.3\%$. These real-potential strengths are essentially indistinguishable from 0 to 40 MeV, as illustrated in **Fig. VI-1**.

The primary impact of asymmetric absorption in the context of ^{208}Pb is, as expected, on the character of the imaginary potential. The strengths of the imaginary potentials (J_w) of **Tables VI-1 to VI-10** are summarized in **Table VI-12**, and illustrated as a function of energy in **Fig. VI-2**. All ten of these potentials suggest that the imaginary strength extrapolates to \approx zero at the Fermi Energy, regardless of the potential asymmetry. This may indicate that energy dependencies of the asymmetries should be referenced to the Fermi Energy rather than to the zero energy in the laboratory system, as

in the above modeling. That alternative energy scale is explored in **Appendix A** and shown to have a minor impact. It is clear from **Fig. VI-2** that after the asymmetry has reached values corresponding to or exceeding values given by $ASYM = 1.0 + 0.20 \bullet E$ the energy dependence of the imaginary strength is approximately linear with energy above 10 MeV without the drop off above ≈ 35 MeV resulting from lower ASYM values. This suggests that the conventional approximation of introducing a volume-absorption term in the modeling should set in at about 10 MeV, as is frequently encountered in the literature.

The energy dependencies of the ^{208}Pb imaginary-potential radii for different asymmetries are summarized in **Table VI-13** and **Fig. VI-3**. When the asymmetry reaches a value of $ASYM = 1.0 + 0.20 \bullet E$ or larger the imaginary radii converge to an average value of $r_w \approx 1.4147 - 0.003485 \bullet E$. The remaining and smaller energy dependence of the parameter may well reflect the non-locality of the nuclear forces (Per63), and dispersion effects. The larger energy-dependencies for small (or zero) asymmetries may be due to an attempt to describe the absorption having a significant volume component with a surface absorption that is inappropriate as suggested by the LDA model of Liege group (JLM77).

The ^{208}Pb a_w determined by the fitting scattered from distribution to distribution but general energy and asymmetry trends were evident as given in **Table VI-14** and illustrated in **Fig. VI-4**. With increasing asymmetry the a_w magnitudes decrease along with their energy dependencies. This again suggests that the volume absorption is significant even at relatively low energies (as discussed below).

The ^{208}Pb total cross sections predicted by the ten potentials of **Tables VI-1** to **VI-10** using increasingly asymmetric imaginary potentials are essentially the same, as illustrated by the comparisons of **Fig. VI-5**, panels **A** through **D**. All ten of the potentials give essentially the same description of the total cross sections irrespective of the shape of the absorptive potential term. In a broader sense, this result suggests that the total cross sections will not give significant guidance as to the relation of volume and surface absorption in conventional optical-model interpretations.

The differential neutron elastic scattering from ^{208}Pb is not sensitive to the asymmetry (ASYM) of the absorption potential up to incident energies of ≈ 15 MeV as illustrated by the examples of **Figs. VI-6** to **VI-11**. All ten of the ASYM potentials give essentially identical results at these lower energies. At higher energies (15 to 40 MeV) the results calculated with the larger values of ASYM are arguably in better agreement with the experimental values. The improvement is not striking and may be entirely due to variations in experimental results. These results suggest that the shape of the absorption potential is not particularly sensitive to the available ^{208}Pb neutron experimental information, and ^{208}Pb is one of the better known experimental cases. Phenomenological experimental evidence does not unequivocally support volume absorption in the neutron interaction with ^{208}Pb at incident neutron energies of $\leq 40 - 50$ MeV. From theoretical or other grounds, volume absorption of various types may be introduced into the modeling but it can not be strongly justified by experimental ^{208}Pb

neutron total and elastic-scattering experimental evidence. Neutrons are the only probe that will reach into the lower energy region where questions of volume versus surface absorption may be the more acute. This uncertainty probably contributes to the variety of neutron ^{208}Pb potentials found in the literature.

The above examination of the ASYM dependence of the imaginary potential term in neutron scattering from ^{208}Pb was repeated using the ^{209}Bi data base described above. The procedures were essentially the same except that full 6-parameter fitting was used throughout as described above in the SOM Baseline derivations. The "K" of Eq. II-B-1 was varied from 0 (symmetric absorption) to 0.5 in steps of 0.1 (i.e. from 0.0 to 0.1, 0.2, 0.3, 0.4 and finally to 0.5). This is a coarser mesh than used for ^{208}Pb but there are many more distributions and full 6-parameter fits were used. The resulting six SOM potentials are given in Tables VI-15 to VI-20. Finally, an additional potential was considered where the imaginary potential was taken to be entirely volume and of the Saxon-Wood form. The latter potential is given in Table VI-21. The corresponding ^{209}Bi SOM depths and strengths are summarized in Tables VI-22 and VI-23 as functions of ASYM. As for ^{208}Pb , there is little if any dependence of the real potential on ASYM. The J_V and J_W energy dependencies are very similar, particularly for the "K" of Eq. II-N-1, ≥ 2 .

The ^{209}Bi neutron total cross sections calculated with the potentials of Tables VI-15 to VI-20, respectively corresponding to $\text{ASYM} = 1 + K \cdot E$ with $K = 0.0, 0.1, 0.2, 0.3, 0.4$ to 0.5 are compared with the measured values in Fig. VI-13. The last section of the figure was obtained using only a Saxon-Woods volume-imaginary potential as defined by the potential of Table VI-21. All of these calculated total cross sections are in qualitative agreement with the measured values but clearly the representation is best for $\text{ASYM} = 1 + 0.2 \cdot E$, $\text{ASYM} = 1 + 0.3 \cdot E$ or $\text{ASYM} = 1 + 0.4 \cdot E$. Replacing the imaginary Saxon-Woods Derivative potential with a simple Saxon-Woods volume potential leads to some deterioration of the experimental descriptions of the total cross sections but not violently so (see the last panel in Fig. VI-13). Similar comparisons between differential experimental and calculated ^{209}Bi elastic scattering cross sections as functions of ASYM are shown in Figs. VI-14 to VI-19. Again corresponding to the potentials of Tables VI-15 to VI-20. Not surprisingly, the results are essentially the same at lower incident energies (e.g., below 5 – 10 MeV) as the definition of Eq. II-B-1 is a linear expression in laboratory energy. The agreement between measurement and calculation is good for all cases at these lower energies. However, as the incident energy increases the comparisons are more sensitive to ASYM with better agreement between measurement and calculation for $\text{ASYM} = 1 + 0.2 \cdot E$ to $\text{ASYM} = 1 + 0.4 \cdot E$. Even the experimental descriptions provided by the simple volume absorption alone remain reasonably good, as shown in Fig. VI-20. This is not surprising as Perey (Per64) long ago showed that proton elastic-scattering distributions from heavy elements are quite insensitive to the choice of surface or volume imaginary-potential forms if the optical potential parameters are obtained by multi-parameter fitting of the data. Illustrative 17 MeV proton scattering results from reference Per64 are shown in Fig. VI-21. Moldauer (Mol80) and others have pointed out that low-energy S_0 and S_1 neutron strength functions are sensitive to the position and character of the SOM imaginary absorption, suggesting a surface absorption outside the

real potential radius. The ^{209}Bi strength functions deduced from low-energy resonance measurements are $S_0 = 0.65 \pm 0.15$ and $S_1 = 0.23 \pm 0.05 (\times 10^{-4})$ (Mug+81, Mug06). The corresponding values calculated with the SOM potential of **Table V-15** (Saxon-Woods-Derivative absorption and no asymmetry) are $S_0 = 0.884$ and $S_1 = 0.3523$. Those calculated with the entirely volume absorption of **Table V-21** (no asymmetry) are $S_0 = 0.493$ and $S_1 = 0.5543$. Comparison of either of these calculated results with the values deduced from measured values does not clearly support the choice of volume or surface absorption in the present ^{209}Bi SOM cases.

As in the above ^{208}Pb considerations, the derivation of ^{209}Bi asymmetric (or other) potentials can be improved if the number of parameters used in the fitting are reduced from six to four. This was done by fixing the real-potential geometries to $r_V = 1.2589 - 0.0019 \cdot E$ (fms) and $a_V = 0.69412$ (fms), where these values are the simple averages of those obtained in the 6-parameter fitting resulting in the ASYM potentials of **Tables VI-15 to VI-20**. The entire ^{209}Bi data base was then refitted searching for the four parameters r_W , a_W , V and W at asymmetry values of $\text{ASYM} = 1 + 0.0 \cdot E$, $\text{ASYM} = 1 + 0.1 \cdot E$, $\text{ASYM} = 1 + 0.2 \cdot E$, $\text{ASYM} = 1 + 0.3 \cdot E$, $\text{ASYM} = 1 + 0.4 \cdot E$ and $\text{ASYM} = 1 + 0.5 \cdot E$ in the same manner used above in the context of the ^{209}Bi 6-parameter fitting. The resulting model parameters, given in **Tables VI-24 to VI-29**, are quite stable and are consistent with those of the above 6-parameter fitting. This is illustrated in the ASYM dependence of the real and imaginary strengths shown in **Fig. VI-22**, and the values of **Tables VI-30 and VI-31**. The same is true of the resulting imaginary potential geometries tabulated in **Tables VI-32 and VI-33**, and illustrated in **Fig. VI-23**. The ^{209}Bi total cross sections calculated with the various ASYM functions of **Tables VI-24 to VI-29** are compared with the energy averaged experimental database in **Fig. VI-24**. All of these calculated results agree quite well with the experimental database, but those made with $\text{ASYM} = 1 + 0.3 \cdot E$ are superior throughout the energy range and particularly at the low-MeV energies. The differential ^{209}Bi elastic-scattering distributions calculated with the same potential of **Table VI-27** are compared with the experimental database in **Fig. VI-25**. The agreement is very good. Perhaps somewhat better than obtained with the above ^{209}Bi 6-parameter fitting. The potential of **Table VI-27** is used with good success elsewhere in these remarks to describe other ^{209}Bi neutron observable.

VII. Energy dependence of the imaginary potential strength

Theoretical justification of the optical-model potential is frequently based on infinite nuclear matter considerations (e.g., Gom59, FPW54, Bru55, etc.) and an assumed nucleon-nucleon interaction (e.g., the Yukawa potential, Yak35). Various approximations are used to apply these nuclear matter concepts to the finite nucleus. Prominent of these is the "local-density approximation (LDA)" widely exploited by the Liege group (JLM77) and others. The interaction of an incident particle with the target nucleus is well represented by an optical potential consisting of real and imaginary terms. The course of the incident particle is governed by the real potential (e.g, shape scattering). In addition, the incident particle may undergo compound-nucleus reactions becoming a part of the target nucleus or be re-emitted into the same or another channel.

These compound-nucleus reactions are represented by the complex (imaginary) portion of the optical potential. As the incident-particle energy decreases it approaches the "Fermi Energy". At that energy all states are filled, and the Pauli Principle forbids the absorption of an additional incoming particle. As the energy of the incident particle decreases the number of open absorption channels rapidly falls until at the Fermi Energy there are none and thus the imaginary optical potential must be zero. At low unbound energies the compound-nucleus processes rapidly fluctuate with energy resulting in a complex of resonance structure. The average energy-dependent trends of those resonances, consistent with the optical model, are difficult to determine from experiment. However, it is clear that the imaginary potential strength should fall with energy and extrapolate into the bound region to zero at the Fermi Energy. This physical behavior should guide optical-model interpretations of experimental measurements at lower energies. It is a region where phenomenological optical models fluctuate with various effects attributed to "the Fermi Surface Anomaly, and dispersive and iso-spin considerations. It is pointed out that the present detailed ^{208}Pb and ^{209}Bi neutron scattering interpretations at or near the double shell closure at $A = 208$ using both spherical optical potentials and collective coupled-channels models extrapolate to imaginary potentials of approximately zero magnitude at the Fermi Energy. This is consistent with the concepts outlined above, and it suggests that phenomenological optical potentials should make use of the above physical concepts in their derivation. Many found in the literature do not.

VIII. A regional potential.

The present work, previously published work by the author and associates, and work by the Los Alamos Group provide the basis for a regional SOM extending from the highly deformed region near $A \approx 150$ to the spherical region near the doubly-closed-shell nuclei at $Z = 82$ and $A = 126$. The real potential strengths of these models are summarized in terms of volume-integrals-per-nucleon in **Table VIII-1** and **VIII-2**. Simple averages reasonably define the real geometries (r_V , a_V) and imaginary (r_W , a_W) geometries as given by the values given in **Tables VIII-1** and **VIII-2**. The mass and energy dependencies of the real and imaginary strengths are a more complex matter as they depend on both incident-particle energy and target mass. This behavior is reasonably systematic for the J_V of the real potential. Assuming a simple linear Mass and energy dependence one gets the approximate regional expression $J_V = 537.72 - 0.5643 \bullet \text{Mass} + (0.2387 - 0.01632 \bullet \text{Mass}) \bullet E \text{ MeV} \cdot \text{fm}^3$. This approximate expression describes the model-deduced J_V values of **Table VIII-1** to within several percent or better. A similar linear approximation of the mass dependence of J_W of **Table VIII-2** is less successful as the individual SOM deduced J_W values are sensitive to the structure of the individual targets, in particularly the effect of low-lying collective states and shell closures (notable the double shell closure at $A=208$). However, using a simple linear expression in Mass and a quadratic expression in energy one can qualitatively describe the imaginary potential strength over the mass range = 150 - 210 and up to ≈ 35 MeV or more with the expression $J_W = 51.664 - 0.1740 \bullet \text{Mass} + (-2.771 + 0.0316 \bullet \text{Mass}) \bullet E + (0.3177 - 0.00190 \bullet \text{Mass}) \bullet E^2 \text{ MeV} \cdot \text{fm}^3$. Away from $A=208$ and strong collective

targets this simple expression leads to SOM J_w values within less than 20% of the values following from the individual models. The above are simple approximations but they will lead to SOM parameters that are qualitatively applicable to a difficult mass region. Such a regional parameterization seems to give reasonable neutron-reaction results from $A = 150 \rightarrow 210$ at energies below ≈ 50 MeV. It needs to now be extended to above $A = 210$ and into the fissile targets. That will take careful consideration of the fission process in many cases. Such work is underway.

References

Note:- The symbol "#" indicates the EXFOR file of the referenced data.

- (ACQ53) Agno M., Cortellesa G. and Querzoli I., Nuovo. Cem. 10 282 (1955), #21263.
- (AFD85) Annand J., Finlay R. and Dietrich F., Nucl. Phys. A443 249 (1985), #12906 and #12903.
- (AG85) Annand J. and Galloway R., J. Phy. G11 1341 (1985), #22029.
- (Ang+71) Angeli I. et al., AHP 30 115 (1971), #30141.
- (BBP49) Barschall H., Bockelman B. and Peterson R., Phys. Rev. 76 1146 (1949), #12228.
- (Bes+92) Bessheuko O. et al. UFZ 37 1314 (1992), #41250.
- (BKF72) Belovitski G. Kolesnikova and Frank I., YF 15 662 (1972), #40288.
- (Blo+03) Bolomgren J. et al., Phys. Rev. C68 064605 (2003), #22847.
- (Bos+59) Bostrom N. et al., Report WADC-TN-59-107 (1959), #11130.
- (BPS58) Bratenahl A., Peterson J. and Stoering J., Phys. Rev. 110 927 (1958), #11155.
- (Bru+55) Brugger H. et al., Hel. Phys. Acta. 28 331 (1955), #21241.
- (Bru+55) Bruekner K. Lockett A. and Rotenberg M., Phys. Rev. 121 255 (1961).
- (BWS56) Beyster J., Walt M. and Salmi E., Phys. Rev. 104 1319 ((1956), #11229.
- (CB67) Carlson A. and Barschall H., Phys. Rev. 158 1142 (1967), #11497.
- (Car+91) Carlton R. et al., Bull. Am. Phys. Soc. 36 1349 (1991), #13041.
- (Cra+81) Crane R., Garbow B., Hillstrom K. and Minkoff M., Argonne Natl. Lab. Report ANL-80-116, Rev.-1 (1981).
- (CGB52) Coon J., Graves E. and Barschall H., Phys. Rev. 88 562 (1952), #11056.
- (CHH55) Coor T., Hill D. and Hornyak W., Phys. Rev. 98 1369 (1955), #11087.
- (Cie+68) Cierjacks S. et al., Report KFK-1000 (1968), #20010.
- (CJ60) Cross W. and Jarvis R. Nucl. Phys. 15 155(1960) #11465.
- (CW59) Carpenter S. and Wilson R., Phys. Rev. 114 510 (1959), #13850.
- (Das+90) Das R. et al., Phys. Rev. C42 1013 (1990), #13199.
- (Day65) Day R., priv. com. to NNDC (1965), #12191.
- (Day71) Day R., priv. com. to NNDC (1971), #12191
- (Del+83) Delaroche J. et al., Phys. Rev. C28 1410 (1983), #13635.
- (Dev80) De Vito T., DA/B 40 5724 (1980), #12701.
- (DH53) Day R. and Henckel R. Phys. Rev. 92 358 (1953), #11060.

- (Div68) Divadeenam T., DA/B 28 3834 (1968), #10523.
- (DM58) Deconninck G. and Martegani A., BCS 44 851 (1958), #20172.
- (Dri+73) Drigo L. et al., Nuovo. Cem. A13 867 (1973), #20664.
- (Duk67) Dukarevich Ju., Nucl. Phys. A92 433 (1967), #40813.
- (Elt61) Elton L., Rev. Mod. Phys. 30 557 (1958), also Nuclear Size, Report, Oxford Univ. Press (1961).
- (ENDF) ENDF/B-VI, Evaluated Nuclear Data File/B, version VI. Available from the National Nuclear Data Center, Brookhaven National Laboratory. ENDF/B-VII has very recently been released. It does not significantly change the present comments.
- (Far+65) Farrell J. et al., Phys. Lett. 17 285 (1965), #12684.
- (FC62) Fowler J. and Campbell E., Phys. Rev. 127 2192 (1962), #12215.
- (Fer+77) Ferrer J. et al., Nucl. Phys. A275 325 (1977), #10633.
- (Fes58) Feshbach H., Ann. Rev. Nucl. Sci. 8 49 (1958).
- (FG71) Foster D. and Glasgow D., Phys. Rev. C3 576 (1971), #10047.
- (Fin+84) Finlay R. et al., Phys. Rev. C30 796 (1984), #12865.
- (Fin+91) Finlay R. et al., priv. com. to NNDC (1991), #13532.
- (Fin+93) Finlay R. et al., Phys. Rev. C47 237 (1993), #13569.
- (FLM63) Firk F., Lynn E. and Moxon M., Nucl. Phys. 44 431 (1963), #21318.
- (Flo81) Floyd C., priv. com. to NNDC (1981), #13685.
- (Fow66) Fowler J., Phys. Rev. 147 870 (1966), #12217.
- (FPW54) Feshbach H., Porter C. and Weisskopf V., Phys. Rev. 96 448 (1954).
- (Fra88) Franz J., Nucl. Phys. A490 667 (1988), #2217.
- (GC65) Gilbert A. and Cameron A., Can. J. Phys. 43 1446 (1965).
- (GHS78) Guenther P., Havel D. and Smith A., Nucl. Sci. Eng. 65 174 (1978), #10664.
- (Gib+56) Gibbons J. et al., Nucl. Phys. 102 1574 (1956), #11864.
- (GM67) Gibbons J. and Macklin R., Phys. Rev. 153 1356 (1967), #12218.
- (Gio+78) Giordana V. et al., Nucl. Phys. A302 83 (1978), #41311.
- (GLM64) Gorlov G., Lebedeva N. and Morozov V., DOK 158 574 (1964), #40221.
- (GLM67) Gorlov G., Lebedeva N. and Morozov V., YF 6 910 (1967), #41311.
- (Gom59) Gomes L., Phys. Rev. 116 1226 (1959).
- (Goo62) Goodman L., Phys. Rev. 88 686 (1962), #11057.
- (GPT68) Greenlees G., Pyle G. and Tang Y., Phys. Rev. 171 1115 (1968), and Phys. Rev. C1 1145 (1970).
- (GSW80) Guenther P., Smith A. and Whalen J., Nucl. Sci. Eng. 75 69 (1980), #10846.
- (Gua+92) Guanren S. et al. CNP 14 234 (1992), #32580.
- (Gue+89) Guenther P. et al., Report, ANL/NDM-109 (1980).
- (Har+72) Harvey J. et al., Report ORNL-4743 (1972), #12816.
- (Hao+82) Haouat G. et al., Nucl. Sci. Eng. 81 491 (1982), #20801.
- (Han+85) Hansen L. et al., Phys. Rev. C31 111 (1985), #12935.
- (Har99) Harvey J., priv. com. to NNDC (1999), #13723.
- (HL50) Hildebrand R. and Leith C. Phys. Rev. 80 842 (1950), #11039.
- (HL55) Hibdon C. and Langsdorf A., Phys. Rev. 98 223 (1955), #11244.

- (Hod63) Hodgson P., *The Optical Model of Elastic Scattering*, Clarendon, Oxford (1963).
- (Hod94) Hodgson P., *The Nucleon Optical Model*, World Scientific, Singapore (1994).
- (HS77) Harvey J. and Smith H., priv. com. to NNDC (1977), #13761.
- (Hud+62) Hudson C. et al., *Phys. Rev.* 128 1271 (1962), #12180.
- (HWH75) Harvey J., Wilson W. and Hill N., priv. com. to NNDC (1975), #10449.
- (HWJ69) Holmqvist B., Wiedling T. and Johansson S., Report AE-366 (1969), #20019.
- (JLM77) Jeukenne J., Lejeune A. and Mahaux C., *Phys. Rev. C* 16 80 (1977).
- (Kha56) Khaletskij M. *DOK* 113 305 (1956), #40709.
- (KMM57) Kimball C., Monahan J. and Mooring P., Report WASH-745 (1957), #12234.
- (Kor+77) Korzh I., et al., *UFZ* 22 87 (1977), #40532.
- (KP74) Kinney W. and Perey F., Report ORNL-4909 (1974), #10412.
- (KVJ72) Kuijper P., Veefkid J. and Jonker D., *Nucl. Phys. A* 181 545 (1972), b#19710.
- (Lan62) Lane A., *Nucl. Phys.* 35 676 (1962), also *Phys. Rev. Lett.* 171 (1962).
- (LGS87) Lawson R., Guenther P. and Smith A., *Phys. Rev. C* 36 1298 (1987), #13120.
- (Lip66) Lipperheide R., *Nucl. Phys.* 89 97 (1966).
- (LR53) Linlor W. and Ragent B., *Phys. Rev.* 92 895 (1953), #12205.
- (LS99) Lawson R. and Smith A., Argonne National Laboratory Reports ANL/NDM-145 and ANL/NDM-147 (1999).
- (LS01) Lawson R. and Smith A., Argonne National Laboratory Report ANL/NDM-152 (2001).
- (Man65) Manero F., *Nucl. Phys.* 65 417 (1965), #20209.
- (Maz+55) Mazari I., et al., *AFE* 1 69 (1955), b#30037.
- (MEF55) McGarry W., Elliot G. and Faust W. Report NRL-4666 (1955), #13050.
- (Mil+52) Miller D. et al., *Phys. Rev.* 88 83 (1952), #11712.
- (MN81) Mahaux C. and Ngo N., *Phys. Lett. B* 100 285 (1981)
- (Mol80) Moldauer P., *Nucl. Phys. A* 344 185 (1980).
- (Mug+81) Mughabghab S., Divadeenam M. and Holden M., *Neutron Cross Sections*, Academic, New York (1981).
- (Mug06) Mughabghab S., *ATLAS of Neutron Resonances*, Elsevier, Amsterdam (2006).
- (ND53) Nereson N. and Darden S., *Phys. Rev.* 89 775 (1953), #11060.
- (NDS) Martin M., *Nucl. Data Sheets* 47 797 (1986) and 63 723 1991, available from the National Nuclear Data Center, Brookhaven Nat. Lab., New York.
- (NNDC) National Nuclear Data Center, Brookhaven National Laboratory, Upton New York.
- (Ols+82) Olsson N. et al., *Nucl. Phys.* 385 285 (1982), # 21825.
- (Ols+87) Olsson N. et al., *Nucl. Phys. A* 472 237 (1987), #22048.
- (OR82) Olsson N. and Ramstrom E., *Nucl. Phys. A* 388 288 (1982).
- (Ort75) Ortega R., INIX-MF-1743 (1975), #30378.
- (Osb+04) Osborne J. et al., *Phys. Rev. C* 70 139046 (2004), #13956.

- (Pas67) Passatori G., Nucl. Phys. A95 694 (1967).
(Pau41) Pauli W., Rev. Mod. Phys. 13 203 (1941).
(PBS60) Peterson J., Bratenhall A. and Stoering J. Phys. Rev. 120 521 (1960), #11108
(Per63) Perey F., Phys. Rev. 131 745 (1963).
(Rap+78) Rapaport J., et al., Nucl. Phys. A296 95 (1978), #10871.
(Rap82) Rapaport J., Phys. Reports 87 25 (1982).
(Ray59) Rayburn L., Phys. Rev. 116 1571 (1959), #11806.
(Ray96) Raynal J., CEA Report CEA-N-2772 (1996) and priv. com.
(Rob+91) Roberts M., et al, Phys. Rev. C44 2006 (1991), #13531.
(SBN67) Seibel F., Bilpuch E. and Newson H., Report WASH-1074 (1967), #10010.
(Sch+73) Schimmerling W., et al., Phys. Rev. C7 248 (1973), #10082.
(Sin+76) Singh U., et al., Phys, Rev C13 124 (1976), #10539.
(Smi+70) Smith A., et al., Nucl. Sci. Eng. 41 63 (1970), #10010.
(SGL86) Smith A., Guenther P. and Lawson. R., Argonne Natl. Lab. Report ANL/NDM-100 (1986).
(Smi05) Smith A., priv. com. from the author (2005).
(Sat83) Satchler G., Direct Nuclear Reactions, Addison-Westley, Reading MA (1983).
(SW54) Snowdon S. and Whitehead W. Phys. Rev. 94 1267 (1954), #11965.
(Tak+88) Takahashi A., et al., JAERI-M-88-102 (1988), #22106.
(Tan+72) Tanaka S., et al., Nucl. Phys. A179 513 (1972), #20337.
(Tul05) Tuli J., Nuclear Wallet Cards, National Nuclear Data Center, Brookhaven Natl. Lab. (2005).
(TUNL) Triangular Universities Nuclear Laboratory, Durham N. C.
(Tut+65) Tutubalin A., et al., Kiev Conf. 2 65 (1977). #40559.
(WB54) Walt M. and Beyster R., Phys. Rev. 98 677 (1954), #11637.
(WB55) Walt M. and Beyster R., Phys. Rev. 98 677 (1985), #11215.
(WG85) Walter R. and Guss P., Proc. Conf. on Nucl. Data for Basic and Applied Sci., Eds. P. Young et al., Gordon and Breach (1985).
(Wil+65) Wilenzick R., et al., Nucl Phys. 62 511 (1965), #11287.
(Wol51) Wolfenstein L., Phys. Rev. 82 690 (1951).
(Zaf+65) Zafiratos C., et al., Phys. Rev. Lett. 14 913 (1965), #12220.
(Yak35) Yakawa H., Proc. Phys. Mat Soc. Japan 17 392 (1935).

Acknowledgements. The author gratefully acknowledges the help of Drs. P. Young, S. Grammel and F. Kondev.

Appendix A. Absorption asymmetry referenced to the Fermi-Energy (EF)

The fitting of **Section V** of the main body of the text suggests that the potential absorption extrapolates to zero at approximately the Fermi Energy, irrespective of the imaginary potential asymmetry, for example as illustrated for example **Tables VI-1 to VI-10** and in **Fig. VI-12**. This suggests that the energy scale should be referenced to the Fermi Energy (≈ -6 MeV) rather than the conventional laboratory energy. This has been suggested from time to time in the literature (e.g. Rap82). This assumption leads to the equation

$$\text{ASYM} = 1 + K \cdot (E - E_F), \quad (\text{A-1})$$

where "K" has the same connotation as in **Eq. II-B-1** of the text. With the assumption of **Eq. A-1**, the four-parameter ^{208}Pb fitting of **Section V** of the main body of the text was repeated for $K = 0.0, 0.1, 0.2, 0.3, 0.4$ and 0.5 with the resulting respective potentials of **Tables A-1 to A-6**. These potentials give essentially the same results as obtained with the prior **Section V** fitting which referenced the energy scale to the laboratory system. This is illustrated by comparing **Tables A-7 and A-8** with **Tables V-13 and V-14**, and by comparisons of **Fig. A-1** with **Figs. VI-2 and VI-4**. Thus, the present phenomenological interpretations do not strongly support either choice of energy scale, although the Fermi-Energy reference point may be more theoretically attractive.

Appendix B. Dispersive ^{209}Bi Considerations

As pointed out in **Section IV-B** of the text, the derivation of the dispersion fraction (illustrated in **Figs. IV-B-1 and IV-B-2**) is sensitive to the potential on which it is based, particularly the energy extrapolations used in the calculations. Some of these matters are mitigated by the dispersive approach used in **Section IV-B**, but others are unavoidable. Therefore, the 6-parameter dispersive ^{209}Bi fitting was repeated, normalizing the dispersive fraction by $1.0 \cdot \text{DISP}$, $0.5 \cdot \text{DISP}$, $0.25 \cdot \text{DISP}$ and $0.01 \cdot \text{DISP}$ (i.e. essentially no dispersion) where **DISP** is the dispersive distribution shown in **Fig. IV-B-2** and as discussed in **Section IV-B**. The resulting potentials are given in **Tables B-1, B-2, B-3 and B-4**. The neutron total cross sections obtained with each of the potentials are compared with the energy-averaged values in **Fig. B-1**. The four potentials give qualitatively the same total cross section results, with those employing the dispersion times 1.0 to 0.5 perhaps being the most desirable. The same conclusion was reached from comparisons of **SOM** and **DOM** calculated and measured differential elastic-scattering distributions and total cross sections. Dispersion effects are an important consideration in lower-energy model development but the considerations remain only qualitative. Other considerations of dispersive effects based on other potentials and models may well lead to differing results but the qualitative features are probably reasonably represented by the current considerations.

Appendix C. Neutron Inelastic-Scattering Cross Sections

The experimental knowledge of inelastic neutron scattering from ^{208}Pb as available at the NNDC is remarkably meager, limited to 22 references, only 7 of which deal with direct experimental determinations of inelastic excitation functions. The remaining citations deal with γ -production measurements or continuum neutron emission measurements. These references are:-

- (C-1) Kinney W. and Perey F., Report ORNL-4909 (1974), #10412. Differential inelastic neutron scattering for E_{in} 5.5 – 8.5 MeV. A number of levels and composites.
- (C-2) Nellis D., Phy. Rev. C9-1972 (1974) #10485, Gamma-production.
- (C-3) Dickens J., Nucl. Sci. and Eng. 63-101 (1977) #10692, Gamma production for $E_{\text{in}} = 5.5 - 8.0$ MeV.
- (C-4) Bainum D., Phy. Rev. C16-1377 (1977) #10699, Differential distributions at 11 and 26 MeV. No values much back of forward hemisphere.
- (C-5) Bostrom N., Report WADC-TR-59-31 (1959) #11341, Gamma-production results.
- (C-6) Finlay R., Phy. Rev. C30-796 (1984) #12865. Neutron angular distributions at 20 and 22 MeV, $E_x = 2.62$ MeV.
- (C-7) Guss P., Phy. Rev. C25-2854 (1982) #13525. Polarizations. $E_{\text{in}} = 9.97$, $E_x = 2.61$ MeV.
- (C-8) Yeh M., Phy, Rev. C54-942 (1996) #13626. Search for 2.485 gamma ray
- (C-9) Kadi M., Phy, Rev. Lett. 76 1208 (1996) #13942, Gamma-production measurements.
- (C-10) Almen-Ramstrom E., Report AE-503 (1974) #20788. Inelastic scattering, $E_{\text{in}} = 3.8-4.5$ MeV, $E_x = 2.61$ MeV.
- (C-11) Towle J. and Gilboy W., Nucl. Phys. 44-256 (1965) #21128. $E_{\text{in}} = 3.2 - 4.5$ MeV, $E_x = 2.62 - 3.48$ MeV.
- (C-12) Yamamoto T., J. Nucl. Sci. Tech. 15-797 (1978) #21394. Gamma-production at $E_{\text{in}} = 14.7$ MeV.
- (C-13) Hlavac S., Nucl. Sci. and Eng. 119-195 (1995) #31450. Gamma-production at $E_{\text{in}} = 14.7$ MeV.
- (C-14) Hongyu Zhou+, Nucl. Sci. and Eng. 134-106 (2000) #31492. Gamma-production from natural lead at 14.9 MeV incident neutron energy.
- (C-15) Belovickij G. +, YF 15-666 (1972) #40700. Neutron scattering at 13.7 incident energy.
- (C-16) Govor L., IZV 54-526 (1990) #41015, Gamma-production.
- (C-17) Lashuk A., YK 1996-59-1912 (1996) #4125. Gamma-production at $E_{\text{in}} = 3.0$ MeV.
- (C-18) Simakov S., INDC(CCCP)-315/L (1990) #41331. Neutron emission at $E_{\text{in}} = 14.7$ MeV.
- (C-19) Degtjarev Ju+, IZV 35-2341 (1971) #40278. Gamma production.
- (C-20) Joensson B., AE 39-295 (1969) #20164. Gamma production at an incident energy of 15 MeV.

(C-21) Vonach H., Phys. Rev. C50-1952 (1994) #13644. Gamma production at incident neutron energies of 3 – 200 MeV.

(C-22) Nellis D., J. BAP 7-120 (1962) #13001. Neutron gamma production at incident energies of 4-15 MeV.

This symbol indicates the EXFOR accession number for data in each of the above references.

The above is only fragmentary experimental evidence of inelastic-neutron scattering from ^{208}Pb , and it is not much assistance with SOM development. This is particularly true as the low-lying excited states are highly collective vibrational excitations as clearly evident from a few of the better quality measured inelastic-neutron angular distributions, and from life-time measurements.

The experimental knowledge of inelastic neutron scattering from ^{209}Bi is more extensive than for ^{208}Pb , as cited in the 49 references below. However, only approximately half deal directly with inelastic-neutron scattering, and less than half of those are at all relevant to the above model considerations. Many of the results are very old, limited, and confined to approximately 14 MeV incident energies.

(C-23) Kiehn R. and Goodman C., Phys. Rev. 95-989 (1954), #11477, n-gamma measurements.

(C-24) Smith A., Nucl. Sci. and Eng. 41-63 (1970), #10010, (n,n') scattering at E_{in} up to 1.5 MeV.

(C-25) Guenther P., Nucl. Sci. and Eng. 75-69 (1980), # 10846, (n,n'), scattering at E_{in} 1.5 – 4.0 MeV.

(C-26) McGregor M., Proc. Paris Conf. (1958), #11205, shell measurement at 14 MeV.

(C-27) Rosen L. and Stewart L., Phys. Rev. 107-824 (1957), #11223, emulsion measurements at 14 MeV.

(C-28) Wilenzick R., Nucl. Phys 62-511 (1965), #11287, scattering at 6 MeV.

(C-29) Cranberg L. and Levin J., Phys. Rev. 103-343 (1956), #11396, scattering at 2.45 MeV.

(C-30) Almen-Ramstrom E., Report, AE-503 (1975), #20788, (n,n') scattering E_{in} 2-4.5 MeV.

(C-31) Takahashi A., Report JAERI-M-88-102 (1988), #22106, double differential emission at 14 MeV.

(C-32) Eliot E., Phys. Rev. 94-144 (1954), #21385, (n,n') scattering at 2.5 E_{in} .

(C-33) Schweitzer T., KE 20-174 (1977), #30463, (n,n') at 3.4 MeV E_{in} .

(C-34) Degtjarev Ju and Protopopov V., AE 23-568 (1967), #40047, (n,n') 1.0-4.0 MeV E_{in}

(C-35) Broder D., IZV 31-327 (1967), #40161, n-gamma production.

(C-36) Korzh I., UFZ 22-87 (1977), #40532, n-gamma production.

(C-37) Lashuk A., YK 1994-26 (1994), #41186, (n,n') $E_{\text{in}} = 1.0 - 5.0$ MeV.

(C-38) Lashuk A. and Sadokhin I., YK 1996 (1959), #41245, gamma-prod. at 3 MeV.

(C-39) Wedell J., Phys. Rev. 104-1069 (1956), #11479, scattering at 4.4 MeV.

(C-40) Stelson P., Nucl. Phys. 68-97 (1965), #11527, scattering at 14 MeV.

(C-41) Scherrer V., Phys. Rev. 96-386 (1954), #11672, gamma-production at 3.2 MeV.

- (C-42) Schectman W. and Anderson J., BAP 10-498 (1965), #11898, scattering at 14 MeV.
- (C-43) Buchanan P., BAP 12-921 (1967), #12689, scattering 1.7-4.0 MeV.
- (C-44) Williams G., DA/B 36-790 (1975), #12690, gamma-production.
- (C-45) McKinney T., (priv. com. to NNDC, (1972), #13034, scattering at 14 MeV.
- (C-46) Cranberg L., Phys. Rev. 159-969 (1967), #13578, scattering at 2.5 MeV.
- (C-47) Joensson J., AE 39-295(1969) #20164, gamma-production at 15 MeV.
- (C-48) Rethmier J., Nucl. Inst. and Methods 17-273 (1962), #20200, scattering at 14.7 MeV.
- (C-49) Kuiper P., Nucl. Phys./A 181-545(1972), #20223, 14 MeV scattering.
- (C-50) Hosoe M., J. Phy. Japan 14-699 (1959), #20286, gamma-production.
- (C-51) Matoba M., Nucl. Phys. A/204-125 (1973), #20308, 14.1 MeV scattering.
- (C-52) Tanaka S., Nucl. Phys. A/179-513 (1972), #20337, scattering 1.5-3.5 MeV.
- (C-53) Habbani F. and Jiggins A., Nucl. Instr. and Meth. 134-545 (1976), #20667, gamma-production at 3.3 MeV.
- (C-54) Towle J. and Gilboy W., Nucl. Phys. A/112-337 (1968), #21231, many differential neutron-scattering distributions.
- (C-55) Poole M., PM 34-1398 (1953), # 21377, inelastic neutron scattering.
- (C-56) Akiyoshi T., Nucl. Sci. and Tech. 11-523 (1974), #21588, 14.1 MeV scattering.
- (C-57) Bertin A., Report CEA-R-3808, #21678, gamma-production at 6.6 and 8.7 MeV.
- (C-58) Galloway R. and Rahighi J., Nucl. Instr. and Methods A/297-452 (1990), #22706, scattering at 14 MeV.
- (C-59) Nath N., Tokyo Conf. (1967), #30056, gamma-production.
- (C-60) Shen Rong-Lin, J. CNP 4-128 (1982), #30656, 14.2 MeV gamma-production.
- (C-61) Bakov A., J. AE-29-238 (1970), #40131, gamma-production in fission spectrum.
- (C-62) Anufrienko V., YF 2-826 (1966), #40133, 14 MeV scattering and temperature.
- (C-63) Ju. Degtjarev and Protopov V., IZV 35-2341 (1971), #40278, gamma-production.
- (C-64) Biryukov N., YF 19-1190 (1974), #40287, scattering at 9.1 MeV.
- (C-65) Trykova V. and Baryba B., YK 19-66 (1975), #40338, temperature data.
- (C-66) Popov V., AE 3-498 (1957), #40467, scattering at 2.9 MeV.
- (C-67) Avchukhov V., Tashkent Conf. 16 (1971), #40526, gamma-production.
- (C-68) Simakov S., YK 5-17 (1982), #40683, scattering at 4-8 MeV.
- (C-69) Prokpets G., YF 32-37 (1980), #41102, scattering at 20.6 MeV.
- (C-70) Simakov S., YF 4-74 (1992), #41155, scattering 5-8.5 MeV.
- (C-71) Annand J., Nucl. Phys. A/443-249 (1985), no #, scattering 4-7 MeV.
- # This symbol indicates EXFOR accession number.

Some of these resources are of limited value in the context of the present work as much of this referenced work is:- 1) the result of gamma-production measurements which do not define neutron excitation functions due to uncertainties in gamma-branching ratios and internal conversion effects, and 2) the scattered-neutron experiment does not fully resolve the contributions from any but the first few excited levels. Much of the data is very old and does not benefit from modern techniques. Thus only the excitations of the first three mean excited states of ²⁰⁹Bi are reasonably defined by neutron inelastic

scattering experiments ($E_x \approx 0.9, \approx 1.6$ and ≈ 2.5 MeV). The latter consists of contributions from as many as seven components,. The corresponding first three low-energy excitations of ^{208}Pb are at $\approx 2.6, \approx 3.2$ and ≈ 3.5 MeV. The experimental results contributing to each of these triplets of effective "levels" were carefully culled by graphical inspections with the resulting composite experimental excitation functions of the first three levels of ^{208}Pb shown in **Fig. A-C-1**, and for ^{209}Bi shown in **Fig. A-C-2**. The same figures show calculated inelastic excitation functions assuming compound-nucleus processes as outlined in the body of the text.. These inelastic excitation functions are used to adjust the statistical temperature above discrete-excitation energies with the results discussed in **Section V** and **Appendix E**.

Appendix D. Scattered-neutron polarizations

Scattered-neutron polarizations have been used for guiding model interpretations. Unfortunately, the experimental measurements upon which such considerations are based are very difficult. As a consequence the available data is limited and often of marginal quality. Many of the best experimental results are from a single institution (TUNL). There are five references to ^{208}Pb neutron scattering polarization measurements at the NNDC as follows:-

- (D-1) Delaroche J., *Phy. Rev. C*/28-1410 (1983), #13635.
- (D-2) Floyd C., *Phy. Rev. C*/25-1682 (1982), #12859
- (D-3) Roberts M., *Phys. Rev. C*/44-2006 (1991), #13531.
- (D-4) Morozov V., *YFI* 14-8 (1972), #40075.
- (D-5) Guss P., *Phys. Rev. C*/25-2854 (1992), #13525.

where "#" denotes EXFOR number.

There are more NNDC references to the measurement of polarization of neutrons scattered from ^{209}Bi , as one would expect from the ready availability of the sample material. However, the experimental results scatter and many are very old and limited. These 13 ^{209}Bi NNDC references are:-

- (D-6) Begum A., *J. Phy. G*/7-535 (1981), #30633.
- (D-7) Hussein A. et al., *Phys. Rev. C*/15-233 (1977), #10645.
- (D-8) Zijp E. and Jonker C., *Nucl. Phys. A*/222-93 (1974), #20777.
- (D-9) Drigo L., *Nuovo. Cem. A*/13-867 (1973), #20664.
- (D-10) Cox S. and Cox D., *Report ANL-7935* (1972), #10332.
- (D-11) Ferguson A., *Nucl. Phys.* 76-269 (1966), #21140.
- (D-12) Gorlov G., *DOK* 158-574 (1964), #40221.
- (D-13) Weisel G., *Phy. Rev C*/54-2410 (1996), #13680.
- (D-14) Annand J. and Galloway R., *J. Phys. G*/11-1341 (1985), #22029.
- (D-15) Ahmed M. and Firk F., *Sante Fe Conf.*-389 (1980), #10855.
- (D-16) Gorlov G., *YF* 8-1086 (1968), #40307.
- (D-17) Katori K., *JPJ* 28-1116 (1970), #209898.
- (D-18) Delaroche J., *Phys. Rev. C*/28- 1410 (1983), #13680.

where , again, "#" denotes EXFOR number.

This database is not sufficiently rigorous to be used for empirical model development analogous to that described in the body of this report. Indeed, attempts to do just that reported in the literature have lead to erroneous conclusions which were later withdrawn by the authors. Here, comparisons are made between the observed polarization of elastically-scattering neutrons and the predictions of the simple SOM potentials of **Table IV-A-1** and **IV-A-2**. **Fig. D-1** (panels one and two) compares measured and calculated elastic-scattered polarization asymmetries for elastic neutron scattering from ^{208}Pb at incident energies of 5.97, 6.96, 7.96, 8.95, 9.95, and 13.90 MeV. The measured data, as given in the above references D-1, D-2 and D-3, is indicated by circular symbols. The curves indicate the results of calculations with the SOM potential on a 6-degree angular mesh. The measured values are all from TUNL work. The agreement between measurement and calculation is qualitatively reasonable, with the larger differences at back angles. That agreement might be improved by introducing dispersion and/or channel coupling into the calculations, but it is doubtful if the experimental data is sufficiently accurate to support such additional model complexity in this ^{208}Pb case.

Similar comparisons of measured and calculated elastically-scattered neutron polarizations for ^{209}Bi are shown in the two panels of **Fig. D-2**. The SOM potential of **Table IV-A-2** was used in the calculations. The incident neutron energies were 0.93, 2.9, 3.0, 3.2, 6.0 and 9.0 MeV as given in the above references D-10, D-6, D-14, D-8 and D-18, respectively. There are obvious discrepancies in the experimental data near incident energies of 3.0, and possibly elsewhere. Given these experimental uncertainties, the comparisons with calculation are about as good as can be expected. This experimental database certainly does not warrant more complex attempts at model interpretation.

As noted in the beginning of this appendix, neutron polarization measurements are difficult, but they do make possible some interesting model considerations, particularly in this "doubly magic" region. Unfortunately, apparently no such measurements are in progress, and the latest reference in the data-center network is 15 years old, with the average far older.

Appendix E. Effects of statistical level densities and dispersion

E-A. Compound-Nucleus and Channel Competition.

The calculations of the above text use the statistical level formalism of Gilbert and Cameron (GC65), supported by the RIPL compilation of parameters (NDS), to describe the distribution of compound-nucleus cross sections at energies above the energies of discrete level excitations. The compound-nucleus contribution to other than elastic and inelastic channels is assumed to be very small at the lower energies where compound-elastic contributions are significant. The excitation of the first two excited states in ^{209}Bi ($E_x = 0.896$ and $= 1.609$ MeV) are now reasonably experimentally resolved to incident energies of 6 MeV (see **Appendix B**). They are very largely particle excitations that can be treated as compound-nucleus excitations. The associated

collective-vibrational excitations are relatively small. The consequences of uncertainties in the low-lying level structure were examined using alternate level-density assumptions. The statistical level temperatures in the ^{208}Pb and ^{209}Bi region are anomalous. Generally, the statistical temperature is a smooth function of mass (See Fig. 9 of ref. GC65) but it peaks very sharply at the double shell closure at $A = 208$. The general mass trend is for a temperature of ≈ 0.4 MeV in the heavier mass region, peaking very sharply to ≈ 1.0 MeV at $A = 208$. The magnitude of this peak must result in low-energy consistency between compound-nucleus elastic and inelastic scattering results in the present considerations.

The impact of the continuum temperature (T) of ^{209}Bi on elastic and inelastic neutron scattering was examined using 6-parameter fitting of the entire elastic-scattering data base with temperatures of $T = 0.4, = 0.7, = 1.0$ and 1.4 MeV, including 13 discrete levels distributed over excitations of 0.0 to 2.826 MeV with spins and parities as given in the Nuclear Data sheets (NDS), and the ASYM of the absorption $\equiv 0.0$. The resulting SOM ^{209}Bi potentials are given in **Tables E-1, E-2, E-3** and **E-4**. All of these potentials give reasonable descriptions of the measured neutron total cross sections, as illustrated by panels E-1 to E-4 of **Fig. E-1**, with potentials of **Tables E-2** and **E-3** probably preferred. Comparisons of the corresponding measured and calculated differential elastic-scattering cross sections are very similar to each other and to those illustrated in the main body of the text. The calculated cross sections for the inelastic excitation of the first two excited states is far more sensitive to the model temperature as illustrated in **Fig. E-2**. The potential of **Table E-3** gives reasonable descriptions of the excitation of these first two states while the potentials of **Tables E-1** and **E-2** lead to far poorer results due to excessive channel competition, and that of **Table E-4** due to too little channel competition. Thus even though there is considerable scatter in the relevant measured inelastic-scattering cross sections, they, combined with the differential elastic-scattering and total cross sections, clearly indicate that the ^{209}Bi statistical temperature is ≈ 1.0 MeV below ≈ 30 MeV incident neutron energy. This value is consistent with that given in ref. GC65 and with that used in the primary calculations of the main text.

The above conclusions were supported by repeating the above 6-parameter fitting assuming 48 discrete levels extending to an excitation of 3.692 MeV with and without a temperature of $T = 1.0$ MeV. Again, the differential elastic-scattering and total cross sections were reasonably described by either alternative but the calculated inelastic excitations of the first two levels are still modestly sensitive to the alternate potential choices at higher energies, as illustrated in the panels of **Fig. E-3**. Though small, the effect of the statistical levels is significant above the upper 3.692 energy limit of the discrete levels.

The exercises of this appendix based upon the SOM and the measured neutron total, elastic-scattering and inelastic-scattering cross sections strongly suggest that a statistical temperature of ≈ 1.0 MeV is suitable for describing the **neutron** interaction of ^{209}Bi up to energies of at least 30 MeV. Such a value is consistent with that of ref. GC65. It is an experimental verification of the value. It is reasonable to assume the same value for ^{208}Pb , as suggested in ref. GC65. However, that can not be verified by interpretations, such as the above, as the definition of the relevant ^{208}Pb inelastic neutron

scattering is not nearly as good as for ^{209}Bi . Also, the inelastic processes probably are far more of a collective vibrational nature and thus not nearly as well described by the SOM compound-nucleus model.

E-B. Dispersive Effects

The above statistical temperature conclusions may be sensitive to dispersive effects. This alternative was explored with 6-parameter ^{209}Bi fitting assuming temperatures of $T = 1.0$ MeV and 48 discrete levels with results as given in the potential of **Table E-6**, but with the full dispersion effect of **Section IV-B** of the main text, and also with the dispersive contribution reduced by 50%. The resulting potentials are given in **Tables E-7** and **E-8**. Both give reasonable representation of measured neutron total, differential elastic, and of the inelastic-scattering cross sections, as illustrated in **Fig. E-1** (panels 7 and 8), and in **Fig. E-4**. The differences between the two inelastic cross sections of **Fig. E-4** as deduced with the full dispersion and half dispersion contributions are very small, probably easily within the variation one might expect from independent statistical fitting procedures. The conclusion is that the temperature $T \approx 1.0$, and is independent of reasonable variations in dispersive contributions.

TABLES

Table IV-A-1. ^{208}Pb Baseline SOM from 6-parameter fitting. Potential depths and energies are in MeV. Potential strengths are in volume-integrals-per-nucleon (J_i , in $\text{MeV}\cdot\text{fm}^3$). Geometries are in fms. $\text{ASYM} = 1 + 0.00\cdot E$ (i.e spherical), temperature $T = 1.0$ MeV, 13 discrete levels.

Real Potential

$$\begin{aligned} \text{Strength } V &= 46.353 - 0.1239\cdot E \\ J_V &\approx 417.25 - 3.2910\cdot E \text{ (approximation)} \\ J_V &= 420.09 - 3.7777\cdot E + 0.01217\cdot E^2 \end{aligned}$$

$$\text{Radius } r_V = 1.2589 - 0.002796\cdot E$$

$$\text{Diffuseness } a_V = 0.6821$$

Imaginary Potential

$$\begin{aligned} \text{Strength } W &= 4.7808 + 0.4409\cdot E - 0.02327\cdot E^2 + 0.0003408\cdot E^3 \\ J_W &\approx 10.864 + 6.0586\cdot E - 0.25661\cdot E^2 + 0.003514\cdot E^3 \text{ (approximation)} \\ J_W &= 11.652 + 5.2408\cdot E - 0.15223\cdot E^2 - 0.00068503\cdot E^3 + \\ &\quad 0.000052478\cdot E^4 \end{aligned}$$

$$\text{Radius } r_W = 1.4024 - 0.01604\cdot E + 0.0001731\cdot E^2$$

$$\text{Diffuseness } b_W = 0.1486 + 0.04376\cdot E - 0.0009751\cdot E^2 + 0.00001007\cdot E^3$$

Spin-Orbit Potential of ref. WG85, real only and fixed.

$$\text{Strength } V_{\text{SO}} = 5.767 - 0.015\cdot E + 2\cdot((N-Z)/A)$$

$$\text{Radius } r_{\text{SO}} = 1.103$$

$$\text{Diffuseness } a_{\text{SO}} = 0.560$$

Table IV-A-2. ^{209}Bi Baseline SOM from 6-parameter fitting. Potential depths and energies are in MeV. Potential strengths are in volume-integrals-per-nucleon (J_i , in $\text{MeV}\cdot\text{fm}^3$). Geometries are in fms. $\text{ASYM} = 1 + 0.00\cdot E$ (i.e. spherical), temperature $T=1.0$ MeV with 13 discrete levels.

Real Potential

$$\begin{aligned} \text{Strength } V &= 44.672 + 0.05854\cdot E \\ J_V &\approx 421.28 - 3.9854\cdot E \text{ (approximation)} \\ J_V &= 422.91 - 4.3766\cdot E + 0.01304\cdot E^2 \end{aligned}$$

$$\text{Radius } r_V = 1.2793 - 0.005232\cdot E$$

$$\text{Diffuseness } a_V = 0.6814$$

Imaginary Potential

$$\begin{aligned} \text{Strength } W &= 6.1762 - 0.07746\cdot E + 0.005975\cdot E^2 - 0.0001105\cdot E^3 \\ J_W &\approx 20.35 + 3.1487\cdot E - 0.05241\cdot E^2 - 0.0001756\cdot E^3 \text{ (approximation)} \\ J_W &= 20.23 + 3.3936\cdot E - 0.09534\cdot E^2 + 0.002148\cdot E^3 - 0.00003864\cdot E^4 \end{aligned}$$

$$\text{Radius } r_W = 1.3580 - 0.008814\cdot E$$

$$\text{Diffuseness } b_W = 0.2091 + 0.04145\cdot E - 0.0005810\cdot E^2$$

Spin Orbit Potential of reference WG85, fixed

Table IV-B-1. ^{208}Pb DOM potential deduced from 6-P fitting. Potential depths and energies are in MeV. Potential strengths are in volume-integrals-per-nucleon (J_i , in $\text{MeV}\cdot\text{fm}^3$). Geometries are in fms. The Fermi Energy was taken to be -6.0 MeV, $\text{ASYM} = 1 + 0.00\bullet\text{E}$, 13 discrete levels to 4.09 MeV and temperature $T = 1.0$ MeV.

Real Potential

$$\begin{aligned} \text{Strength } V &= 45.611 - 0.09136\bullet\text{E} \\ J_V &= 393.36 - 4.1109\bullet\text{E} + 0.01522\bullet\text{E}^2 \\ J_V &\approx 389.81 - 3.5020\bullet\text{E} \\ \text{Radius } r_V &= 1.2376 - 0.003670\bullet\text{E} \\ \text{Diffuseness } a_V &= 0.6827 \end{aligned}$$

Imaginary Potential

$$\begin{aligned} \text{Strength } W &= 4.7896 + 0.3010\bullet\text{E} - 0.007332\bullet\text{E}^2 \\ J_W &= 19.267 + 2.7140\bullet\text{E} - 0.004951\bullet\text{E}^2 - 0.001056\bullet\text{E}^3 \\ J_W &\approx 17.050 + 3.6692\bullet\text{E} - 0.06828\bullet\text{E}^2 \\ \text{Radius } r_W &= 1.3295 - 0.007400\bullet\text{E} \\ \text{Diffuseness } b_W &= 0.2707 + 0.01975\bullet\text{E} - 0.00001292\bullet\text{E}^2 \end{aligned}$$

Spin-Orbit Potential of reference WG85, fixed.

$$\text{Dispersion Fraction DISP} = 0.9223 - 0.02770\bullet\text{E} + 0.0009277\bullet\text{E}^2 - 0.00001504\bullet\text{E}^3$$

Table IV-B-2. ^{209}Bi DOM potential deduced from 6-P fitting. Potential depths and energies are in MeV. Potential strengths are in volume-integrals-per-nucleon (J_i , in $\text{MeV}\cdot\text{fm}^3$). Geometries are in fms. The Fermi Energy is taken to be -5.87 MeV, $\text{ASYM} \equiv 1$, 13 discrete levels to 2.83 MeV and a statistical temperature of $T = 1.0$ MeV.

Real Potential

$$\begin{aligned} \text{Strength } V &= 45.496 + 0.002035\bullet\text{E} \\ J_V &= 398.55 - 5.6652\bullet\text{E} + 0.02572\bullet\text{E}^2 \\ J_V &\approx 395.34 - 4.8934\bullet\text{E} \\ \text{Radius } r_V &= 1.2455 - 0.006256\bullet\text{E} \\ \text{Diffuseness } a_V &= 0.6757 \end{aligned}$$

Imaginary Potential

$$\begin{aligned} \text{Strength } W &= 5.5323 - 0.1019\bullet\text{E} + 0.02886\bullet\text{E}^2 - 0.001472\bullet\text{E}^3 + 0.00002089\bullet\text{E}^4 \\ J_W &= 22.594 + 2.5943\bullet\text{E} + 0.008846\bullet\text{E}^2 - 0.002045\bullet\text{E}^3 \\ J_W &\approx 21.061 + 3.6165\bullet\text{E} - 0.08315\bullet\text{E}^2 \\ \text{Radius } r_W &= 1.3210 - 0.006788\bullet\text{E} \\ \text{Diffuseness } a_W &= 0.2809 + 0.03354\bullet\text{E} - 0.0004784\bullet\text{E}^2 \end{aligned}$$

Spin-orbit Potential of reference WG85, fixed.

$$\text{Dispersive fraction DISP} = 1.0163 - 0.03466\bullet\text{E} + 0.001339\bullet\text{E}^2 - 0.0000.2654\bullet\text{E}^3$$

Table V-1. ^{208}Pb potential parameters deduced with the two-level (0+, 3-) vibrational model described in the text. The deformation $\beta_3 = 0.0$. This should be comparable with the SOM baseline potential although the model codes used are different. Potential depths are in MeV, potential strengths (J_i) in volume-integrals-per-nucleon (MeV- fm³), and dimensions in fermis.

Real Potential

$$\text{Strength } V = 45.767 - 0.1123 \bullet E$$

$$J_V = 413.35 - 2.8107 \bullet E$$

$$\text{Radius } r_V = 1.2611 - 0.002290 \bullet E$$

$$\text{Diffuseness } a_V = 0.6755$$

Imaginary Potential

$$\text{Strength } W = 1.3038 + 1.3741 \bullet E - 0.1027 \bullet E^2 + 0.002956 \bullet E^3 - 0.00002906 \bullet E^4$$

$$J_W = 3.3128 + 8.0398 \bullet E - 0.4546 \bullet E^2 + 0.01110 \bullet E^3 - 0.00009316 \bullet E^4$$

$$\text{Radius } r_W = 1.4360 - 0.02023 \bullet E + 0.0002616 \bullet E^2$$

$$\text{Diffuseness } a_W = 0.1781 + 0.03444 \bullet E - 0.0003356 \bullet E^2$$

Spin-orbit Potential of reference WG85, fixed.

Table V-2. ^{208}Pb potential parameters deduced with the two-level (0+, 3-) vibrational model. The deformation $\beta_3 = 0.100$. Otherwise nomenclature is identical to that of **Table V-1**, above.

Real Potential

$$\text{Strength } V = 46.031 - 0.1338 \bullet E$$

$$J_V = 416.35 - 3.2597 \bullet E + 0.008717 \bullet E^2$$

$$\text{Radius } r_V = 1.2592 - 0.002189 \bullet E$$

$$\text{Diffuseness } a_V = 0.6789$$

Imaginary Potential

$$\text{Strength } W = 0.7412 + 1.4519 \bullet E - 0.1183 \bullet E^2 + 0.003711 \bullet E^3 - 0.00003926 \bullet E^4$$

$$J_W = 0.2881 + 8.6167 \bullet E - 0.5633 \bullet E^2 + 0.01637 \bullet E^3 - 0.0001658 \bullet E^4$$

$$\text{Radius } r_W = 1.4826 - 0.02634 \bullet E + 0.0003968 \bullet E^2$$

$$\text{Diffuseness } a_W = 0.1042 + 0.04645 \bullet E + 0.0006052 \bullet E^2$$

Spin-orbit potential of reference WG85, fixed.

Table V-3. ^{208}Pb potential parameters deduced with the two-level (0+, 3-) vibrational model. The deformation $\beta_3 = 0.150$. Otherwise the nomenclature is identical to **Table V-1**.

Real Potential

$$\text{Strength } V = 45.307 - 0.08811 \bullet E$$

$$J_V = 420.00 - 3.4652 \bullet E + 0.01008 \bullet E^2$$

$$\text{Radius } r_V = 1.2677 - 0.002826 \bullet E$$

$$\text{Diffuseness } a_V = 0.7024$$

Imaginary Potential

$$\text{Strength } W = 1.5573 + 1.0891 \bullet E - 0.08694 \bullet E^2 + 0.002646 \bullet E^3 - 0.00002711 \bullet E^4$$

$$J_W = 2.6391 + 7.0312 \bullet E - 0.4040 \bullet E^2 + 0.01071 \bullet E^3 - 0.00009986 \bullet E^4$$

$$\text{Radius } r_W = 1.4345 - 0.01787 \bullet E + 0.0002077 \bullet E^2$$

$$\text{Diffuseness } a_W = 0.1294 + 0.04245 \bullet E - 0.0004659 \bullet E^2$$

Spin-orbit potential of reference WG85, fixed.

Table V-4. ^{208}Pb potential parameters deduced with the two-level (0+, 3-) vibrational model. The deformation $\beta_3 = 0.200$. Otherwise the nomenclature is identical to that of **Table V-1**.

Real Potential

$$\text{Strength } V = 44.910 - 0.06702 \bullet E$$

$$J_V = 428.07 - 3.8206 \bullet E + 0.01179 \bullet E^2$$

$$\text{Radius } r_V = 1.2791 - 0.003367 \bullet E$$

$$\text{Diffuseness } a_V = 0.7133$$

Imaginary Potential

$$\text{Strength } W = 0.4986 + 1.3454 \bullet E - 0.1114 \bullet E^2 + 0.003521 \bullet E^3 - 0.00003742 \bullet E^4$$

$$J_W = 1.5411 + 6.6953 \bullet E - 0.4142 \bullet E^2 + 0.01237 \bullet E^3 - 0.0001304 \bullet E^4$$

$$\text{Radius } r_W = 1.4212 - 0.01486 \bullet E + 0.0001550 \bullet E^2$$

$$\text{Diffuseness } a_W = 0.09660 + 0.04215 \bullet E - 0.0004527 \bullet E^2$$

Spin-orbit potential of reference WG85, fixed.

Table V-5. ^{208}Pb potential parameters deduced with the two-level (0+,3-) vibrational model. The deformation $\beta_3 = 0.300$. Otherwise the nomenclature is identical to that of **Table V-1**.

Real Potential

$$\text{Strength } V = 43.683 - 0.009985 \cdot E$$

$$J_V = 436.49 - 3.9258 \cdot E + 0.01158 \cdot E^2$$

$$\text{Radius } r_V = 1.2936 - 0.004042 \cdot E$$

$$\text{Diffuseness } a_V = 0.7793$$

Imaginary Potential

$$\text{Strength } W = 0.5069 + 0.9693 \cdot E - 0.06257 \cdot E^2 + 0.001536 \cdot E^3 - 0.00001272 \cdot E^4$$

$$J_W = 1.1982 + 4.0667 \cdot E - 0.1216 \cdot E^2 + 0.0009579 \cdot E^3 + 0.000008656 \cdot E^4$$

$$\text{Radius } r_W = 1.4124 - 0.01492 \cdot E + 0.0005857 \cdot E^2 - 0.00001065 \cdot E^3$$

$$\text{Diffuseness } a_W = 0.1774 + 0.02204 \cdot E + 0.00002817 \cdot E^2$$

Spin-orbit potential of reference WG85, fixed.

Table V-6. ^{208}Pb potential parameters deduced from coupling the three levels 0+ (g.s), 3- (2.614 MeV), and 5- (3.197 MeV) assuming an octupole vibrational system with $\beta_3 = 0.150$. Otherwise the nomenclature is identical to that of **Table V-1**.

Real Potential

$$\text{Strength } V = 45.773 - 0.1140 \cdot E$$

$$J_V = 416.87 - 3.2438 \cdot E + 0.008751 \cdot E^2$$

$$\text{Radius } r_V = 1.2604 - 0.002356 \cdot E$$

$$\text{Diffuseness } a_V = 0.6969$$

Imaginary Potential

$$\text{Strength } W = 0.6033 + 1.1720 \cdot E - 0.08263 \cdot E^2 + 0.002304 \cdot E^3 - 0.00002204 \cdot E^4$$

$$J_W = 1.3436 + 6.7122 \cdot E - 0.3373 \cdot E^2 + 0.007539 \cdot E^3 - 0.00005707 \cdot E^4$$

$$\text{Radius } r_W = 1.4316 - 0.01763 \cdot E + 0.0002003 \cdot E^2$$

$$\text{Diffuseness } a_W = 0.1899 + 0.03385 \cdot E - 0.0003178 \cdot E^2$$

Spin-orbit potential of reference WG85, fixed.

Table VI-1. ^{208}Pb SOM parameters determined from 4 - P fitting with fixed real geometry. Potential depths and energies are in MeV. Potential strengths are in volume-integral-per-nucleon (J_i , MeV-fm³). Geometries are in fermis. ASYM = 1 + 0.0•E, i.e. no asymmetry. 13 discrete levels were considered, the temperature T = 1.0 MeV, and there was no dispersion contribution.

Real Potential

$$\text{Strength } V = 47.701 - 0.2710 \bullet E$$

$$J_V = 407.35 - 2.3142 \bullet E$$

$$\text{Radius } r_V = 1.2342 \text{ (fixed)}$$

$$\text{Diffuseness } a_V = 0.6806 \text{ (fixed)}$$

Imaginary Potential

$$\text{Strength } W = 4.0620 + 0.3409 \bullet E - 0.003867 \bullet E^2$$

$$J_W = 16.682 + 3.1364 \bullet E - 0.031748 \bullet E^2 - 0.0003722 \bullet E^3$$

$$\text{Radius } r_W = 1.3702 - 0.008577 \bullet E$$

$$\text{Diffuseness } a_W = 0.2673 + 0.01979 \bullet E - 0.0002699 \bullet E^2$$

Table VI-2. ^{208}Pb SOM parameters deduced from 4 - P fitting with fixed real geometry. Potential depths and energies are in MeV. Potential strengths are in volume-integrals-per-nucleon (J_i , MeV-fm³). Geometries are in fermis. ASYM = 1 + 0.05•E, thirteen discrete levels were considered, the temperature T = 1.0 MeV.

Real Potential

$$\text{Strength } V = 47.725 - 0.2747 \bullet E$$

$$J_V = 407.51 - 2.345 \bullet E$$

$$\text{Radius } r_V = 1.2342 \text{ (fixed)}$$

$$\text{Diffuseness } a_V = 0.6806 \text{ (fixed)}$$

Imaginary Potential

$$\text{Strength } W = 4.2569 + 0.2550 \bullet E - 0.003863 \bullet E^2$$

$$J_W = 19.385 + 2.6971 \bullet E - 0.019142 \bullet E^2 - 0.0004508 \bullet E^3$$

$$\text{Radius } r_W = 1.3699 - 0.006080 \bullet E$$

$$\text{Diffuseness } a_W = 0.2936 + 0.01136 \bullet E - 0.0001311 \bullet E^2$$

Spin-Obit Potential of reference. WG85, fixed.

Table VI-3. ^{208}Pb SOM parameters deduced from 4 – P fitting with fixed real geometries. Potential depths and energies are in MeV. Potential strengths are in volume-integrals-per-nucleon (J_i , MeV–fm³). Geometries are in fermis. ASYM = 1 + 0.1•E. The temperature T = 1.0 MeV, 13 discrete levels are considered, and no dispersion.

Real Potential

$$\text{Strength } V = 47.816 - 0.2813 \bullet E$$

$$J_V = 409.22 - 2.4080 \bullet E$$

$$\text{Radius } r_V = 1.2342 \text{ (fixed)}$$

$$\text{Diffuseness } a_V = 0.6806 \text{ (fixed)}$$

Imaginary Potential

$$\text{Strength } W = 4.8503 + 0.1274 \bullet E - 0.001454 \bullet E^2$$

$$J_W = 21.386 + 2.4507 \bullet E - 0.02072 \bullet E^2 - 0.0002503 \bullet E^3$$

$$\text{Radius } r_W = 1.3702 - 0.004659 \bullet E$$

$$\text{Diffuseness } a_W = 0.2815 + 0.009289 \bullet E - 0.0001150 \bullet E^2$$

Spin-Orbit Potential of reference WG85, fixed.

Table VI - 4. ^{208}Pb SOM parameters deduced from 4 – P fitting with fixed real geometry. Potential depths and energies are in MeV. Potential strengths are in volume-integrals-per-nucleon (J_i , Mev – fm³). Geometries are in fermis. ASYM = 1 + 0.15•E. The temperature is T = 1.0, with 13 discrete levels and no dispersion.

Real Potential

$$\text{Strength } V = 47.765 - 0.2730 \bullet E$$

$$J_V = 408.34 - 2.4032 \bullet E$$

$$\text{Radius } r_V = 1.2342 \text{ (fixed)}$$

$$\text{Diffuseness } a_V = 0.6806 \text{ (fixed)}$$

Imaginary Potential

$$\text{Strength } W = 4.9330 + 0.05364 \bullet E + 0.0002863 \bullet E^2$$

$$J_W = 21.450 + 2.4280 \bullet E - 0.030437 \bullet E^2 - 0.000044685 \bullet E^3$$

$$\text{Radius } r_W = 1.3736 - 0.003694 \bullet E$$

$$\text{Diffuseness } a_W = 0.2742 + 0.008252 \bullet E - 0.0001304 \bullet E^2$$

Spin-Orbit Potential of reference WG85, fixed.

Table VI-5. ^{208}Pb SOM parameters deduced from 4 – P fitting with fixed real geometry. Potential depths and energies are in MeV. Potential strengths are in volume-integrals-per-nucleon (J_i , MeV – fm³). Geometries are in fermis. ASYM = 1 + 0.20•E, Temperature T = 1.0 MeV, with 13 discrete levels and no dispersion.

Real Potential

$$\text{Strength } V = 47.667 - 0.2679 \bullet E$$

$$J_V = 407.61 - 2.349 \bullet E$$

$$\text{Radius } r_V = 1.2342 \text{ (fixed)}$$

$$\text{Diffuseness } a_V = 0.6806 \text{ (fixed)}$$

Imaginary Potential

$$\text{Strength } W = 5.4220 - 0.01516 \bullet E + 0.001739 \bullet E^2$$

$$J_W = 19.424 + 2.8276 \bullet E - 0.050191 \bullet E^2 + 0.00035039 \bullet E^3$$

$$\text{Radius } r_W = 1.3924 - 0.003802 \bullet E$$

$$\text{Diffuseness } a_W = 0.2191 + 0.01093 \bullet E - 0.0001854 \bullet E^2$$

Spin-Obit Potential as per reference. WG85, fixed

Table VI-6. ^{208}Pb SOM parameters deduced from 4 – P fitting with fixed real geometry. Potential depths and energies are in MeV. Potential strengths are in volume-integrals-per-nucleon (J_i , MeV – fm³). Geometries are in fermis, ASYM = 1 + 0.25•E, Temperature T=1.0 MeV, with 13 discrete levels and no dispersion.

Real Potential

$$\text{Strength } V = 47.550 - 0.2646 \bullet E$$

$$J_V = 406.04 - 2.260 \bullet E$$

$$\text{Radius } r_V = 1.2342 \text{ (fixed)}$$

$$\text{Diffuseness } a_V = 0.6806 \text{ (fixed)}$$

Imaginary Potential

$$\text{Strength } W = 5.5781 - 0.05154 \bullet E + 0.002388 \bullet E^2$$

$$J_W = 18.358 + 3.0673 \bullet E - 0.066278 \bullet E^2 + 0.00063682 \bullet E^3$$

$$\text{Radius } r_W = 1.4032 - 0.003729 \bullet E$$

$$\text{Diffuseness } a_W = 0.1969 + 0.01092 \bullet E - 0.0001713 \bullet E^2$$

Spin-Obit Potential as per reference WG85, fixed.

Table VI - 7. ^{208}Pb SOM parameters deduced from 4 - P fitting with fixed real geometry. Potential depths and energies are in MeV. Potential strengths are in volume-integrals-per-nucleon (J_i , MeV - fm³). Geometries are in fermis, ASYM = 1 + 0.30•E, temperature T = 1.0 MeV, with 13 discrete levels and no dispersion.

Real Potential

$$\text{Strength } V = 47.641 - 0.2698 \bullet E$$

$$J_V = 406.70 - 2.302 \bullet E$$

$$\text{Radius } r_V = 1.2342 \text{ (fixed)}$$

$$\text{Diffuseness } a_V = 0.6806 \text{ (fixed)}$$

Imaginary Potential

$$\text{Strength } W = 5.1170 - 0.03175 \bullet E + 0.002074 \bullet E^2$$

$$J_W = 19.491 + 2.8118 \bullet E - 0.060969 \bullet E^2 + 0.00065811 \bullet E^3$$

$$\text{Radius } r_W = 1.4076 - 0.003476 \bullet E$$

$$\text{Diffuseness } a_W = 0.2244 + 0.005937 \bullet E - 0.00007101 \bullet E^2$$

Spin-Obit Potential as per reference WG85, fixed.

Table VI-8. ^{208}Pb SOM parameters deduced from 4 - P fitting with fixed real geometry. Potential depths and energies are in MeV. Potential strengths are in volume-integrals-per-nucleon (J_i , MeV - fm³). Geometries are in fermis, temperature T = 1.0 MeV, with 13 discrete levels and no dispersion, ASYM = 1 + 0.35•E.

Real Potential

$$\text{Strength } V = 47.580 - 0.2649 \bullet E$$

$$J_V = 406.32 - 2.263 \bullet E$$

$$\text{Radius } r_V = 1.2342 \text{ (fixed)}$$

$$\text{Diffuseness } a_V = 0.6806 \text{ (fixed)}$$

Imaginary Potential

$$\text{Strength } W = 5.0167 - 0.02987 \bullet E + 0.002039 \bullet E^2$$

$$J_W = 17.777 + 2.9985 \bullet E - 0.067280 \bullet E^2 + 0.00073178 \bullet E^3$$

$$\text{Radius } r_W = 1.4070 - 0.002884 \bullet E$$

$$\text{Diffuseness } a_W = 0.2082 + 0.005816 \bullet E - 0.00008287 \bullet E^2$$

Spin-Obit Potential as per reference WG85, fixed.

Table VI-9. ^{208}Pb SOM parameters deduced from 4 – P fitting with fixed real geometry. Potential depths and energies are in MeV. Potential strengths are in volume-integrals-per-nucleon (J_i , MeV – fm³). Geometries are in fermis, temperature T = 1.0 MeV, 13 discrete levels, no dispersion, ASYM = 1 + 0.40•E.

Real Potential

$$\text{Strength } V = 47.378 - 0.2599 \bullet E$$

$$J_V = 404.56 - 2.219 \bullet E$$

$$\text{Radius } r_V = 1.2342 \text{ (fixed)}$$

$$\text{Diffuseness } a_V = 0.6806 \text{ (fixed)}$$

Imaginary Potential

$$\text{Strength } W = 4.6457 - 0.003209 \bullet E + 0.001533 \bullet E^2$$

$$J_W = 16.546 + 3.1278 \bullet E - 0.070176 \bullet E^2 + 0.00073472 \bullet E^3$$

$$\text{Radius } r_W = 1.4237 - 0.003677 \bullet E$$

$$\text{Diffuseness } a_W = 0.2049 + 0.004287 \bullet E - 0.00002378 \bullet E^2$$

Spin-Obit Potential as per reference WG85, fixed.

Table VI-10. ^{208}Pb SOM parameters deduced from 4 – P fitting with fixed real geometry. Potential depths and energies are in MeV. Potential strengths are in volume-integrals-per-nucleon (J_i , MeV – fm³). Geometries are in fermis, temperature T = 1.0 MeV, 13 discrete levels, ASYM = 1 + 0.5•E, no dispersion.

Real Potential

$$\text{Strength } V = 47.505 - 0.2626 \bullet E$$

$$J_V = 406.34 - 2.275 \bullet E$$

$$\text{Radius } r_V = 1.2342 \text{ (fixed)}$$

$$\text{Diffuseness } a_V = 0.6806 \text{ (fixed)}$$

Imaginary Potential

$$\text{Strength } W = 5.0167 - 0.05746 \bullet E + 0.002678 \bullet E^2$$

$$J_W = 17.137 + 3.2345 \bullet E - 0.087625 \bullet E^2 + 0.0011113 \bullet E^3$$

$$\text{Radius } r_W = 1.4321 - 0.003657 \bullet E$$

$$\text{Diffuseness } a_W = 0.1888 + 0.003448 \bullet E + 0.000003791 \bullet E^2$$

Spin-Obit Potential as per reference WG85, fixed.

Table VI-11. ^{208}Pb SOM real potential depths (V) and strengths (J_V) as a function of asymmetry resulting from 4 - P fitting with the fixed real geometry of $r_v = 1.234$ and $a_v = 0.6806$ fermis. Energies E and potential depths are in MeV, potential strengths in $\text{MeV}\cdot\text{fm}^3$.

ASYM	Potential Depth	Strength in Volume Integrals-per-Nucleon
1+0.00•E	$V = 47.701 - 0.2710\bullet E$	$J_V = 407.35 - 2.314\bullet E$
1+0.05•E	$V = 47.725 - 0.2747\bullet E$	$J_V = 407.51 - 2.345\bullet E$
1+0.10•E	$V = 47.816 - 0.2813\bullet E$	$J_V = 409.22 - 2.408\bullet E$
1+0.15•E	$V = 47.765 - 0.2730\bullet E$	$J_V = 408.34 - 2.403\bullet E$
1+0.20•E	$V = 47.667 - 0.2679\bullet E$	$J_V = 407.61 - 2.349\bullet E$
1+0.25•E	$V = 47.550 - 0.2646\bullet E$	$J_V = 406.04 - 2.260\bullet E$
1+0.30•E	$V = 47.641 - 0.2698\bullet E$	$J_V = 406.70 - 2.302\bullet E$
1+0.35•E	$V = 47.580 - 0.2649\bullet E$	$J_V = 406.32 - 2.263\bullet E$
1+0.40•E	$V = 47.378 - 0.2599\bullet E$	$J_V = 404.56 - 2.219\bullet E$
1+0.50•E	$V = 47.505 - 0.2626\bullet E$	$J_V = 406.34 - 2.275\bullet E$

Averages

$$V = 47.633(\pm 0.18\%) - 0.2690(\pm 2.0\%)\bullet E$$

$$J_V = 406.998(\pm 0.12\%) - 2.3138(\pm 1.3\%)\bullet E$$

Table VI - 12. ^{208}Pb SOM potential imaginary depths (W) and strengths (J_w) as functions of asymmetry resulting from 4 - P fitting with fixed real-potential geometries of $r_V = 1.234$ and $a_V = 0.6806$ fermis. Energies and potential depths in MeV, and strengths in MeV - fm³.

ASYM	Potential Depth/Strength in volume integral-per-nucleon
1+0.00•E	$W = 4.0620 + 0.3409\bullet E - 0.003867\bullet E^2$ $J_w = 16.682 + 3.1364\bullet E - 0.031748\bullet E^2 - 0.0003722\bullet E^3$
1+0.05•E	$W = 4.2569 + 0.2550\bullet E - 0.003863\bullet E^2$ $J_w = 19.385 + 2.6971\bullet E - 0.019142\bullet E^2 - 0.0004508\bullet E^3$
1+0.10•E	$W = 4.8503 + 0.1274\bullet E - 0.001454\bullet E^2$ $J_w = 21.386 + 2.4507\bullet E - 0.020720\bullet E^2 - 0.0002503\bullet E^3$
1+0.15•E	$W = 4.9330 + 0.05364\bullet E + 0.0002863\bullet E^2$ $J_w = 21.450 + 2.4280\bullet E - 0.030437\bullet E^2 - 0.000044685\bullet E^3$
1+0.20•E	$W = 5.4220 - 0.01516\bullet E + 0.001739\bullet E^2$ $J_w = 19.424 + 2.8276\bullet E - 0.050191\bullet E^2 + 0.00035039\bullet E^3$
1+0.25•E	$W = 5.5781 - 0.05154\bullet E + 0.002388\bullet E^2$ $J_w = 18.358 + 3.0673\bullet E - 0.066278\bullet E^2 + 0.00063682\bullet E^3$
1+0.30•E	$W = 5.1170 - 0.03175\bullet E + 0.002074\bullet E^2$ $J_w = 19.491 + 2.8118\bullet E - 0.060969\bullet E^2 + 0.00065811\bullet E^3$
1+0.35•E	$W = 5.0167 - 0.02987\bullet E + 0.002039\bullet E^2$ $J_w = 17.777 + 2.9985\bullet E - 0.067280\bullet E^2 + 0.00073178\bullet E^3$
1+0.40•E	$W = 4.6457 - 0.003209\bullet E + 0.001533\bullet E^2$ $J_w = 16.546 + 3.1278\bullet E - 0.070176\bullet E^2 + 0.00073472\bullet E^3$
1+0.50•E	$W = 5.0167 - 0.057460\bullet E + 0.002678\bullet E^2$ $J_w = 17.137 + 3.2345\bullet E - 0.087625\bullet E^2 + 0.00111130\bullet E^3$

Table VI-13. ^{208}Pb SOM reduced imaginary radii (r_w) as a function of asymmetry resulting from 4-P fitting with the real geometries fixed to $r_V = 1.2340$ and $a_V = 0.6806$ fms. Energies are in MeV.

ASYM	r_w (fms)
1 + 0.00•E	1.3702 – 0.008577•E
1 + 0.05•E	1.3699 – 0.006080•E
1 + 0.10•E	1.3702 – 0.004659•E
1 + 0.15•E	1.3736 – 0.003694•E
1 + 0.20•E	1.3924 – 0.003802•E
1 + 0.25•E	1.4032 – 0.003729•E
1 + 0.30•E	1.4076 – 0.003476•E
1 + 0.35•E	1.4070 – 0.002884•E
1 + 0.40•E	1.4237 – 0.003677•E
1 + 0.50•E	1.4321 – 0.003657•E

Table VI-14. ^{208}Pb SOM imaginary diffuseness (a_w) as a function of asymmetry resulting from 4-P fitting with the real geometries fixed to $r_w = 1.2340$ and $a_w = 0.6806$ fms. Energies are in MeV.

ASYM	a_w (fms)
1 + 0.00•E	0.2673 + 0.01979•E – 0.0002699•E ²
1 + 0.05•E	0.2936 + 0.01136•E – 0.0001311•E ²
1 + 0.10•E	0.2815 + 0.009289•E – 0.0001150•E ²
1 + 0.15•E	0.2742 + 0.008252•E – 0.0001304•E ²
1 + 0.20•E	0.2191 + 0.010930•E – 0.0001854•E ²
1 + 0.25•E	0.1969 + 0.010920•E – 0.0001713•E ²
1 + 0.30•E	0.2244 + 0.005937•E – 0.00007101•E ²
1 + 0.35•E	0.2082 + 0.005816•E – 0.00008287•E ²
1 + 0.40•E	0.2049 + 0.004287•E – 0.00002378•E ²
1 + 0.50•E	0.1888 + 0.003448•E + 0.000003791•E ²

Table VI – 15. ^{209}Bi SOM potential deduced from 6-parameter fitting with $\text{ASYM} = 1 + 0.00 \bullet E$. This is the simple SOM potential. Potential strengths (J_i) are in volume-integrals-per-nucleon ($\text{MeV}\text{-fm}^3$), and depths and energies in MeV, statistical temperature is $T = 1.0$ MeV, with 13 discrete levels and no dispersion.

Real Potential

$$\text{Strength } V = 44.524 + 0.05825 \bullet E$$

$$J_V = 423.57 - 4.4448 \bullet E + 0.01340 \bullet E^2$$

$$J_V \approx 421.89 - 4.0429 \bullet E$$

$$\text{Radius } r_V = 1.2831 - 0.005314 \bullet E$$

$$\text{Diffuseness } a_V = 0.6698$$

Imaginary Potential

$$\text{Strength } W = 5.5047 + 0.03334 \bullet E - 0.0008421 \bullet E^2$$

$$J_W = 21.11 + 3.3396 \bullet E - 0.07990 \bullet E^2 + 0.0002711 \bullet E^3$$

$$J_W \approx 21.22 + 3.2040 \bullet E - 0.06777 \bullet E^2$$

$$\text{Radius } r_W = 1.3372 - 0.007674 \bullet E$$

$$\text{Diffuseness } b_W = 0.2517 + 0.04020 \bullet E - 0.0006174 \bullet E^2$$

Spin Orbit Potential of reference WG85, fixed.

Table VI-16. ^{209}Bi SOM deduced from 6-parameter fitting with $\text{ASYM} = 1 + 0.10 \bullet E$, 13 discrete levels, with no dispersion, temperature $T = 1.0$ MeV.

Real Potential

$$\text{Strength } V = 44.691 - 0.01022 \bullet E$$

$$J_V = 423.37 - 3.9676 \bullet E + 0.012488 \bullet E^2$$

$$J_V \approx 421.81 - 3.5930 \bullet E$$

$$\text{Radius } r_V = 1.2814 - 0.004107 \bullet E$$

$$\text{Diffuseness } a_V = 0.6672$$

Imaginary Potential

$$\text{Strength } W = 5.6540 - 0.06204 \bullet E + 0.0002317 \bullet E^2$$

$$J_W = 23.08 + 3.0959 \bullet E - 0.08775 \bullet E^2 + 0.0005445 \bullet E^3$$

$$J_W \approx 23.49 + 2.8236 \bullet E - 0.06323 \bullet E^2$$

$$\text{Radius } r_W = 1.3277 - 0.001839 \bullet E$$

$$\text{Diffuseness } b_W = 0.2739 + 0.02486 \bullet E - 0.0004074 \bullet E^2$$

Spin-orbit potential same as reference WG85, fixed.

Table VI-17. ^{209}Bi SOM potential deduced from 6-parameter fitting with $\text{ASYM} = 1 + 0.2 \bullet E$, 13 discrete levels, temperature $T = 1.0 \text{ MeV}$, and no dispersion.

Real Potential

$$\text{Strength } V = 44.855 - 0.06180 \bullet E$$

$$J_V = 419.77 - 3.5726 \bullet E + 0.021168 \bullet E^2$$

$$J_V \approx 417.12 - 2.9375 \bullet E$$

$$\text{Radius } r_V = 1.2751 - 0.002862 \bullet E$$

$$\text{Diffuseness } a_V = 0.6797$$

Imaginary Potential

$$\text{Strength } W = 5.5291 + 0.03989 \bullet E - 0.002911 \bullet E^2$$

$$J_W = 22.91 + 3.0324 \bullet E - 0.05004 \bullet E^2 - 0.0005378 \bullet E^3$$

$$J_W \approx 22.50 + 3.3012 \bullet E - 0.07423 \bullet E^2$$

$$\text{Radius } r_W = 1.3420 + 0.0006631 \bullet E$$

$$\text{Diffuseness } b_W = 0.2723 + 0.007540 \bullet E - 0.00005994 \bullet E^2$$

Spin-Orbit potential same as reference WG85, fixed.

Table VI-18. ^{209}Bi SOM potential deduced from 6-parameter fitting with $\text{ASYM} = 1 + 0.30 \bullet E$, 13 levels, temperature $T = 1.0 \text{ MeV}$, and no dispersion.

Real Potential

$$\text{Strength } V = 45.231 - 0.1334 \bullet E$$

$$J_V = 417.76 - 2.6297 \bullet E + 0.005302 \bullet E^2$$

$$J_V \approx 417.10 - 2.4706 \bullet E$$

$$\text{Radius } r_V = 1.2687 - 0.001502 \bullet E$$

$$\text{Diffuseness } a_V = 0.6823$$

Imaginary Potential

$$\text{Strength } W = 5.0806 + 0.08123 \bullet E - 0.001924 \bullet E^2$$

$$J_W = 21.68 + 3.2525 \bullet E - 0.08806 \bullet E^2 + 0.0005556 \bullet E^3$$

$$J_W \approx 22.10 + 2.9747 \bullet E - 0.06305 \bullet E^2$$

$$\text{Radius } r_W = 1.3488 - 0.001517 \bullet E$$

$$\text{Diffuseness } b_W = 0.2766 + 0.001582 \bullet E - 0.00009255 \bullet E^2$$

Spin-Orbit potential the same as in reference WG85, fixed.

Table VI-19. ^{209}Bi SOM potential deduced from 6-parameter fitting with $\text{ASYM} = 1 + 0.4 \cdot E$, 13 discrete levels, temperature $T = 1.0$ MeV, and no dispersion.

Real Potential

$$\begin{aligned} \text{Strength } V &= 45.239 - 0.1341 \cdot E \\ J_V &= 417.18 - 2.5545 \cdot E + 0.005116 \cdot E^2 \\ J_V &\approx 416.54 - 2.4010 \cdot E \\ \text{Radius } r_V &= 1.2678 - 0.001413 \cdot E \\ \text{Diffuseness } a_V &= 0.6844 \end{aligned}$$

Imaginary Potential

$$\begin{aligned} \text{Strength } W &= 5.4279 - 0.01054 \cdot E + 0.0006415 \cdot E^2 \\ J_W &= 22.29 + 3.4418 \cdot E - 0.1098 \cdot E^2 + 0.001451 \cdot E^3 \\ J_W &\approx 23.38 + 2.7162 \cdot E - 0.0444 \cdot E^2 \\ \text{Radius } r_W &= 1.3416 + 0.002371 \cdot E \\ \text{Diffuseness } b_W &= 0.2671 - 0.0003348 \cdot E - 0.00006020 \cdot E^2 \end{aligned}$$

Spin-Orbit potential the same as reference WG85, fixed.

Table VI-20. ^{209}Bi SOM potential determined from 6-parameter fitting, $\text{ASYM} = 1.0 + 0.5 \cdot E$, 13 discrete levels, temperature $T = 1.0$ MeV, and no dispersion.

Real Potential

$$\begin{aligned} \text{Strength } V &= 45.080 - 0.1252 \cdot E \\ J_V &= 418.21 - 2.5789 \cdot E + 0.005406 \cdot E^2 \\ J_V &\approx 417.53 - 2.4166 \cdot E \\ \text{Radius } r_V &= 1.2702 - 0.001516 \cdot E \\ \text{Diffuseness } a_V &= 0.6872 \end{aligned}$$

Imaginary Potential

$$\begin{aligned} \text{Strength } W &= 5.9893 - 0.06405 \cdot E + 0.002006 \cdot E^2 \\ J_W &= 21.81 + 3.5584 \cdot E - 0.16084 \cdot E^2 + 0.002440 \cdot E^3 \\ J_W &\approx 23.64 + 2.3383 \cdot E - 0.05103 \cdot E^2 \\ \text{Radius } r_W &= 1.3555 - 0.002486 \cdot E \\ \text{Diffuseness } b_W &= 0.2308 - 0.001263 \cdot E - 0.00004503 \cdot E^2 \end{aligned}$$

Spin-Orbit Potential the same as reference WG85, fixed.

Table VI-21. ^{209}Bi SOM Potential determined by 6-parameter fitting using a Saxon-Woods (non-derivative) volume imaginary potential form, as described in the text. This volume absorption corresponds essentially to an infinite ASYM. Potential depths and energies are in MeV and potential strengths in volume integrals-per-nucleon (J_i). 13 discrete levels were used, the temperature $T = 1.0$ MeV, and no dispersion.

Real Potential

$$\text{Strength } V = 45.371 + 0.004975 \bullet E.$$

$$J_V = 422.98 - 4.8817 \bullet E + 0.01805 \bullet E^2$$

$$J_V \approx 420.72 - 4.3401 \bullet E$$

$$\text{Radius } r_V = 1.2778 - 0.005189 \bullet E$$

$$\text{Diffuseness } a_V = 0.6240$$

Imaginary Potential

$$\text{Strength } W = 0.6332 + 0.2330 \bullet E - 0.005905 \bullet E^2$$

$$J_W = 9.073 + 3.4079 \bullet E - 0.05186 \bullet E^2 - 0.0008044 \bullet E^3$$

$$J_W \approx 8.469 + 3.8101 \bullet E - 0.08805 \bullet E^2$$

$$\text{Radius } r_W = 1.4972 + 0.004589 \bullet E$$

$$\text{Diffuseness } a_W = 0.3830$$

Spin-Orbit Potential is the same as given in reference WG85, fixed.

Table VI-22. ^{209}Bi SOM real potential depths (V) and strengths (J_V) as a function of asymmetry (ASYM) resulting from 6-P fitting.

ASYM	Potential	Strengths in volume-integrals-per nucleon
1+0.0•E	$V = 44.524 + 0.05825\bullet E$	$J_V \approx 421.89 - 4.0429\bullet E$
1+0.1•E	$V = 44.691 - 0.01022\bullet E$	$J_V \approx 421.81 - 3.5930\bullet E$
1+0.2•E	$V = 44.855 - 0.06180\bullet E$	$J_V \approx 417.12 - 2.9375\bullet E$
1+0.3•E	$V = 45.231 - 0.13340\bullet E$	$J_V \approx 417.10 - 2.4706\bullet E$
1+0.4•E	$V = 45.239 - 0.13410\bullet E$	$J_V \approx 416.54 - 2.4010\bullet E$
1+0.5•E	$V = 45.080 - 0.12520\bullet E$	$J_V \approx 417.53 - 2.4166\bullet E$
Volume imaginary only		
-----	$V = 45.371 + 0.004975\bullet E$	$J_V \approx 420.72 - 4.3401\bullet E$

Table VI-23. ^{209}Bi SOM imaginary potential depths (W) and strengths (J_W) as functions of asymmetry (ASYM) resulting from 6-parameter fitting

ASYM	Potential (in MeV). Strengths in volume-integral-per-nucleon
1+0.0•E	$W = 5.5047 + 0.03334\bullet E - 0.0008421\bullet E^2$ $J_W = 21.11 + 3.3396\bullet E - 0.07990\bullet E^2 + 0.0002711\bullet E^3$
1+0.1•E	$W = 5.6540 - 0.06204\bullet E + 0.0002317\bullet E^2$ $J_W = 23.08 + 3.0959\bullet E - 0.08775\bullet E^2 + 0.0005445\bullet E^3$
1+0.2•E	$W = 5.5291 + 0.03989\bullet E - 0.002911\bullet E^2$ $J_W = 22.91 + 3.0324\bullet E - 0.05004\bullet E^2 - 0.0005378\bullet E^3$
1+0.3•E	$W = 5.0806 + 0.08123\bullet E - 0.001924\bullet E^2$ $J_W = 21.68 + 3.2525\bullet E - 0.08806\bullet E^2 + 0.0005556\bullet E^3$
1+0.4•E	$W = 5.4279 - 0.001054\bullet E + 0.0006415\bullet E^2$ $J_W = 22.29 + 3.4418\bullet E - 0.1098\bullet E^2 + 0.001451\bullet E^3$
1+0.5•E	$W = 5.9893 - 0.06405\bullet E + 0.002006\bullet E^2$ $J_W = 21.81 + 3.5584\bullet E - 0.16084\bullet E^2 + 0.002440\bullet E^3$
Volume imaginary only	
-----	$W = 0.6332 + 0.2330\bullet E - 0.005905\bullet E^2$ $J_W = 9.073 + 3.4079\bullet E - 0.05186\bullet E^2 - 0.0008044\bullet E^3$

Table VI-24. ^{209}Bi SOM potential derived with $\text{ASYM} = 1 + 0.0 \bullet E$ using 4 – parameter fitting with the real-potential geometries fixed to $r_V = 1.2589 - 0.0019 \bullet E$ and $a_V = 0.69412$. Energies and potential depths are given in MeV, geometries in fms, and potential strengths (J_i) in volume-integrals- per-nucleon ($\text{MeV}\cdot\text{fm}^3$). In this particular case the ASYM implies the spherical surface-absorption optical model.

Real Potential

$$\text{Strength } V = 45.704 - 0.1049 \bullet E$$

$$J_V = 414.5 - 2.7267 \bullet E + 0.006376 \bullet E^2$$

$$J_V \approx 413.7 - 2.5354 \bullet E$$

$$\text{Radius } r_V = 1.2589 - 0.0019 \bullet E, \text{ fixed.}$$

$$\text{Diffuseness } a_V = 0.69412, \text{ fixed.}$$

Imaginary Potential

$$\text{Strength } W = 5.5467 + 0.1689 \bullet E - 0.002645 \bullet E^2$$

$$J_W = 15.51 + 4.2591 \bullet E - 0.09118 \bullet E^2 - 0.0005955 \bullet E^3$$

$$J_W \approx 15.06 + 4.5568 \bullet E - 0.11797 \bullet E^2$$

$$\text{Radius } r_W = 1.3547 - 0.007012 \bullet E$$

$$\text{Diffuseness } b_W = 0.1818 + 0.04117 \bullet E - 0.001032 \bullet E^2$$

Spin Orbit Potential of reference WG85.

Table VI-25. ^{209}Bi SOM potential derived with $\text{ASYM} = 1 + 0.1 \bullet E$ using 4–parameter fitting with fixed real-potential geometries. Otherwise, the nomenclature is the same as that of **Table VI-24**.

Real Potential

$$\text{Strength } V = 45.768 - 0.1143 \bullet E$$

$$J_V = 414.60 - 2.8050 \bullet E + 0.006658 \bullet E^2$$

$$J_V \approx 413.77 - 2.6054 \bullet E$$

$$\text{Radius } r_V = 1.2589 - 0.0019 \bullet E, \text{ fixed.}$$

$$\text{Diffuseness } a_V = 0.69412, \text{ fixed.}$$

Imaginary Potential

$$\text{Strength } W = 5.2526 + 0.1205 \bullet E - 0.003679 \bullet E^2$$

$$J_W = 16.88 + 3.5259 \bullet E - 0.03432 \bullet E^2 - 0.001218 \bullet E^3$$

$$J_W \approx 15.97 + 4.1347 \bullet E - 0.08912 \bullet E^2$$

$$\text{Radius } r_W = 1.3462 - 0.002414 \bullet E$$

$$\text{Diffuseness } b_W = 0.2124 + 0.02330 \bullet E - 0.0004727 \bullet E^2$$

Spin Orbit potential of reference WG85.

Table VI-26. ^{209}Bi SOM potential derived with $\text{ASYM} = 1 + 0.2 \cdot E$ using 4-parameter fitting with the real geometries fixed. Otherwise the nomenclature is the same as in **Table VI-24**.

Real Potential

$$\text{Strength } V = 45.742 - 0.1162 \cdot E$$

$$J_V = 414.37 - 2.8218 \cdot E + 0.006730 \cdot E^2$$

$$J_V \approx 413.53 - 2.6199 \cdot E$$

$$\text{Radius } r_V = 1.2589 - 0.0019 \cdot E, \text{ fixed.}$$

$$\text{Diffuseness } a_V = 0.69412, \text{ fixed.}$$

Imaginary Potential

$$\text{Strength } W = 4.6375 + 0.1353 \cdot E - 0.003994 \cdot E^2$$

$$J_W = 17.85 + 3.2847 \cdot E - 0.02719 \cdot E^2 - 0.001111 \cdot E^3$$

$$J_W \approx 17.02 + 3.8402 \cdot E - 0.07718 \cdot E^2$$

$$\text{Radius } r_W = 1.3481 + 0.00005042 \cdot E$$

$$\text{Diffuseness } b_W = 0.2525 + 0.01051 \cdot E - 0.0001942 \cdot E^2$$

Spin Orbit potential of reference WG85, fixed.

Table VI - 27. ^{209}Bi SOM potential derived with $\text{ASYM} = 1 + 0.3 \cdot E$ and 4-parameter fitting with the real-potential geometries fixed. Otherwise, the nomenclature is the same as **Table VI-24**.

Real Potential

$$\text{Strength } V = 45.745 - 0.1182 \cdot E$$

$$J_V = 414.40 - 2.8394 \cdot E + 0.006786 \cdot E^2$$

$$J_V \approx 413.55 - 2.6358 \cdot E$$

$$\text{Radius } r_V = 1.2589 - 0.0019 \cdot E, \text{ fixed.}$$

$$\text{Diffuseness } a_V = 0.69412, \text{ fixed.}$$

Imaginary Potential

$$\text{Strength } W = 4.8421 + 0.06658 \cdot E - 0.002369 \cdot E^2 + 0.00002724 \cdot E^3$$

$$J_W = 19.35 + 3.2714 \cdot E - 0.06582 \cdot E^2 + 0.000008946 \cdot E^3$$

$$J_W \approx 19.36 + 3.2669 \cdot E - 0.06541 \cdot E^2$$

$$\text{Radius } r_W = 1.3518 + 0.001821 \cdot E$$

$$\text{Diffuseness } b_W = 0.2586 + 0.003716 \cdot E - 0.00009609 \cdot E^2$$

Spin Orbit potential of reference WG85, fixed.

Table VI-28. ^{209}Bi SOM potential derived with $\text{ASYM} = 1 + 0.4 \cdot E$ using 4-parameter fitting with fixed real-potential geometries. Otherwise, the nomenclature is identical to that of **Table VI-24**.

Real Potential

$$\begin{aligned} \text{Strength } V &= 45.767 - 0.1203 \cdot E \\ J_V &= 414.60 - 2.8596 \cdot E + 0.006874 \cdot E^2 \\ J_V &\approx 413.74 - 2.6534 \cdot E \\ \text{Radius } r_V &= 1.2589 - 0.0019 \cdot E, \text{ fixed.} \\ \text{Diffuseness } a_V &= 0.69412, \text{ fixed.} \end{aligned}$$

Imaginary Potential

$$\begin{aligned} \text{Strength } W &= 4.7177 + 0.07413 \cdot E - 0.002723 \cdot E^2 + 0.00001617 \cdot E^3 \\ J_W &= 17.89 + 3.6011 \cdot E - 0.08361 \cdot E^2 + 0.0002844 \cdot E^3 \\ J_W &\approx 18.10 + 3.4589 \cdot E - 0.07081 \cdot E^2 \\ \text{Radius } r_W &= 1.3523 + 0.002899 \cdot E \\ \text{Diffuseness } b_W &= 0.2447 + 0.001163 \cdot E - 0.00004476 \cdot E^2 \end{aligned}$$

Spin Orbit potential of reference WG85, fixed.

Table VI-29. ^{209}Bi SOM potential derived with $\text{ASYM} = 1 + 0.5 \cdot E$ using 4-parameter fitting with fixed real geometries. Otherwise the nomenclature is identical to that of **Table VI-24**.

Real Potential

$$\begin{aligned} \text{Strength } V &= 45.764 - 0.1222 \cdot E \\ J_V &= 414.57 - 2.8767 \cdot E + 0.006936 \cdot E^2 \\ J_V &\approx 413.71 - 2.6686 \cdot E \\ \text{Radius } r_V &= 1.2589 - 0.0019 \cdot E, \text{ fixed.} \\ \text{Diffuseness } a_V &= 0.69412, \text{ fixed.} \end{aligned}$$

Imaginary Potential

$$\begin{aligned} \text{Strength } W &= 4.4112 + 0.09521 \cdot E - 0.002028 \cdot E^2 \\ J_W &= 16.73 + 3.8467 \cdot E - 0.09475 \cdot E^2 + 0.0006245 \cdot E^3 \\ J_W &\approx 17.20 + 3.5344 \cdot E - 0.06664 \cdot E^2 \\ \text{Radius } r_W &= 1.3630 + 0.003406 \cdot E \\ \text{Diffuseness } b_W &= 0.2398 - 0.001284 \cdot E - 0.00006157 \cdot E^2 \end{aligned}$$

Spin-Orbit potential of reference WG85, fixed.

Table VI-30. ^{209}Bi SOM real potential depths (V) and strengths (J_V) as a function of asymmetry (ASYM) resulting from 4 - P fitting.

ASYM	Potential	Strengths in volume-integrals-per nucleon
1+0.0•E	$V = 45.704 - 0.1049\bullet E$	$J_V = 414.50 - 2.7267\bullet E + 0.006376\bullet E^2$
1+0.1•E	$V = 45.768 - 0.1143\bullet E$	$J_V = 414.60 - 2.8050\bullet E + 0.006658\bullet E^2$
1+0.2•E	$V = 45.742 - 0.1162\bullet E$	$J_V = 414.37 - 2.8218\bullet E + 0.006730\bullet E^2$
1+0.3•E	$V = 45.745 - 0.1182\bullet E$	$J_V = 414.40 - 2.8394\bullet E + 0.006786\bullet E^2$
1+0.4•E	$V = 45.767 - 0.1203\bullet E$	$J_V = 414.60 - 2.8596\bullet E + 0.006874\bullet E^2$
1+0.5•E	$V = 45.764 - 0.1222\bullet E$	$J_V = 414.57 - 2.8767\bullet E + 0.006936\bullet E^2$

Table VI-31. ^{209}Bi SOM imaginary potential depths (W) and strengths (J_W) as functions of asymmetry (ASYM) resulting from 4 - parameter fitting.

ASYM	Potential (in MeV).	Strengths in volume-integral-per-nucleon
1+0.0•E	$W = 5.5467 + 0.1689\bullet E - 0.002645\bullet E^2$	$J_W = 15.51 + 4.2591\bullet E - 0.091180\bullet E^2 - 0.0005955\bullet E^3$
1+0.1•E	$W = 5.2526 + 0.1205\bullet E - 0.003679\bullet E^2$	$J_W = 16.88 + 3.5259\bullet E - 0.034320\bullet E^2 - 0.0012180\bullet E^3$
1+0.2•E	$W = 4.6375 + 0.1353\bullet E - 0.003994\bullet E^2$	$J_W = 17.85 + 3.2847\bullet E - 0.027190\bullet E^2 - 0.001111\bullet E^3$
1+0.3•E	$W = 4.8421 + 0.06658\bullet E - 0.002369\bullet E^2 + 0.0002724\bullet E^3$	$J_W = 19.35 + 3.27140\bullet E - 0.065820\bullet E^2 - 0.000008946\bullet E^3$
1+0.4•E	$W = 4.7177 + 0.07413\bullet E - 0.002723\bullet E^2 + 0.000016170\bullet E^3$	$J_W = 17.89 + 3.60110\bullet E - 0.083610\bullet E^2 - 0.0002844\bullet E^3$
1+0.5•E	$W = 4.4112 + 0.09521\bullet E - 0.002028\bullet E^2$	$J_W = 16.73 + 3.84670\bullet E - 0.094750\bullet E^2 + 0.0006245\bullet E^3$

Table VI-32. ^{209}Bi SOM imaginary potential radii (r_w) as functions of asymmetry (ASYM) resulting from 4 – parameter fitting.

ASYM	Imaginary radii in fms.
1 + 0.0•E	$r_w = 1.3547 - 0.007012 \bullet E$
1 + 0.1•E	$r_w = 1.3462 - 0.002414 \bullet E$
1 + 0.2•E	$r_w = 1.3481 + 0.000050 \bullet E$
1 + 0.3•E	$r_w = 1.3518 + 0.001821 \bullet E$
1 + 0.4•E	$r_w = 1.3523 + 0.002899 \bullet E$
1 + 0.5•E	$r_w = 1.3630 + 0.003406 \bullet E$

Table VI-33. ^{209}Bi SOM imaginary potential diffuseness (b_w) as a functions of asymmetry (ASYM) resulting from 4 – parameter fitting.

ASYM	Imaginary diffuseness in fms
1 + 0.0•E	$b_w = 0.1818 + 0.04117 \bullet E - 0.001032 \bullet E^2$
1 + 0.1•E	$b_w = 0.2124 + 0.02330 \bullet E - 0.0004727 \bullet E^2$
1 + 0.2•E	$b_w = 0.2525 + 0.01051 \bullet E - 0.0001942 \bullet E^2$
1 + 0.3•E	$b_w = 0.2586 + 0.003716 \bullet E - 0.00009609 \bullet E^2$
1 + 0.4•E	$b_w = 0.2447 + 0.001163 \bullet E - 0.00004476 \bullet E^2$
1 + 0.5•E	$b_w = 0.2398 - 0.001284 \bullet E - 0.00006157 \bullet E^2$

Table VIII-1. Regional real potential strengths in volume integrals per nucleon, J_V .
 SYM = elemental symbol, Z = charge, A = mass, asymmetry ($\eta=(N - Z)/A$), deformation
 β (usually β_2), $J_V(\text{MeV}\cdot\text{fm}^3)$ as a function of energy, and the reference are given.
 Average real-potential reduced radius (r_V) and diffuseness (a_V) are given in fms.

SYM	Z	A	η	β	J_V	Reference
Eu	63	151.9	0.171	0.160	$= 463.83 - 3.2009 \bullet E$,	LA-10915-pr31 (1987)
Gd	64	157.3	0.186	0.308	$= 434.49 - 0.7961 \bullet E$,	NDM-157 (2004)
Gd	64	157.3	0.186	0.308	$= 434.45 - 1.9482 \bullet E$,	LA-10915-pr31 (1987)
Ho	67	164.9	0.187	0.300	$= 444.38 - 3.5580 \bullet E$	NDM-151 (2000)
Ho	67	164.9	0.187	0.300	$= 450.00 - 3.1254 \bullet E$	LA-10915-pr31 (1987)
Hf	72	178.5	0.193	0.287	$= 457.03 - 2.5823 \bullet E$	NDM-153 (2001)
Ta	73	180.9	0.193	0.269	$= 441.05 - 2.4610 \bullet E$	NDM-160 (2005)
Re	75	186.2	0.194	0.220	$= 430.78 - 2.9740 \bullet E$	NDM-155 (2003)
Re	75	186.2	0.194	0.220	$= 432.77 - 2.7804 \bullet E$	NS+E-97-239 (1987)
Au	79	197.0	0.198	-0.131	$= 416.56 - 1.5995 \bullet E$	NDM-161 (2005)
Pb	82	208.0	0.212	0.125	$= 417.25 - 3.2910 \bullet E$	This Work
Bi	83	209.0	0.206	0.000	$= 421.28 - 3.9854 \bullet E$	This Work

$$r_V \approx 1.2462 \pm 0.67\%$$

$$a_V \approx 0.6435 \pm 1.32\%$$

Table VIII-2. Regional imaginary potential strengths in volume integrals per nucleon,
 J_W . The nomenclature is the same as for **Table VIII-1**.

SYM	Z	A	η	β	J_W	References as per Table VIII-1
Eu	63	151.9	0.171	0.160	$= 24.22 + 3.2482 \bullet E - 0.02194 \bullet E^2$	
Gd	64	157.3	0.186	0.308	$= 25.90 + 2.4564 \bullet E + 0.000006587 \bullet E^2$	
Gd	64	157.3	0.186	0.308	$= 19.77 + 2.6426 \bullet E - 0.01409 \bullet E^2$	
Ho	67	164.9	0.187	0.300	$= 22.39 + 2.1506 \bullet E - 0.000002984 \bullet E^2$	
Ho	67	164.9	0.187	0.300	$= 28.72 + 2.0467 \bullet E - 0.01767 \bullet E^2$	
Hf	72	178.5	0.193	0.287	$= 19.49 + 2.4196 \bullet E - 0.000007651 \bullet E^2$	
Ta	73	181.0	0.193	0.269	$= 21.60 + 0.7208 \bullet E + 0.1578 \bullet E^2$	
Re	75	186.2	0.194	0.220	$= 18.78 + 2.0778 \bullet E + 0.004880 \bullet E^2$	
Re	75	186.2	0.194	0.220	$= 20.43 + 4.1612 \bullet E - 0.05574 \bullet E^2$	
Au	79	197.0	0.198	-0.131	$= 14.97 + 3.3220 \bullet E - 0.0000006554 \bullet E^2$	
Pb	82	208.0	0.212	0.125	$= 10.86 + 6.0586 \bullet E - 0.2566 \bullet E^2 + 0.003514 \bullet E^3$	
Bi	83	209.0	0.206	0.0	$= 20.35 + 3.1487 \bullet E - 0.05241 \bullet E^2 - 0.0001756 \bullet E^3$	

$$r_W \approx 1.2637 \pm 0.66\%$$

$$a_W \approx 0.5000 \pm 4.0\%$$

Table A-1. ^{208}Pb SOM parameters from 4 – P fitting with fixed real geometries. Potential depths and energies are in MeV. Potential strengths are in volume-integrals-per-nucleon (J_i). Geometries are in fermis. The $\text{ASYM} = 1 + 0.00 \bullet (E - EF)$. No dispersion.

Real Potential

$$\text{Strength } V = 47.732 - 0.2708 \bullet E$$

$$J_V = 407.48 - 2.3114 \bullet E$$

$$\text{Radius } r_V = 1.2342 \text{ (fixed)}$$

$$\text{Diffuseness } a_V = 0.6806 \text{ (fixed)}$$

Imaginary Potential

$$\text{Strength } W = 4.5113 + 0.2885 \bullet E - 0.002665 \bullet E^2$$

$$J_W = 18.508 + 2.9669 \bullet E - 0.02831 \bullet E^2 - 0.0003692 \bullet E^3$$

$$\text{Radius } r_W = 1.3659 - 0.008313 \bullet E$$

$$\text{Diffuseness } a_W = 0.2661 + 0.02057 \bullet E - 0.0002970 \bullet E^2$$

Spin-Orbit potential as per reference WG85, fixed.

Table A-2. ^{208}Pb SOM parameters from 4 – P fitting with fixed real geometries. Potential depths and energies are in MeV. Potential strengths are in volume-integrals-per-nucleon (J_i). Geometries are in fermis. $\text{ASYM} = 1 + 0.1 \bullet (E - EF)$. No dispersion.

Real Potential

$$\text{Strength } V = 47.665 - 0.2706 \bullet E$$

$$J_V = 406.93 - 2.3105 \bullet E$$

$$\text{Radius } r_V = 1.2342 \text{ (fixed)}$$

$$\text{Diffuseness } a_V = 0.6806 \text{ (fixed)}$$

Imaginary Potential

$$\text{Strength } W = 4.5276 + 0.08912 \bullet E - 0.0001545 \bullet E^2$$

$$J_W = 21.42 + 2.3022 \bullet E - 0.02009 \bullet E^2 - 0.0001399 \bullet E^3$$

$$\text{Radius } r_W = 1.3967 - 0.005143 \bullet E$$

$$\text{Diffuseness } a_W = 0.2331 + 0.01160 \bullet E - 0.0001584 \bullet E^2$$

Spin-Orbit potential as per reference WG85, fixed.

Table A-3. ^{208}Pb SOM parameters from 4 – P fitting with fixed real geometries. Potential depths and energies are in MeV. Potential strengths are in volume-integrals-per-nucleon (J_i), geometries are in fermis, $\text{ASYM} = 1 + 0.20 \cdot (E - EF)$, no dispersion.

Real Potential

$$\text{Strength } V = 47.627 - 0.2695 \cdot E$$

$$J_V = 406.59 - 2.3008 \cdot E$$

$$\text{Radius } r_V = 1.2342 \text{ (fixed)}$$

$$\text{Diffuseness } a_V = 0.6806 \text{ (fixed)}$$

Imaginary Potential

$$\text{Strength } W = 4.9959 - 0.01563 \cdot E + 0.001865 \cdot E^2$$

$$J_W = 19.97 + 2.6890 \cdot E - 0.04626 \cdot E^2 + 0.0003687 \cdot E^3$$

$$\text{Radius } r_W = 1.4281 - 0.004743 \cdot E$$

$$\text{Diffuseness } a_W = 0.1519 + 0.01233 \cdot E - 0.0001602 \cdot E^2$$

Spin-Orbit potential is as per reference WG85, fixed.

Table A-4. ^{208}Pb SOM parameters from 4 – P fitting with fixed real geometries. Potential depths and energies are in MeV. Potential strengths are in volume-integrals-per-nucleon (J_i), geometries are in fermis, $\text{ASYM} = 1 + 0.30 \cdot (E - EF)$, no dispersion.

Real Potential

$$\text{Strength } V = 47.554 - 0.2654 \cdot E$$

$$J_V = 405.90 - 2.2639 \cdot E$$

$$\text{Radius } r_V = 1.2342 \text{ (fixed)}$$

$$\text{Diffuseness } a_V = 0.6806 \text{ (fixed)}$$

Imaginary Potential

$$\text{Strength } W = 3.8983 + 0.07716 \cdot E - 0.0001181 \cdot E^2$$

$$J_W = 19.89 + 2.4227 \cdot E - 0.02992 \cdot E^2 + 0.00009150 \cdot E^3$$

$$\text{Radius } r_W = 1.4443 - 0.004361 \cdot E$$

$$\text{Diffuseness } a_W = 0.1701 + 0.004651 \cdot E + 0.000001181 \cdot E^2$$

Spin-Orbit potential is as per reference WG85, fixed.

Table A-5. ^{208}Pb SOM parameters from 4 – P fitting with fixed real geometries. Potential depths and energies are in MeV. Potential strengths are in volume-integrals-per-nucleon (J_i), geometries are in fermis, $\text{ASYM} = 1 + 0.40 \cdot (E - EF)$, no dispersion.

Real Potential

$$\text{Strength } V = 47.550 - 0.2653 \cdot E$$

$$J_V = 405.93 - 2.2650 \cdot E$$

$$\text{Radius } r_V = 1.2342 \text{ (fixed)}$$

$$\text{Diffuseness } a_V = 0.6806 \text{ (fixed)}$$

Imaginary Potential

$$\text{Strength } W = 4.7718 - 0.03156 \cdot E + 0.002201 \cdot E^2$$

$$J_W = 19.684 + 2.7015 \cdot E - 0.05694 \cdot E^2 + 0.0006434 \cdot E^3$$

$$\text{Radius } r_W = 1.4564 - 0.004352 \cdot E$$

$$\text{Diffuseness } a_W = 0.1138 + 0.007424 \cdot E - 0.00005195 \cdot E^2$$

Spin-Orbit potential is as per reference WG85, fixed.

Table A-6. ^{208}Pb SOM parameters from 4 – P fitting with fixed real geometries. Potential depths and energies are in MeV. Potential strengths are in volume-integrals-per-nucleon (J_i), geometries are in fermis, $\text{ASYM} = 1 + 0.5 \cdot (E - EF)$, no dispersion.

Real Potential

$$\text{Strength } V = 47.588 - 0.2671 \cdot E$$

$$J_V = 406.27 - 2.2805 \cdot E$$

$$\text{Radius } r_V = 1.2342 \text{ (fixed)}$$

$$\text{Diffuseness } a_V = 0.6806 \text{ (fixed)}$$

Imaginary Potential

$$\text{Strength } W = 4.1784 + 0.02357 \cdot E + 0.001053 \cdot E^2$$

$$J_W = 18.701 + 2.6916 \cdot E - 0.04933 \cdot E^2 + 0.0004586 \cdot E^3$$

$$\text{Radius } r_W = 1.4656 - 0.004171 \cdot E$$

$$\text{Diffuseness } a_W = 0.1107 + 0.004713 \cdot E + 0.0000000101 \cdot E^2$$

Spin-Orbit potential is as per reference WG85, fixed.

Table A-7. ^{208}Pb SOM real-potential strengths as a function of the asymmetry of the absorption potential following from 4-parameter fitting referencing the energy dependence of the absorption asymmetry to the Fermi energy (EF), as described in the text.

ASYM	Strengths (J_V) in volume-integrals-per.nucleon, MeV-fm ³
$1.0 + 0.0 \cdot (E - EF)$	$J_V = 407.48 - 2.3114 \cdot E$
$1.0 + 0.1 \cdot (E - EF)$	$J_V = 406.93 - 2.3105 \cdot E$
$1.0 + 0.2 \cdot (E - EF)$	$J_V = 406.59 - 2.3008 \cdot E$
$1.0 + 0.3 \cdot (E - EF)$	$J_V = 405.90 - 2.2639 \cdot E$
$1.0 + 0.4 \cdot (E - EF)$	$J_V = 405.93 - 2.2650 \cdot E$
$1.0 + 0.5 \cdot (E - EF)$	$J_V = 406.27 - 2.2805 \cdot E$

Table A-8. ^{208}Pb SOM imaginary-potential strengths as a function of the asymmetry of the absorption potential referenced to the Fermi Energy (EF), as described in the text.

ASYM	Strength (J_W) in volume-integrals-per nucleon, MeV-fm ³
$1.0 + 0.0 \cdot (E - EF)$	$J_W = 18.508 + 2.9669 \cdot E - 0.02831 \cdot E^2 - 0.0003692 \cdot E^3$
$1.0 + 0.1 \cdot (E - EF)$	$J_W = 21.417 + 2.3022 \cdot E - 0.02009 \cdot E^2 - 0.0001399 \cdot E^3$
$1.0 + 0.2 \cdot (E - EF)$	$J_W = 19.980 + 2.6890 \cdot E - 0.04626 \cdot E^2 + 0.0003687 \cdot E^3$
$1.0 + 0.3 \cdot (E - EF)$	$J_W = 19.890 + 2.4227 \cdot E - 0.02992 \cdot E^2 + 0.0000915 \cdot E^3$
$1.0 + 0.4 \cdot (E - EF)$	$J_W = 19.684 + 2.7015 \cdot E - 0.05694 \cdot E^2 + 0.0006434 \cdot E^3$
$1.0 + 0.5 \cdot (E - EF)$	$J_W = 18.701 + 2.6916 \cdot E - 0.04933 \cdot E^2 + 0.0004586 \cdot E^3$

Table B-1, ^{209}Bi DOM 6 – P fit, no ASYM, Full dispersion (DISP) contribution calculated with the SOM. Effective dispersion = $1.0 \cdot \text{DISP}$ where DISP is shown in Fig. IV-B-5, as discussed in Section IV-B.

Real Potential

$$\begin{aligned} \text{Strength } V &= 47.623 - 0.1072 \cdot E \\ J_V &= 370.58 - 3.9776 \cdot E + 0.01944 \cdot E^2 \\ J_V &\approx 368.15 - 3.3948 \cdot E \\ \text{Radius } r_V &= 1.1845 - 0.002307 \cdot E \\ \text{Diffuseness } a_V &= 0.7684 - 0.01134 \cdot E \end{aligned}$$

Imaginary Potential

$$\begin{aligned} \text{Strength } W &= 6.0633 - 0.1194 \cdot E + 0.007067 \cdot E^2 - 0.0001374 \cdot E^3 \\ J_W &= 24.33 + 1.7412 \cdot E + 0.021215 \cdot E^2 - 0.0007645 \cdot E^3 \\ J_W &\approx 23.75 + 2.1234 \cdot E - 0.01318 \cdot E^2 \\ \text{Radius } r_W &= 1.3090 - 0.005857 \cdot E \\ \text{Diffuseness } b_W &= 0.2735 + 0.03115 \cdot E + 0.000004075 \cdot E^2 \end{aligned}$$

Spin Orbit potential from reference WG85, fixed.

Table B-2, ^{209}Bi DOM 6 – P fit, no ASYM, Full dispersion contribution (DISP) calculated with the SOM. Effective dispersion = $0.5 \cdot \text{DISP}$.

Real Potential

$$\begin{aligned} \text{Strength } V &= 45.965 - 0.04206 \cdot E \\ J_V &= 399.24 - 4.3506 \cdot E + 0.01592 \cdot E^2 \\ J_V &\approx 397.25 - 3.8732 \cdot E \\ \text{Radius } r_V &= 1.2364 - 0.003914 \cdot E \\ \text{Diffuseness } a_V &= 0.7280 - 0.004471 \cdot E \end{aligned}$$

Imaginary Potential

$$\begin{aligned} \text{Strength } W &= 4.4708 + 0.2930 \cdot E - 0.007469 \cdot E^2 \\ J_W &= 17.76 + 3.1020 \cdot E + 0.037238 \cdot E^2 - 0.0021599 \cdot E^3 \\ J_W &\approx 16.14 + 4.1820 \cdot E - 0.05995 \cdot E^2 \\ \text{Radius } r_W &= 1.3445 - 0.009456 \cdot E \\ \text{Diffuseness } b_W &= 0.2599 + 0.02903 \cdot E + 0.0001080 \cdot E^2 \end{aligned}$$

Spin- Orbit potential from reference WG85, fixed.

Table B-3. ^{209}Bi DOM 6 – P fit, no ASYM, Dispersion contribution (DISP) calculated with the SOM. Effective dispersion = $0.25 \cdot \text{DISP}$.

Real Potential

$$\text{Strength } V = 45.428 - 0.007032 \cdot E$$

$$J_V = 410.86 - 4.5734 \cdot E + 0.01622 \cdot E^2$$

$$J_V \approx 408.83 - 4.0869 \cdot E$$

$$\text{Radius } r_V = 1.2577 - 0.004649 \cdot E$$

$$\text{Diffuseness } a_V = 0.6934 - 0.002130 \cdot E$$

Imaginary Potential

$$\text{Strength } W = 4.9959 + 0.03516 \cdot E - 0.0005835 \cdot E^2$$

$$J_W = 18.27 + 3.2916 \cdot E - 0.061325 \cdot E^2 + 0.00022259 \cdot E^3$$

$$J_W \approx 18.29 + 3.2805 \cdot E - 0.06032 \cdot E^2$$

$$\text{Radius } r_W = 1.3442 - 0.007824 \cdot E$$

$$\text{Diffuseness } b_W = 0.2365 + 0.04388 \cdot E - 0.0006068 \cdot E^2$$

Spin Orbit potential from reference WG85, fixed.

Table B-4. ^{209}Bi DOM 6 – P fit, no ASYM, Dispersion contribution (DISP) calculated with the SOM. Normalization of DISP fraction is 0.01, i.e. essentially no DOM.

Real Potential

$$\text{Strength } V = 45.757 - 0.007393 \cdot E$$

$$J_V = 414.98 - 4.3091 \cdot E + 0.024387 E^2$$

$$J_V \approx 411.93 - 3.5775 \cdot E$$

$$\text{Radius } r_V = 1.2568 - 0.004193 \cdot E$$

$$\text{Diffuseness } a_V = 0.7086 - 0.002207 \cdot E$$

Imaginary Potential

$$\text{Strength } W = 5.0572 + 0.09386 \cdot E - 0.001898 \cdot E^2$$

$$J_W = 15.58 + 3.5765 \cdot E - 0.0533975 \cdot E^2 - 0.00035775 \cdot E^3$$

$$J_W \approx 15.58 + 3.7554 \cdot E - 0.069491 \cdot E^2$$

$$\text{Radius } r_W = 1.3608 - 0.008787 \cdot E$$

$$\text{Diffuseness } b_W = 0.2002 + 0.04203 \cdot E - 0.0005448 \cdot E^2$$

Spin Orbit potential from reference WG85, fixed.

Table E-1. ^{209}Bi SOM potential deduced from 6-parameter fitting. $\text{ASYM} = 1 + 0.00 \bullet E$, temperature $T = 0.4$ MeV, 13 discrete levels and no dispersion. Potential strengths (J_i) are in volume-integrals-per nucleon ($\text{MeV}\cdot\text{fm}^3$), depths and energies in MeV, and dimensions in fermis.

Real Potential

$$\text{Strength } V = 45.920 - 0.009160 \bullet E$$

$$J_V = 412.18 - 3.5299 \bullet E$$

$$\text{Radius } r_V = 1.2553 - 0.004081 \bullet E$$

$$\text{Diffuseness } a_V = 0.7007$$

Imaginary Potential

$$\text{Strength } W = 5.0965 + 0.03045 \bullet E + 0.005764 \bullet E^2 - 0.0001657 \bullet E^3$$

$$J_W = 19.82 + 2.3136 \bullet E + 0.2703 \bullet E^2 - 0.001796 \bullet E^3$$

$$\text{Radius } r_W = 1.3456 - 0.006699 \bullet E$$

$$\text{Diffuseness } b_W = 0.2520 + 0.03286 \bullet E - 0.0004521 \bullet E^2$$

Spin orbit potential is from reference WG85, fixed.

Table E-2. ^{209}Bi SOM deduced from 6-parameter fitting. $\text{ASYM} = 1 + 0.00 \bullet E$, 13 discrete levels, temperature $T = 0.7$ MeV, no dispersion.

Real Potential

$$\text{Strength } V = 44.898 + 0.06643 \bullet E$$

$$J_V = 413.78 - 3.4581 \bullet E$$

$$\text{Radius } r_V = 1.2681 - 0.004741 \bullet E$$

$$\text{Diffuseness } a_V = 0.6924$$

Imaginary Potential

$$\text{Strength } W = 7.0858 - 0.3765 \bullet E + 0.02643 \bullet E^2 - 0.0004313 \bullet E^3$$

$$J_W = 20.70 + 1.9659 \bullet E + 0.04780 \bullet E^2 - 0.001727 \bullet E^3$$

$$\text{Radius } r_W = 1.3499 - 0.007926 \bullet E$$

$$\text{Diffuseness } a_W = 0.1831 + 0.04484 \bullet E - 0.0007413 \bullet E^2$$

Spin-orbit potential of reference WG(85), fixed

Table E-3. ^{209}Bi SOM deduced from 6-parameter fitting. $\text{ASYM} = 1 + 0.00 \bullet E$, 13 levels, temperature $T = 1.0$ and no dispersion.

Real Potential

$$\text{Strength } V = 44.848 + 0.03268 \bullet E$$

$$J_V = 420.12 - 3.8198 \bullet E$$

$$\text{Radius } r_V = 1.2763 - 0.004791 \bullet E$$

$$\text{Diffuseness } a_V = 0.6811$$

Imaginary Potential

$$\text{Strength } W = 5.6084 + 0.03081 \bullet E + 0.0007269 \bullet E^2$$

$$J_W = 20.11 + 3.3235 \bullet E - 0.06635 \bullet E^2 + 0.0001311 \bullet E^3$$

$$\text{Radius } r_W = 1.3526 - 0.008420 \bullet E$$

$$\text{Diffuseness } a_W = 0.2306 + 0.04007 \bullet E - 0.0006794 \bullet E^2$$

Spin-orbit potential is that of reference WG85, fixed.

Table E-4. ^{209}Bi SOM deduced from 6-parameter fitting. $\text{ASYM} = 1 + 0.00 \bullet E$, 13 levels, temperature $T = 1.4$ MeV and no dispersion.

Real Potential

$$\text{Strength } V = 44.655 + 0.04805 \bullet E$$

$$J_V = 423.00 - 3.9745 \bullet E$$

$$\text{Radius } r_V = 1.2823 - 0.005108 \bullet E$$

$$\text{Diffuseness } a_V = 0.6713$$

Imaginary Potential

$$\text{Strength } W = 6.2828 + 0.01382 \bullet E - 0.001371 \bullet E^2$$

$$J_W = 18.20 + 4.1308 \bullet E - 0.1143 \bullet E^2 + 0.0005755 \bullet E^3$$

$$\text{Radius } r_W = 1.3456 - 0.008542 \bullet E$$

$$\text{Diffuseness } a_W = 0.1889 + 0.04402 \bullet E - 0.0006398 \bullet E^2$$

Spin-orbit potential is from reference WG85, fixed..

Table E-5. ^{209}Bi SOM determined from 6-parameter fitting. $\text{ASYM} = 1 + 0.00 \bullet E$, 48 levels, no temperature, no dispersion.

Real Potential

$$\text{Strength } V = 44.155 + 0.02098 \bullet E$$

$$J_V = 430.63 - 5.0649 \bullet E$$

$$\text{Radius } r_V = 1.3007 - 0.005303 \bullet E$$

$$\text{Diffuseness } a_V = 0.6292$$

Imaginary Potential

$$\text{Strength } W = 6.3915 + 0.01450 \bullet E + 0.005181 \bullet E^2 - 0.0001439 \bullet E^3$$

$$J_W = 23.60 + 2.8071 \bullet E + 0.01028 \bullet E^2 - 0.001451 \bullet E^3$$

$$\text{Radius } r_W = 1.3259 - 0.006265 \bullet E$$

$$\text{Diffuseness } a_W = 0.2463 + 0.03324 \bullet E - 0.0004000 \bullet E^2$$

Spin-orbit potential is the same as reference WG85, fixed.

Table E-6. ^{209}Bi SOM deduced from 6-parameter fitting. $\text{ASYM} = 1 + 0.00 \bullet E$, 48 levels, temperature $T = 1.0$, no dispersion.

Real Potential

$$\text{Strength } V = 44.489 + 0.06643 \bullet E$$

$$J_V = 421.22 - 4.0326 \bullet E$$

$$\text{Radius } r_V = 1.2809 - 0.005371 \bullet E$$

$$\text{Diffuseness } a_V = 0.6830$$

Imaginary Potential

$$\text{Strength } W = 5.2271 + 0.1831 \bullet E - 0.009324 \bullet E^2 + 0.0001331 \bullet E^3$$

$$J_W = 20.532 + 3.6138 \bullet E - 0.09157 \bullet E^2 + 0.0005711 \bullet E^3$$

$$\text{Radius } r_W = 1.3598 - 0.008183 \bullet E$$

$$\text{Diffuseness } a_W = 0.2522 + 0.03287 \bullet E - 0.0003363 \bullet E^2$$

Spin-orbit potential is the same as reference WG85, fixed.

Table E-7. ^{209}Bi SOM deduced from 6-parameter fitting. $\text{ASYM} = 1 + 0.00 \bullet E$, 48 discrete levels, temperature $T = 1.0$ MeV, and with full dispersion.

Real Potential

$$\text{Strength } V = 45.376 + 0.05549 \bullet E$$

$$J_V = 385.34 - 4.5339 \bullet E$$

$$\text{Radius } r_V = 1.2323 - 0.006397 \bullet E$$

$$\text{Diffuseness } a_V = 0.6999$$

Imaginary Potential

$$\text{Strength } W = 5.0430 + 0.2421 \bullet E - 0.009016 \bullet E^2$$

$$J_W = 23.18 + 2.6856 \bullet E - 0.008700 \bullet E^2 - 0.001825 \bullet E^3$$

$$\text{Radius } r_W = 1.3035 - 0.004936 \bullet E$$

$$\text{Diffuseness } a_W = 0.3185 + 0.02197 \bullet E - 0.00005345 \bullet E^2$$

Spin-orbit potential is the same as reference WG85, fixed.

Table E-8. ^{209}Bi SOM deduced from 6-parameter fitting. $\text{ASYM} = 1 + 0.00 \bullet E$, 48 discrete levels, temperature $T = 1.0$ MeV, and with the dispersion normalized by 0.5.

Real Potential

$$\text{Strength } V = 45.166 + 0.06014 \bullet E$$

$$J_V = 402.57 - 4.4180 \bullet E$$

$$\text{Radius } r_V = 1.2533 - 0.005992 \bullet E$$

$$\text{Diffuseness } a_V = 0.6979$$

Imaginary Potential

$$\text{Strength } W = 5.9436 + 0.1395 \bullet E - 0.009108 \bullet E^2 + 0.0001539 \bullet E^3$$

$$J_W = 22.63 + 3.1753 \bullet E - 0.07629 \bullet E^2 + 0.0008111 \bullet E^3$$

$$\text{Radius } r_W = 1.3422 - 0.006899 \bullet E$$

$$\text{Diffuseness } a_W = 0.2503 + 0.02778 \bullet E - 0.00008887 \bullet E^2$$

Spin-orbit potential is the same as reference WG85, fixed.

FIGURES

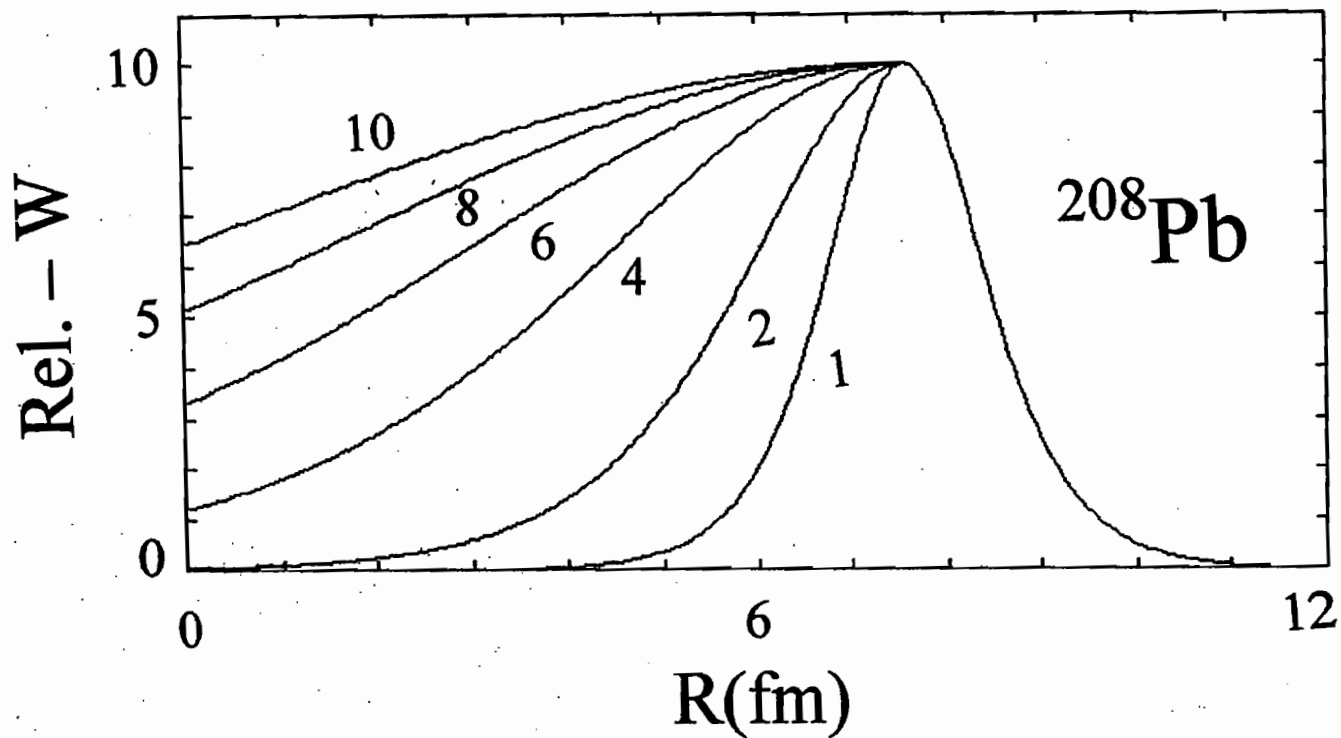


Fig. II-B-1. Relative surface-absorption potential forms as a function of radius obtained with the diffuseness b_{w_i} interior to the imaginary radius increasing from $1 \rightarrow 10$ times that of the diffuseness b_{w_o} exterior to the imaginary radius. This corresponds to $ASYM = 1, 2, 4, 6, 8,$ and 10 of Eq. II-B-1, as numerically noted in the figure.

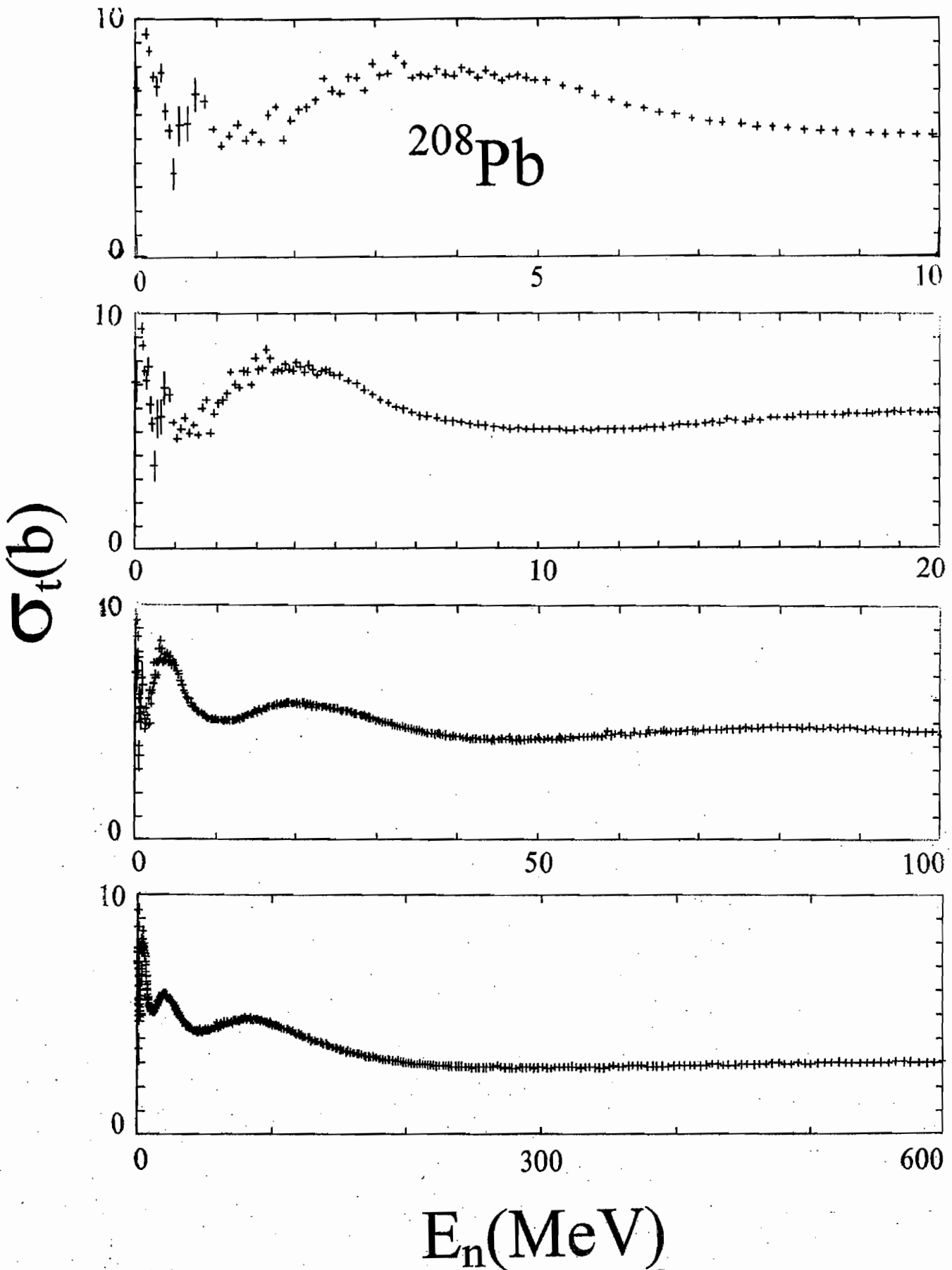


Fig. III-A-1-1. Energy averages of measured ^{208}Pb neutron total cross-sections from ≈ 10 keV to 600 MeV. "+" symbols indicate the averaged experimental values as discussed in the text.

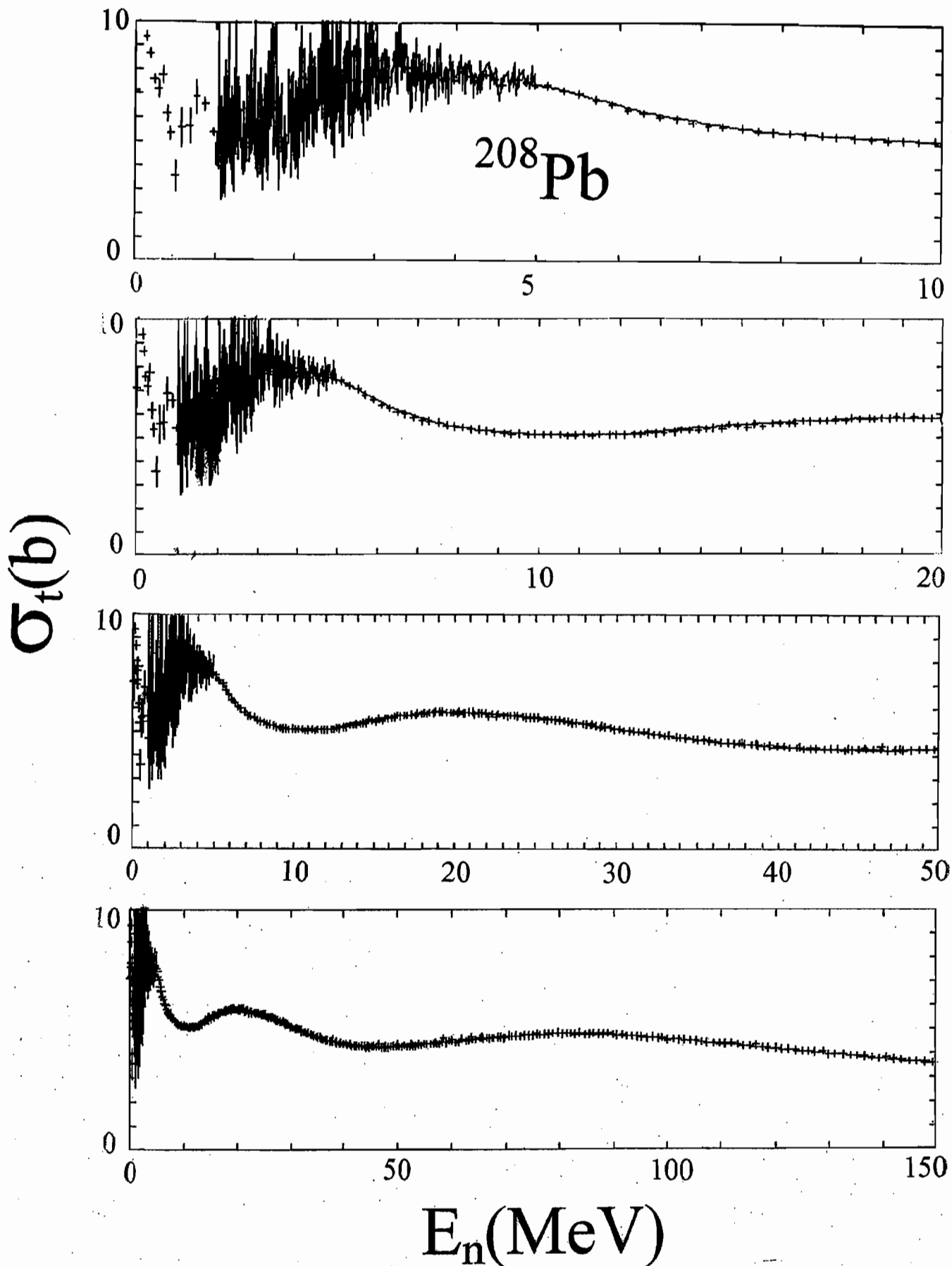


Fig. III-A-1-2. Energy-averaged measured total cross sections of ^{208}Pb compared with the corresponding ENDF/B-VI (ENDF) evaluated cross sections. "+" symbols indicate the present experimental averages and the curves the evaluation.

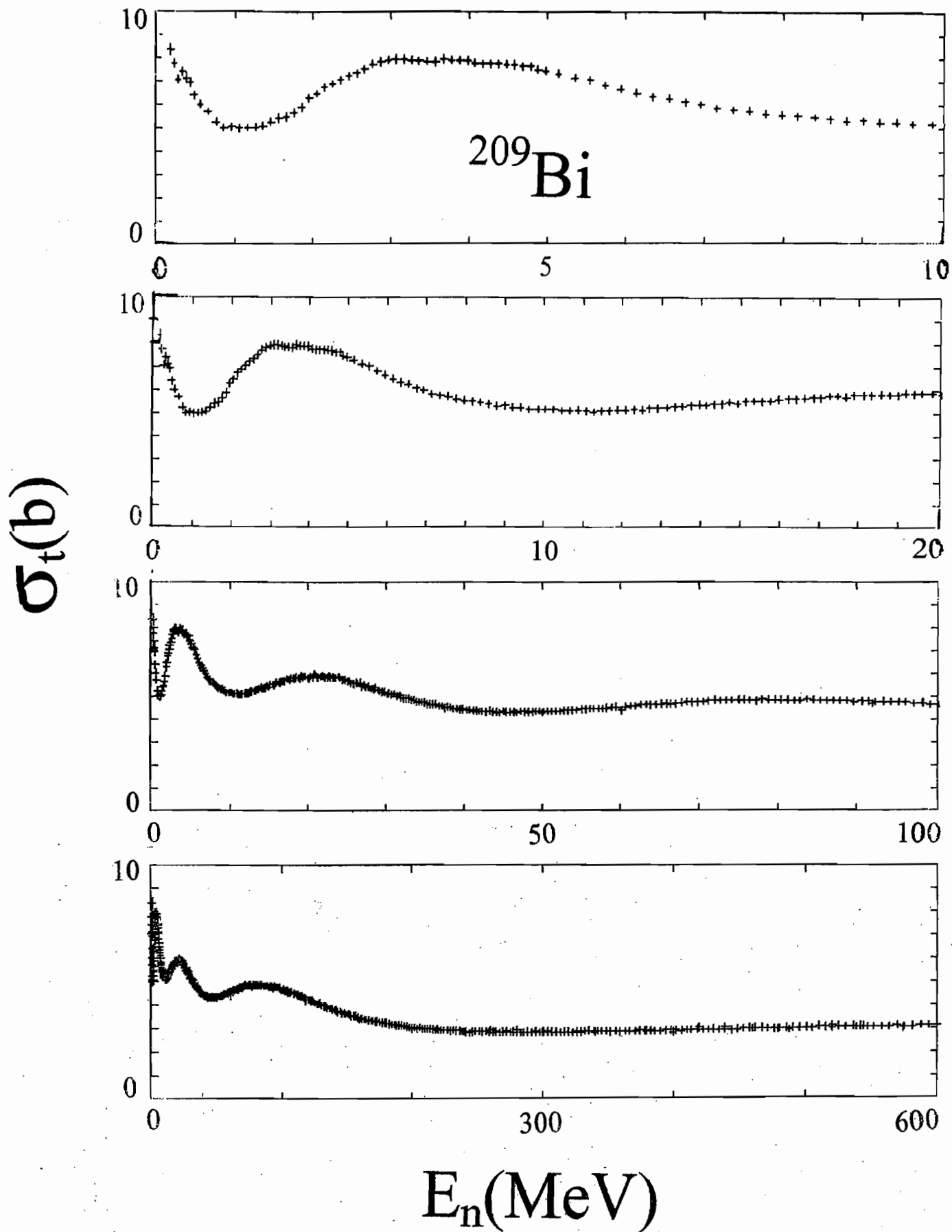


Fig. III-A-2-1. Energy-averaged ^{209}Bi experimental neutron total cross sections (symbols) constructed from the measured values as outlined in the text. The four panels show the same data over different energy ranges.

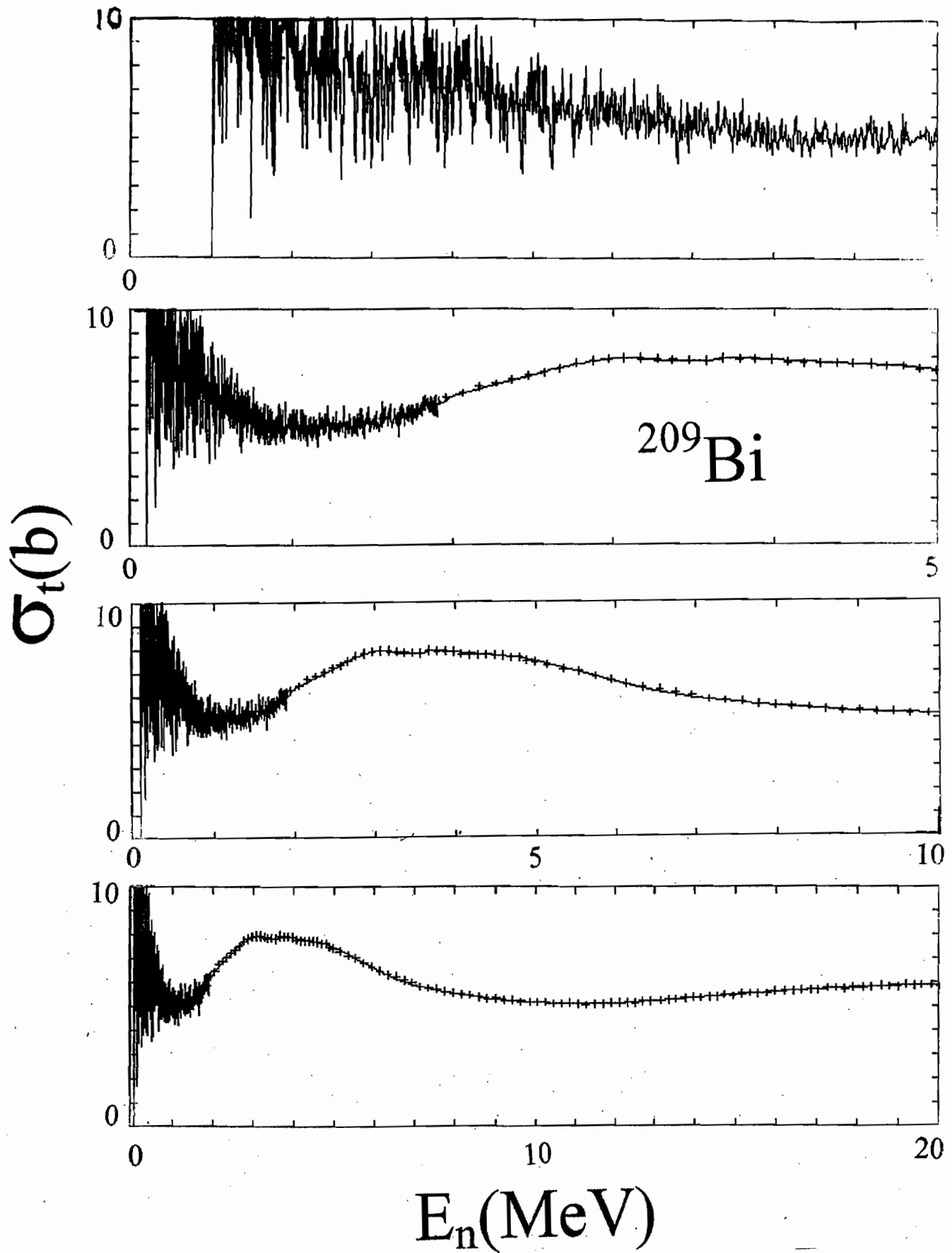


Fig. III-A-2-2. The present energy-averaged ^{209}Bi total cross sections (crosses) compared with the ENDF/B-VI values (curves).

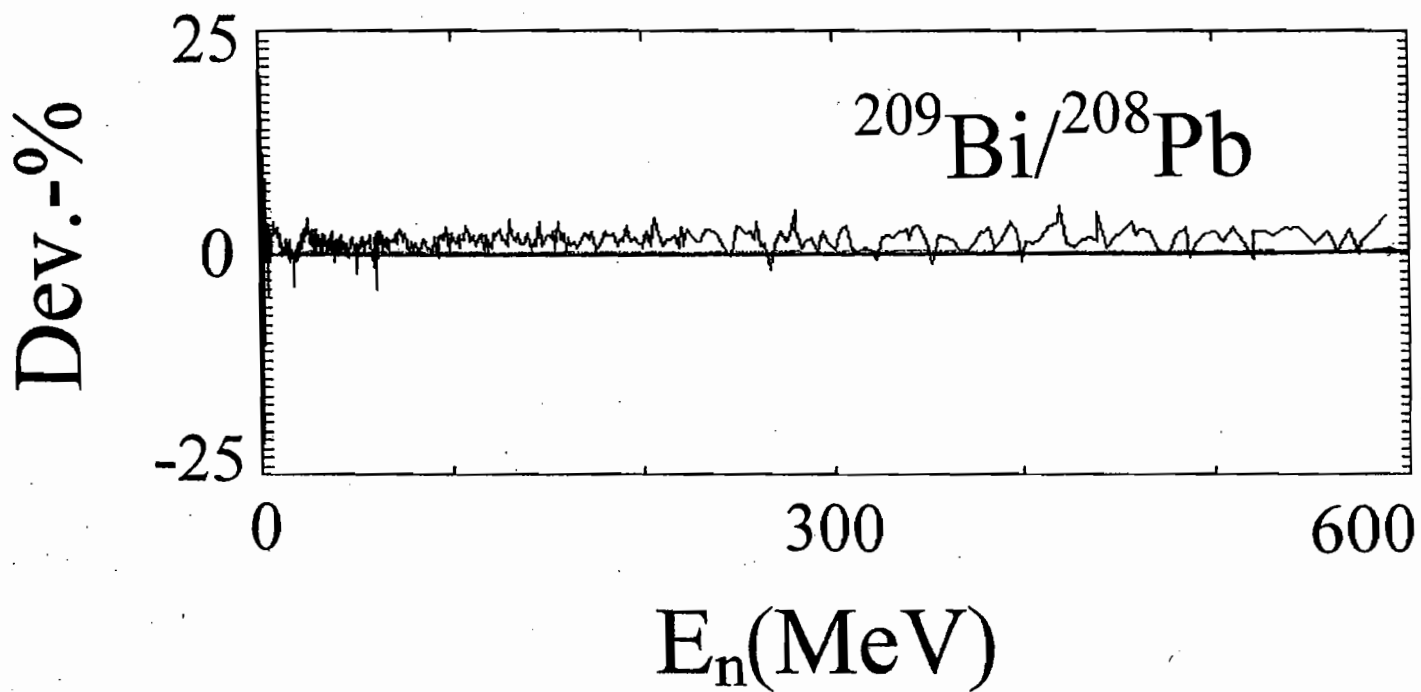


Fig. III-A-2-3. Percentage deviations between energy-averaged ²⁰⁹Bi and ²⁰⁸Pb neutron total cross sections as a function of energy (jagged curve). The heavy solid line indicates zero.

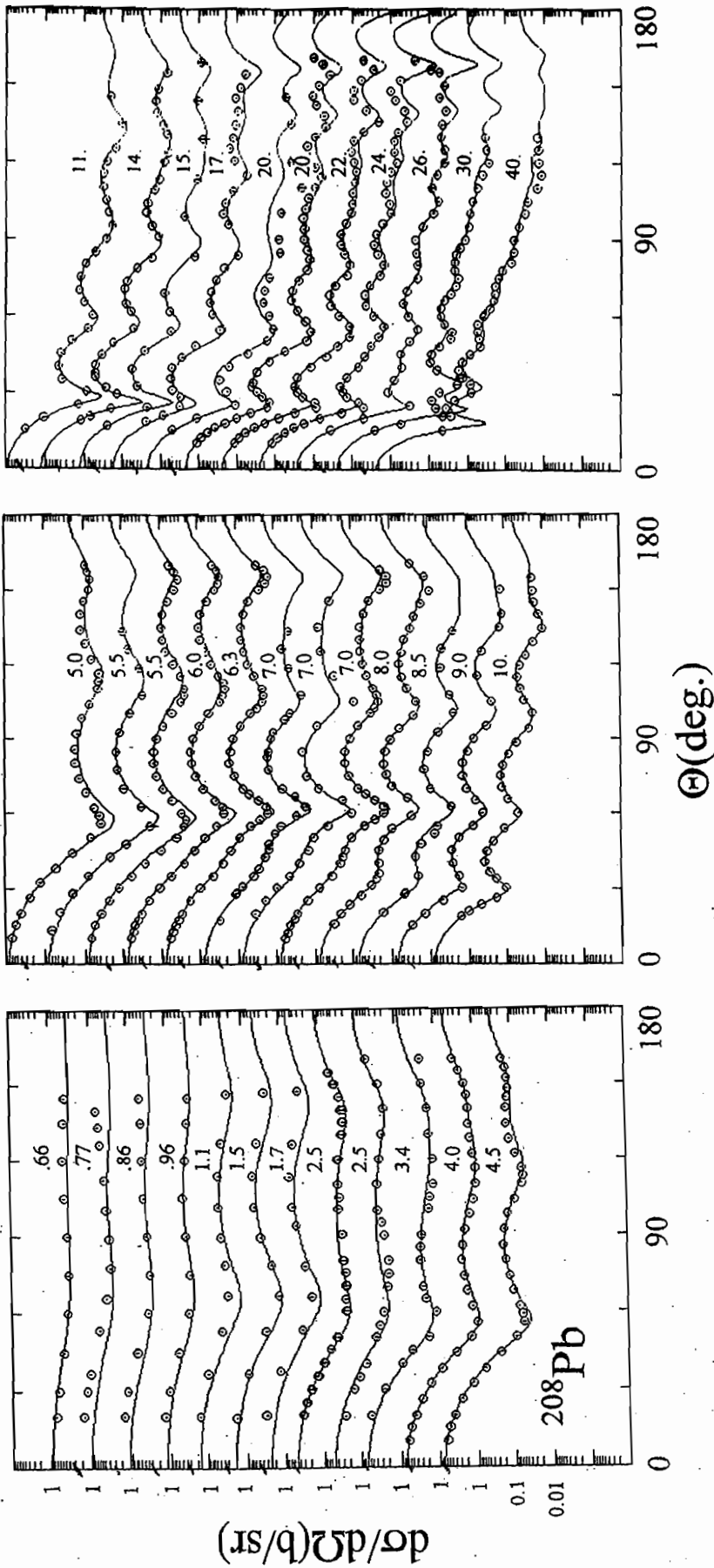


Fig. III-B-1-1. Measured differential neutron elastic-scattering cross sections of ^{208}Pb are indicated by circular symbols. Below 2 MeV the values are energy averages as described in the text. Curves denote the results of SOM fitting as described in Section IV of the text. Incident energies are numerically noted in MeV. Herein all differential data are presented in the laboratory coordinate system.

PANEL-1

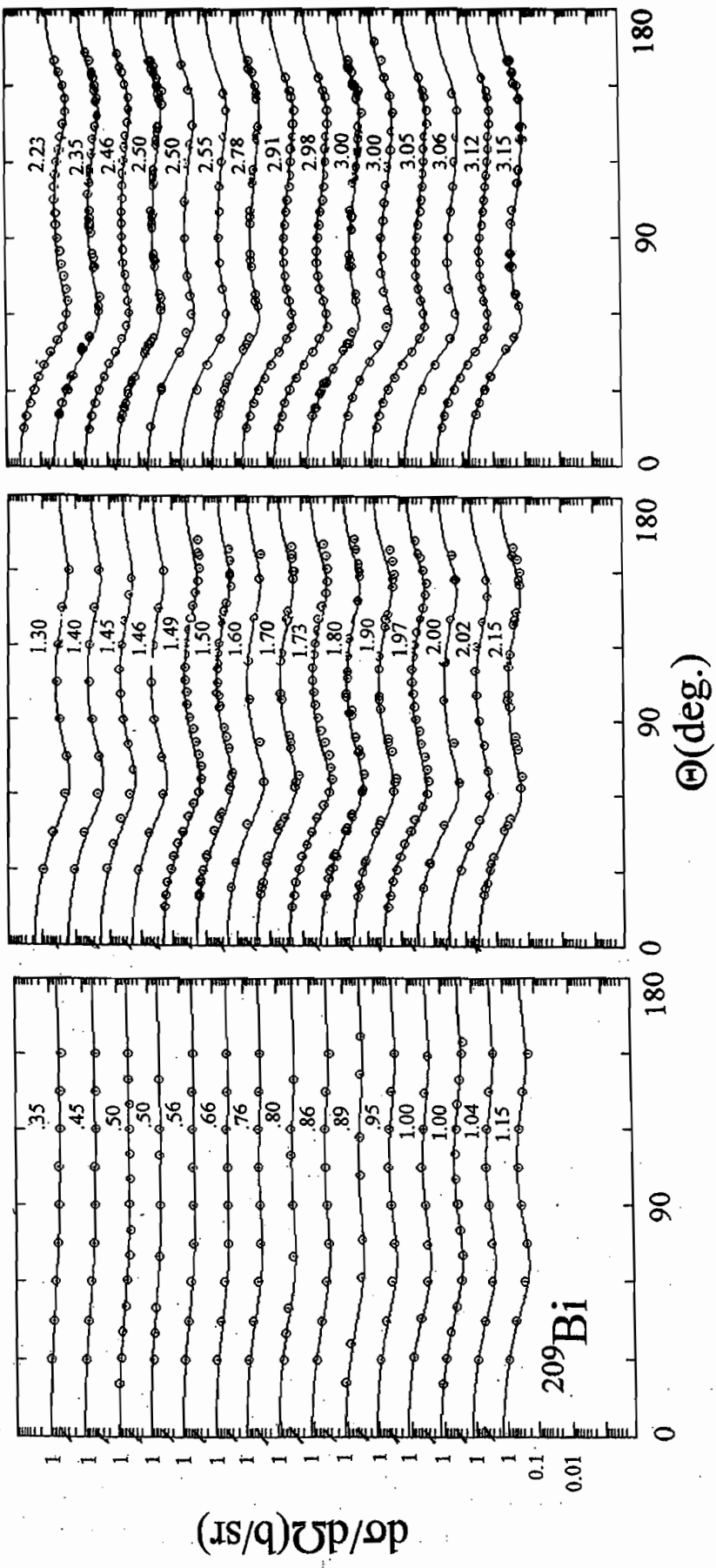
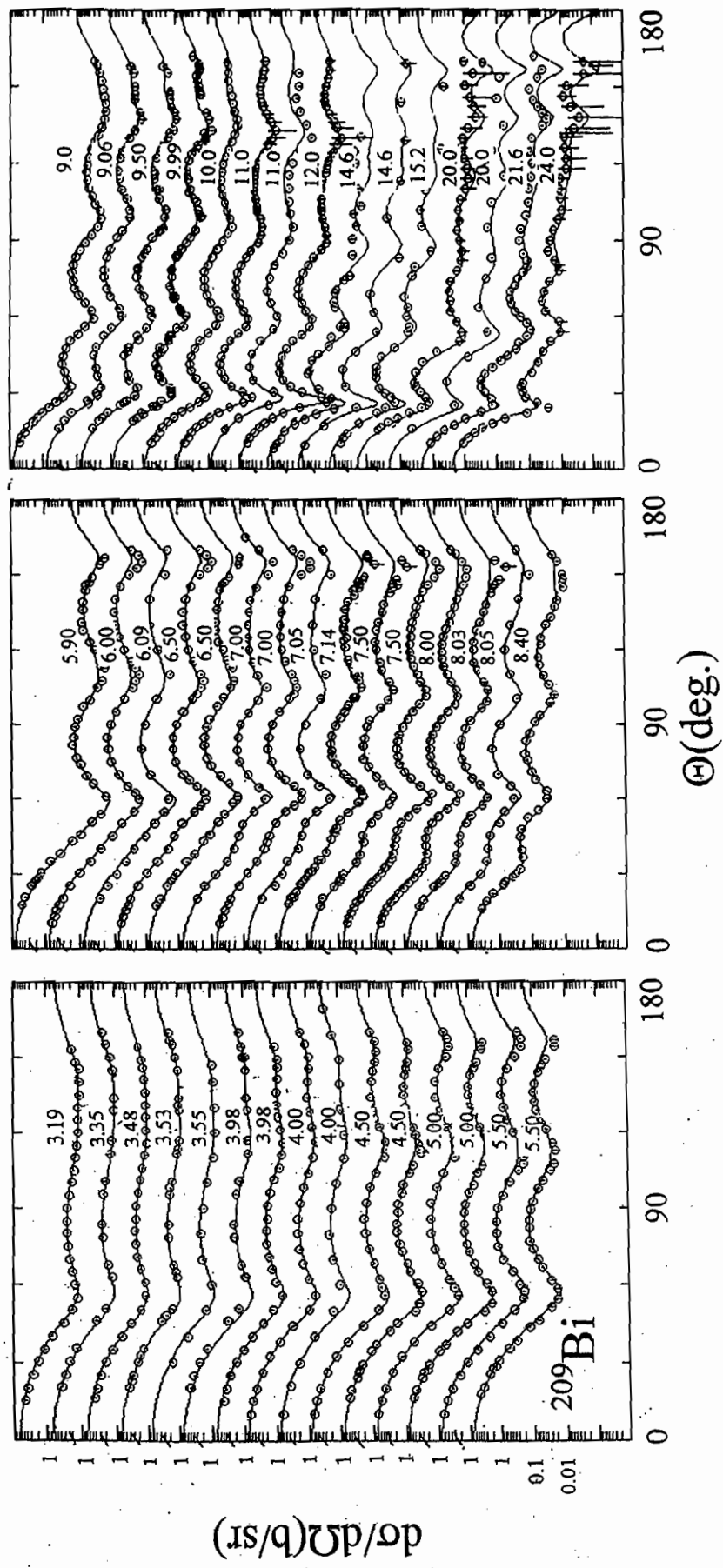


Fig. III-B-2-1. Neutron differential elastic-scattering cross sections of ^{209}Bi . Circular symbols indicate the measured values and curves of calculations using the SOM Base Potential of Table IV-A-2. Incident energies are numerically noted in MeV. There are two panels to this figure.

PANEL-2



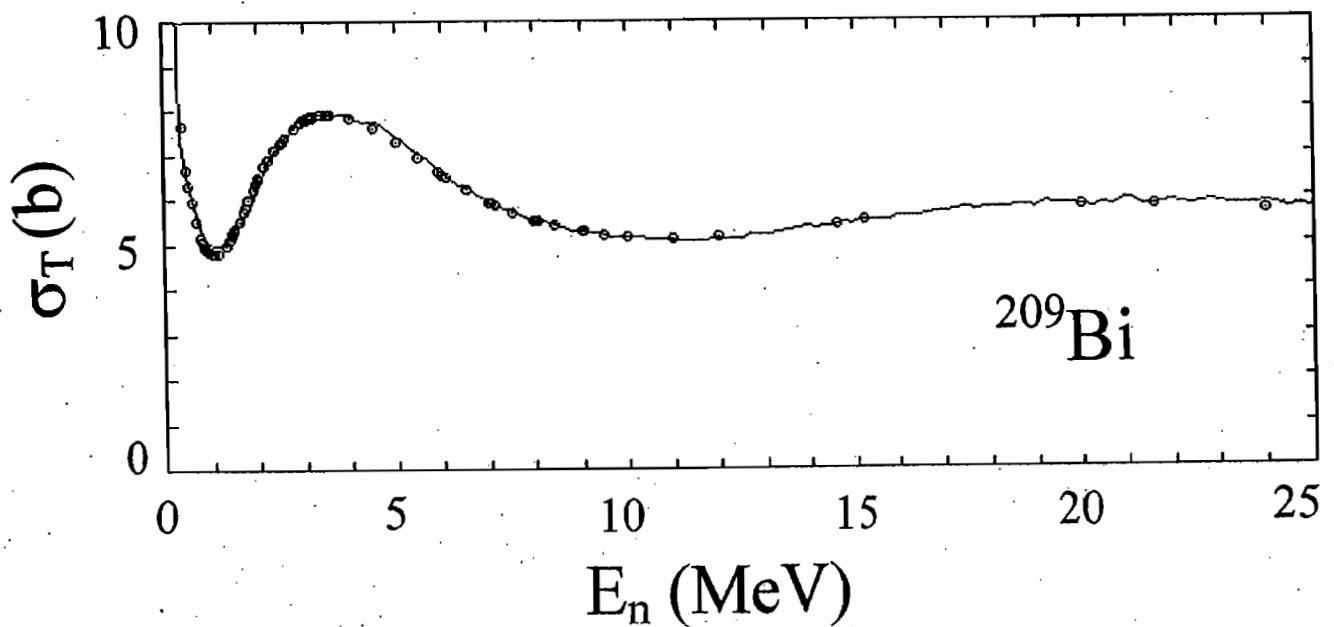
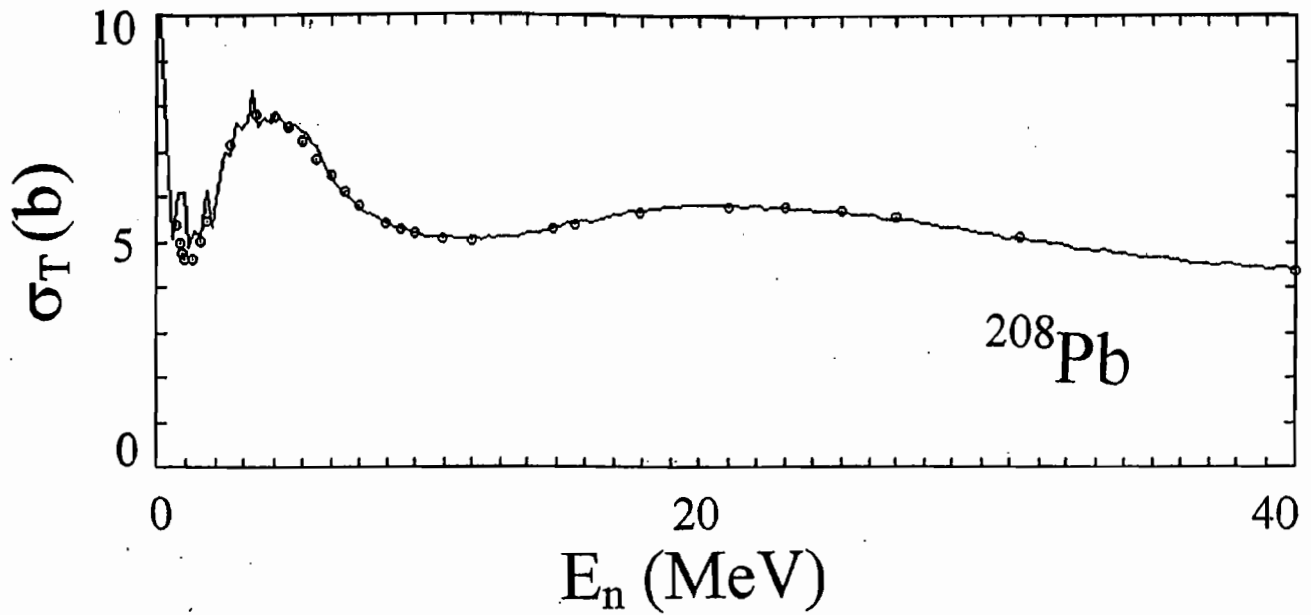


Fig. IV-A-1. Comparison of energy-averaged experimental neutron total cross sections (solid curves) and values calculated with the SOM Baseline potentials of the text at the energies of the experimental elastic-scattering distributions (symbols). The upper panel pertains the ^{208}Pb and the lower to ^{209}Bi .

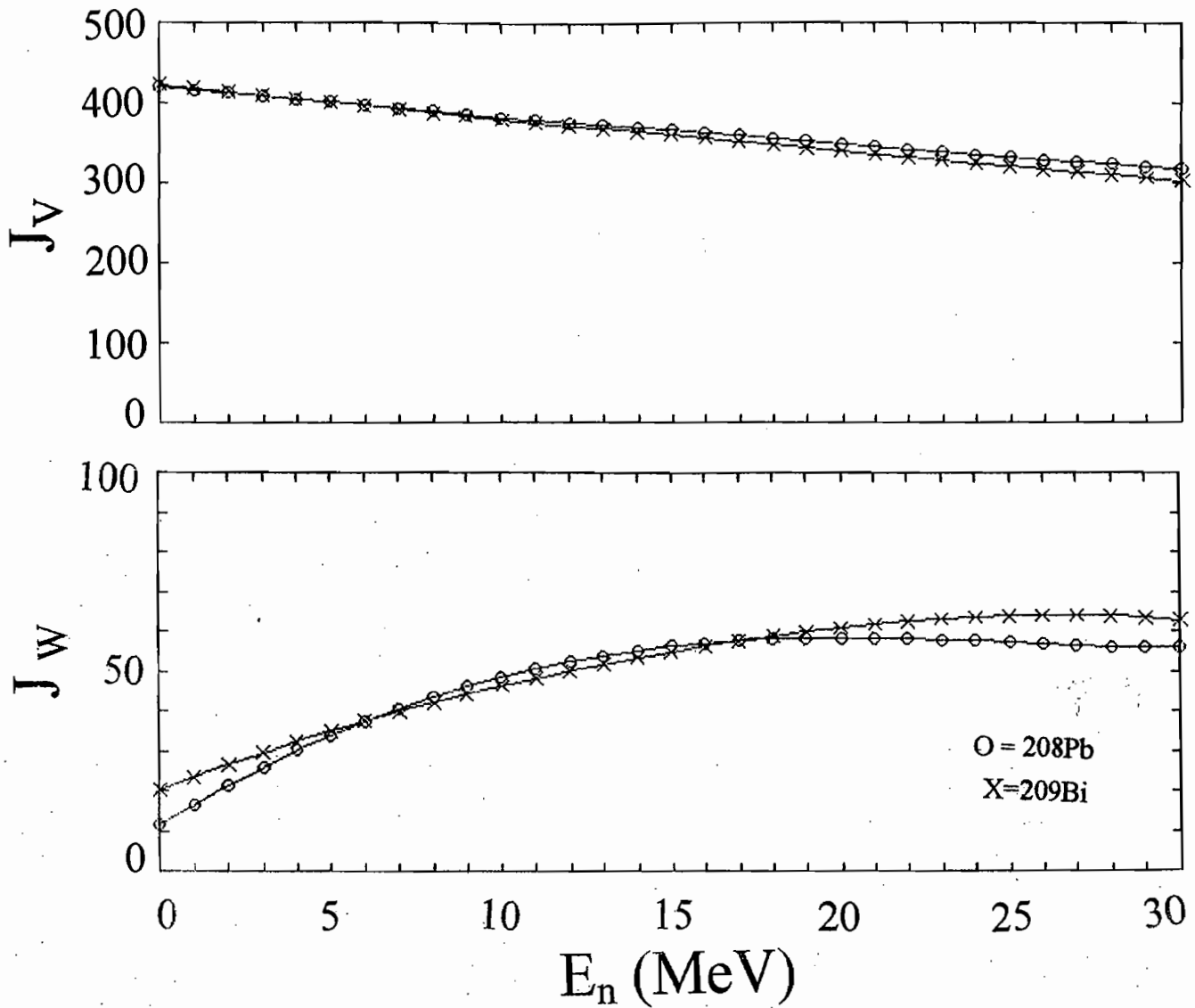


Fig. IV-A-2. Comparisons of the energy distributions of the real (J_v) and imaginary (J_w) SOM Baseline potential strengths of ^{209}Bi and ^{208}Pb as given in Tables IV-A-1 and IV-A-2. Strengths (J_i) are given as volume-integrals-per nucleon. Each panel has two curves with symbols, corresponding to ^{209}Bi ("X" symbols) and ^{208}Pb ("O" symbols) values.

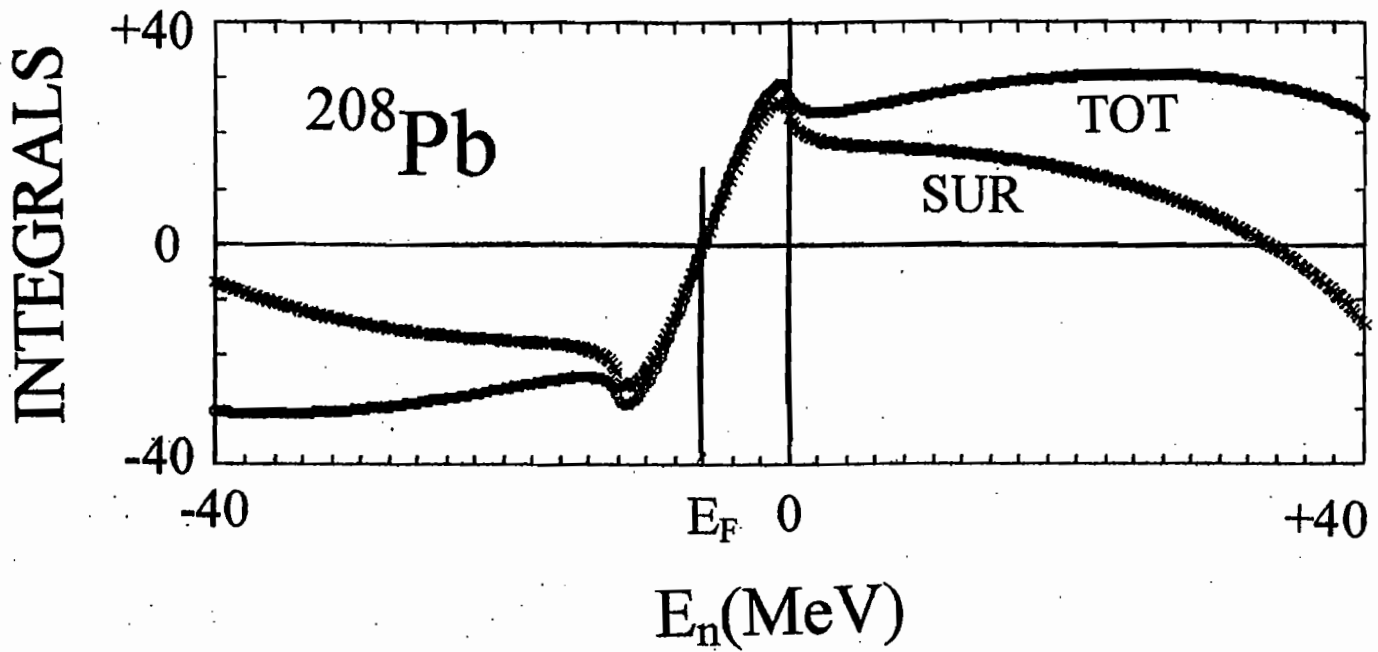


Fig. IV-B-1. ^{208}Pb total (TOT) and surface (SUR) dispersion contributions to the real potential (in units of $\text{MeV}\cdot\text{fm}^3$) as a function of incident neutron energy in MeV.

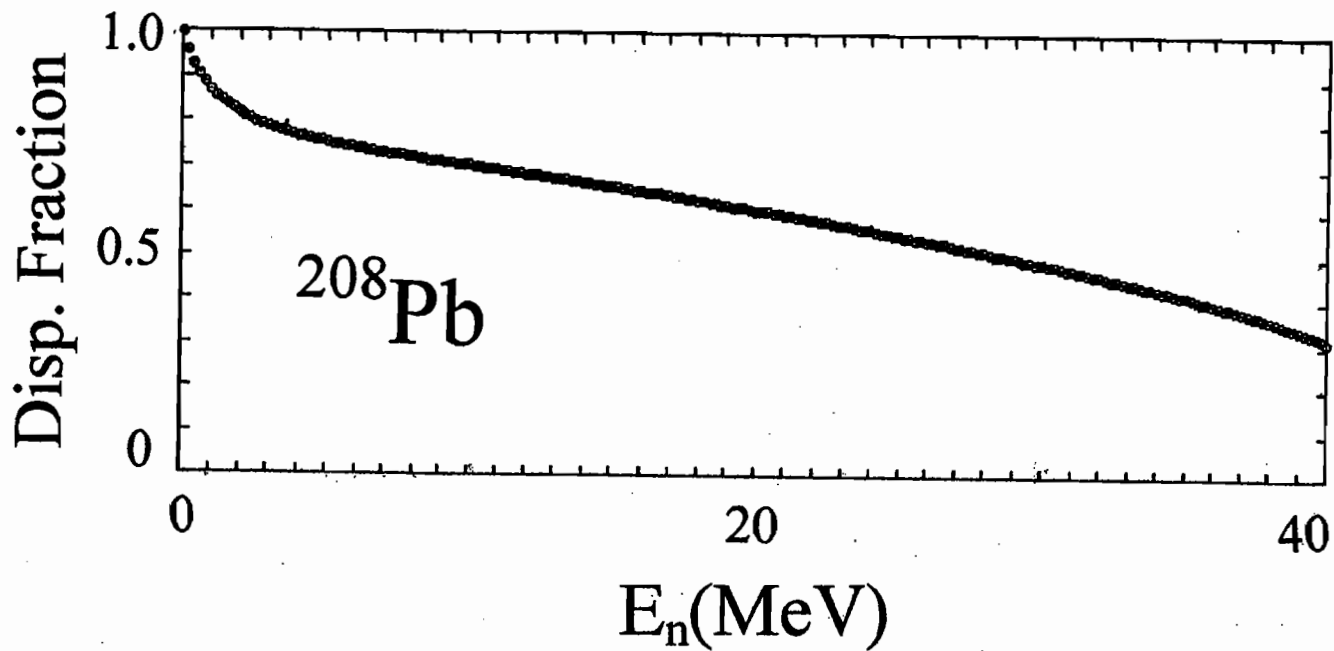


Fig. IV-B-2. The fraction of the surface-imaginary ^{208}Pb potential that is added to the real potential as a function of laboratory energy in the DOM.

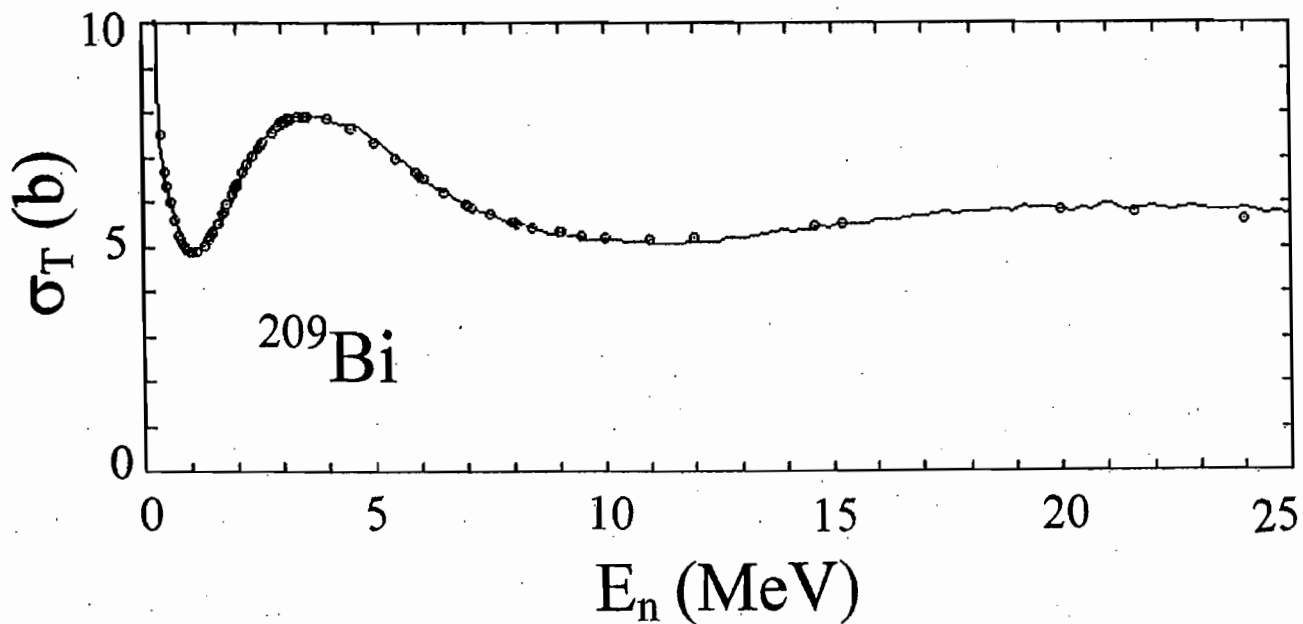
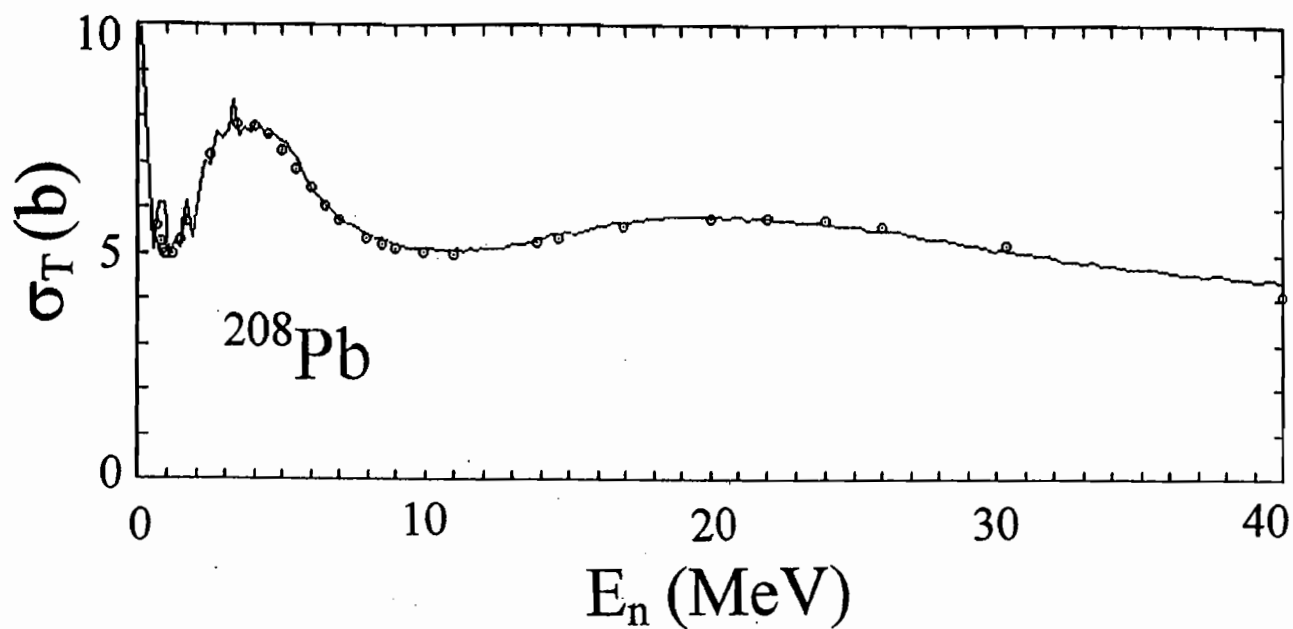


Fig. IV-B-3. Comparison of measured and calculated ^{208}Pb and ^{209}Bi neutron total cross sections. The calculations were made with the DOM potentials of Tables IV-B-1 and IV-B-2. The nomenclature is the same as that of Fig. IV-A-1.

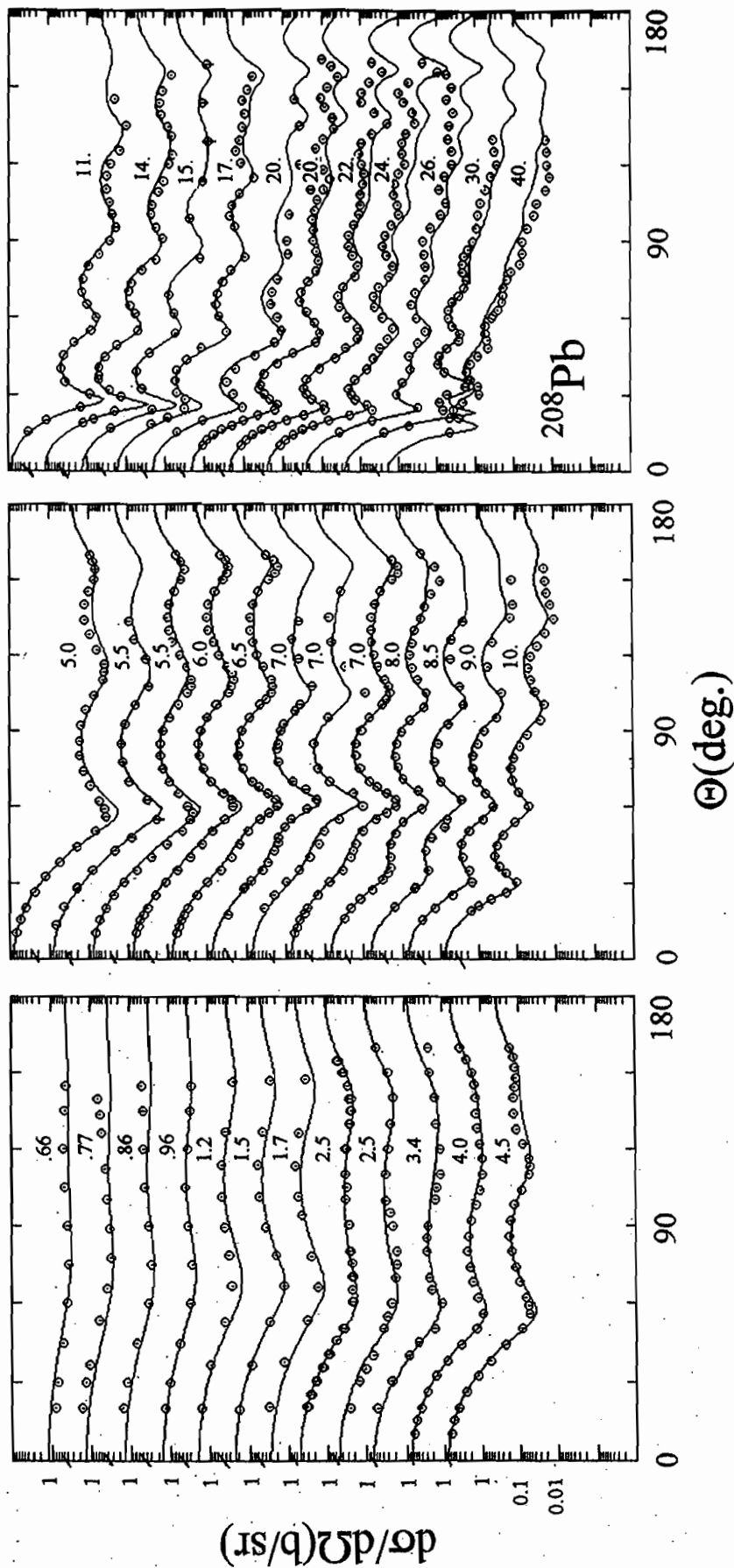


Fig. IV-B-4. Comparison of measured (symbols) and calculated (curves) neutron elastic-scattering cross section of ^{208}Pb . The calculations employed the DOM potential of Table IV-B-1. The nomenclature is the same as that of Fig. III-B-1.

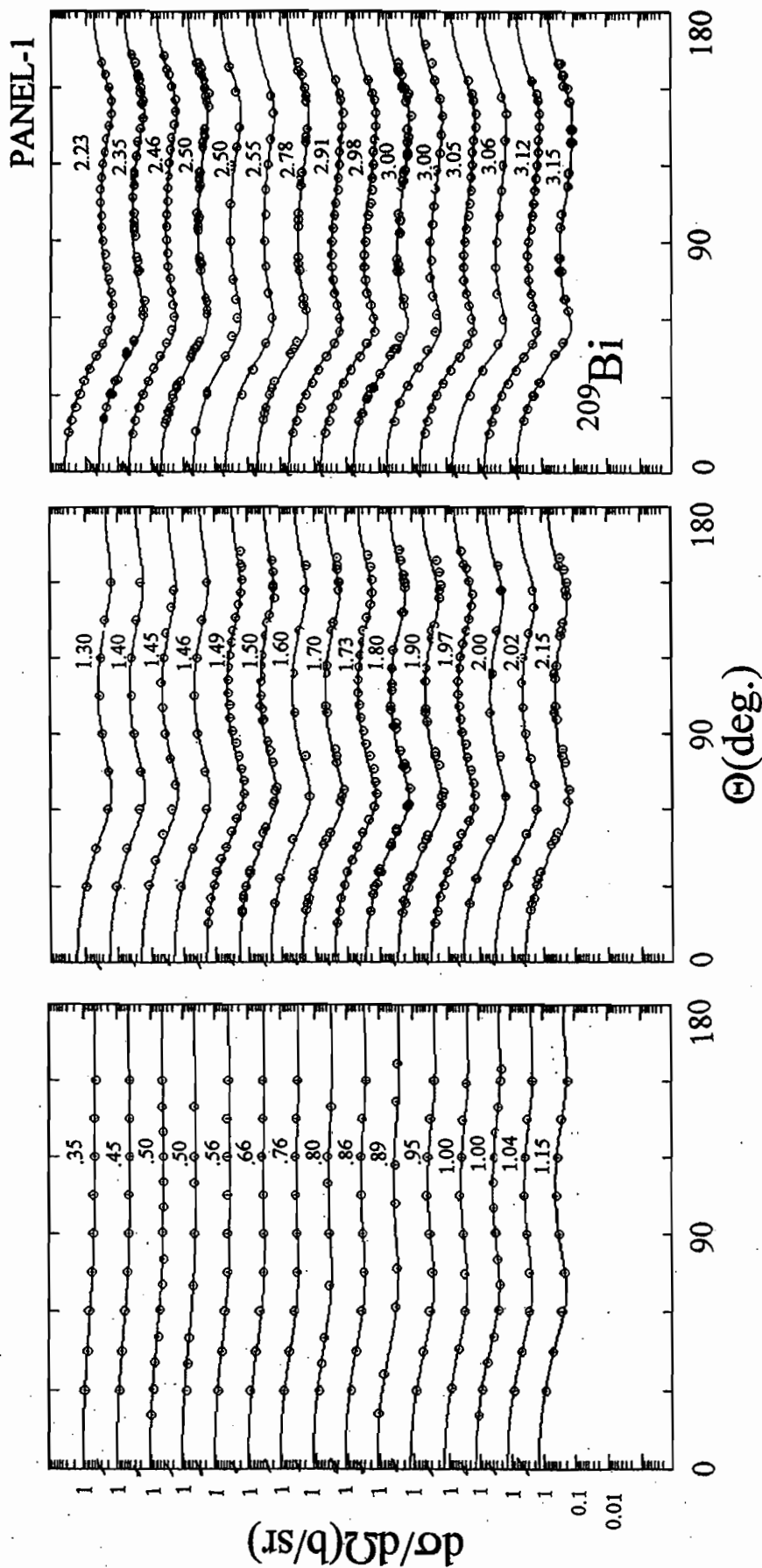
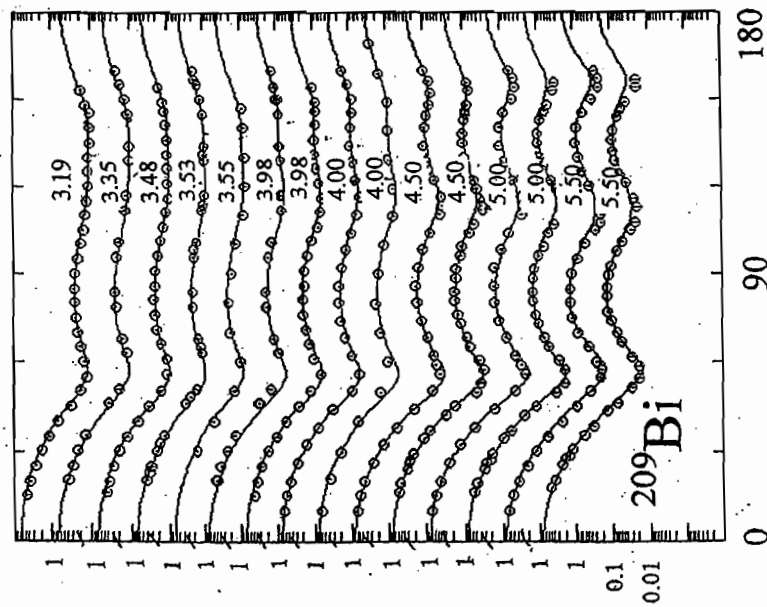
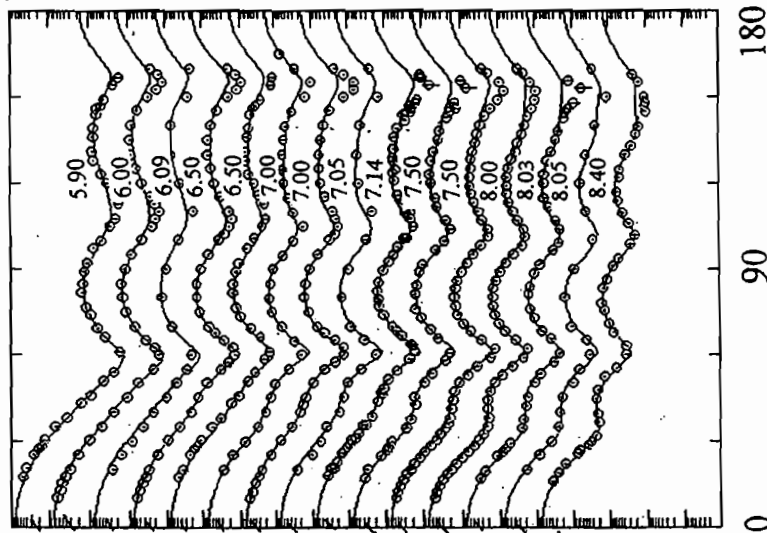
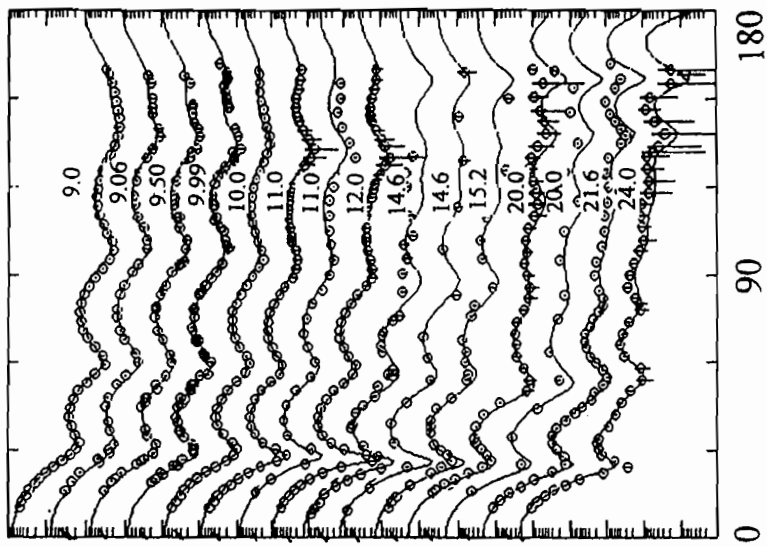


Fig. IV-B-5. Comparison of measured (symbols) and calculated (curves) neutron elastic scattering cross sections of ^{209}Bi . The calculations used the DOM potential of Table IV-B-2. The nomenclature is the same of Fig. III-B-2-1, again with two panels.

PANEL-2



$d\sigma/d\Omega$ (b/sr)

180 0 90 Θ (deg.)

180 0 90

0.1
0.01

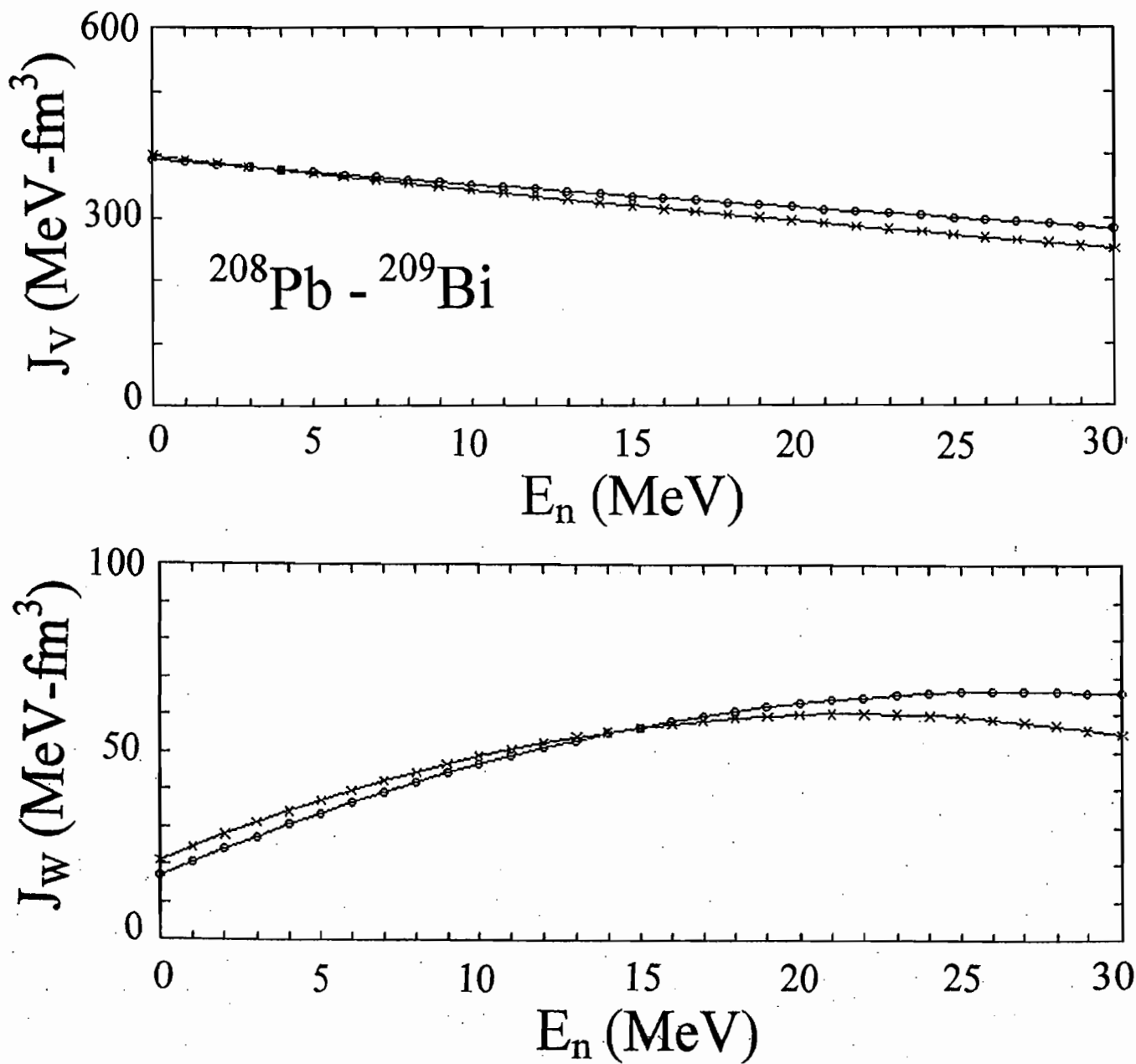


Fig. IV-B-6. Comparisons of ^{208}Pb (crosses) and ^{209}Bi (circles) DOM real (J_V) and imaginary (J_W) potential strengths in terms of volume-integrals-per-nucleon. These curves with symbols represent the values of Tables IV-B-1 and IV-B-2.

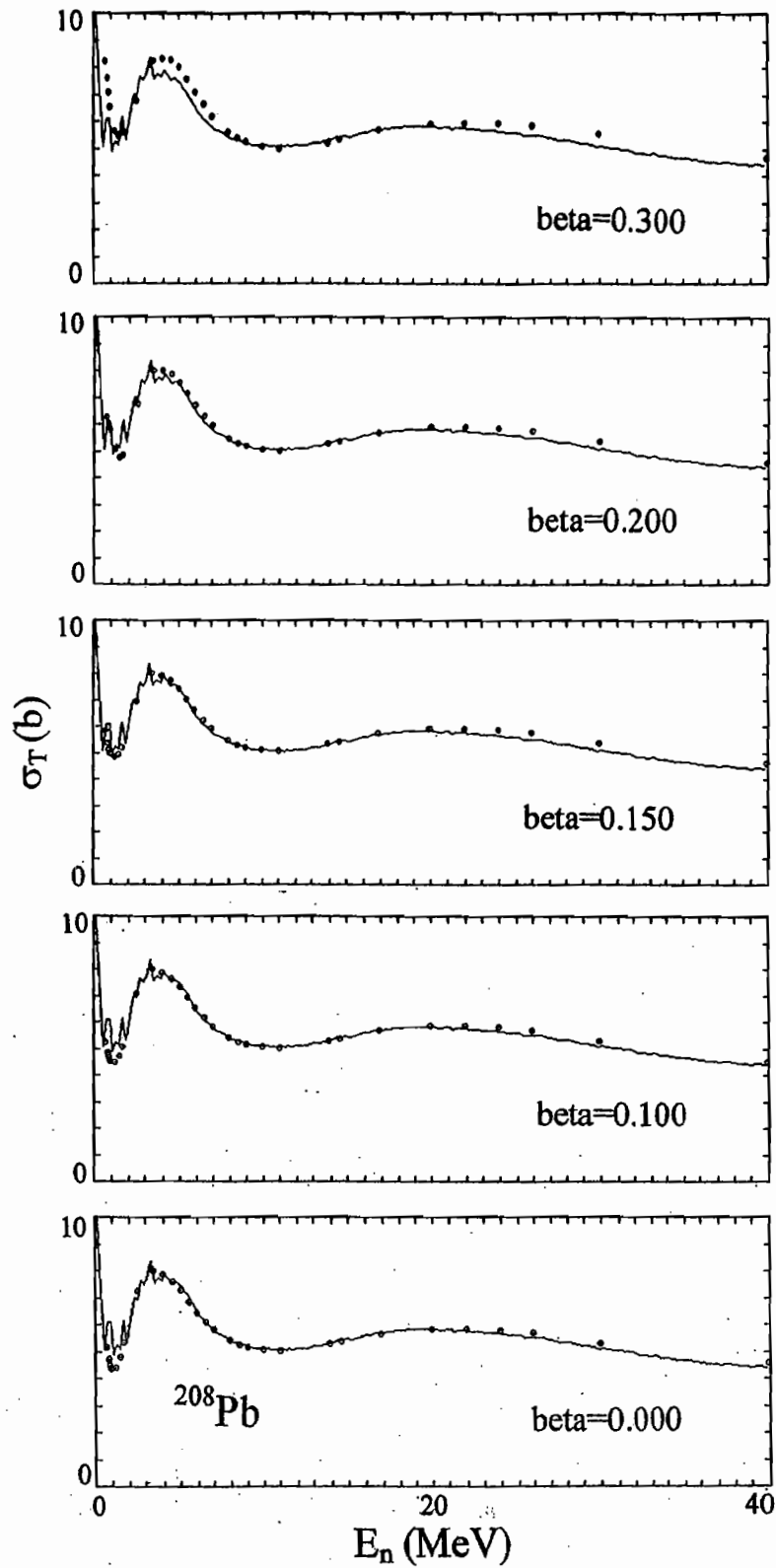


Fig. V-1. ^{208}Pb neutron total cross sections. The energy-averaged experimental values are indicated by the curves. Results calculate at the energies of the elastic-scattering data are indicated by circular symbols. The calculations used the two level ($0+,3-$) vibrational model of the text. The β_3 varied from 0 to 0.1, 0.15, 0.2 and 0.3 as noted on the various panels of the figure.

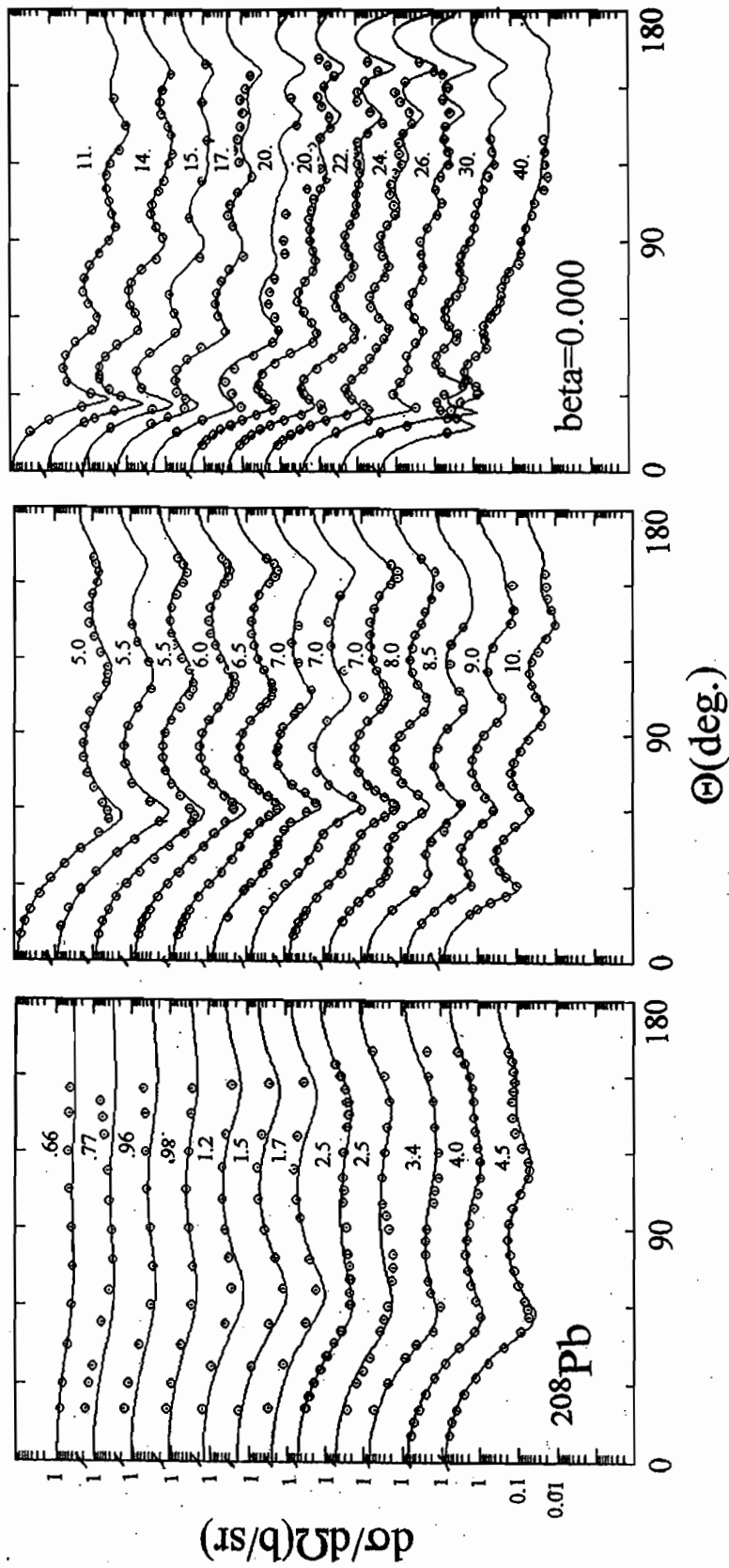


Fig. V-2. Comparisons of measured (symbols) and calculated (curves) ^{208}Pb elastic scattering cross sections. Incident energies are numerically noted. The calculations used the two-level vibrational model of the text with $\beta_3 = 0.00$ (i.e. spherical model).

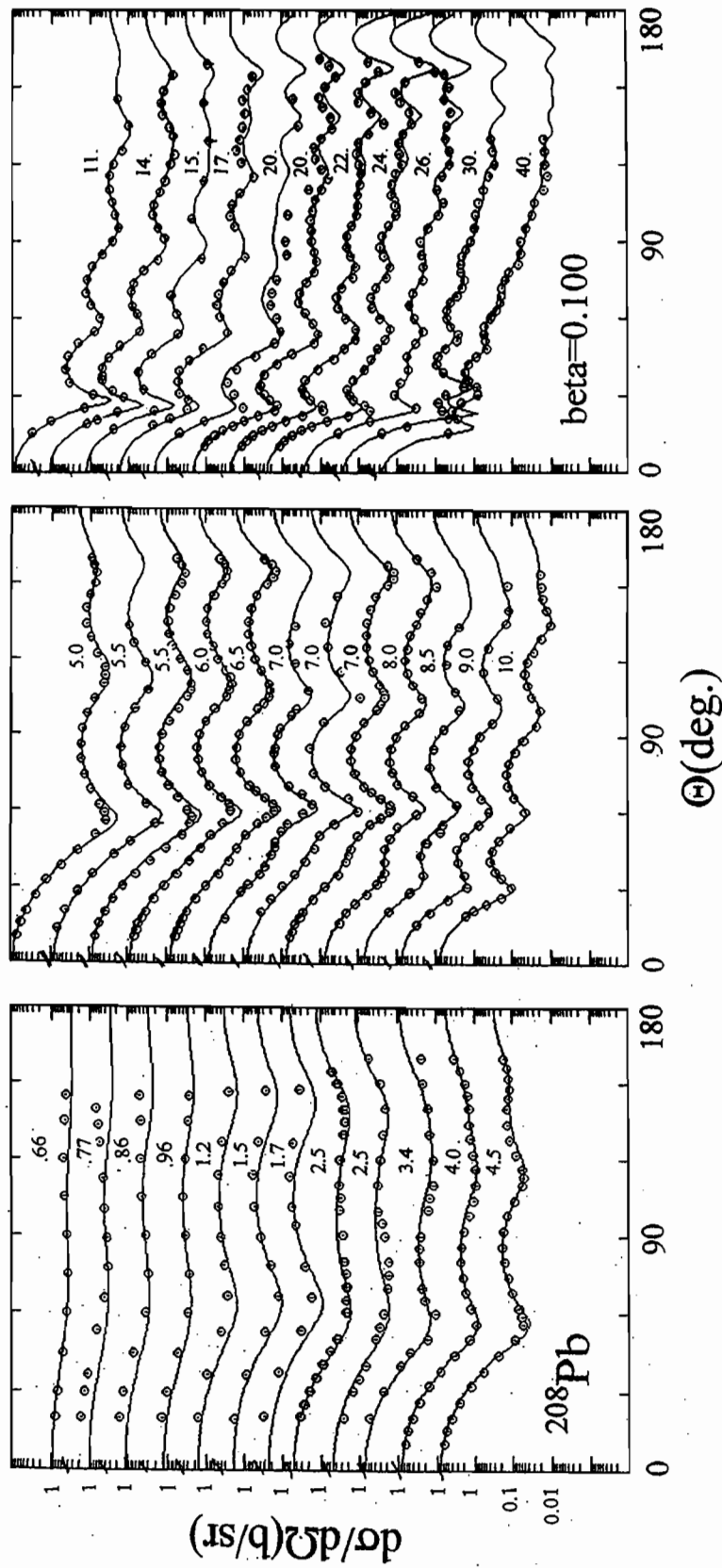


Fig. V-3. Same as Fig. V-2 but with $\beta_3 = 0.10$.

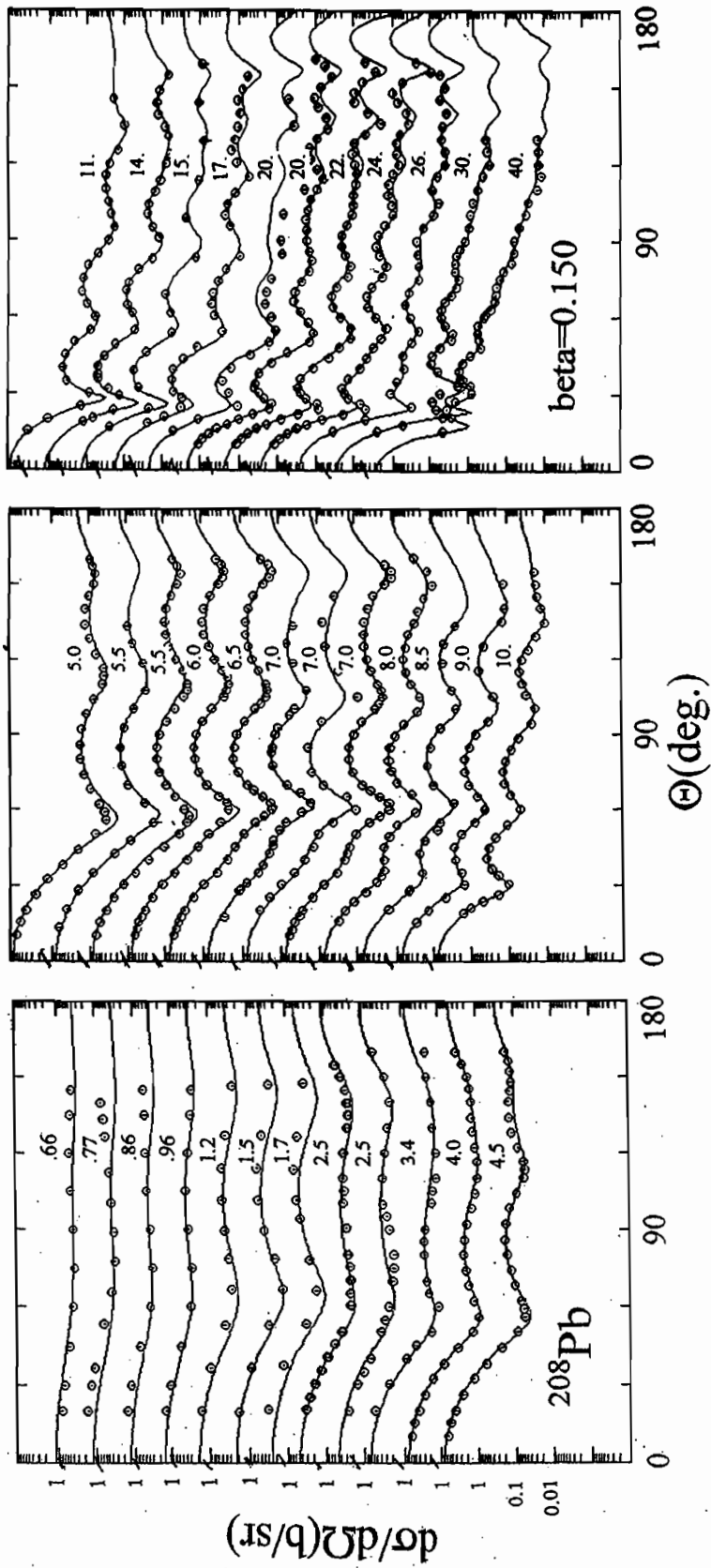


Fig. V-4. Same as Fig. V-2 but with $\beta_3 = 0.15$.

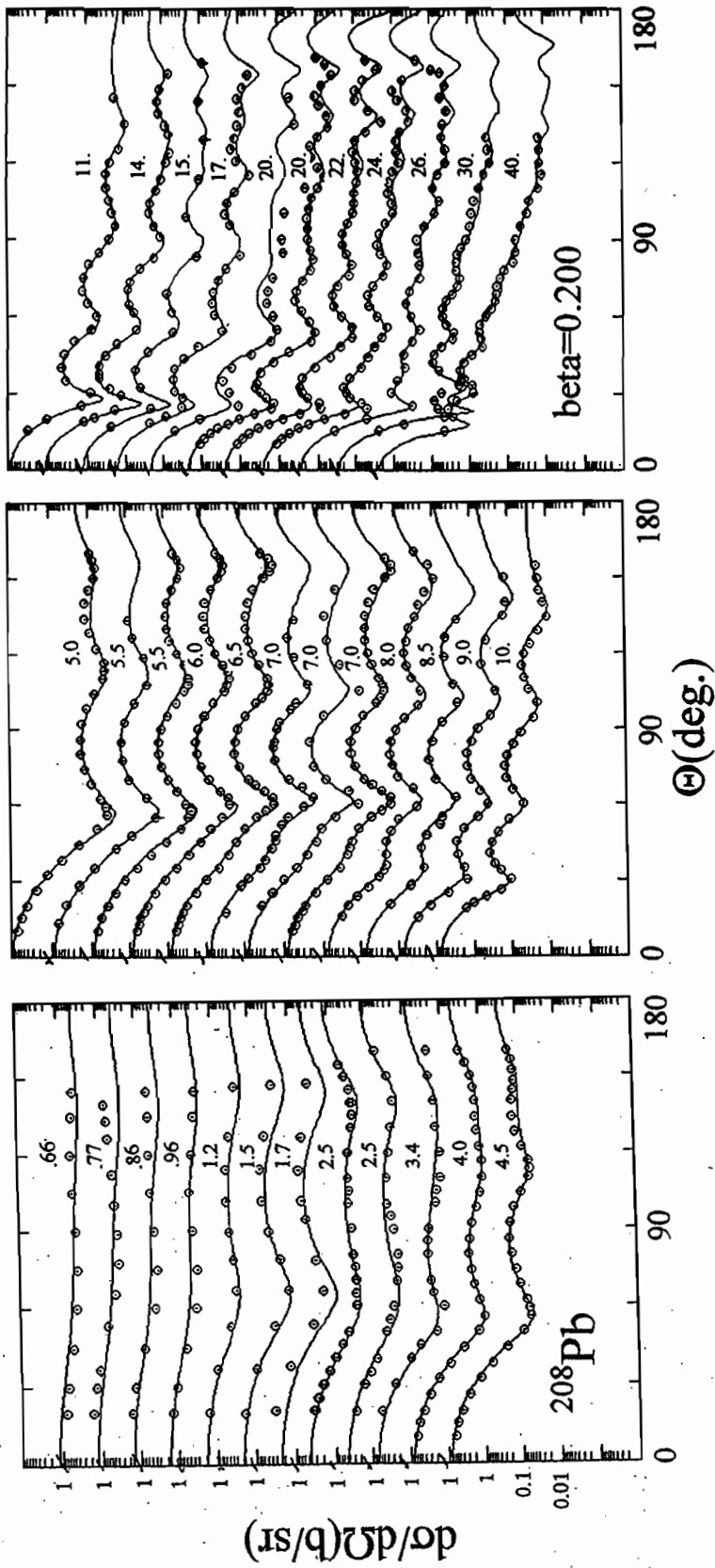


Fig. V-5. Same as Fig. V-2 but with $\beta_3 = 0.20$.

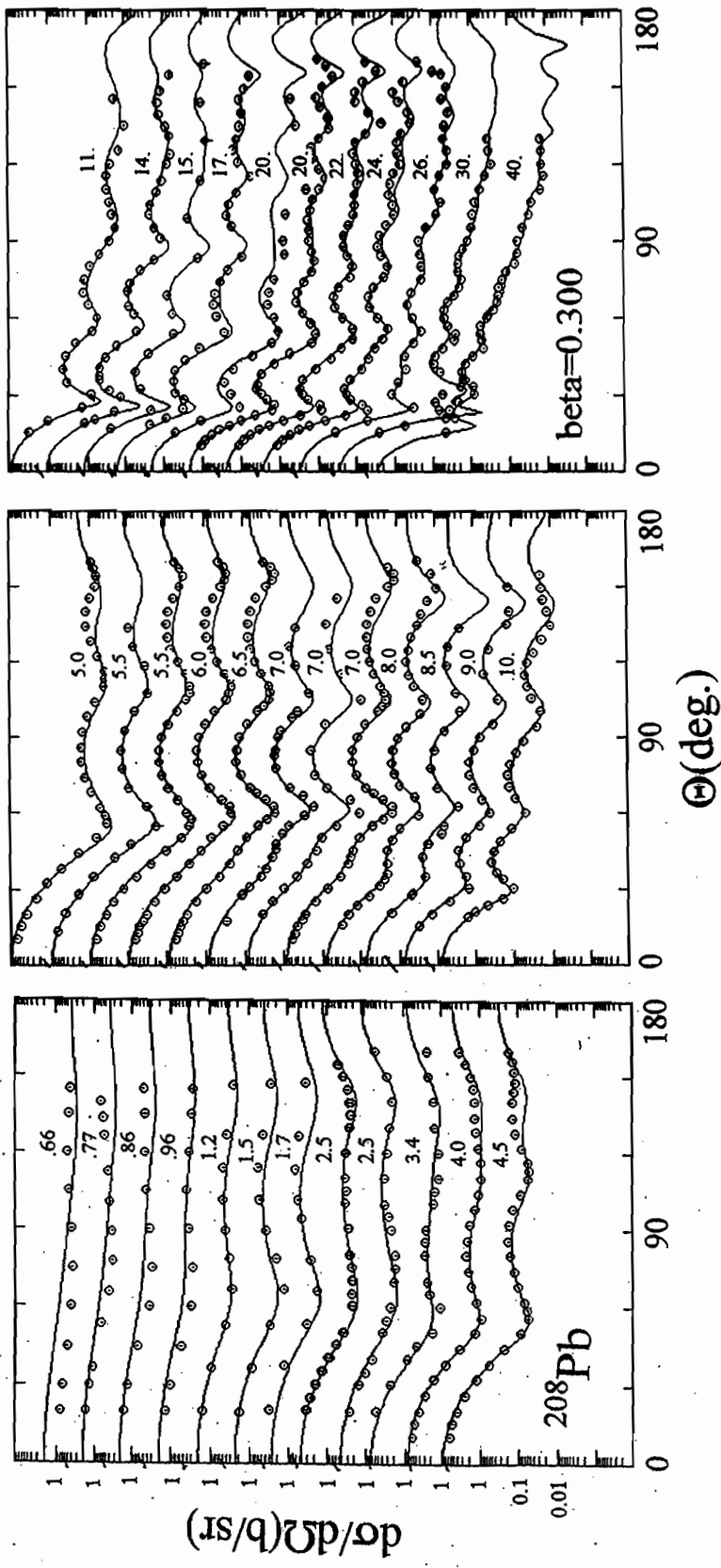


Fig. V-6. Same as Fig. V-2 but with $\beta_3 = 0.30$.

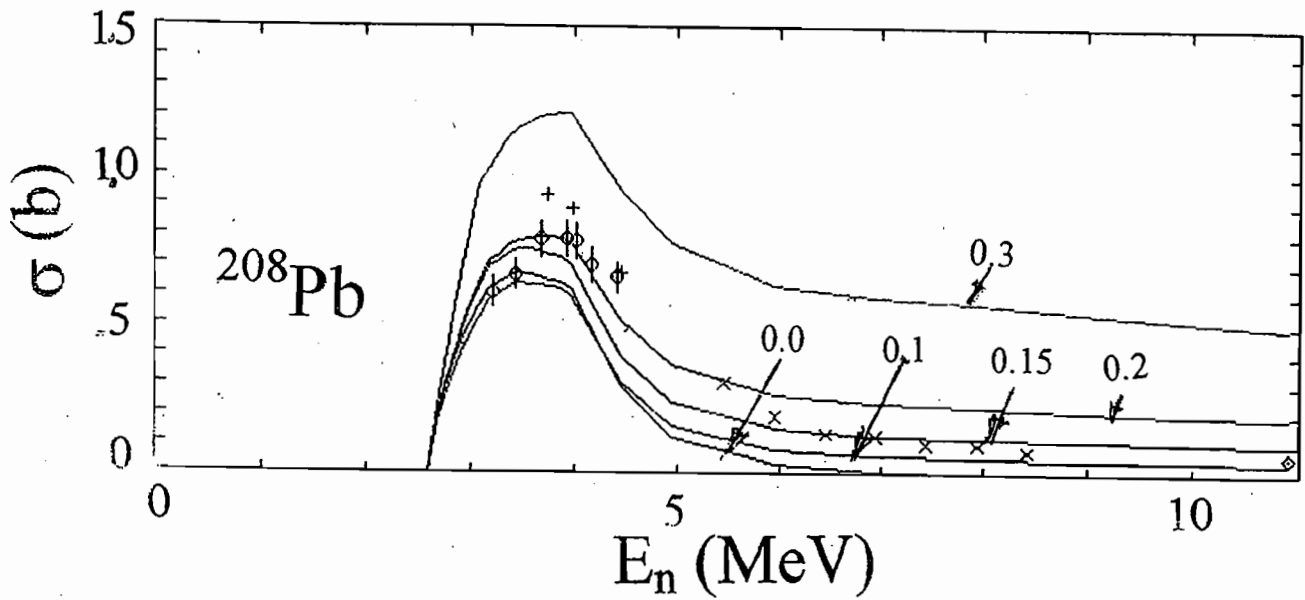


Fig. V-7. Comparison of measured and calculated inelastic neutron-scattering cross section for the excitation of the 2.61 MeV 3- levels in ^{208}Pb . Curves indicate the results of calculations using the indicated β_3 values as described in the text. Symbols indicate the results of measurements as referenced in the text.

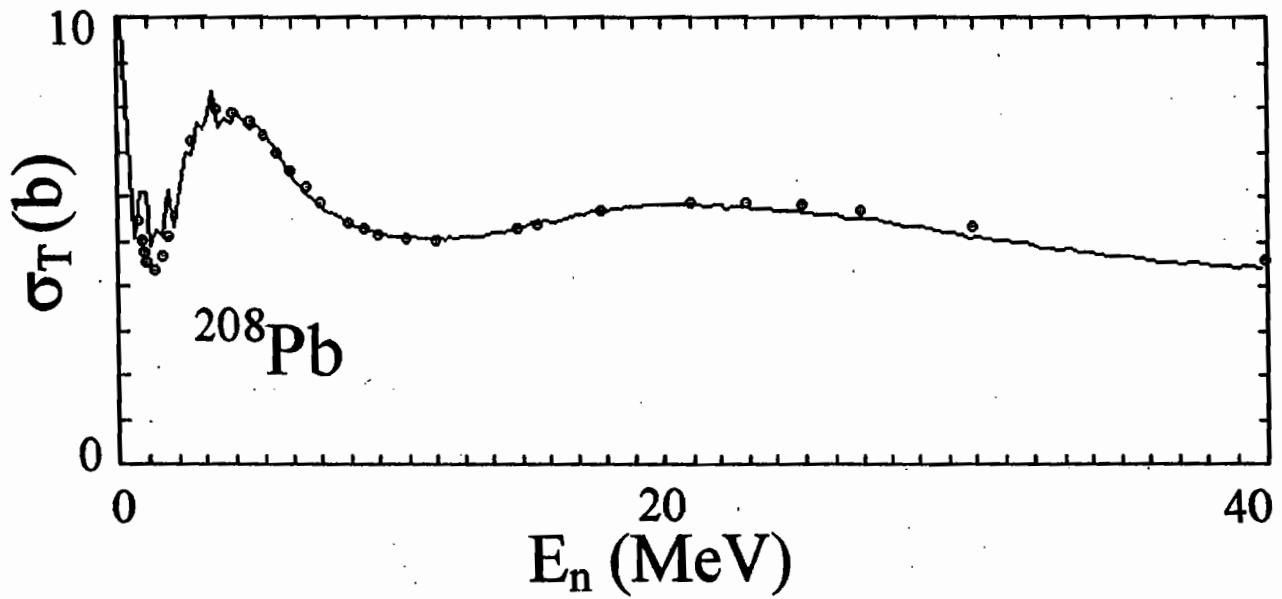


Fig. V-8. Comparisons of measured (curve) and calculated (symbols) neutron total cross sections of ^{208}Pb . The calculations used the three-level vibrational model of Table V-6 as described in the text.

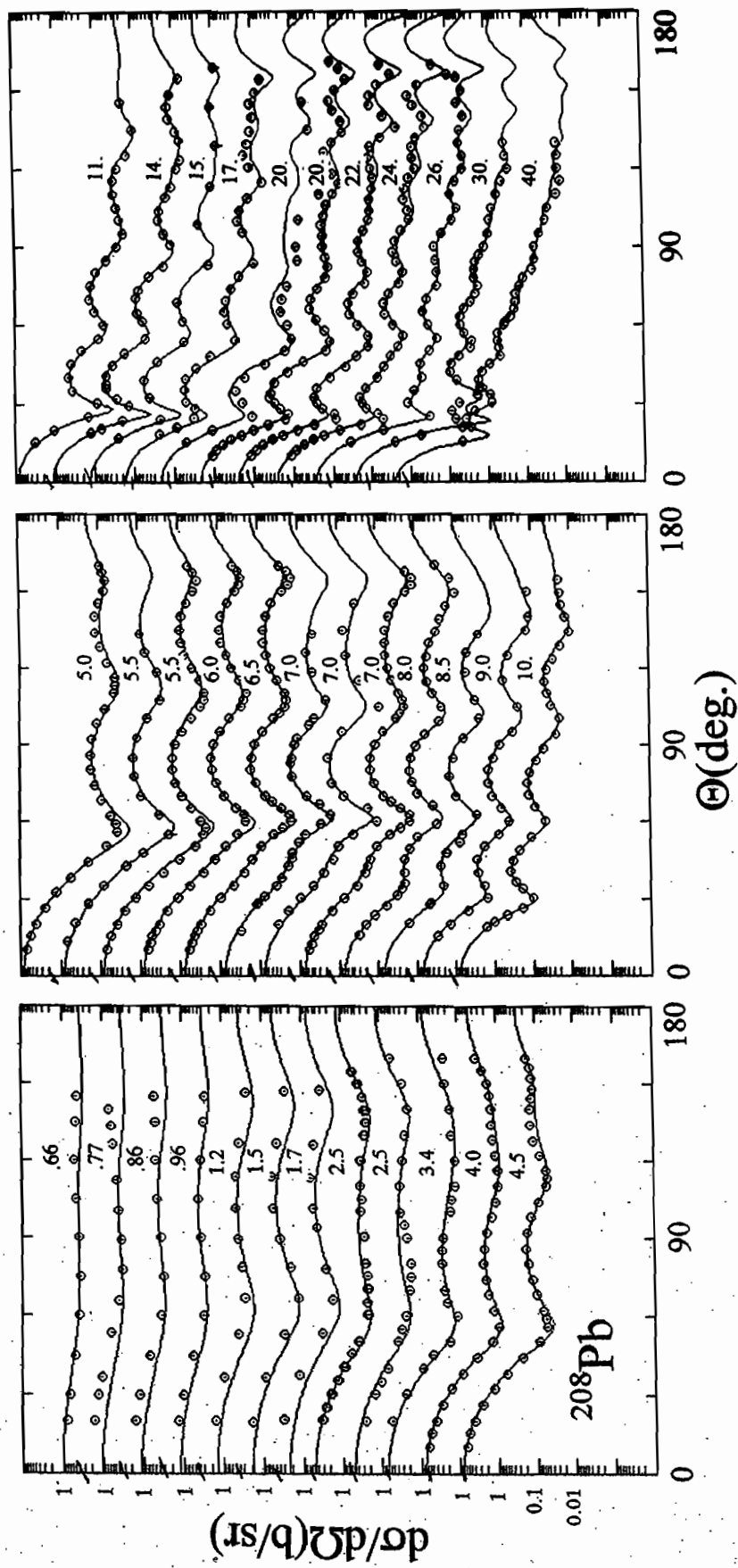


Fig. V-9. Comparisons of measured (symbols) and calculated (curves) ^{208}Pb elastic-scattering angular distributions. The calculations used the three-level vibrational model described in the text with the parameters of Table V-6.

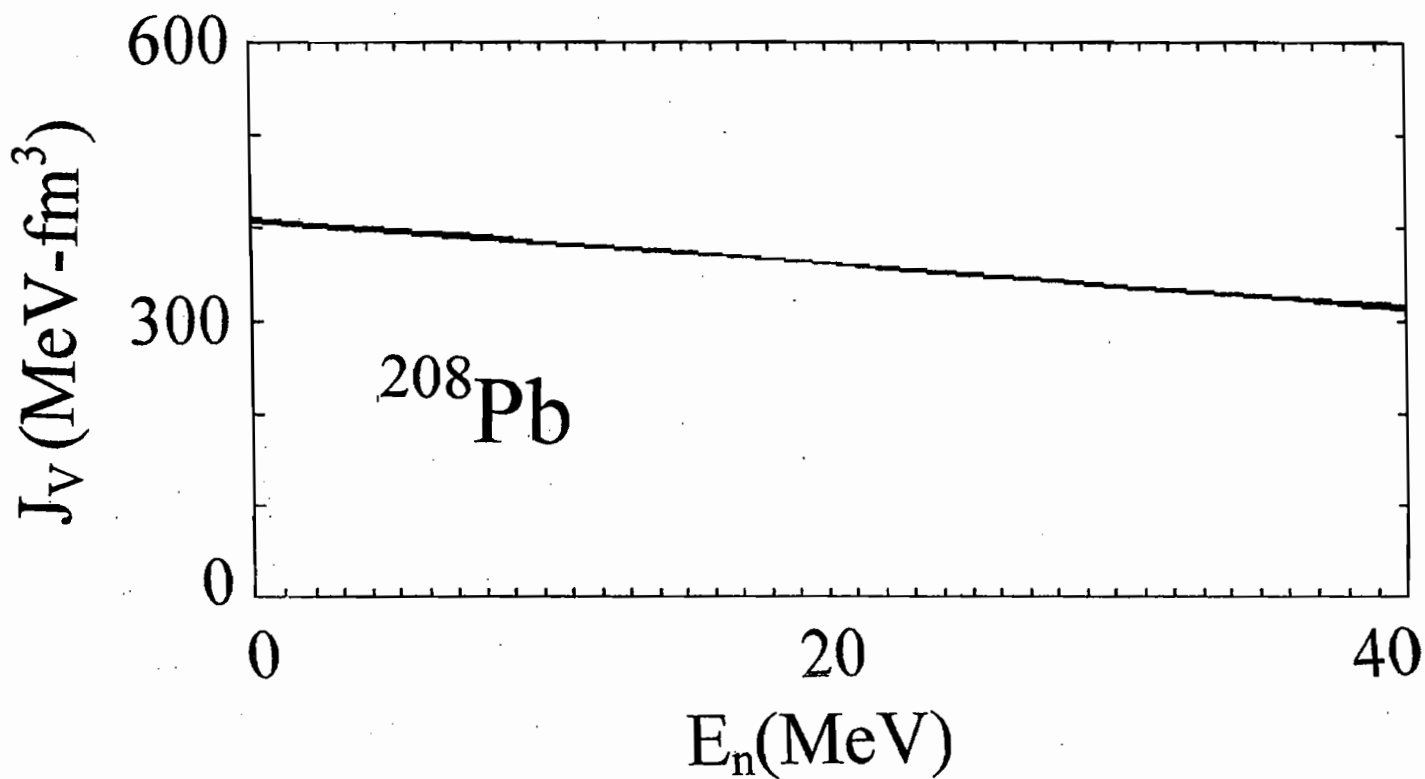


Fig. VI-1. Real-potential strengths as a function of energy for the ten ASYM values of **Tables V-1 to V-10**. These strengths are indicated by ten curves. They are essentially indistinguishable from one another.

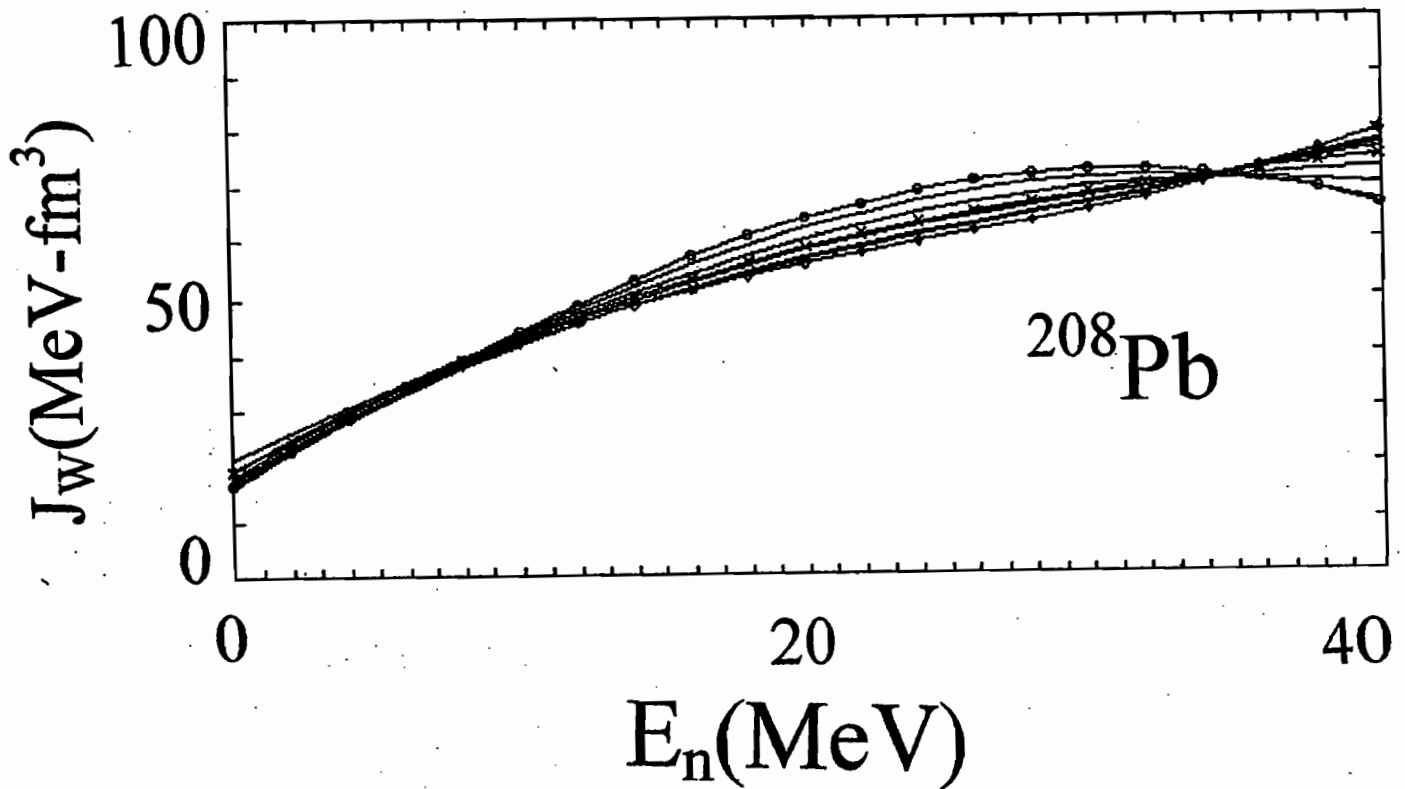


Fig. VI-2. Imaginary potential strengths, J_w , of Tables VI-1 to VI-10 as a function of energy. These ten curves systematically change from $\text{ASYM} = 1.0 + 0.00 \cdot E$ (O symbols), to $\text{ASYM} = 1.0 + 0.50 \cdot E$ (\blacklozenge symbols). The J_w values steadily decrease with asymmetry to ≈ 35 MeV.

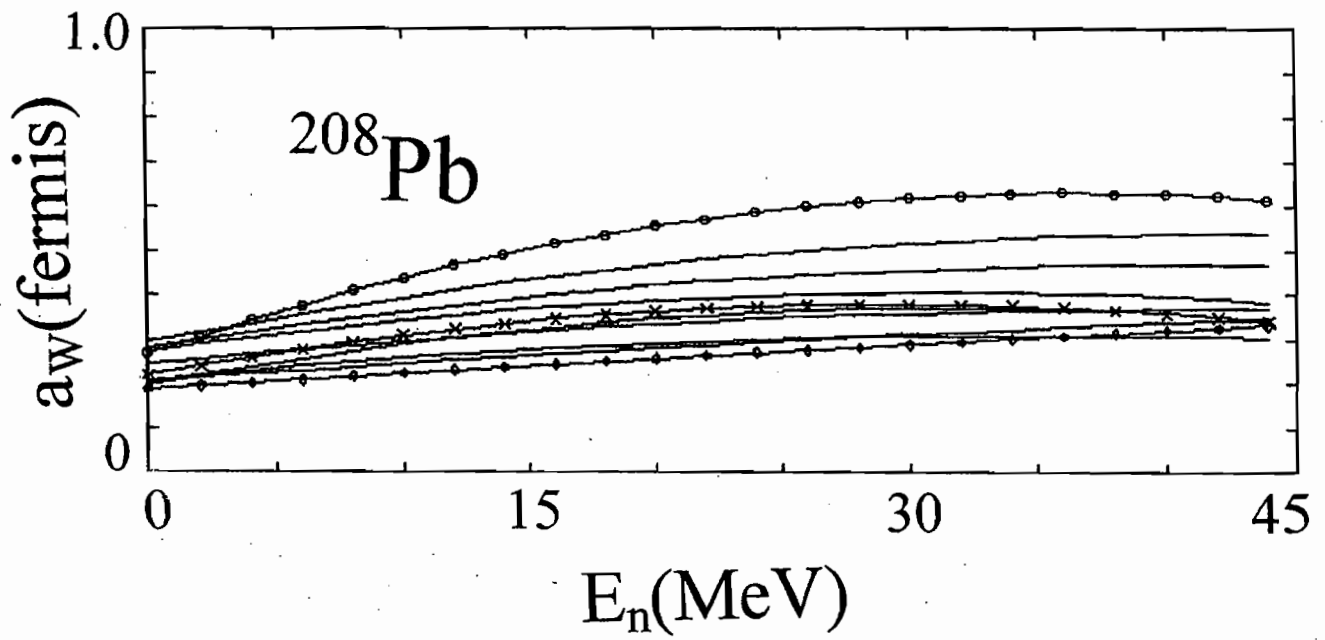


Fig. VI-4. Energy dependencies of the a_w values of the asymmetric potentials of Tables VI-1 to VI-10. The symbols have the same connotations as in Fig. V-2.

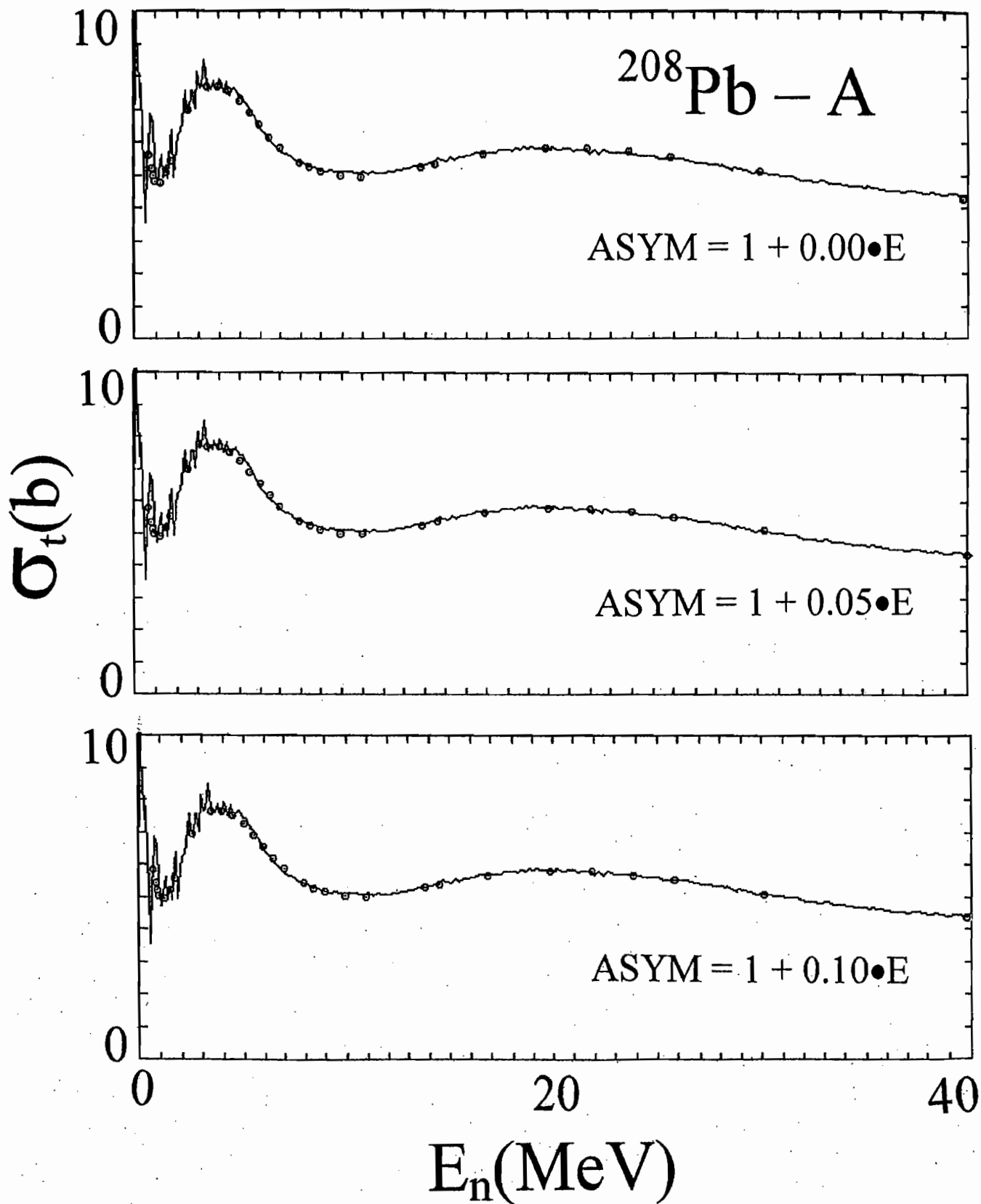
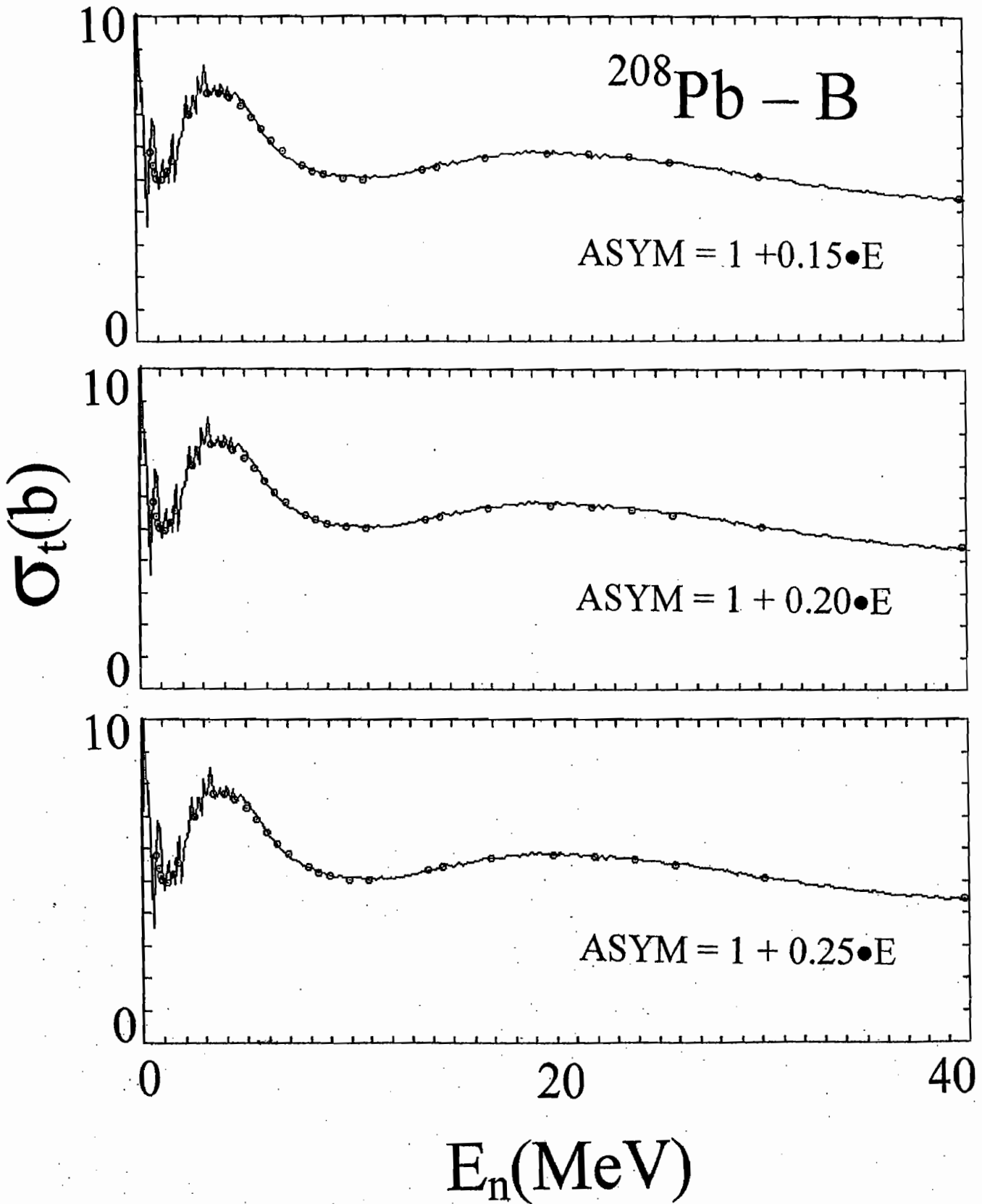
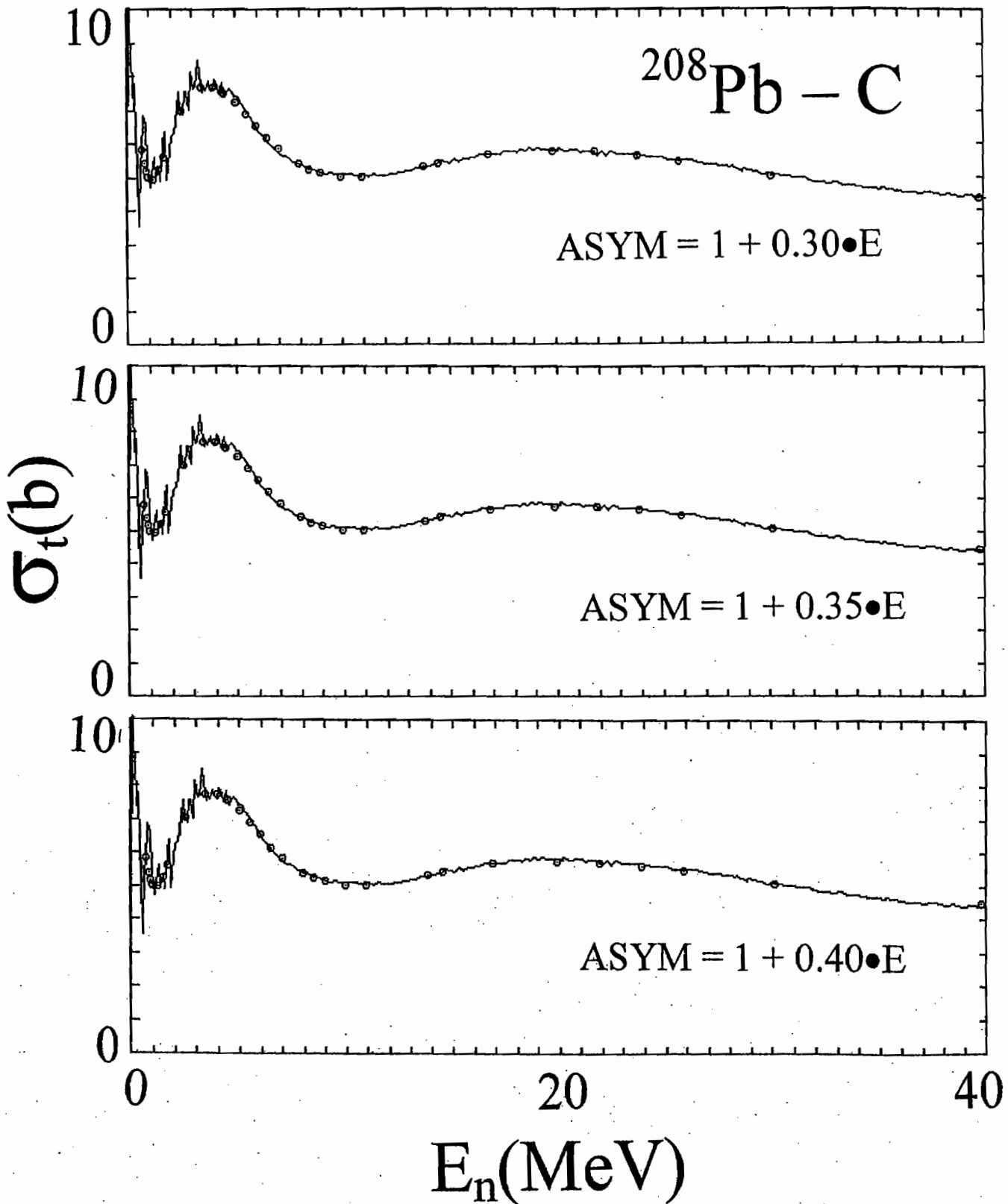
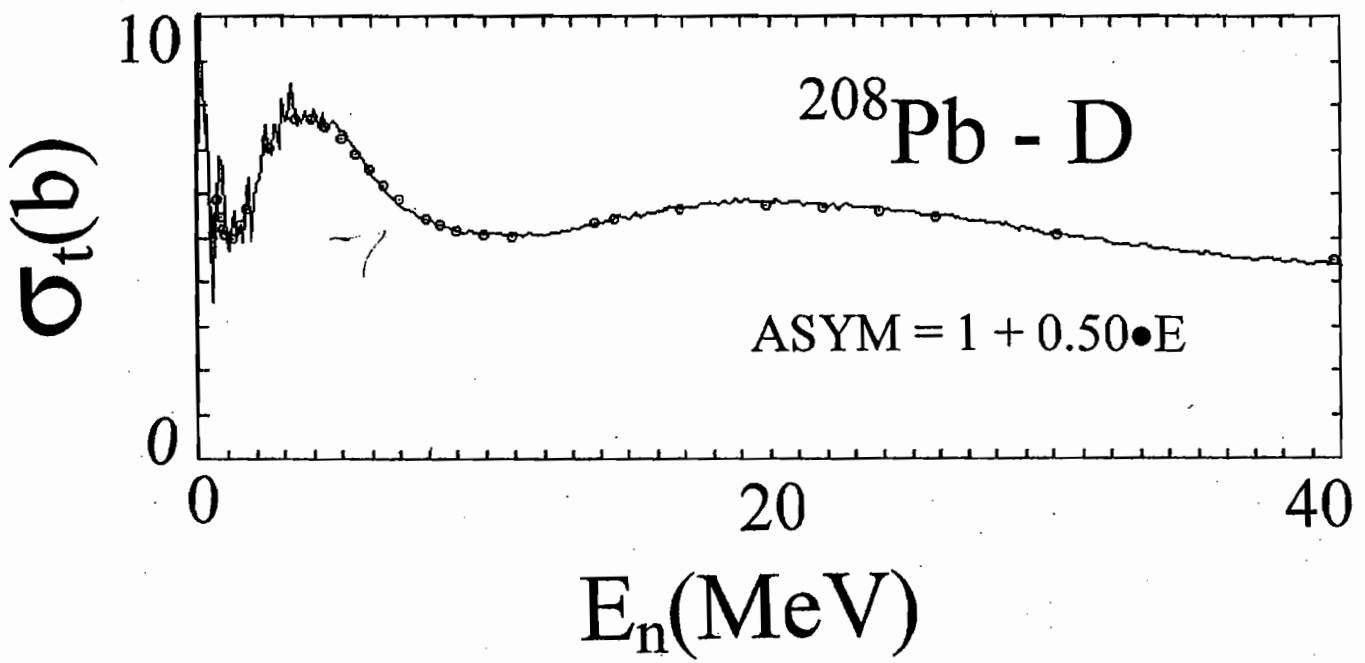


Fig. VI-5. Comparisons of averaged ^{209}Pb total cross sections (curves) with values calculated with various ASYM values (symbols) as noted on panels A through D of the figure.







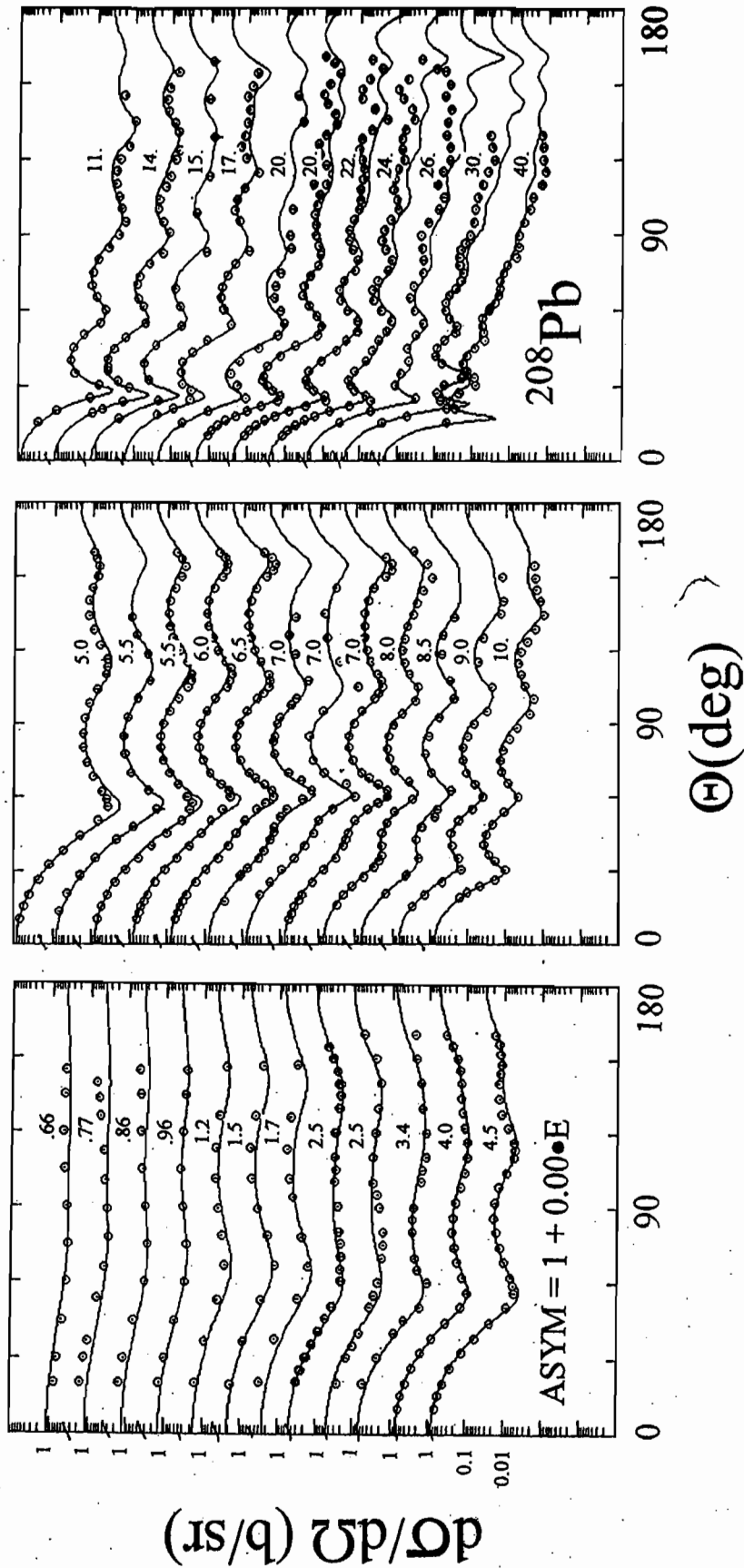


Fig. VI-6. Comparisons of measured and calculated ^{208}Pb elastic-scattering cross sections. The measured values are indicated by symbols and the calculations by curves. The potential is that of Table VI-1 where $ASYM = 0.00E$, i.e. comparable to the simple SOM model. Incident energies are numerically noted.

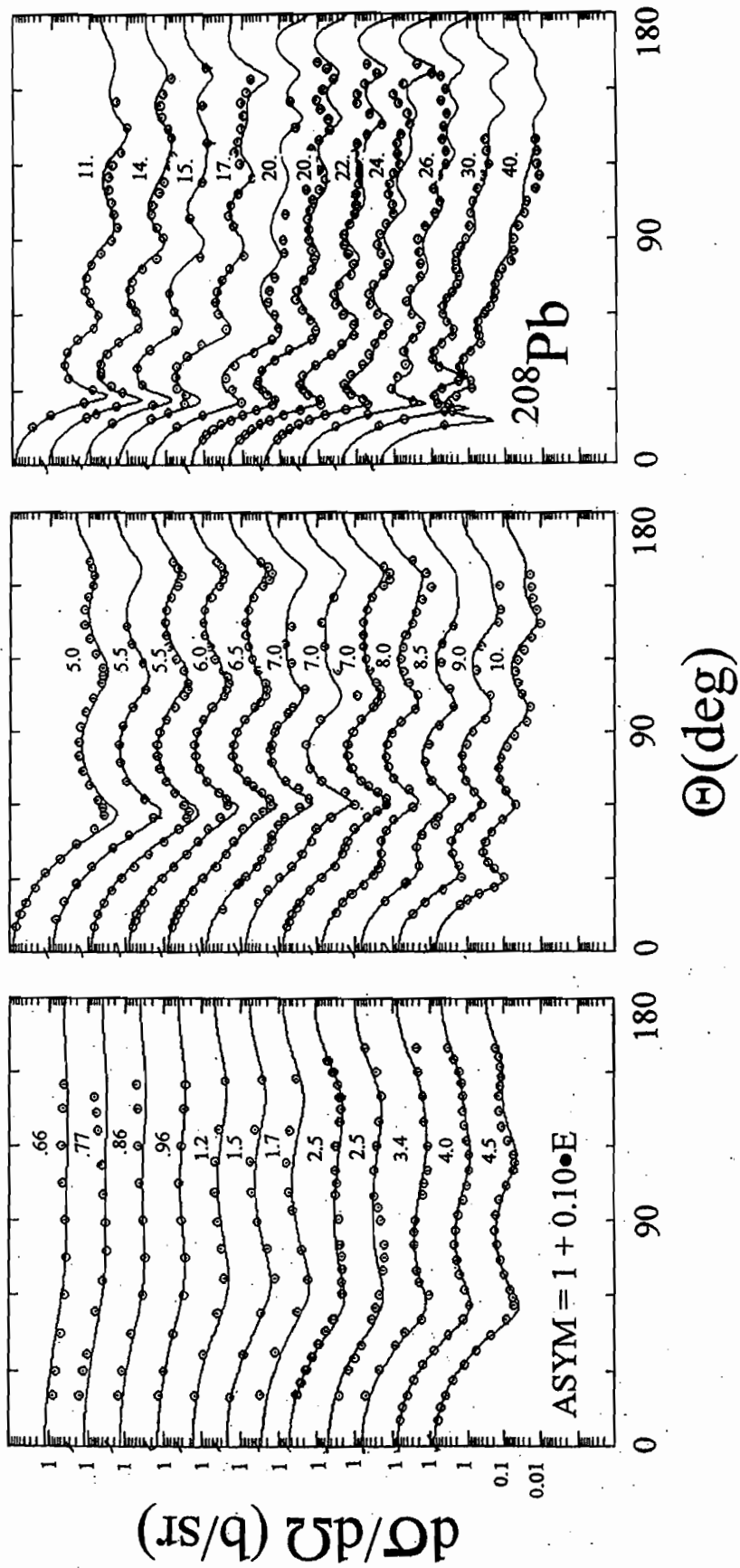


Fig. VI-7. Same as Fig. VI-6, but using the potential of Table VI-3 where $\text{ASYM} = 1.0 + 0.10 \bullet E$.

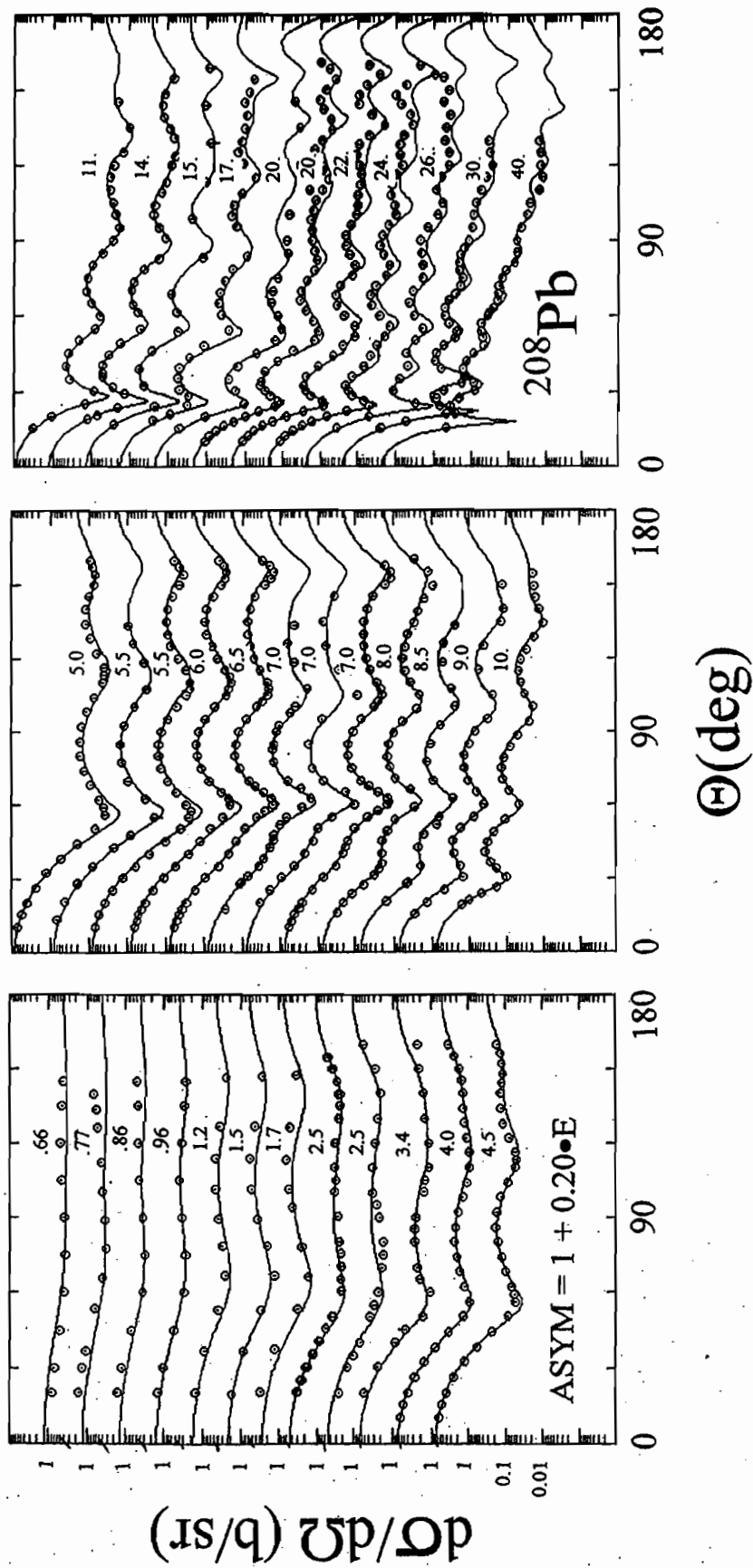


Fig. VI-8. Same as Fig. VI-6, but using the potential of Table VI-5 where $\text{ASTM} = 1.0 + 0.20 \bullet E$.

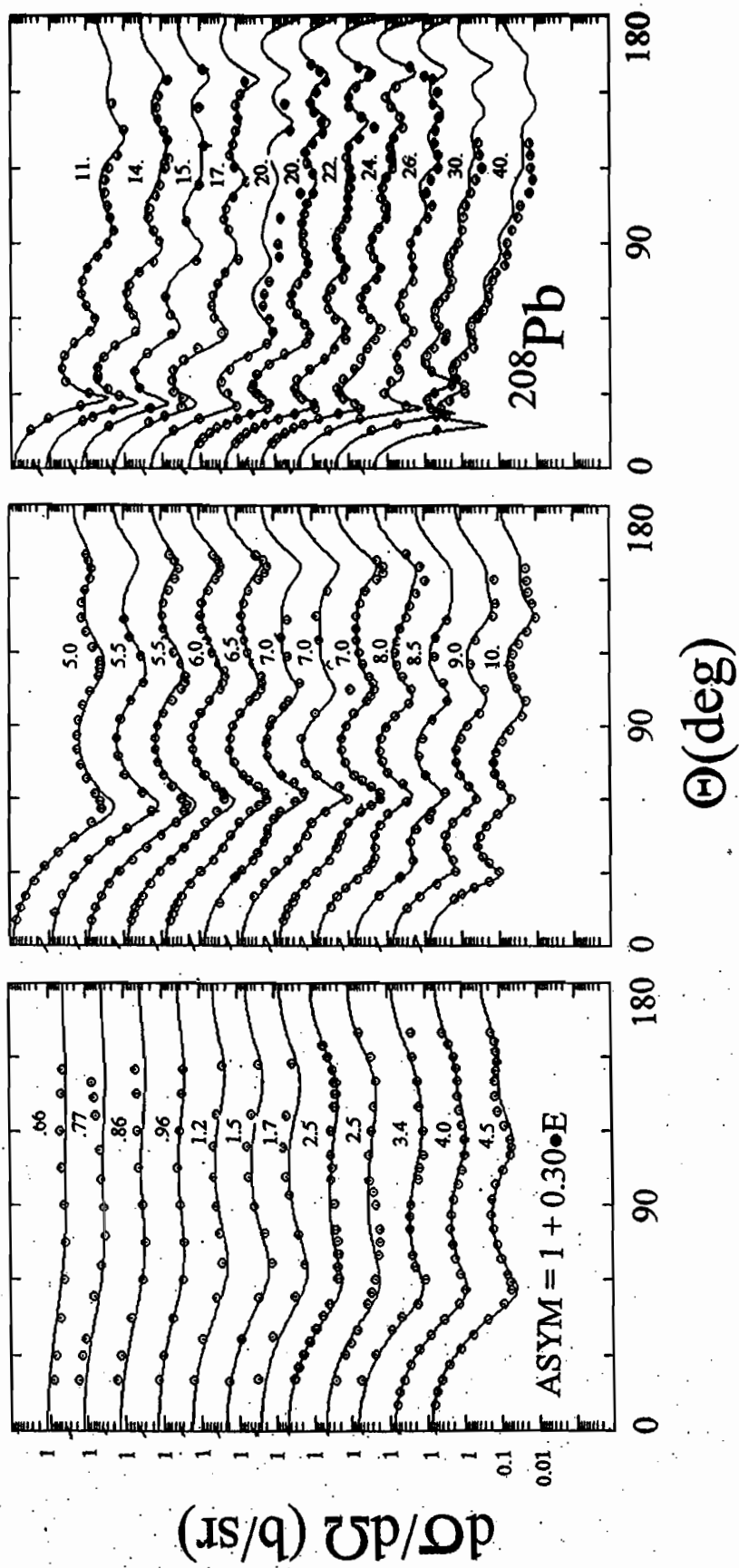


Fig. VI-9. Same as Fig. VI-6, but using the potential of Table VI-7 where $ASYM = 1.0 + 0.30E$.

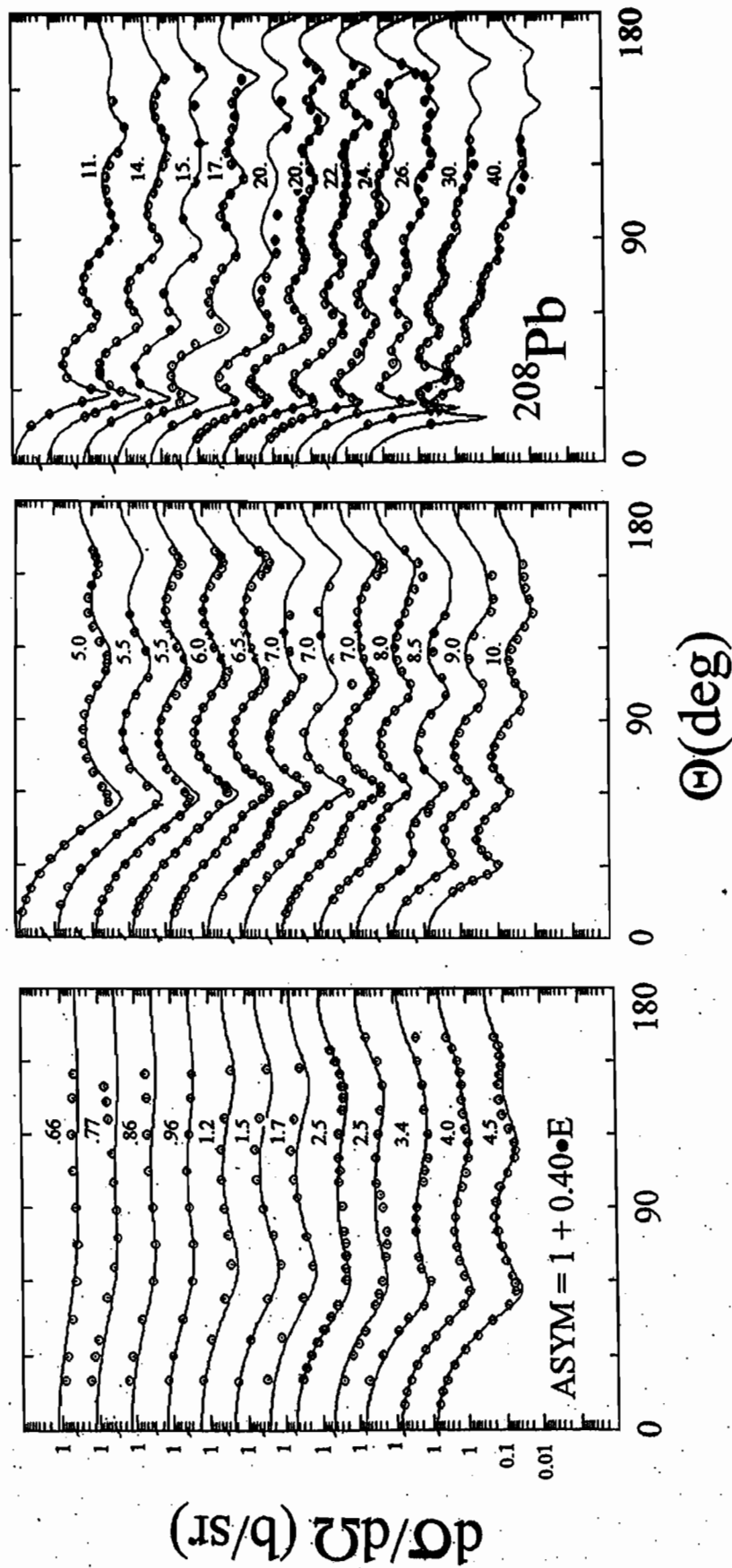


Fig. VI-10. Same as Fig. VI-6, but using the potential of Table VI-9 where $\text{ASYM} = 1.0 + 0.40 \bullet E$.

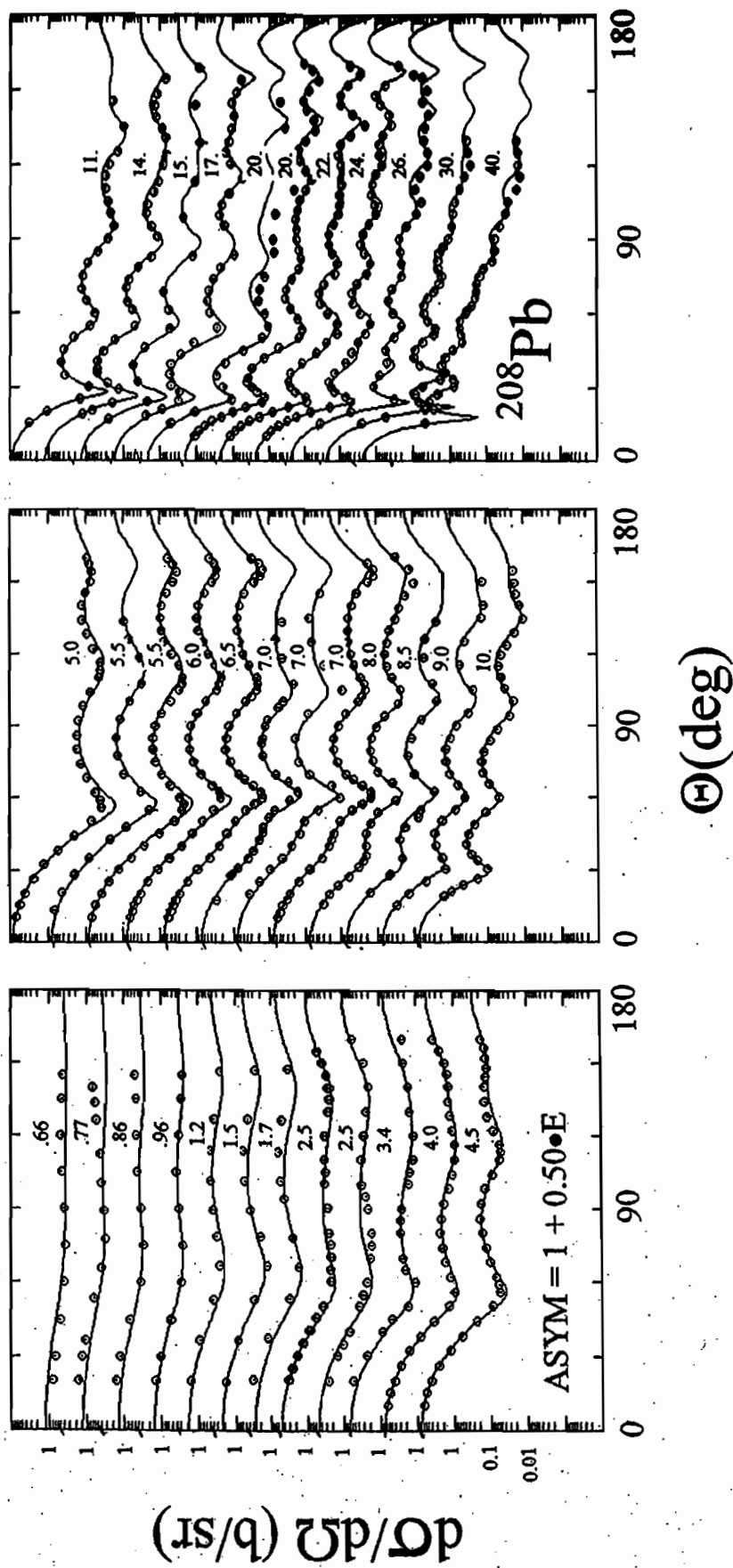


Fig. VI-11. Same as Fig. VI-6, but using the potential of Table VI-10 where ASYM = $1.0 + 0.50 \bullet E$.

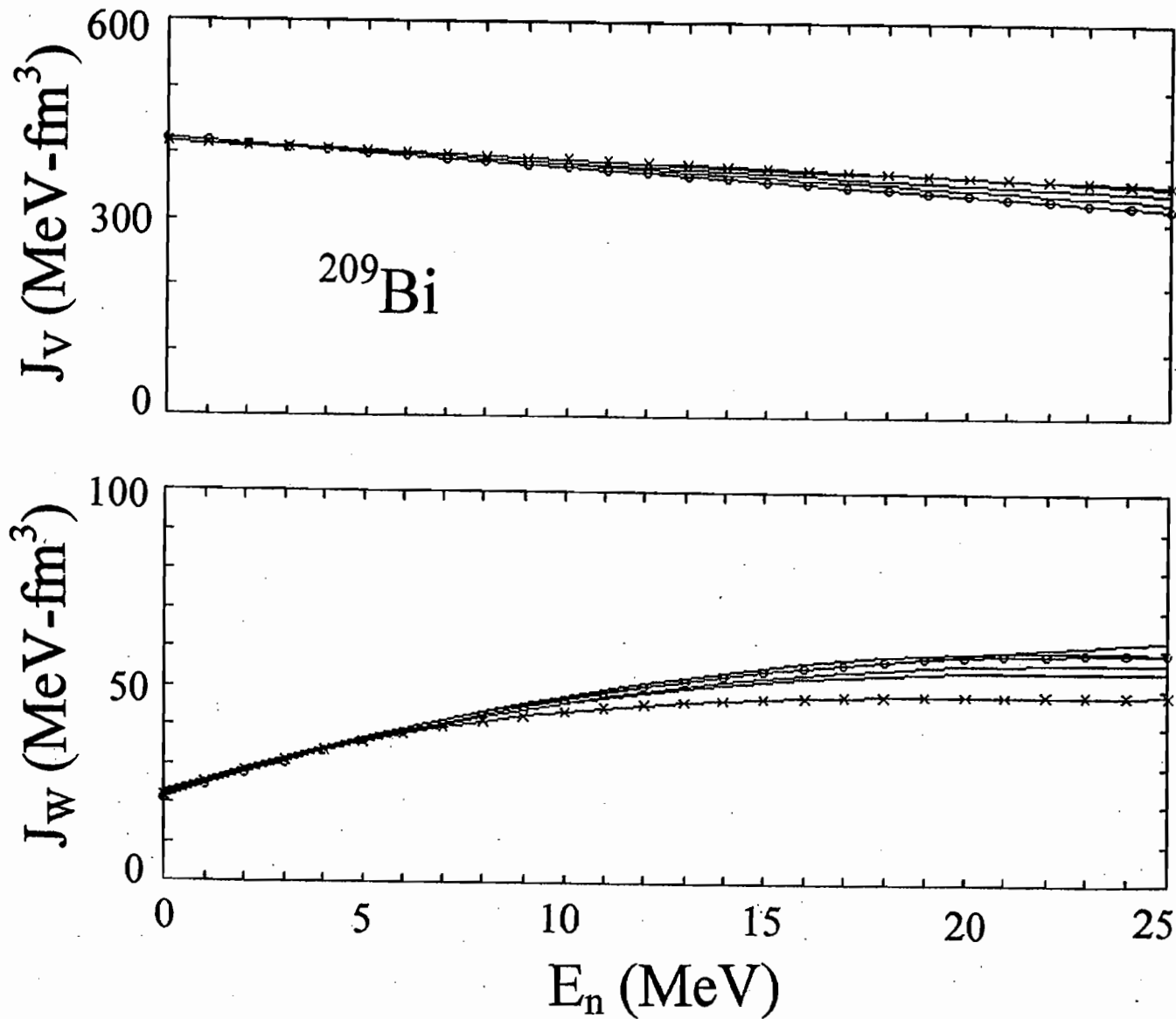


Fig. VI-12. Energy dependencies of the real (J_V) and imaginary (J_W) potential strengths resulting from 6-parameter fitting of the ^{209}Bi data base. The curves indicate increasing ASYM values from $ASYM = 1 + 0.00 \cdot E$ ("O" symbols) to $ASYM = 1 + 0.50 \cdot E$ ("X" symbols).

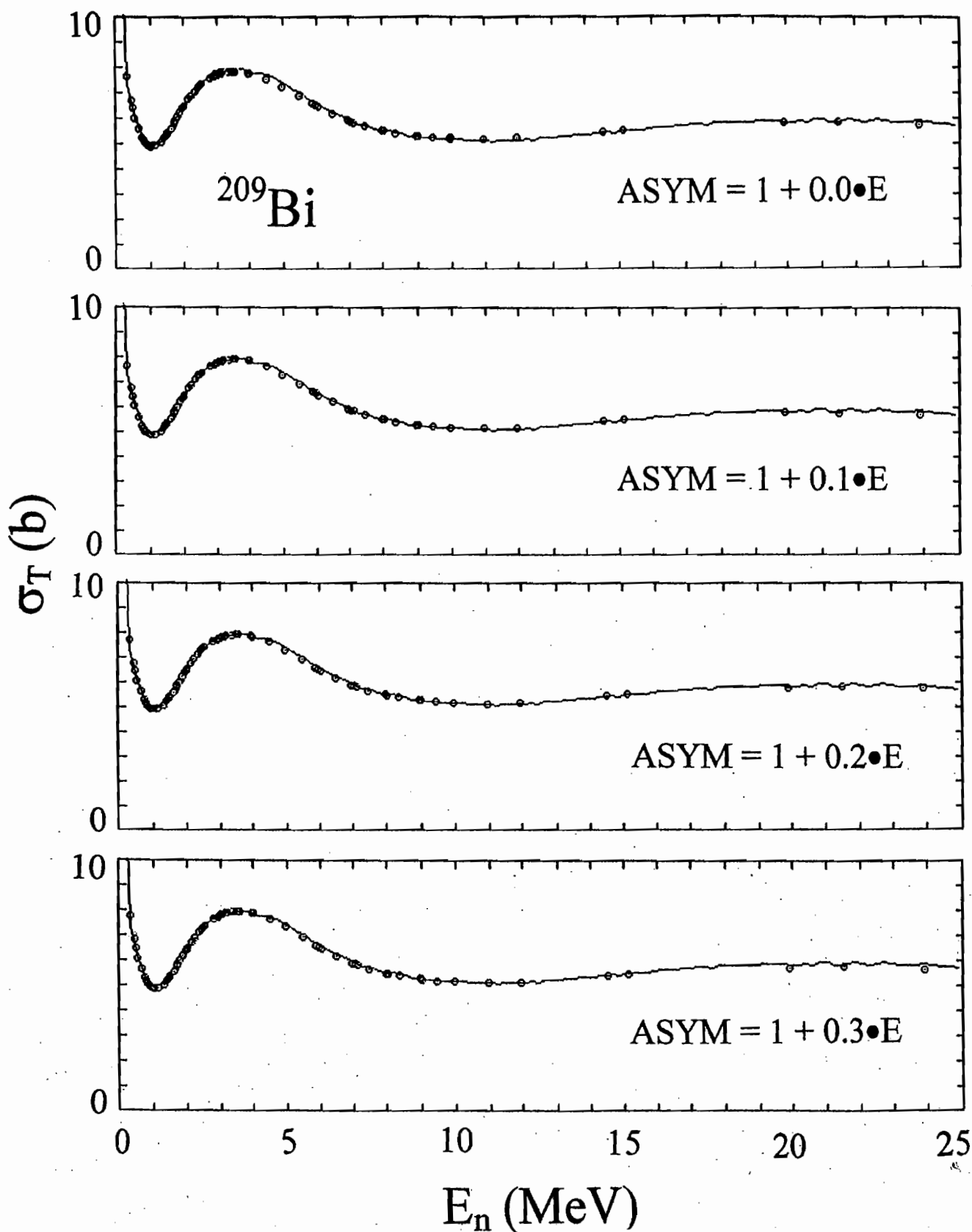
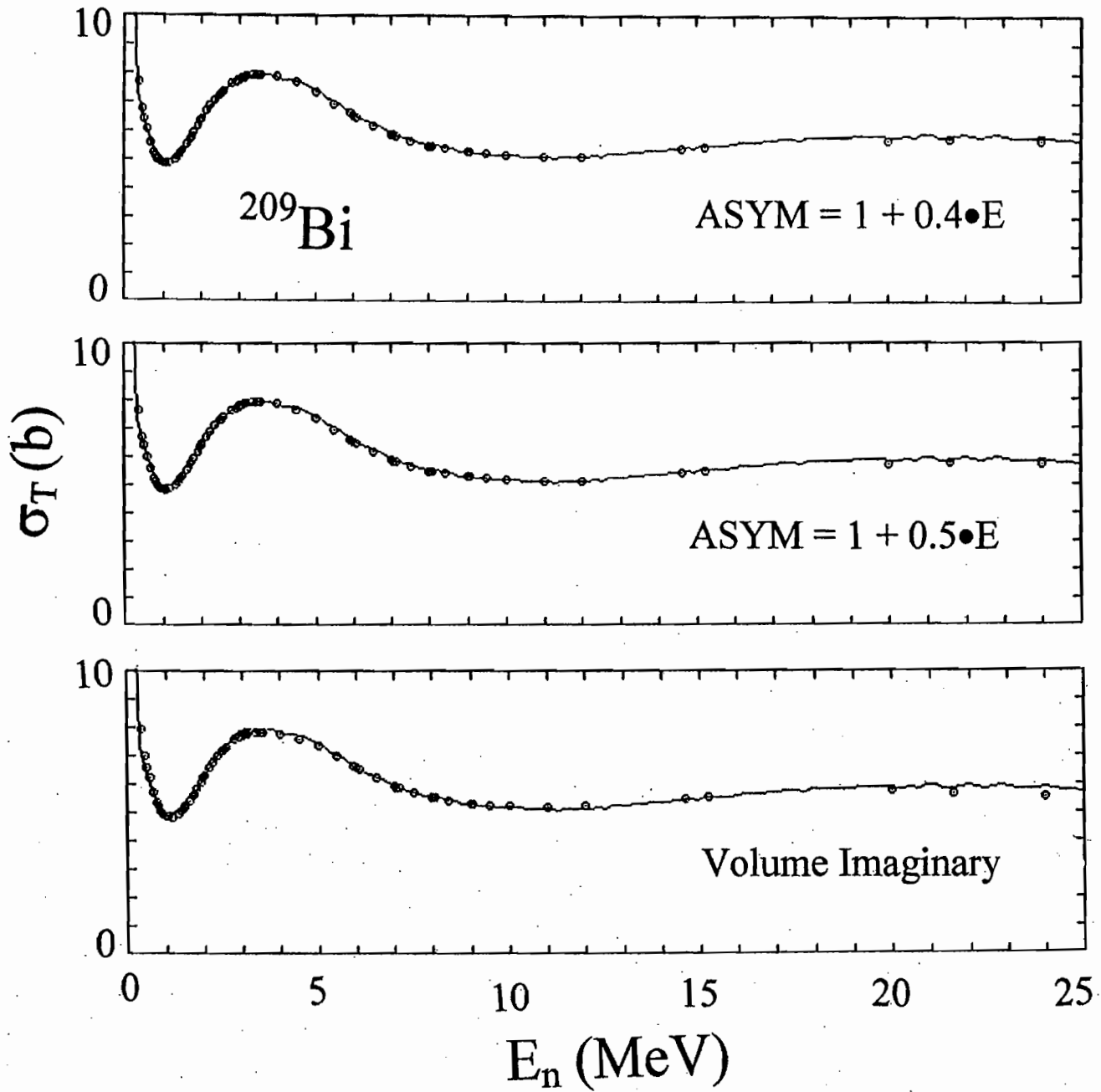


Fig. VI-13. Comparisons of measured (curves) and calculated (symbols) ^{209}Bi neutron total cross sections using ASYM = $1 + 0.0 \cdot E$ to ASYM = $1 + 0.5 \cdot E$ and the corresponding potentials of **Tables VI-15 to VI-20**. The final panel of the figure makes the same comparisons using a Saxon-Woods volume absorption as per **Table VI-21**.



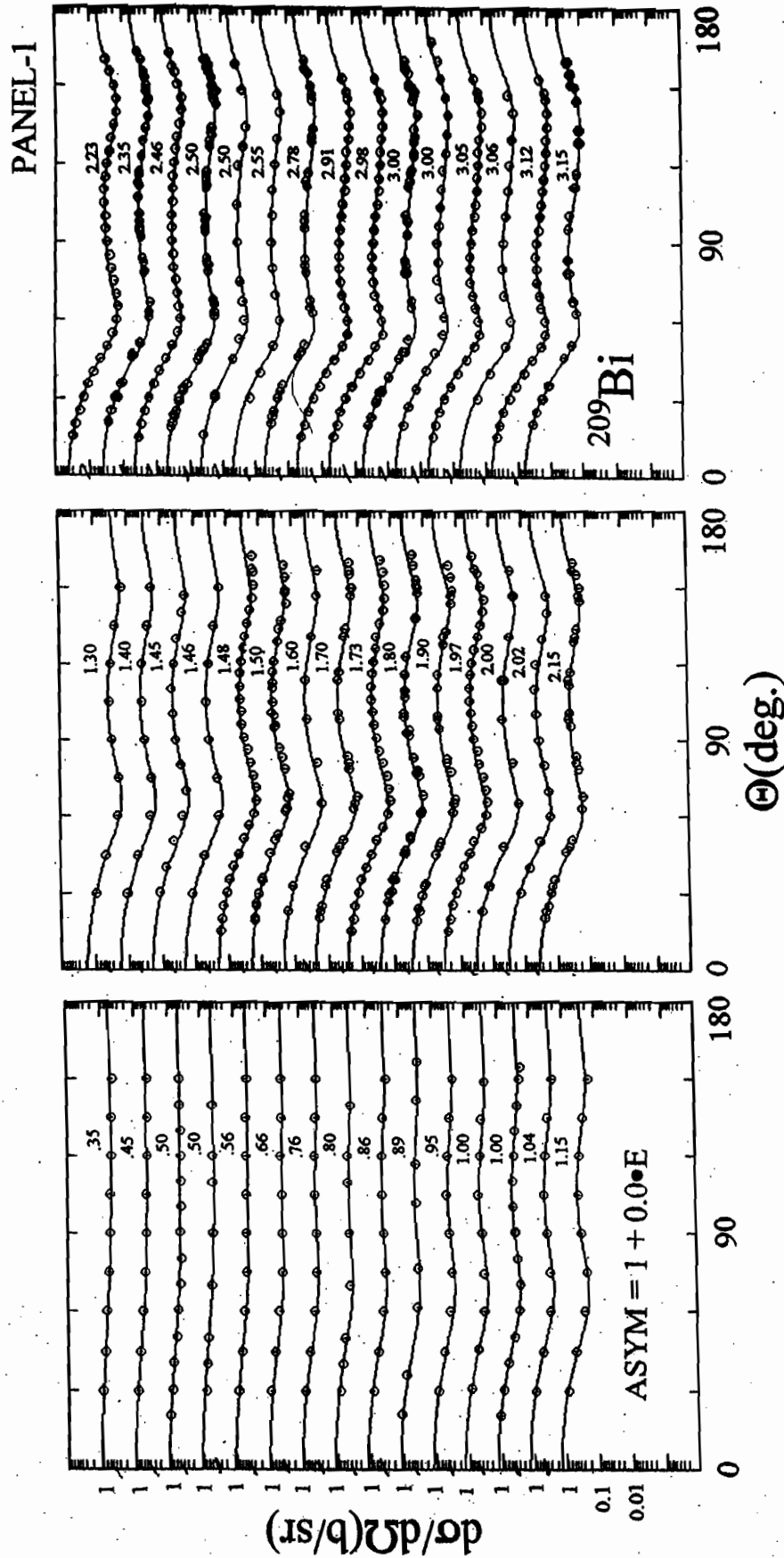
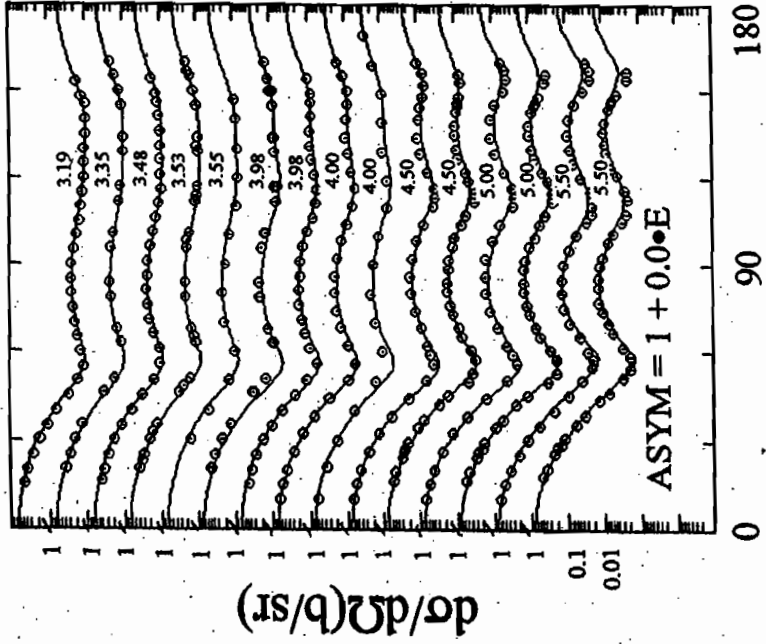
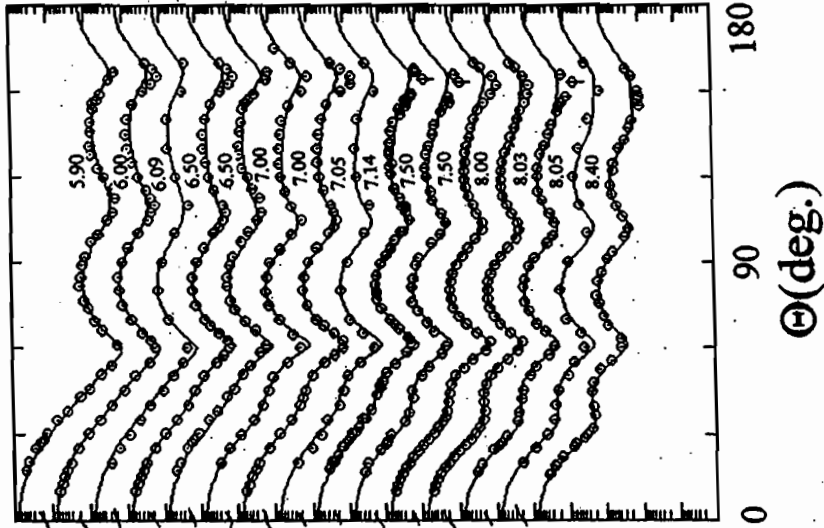
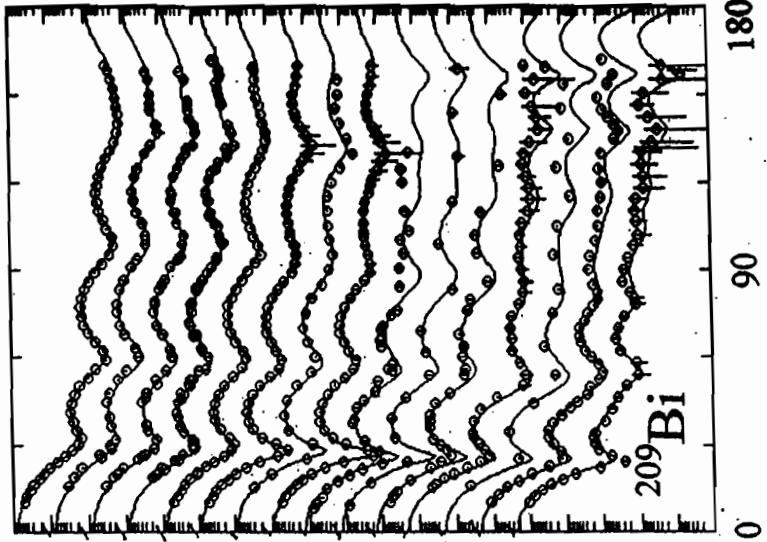


Fig. VI-14. Comparisons of measured (symbols) and calculated (curves) differential elastic scattering cross sections of ^{209}Bi . The calculations used the potential of Table V-15 where ASYM = 1 + 0.00E, i.e. a spherical calculation. The incident neutron laboratory energies are numerically cited for each distribution. The two panels of the figure represent results from 0.35 to 24.0 MeV.

PANEL-2



PANEL-1

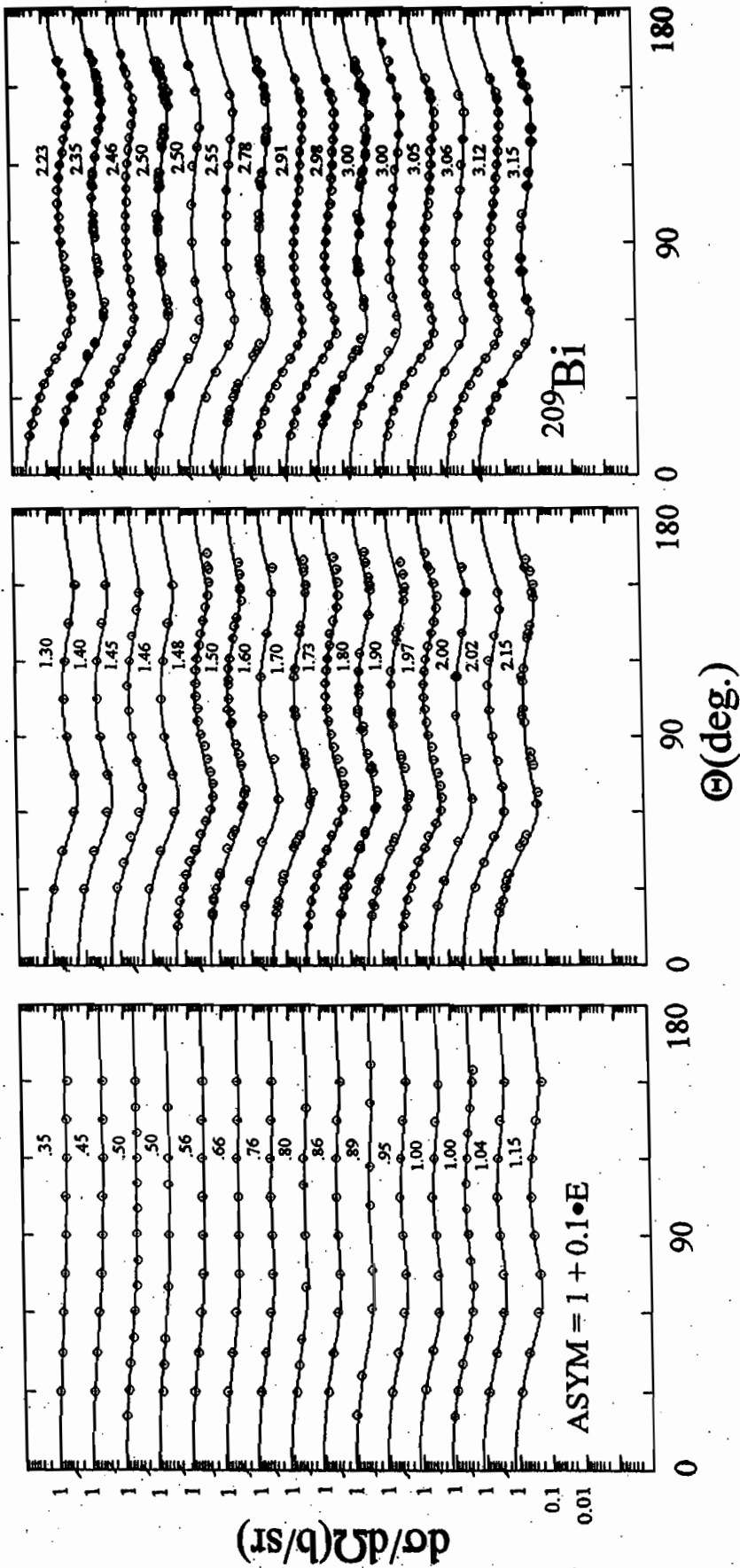
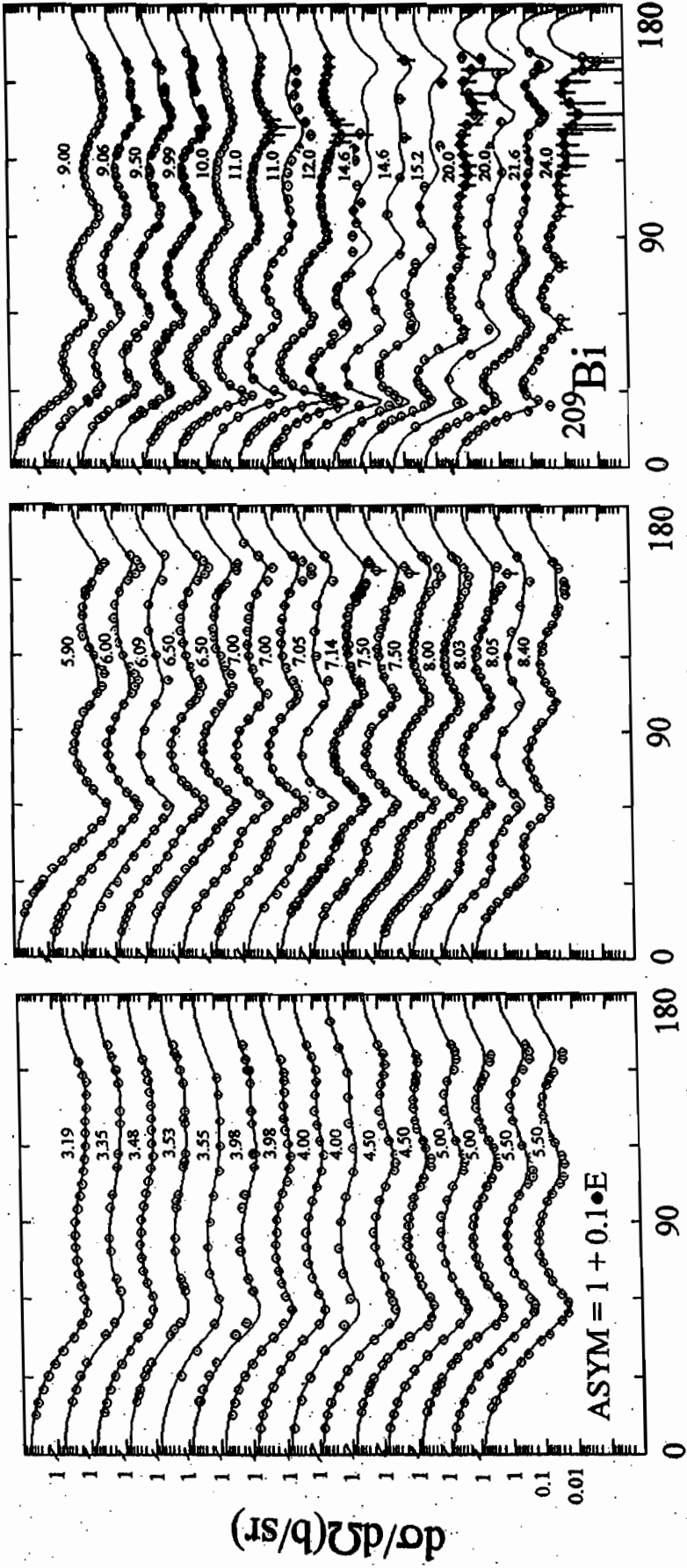


Fig. VI-15. Comparisons of measured (symbols) and calculated (curves) differential elastic scattering cross sections of ^{209}Bi . The calculations used the potential of Table V-16 where $\text{ASYM} = 1 + 0.10 \cdot E$. Otherwise the nomenclature is the same as that of Fig. V-14.

PANEL-2



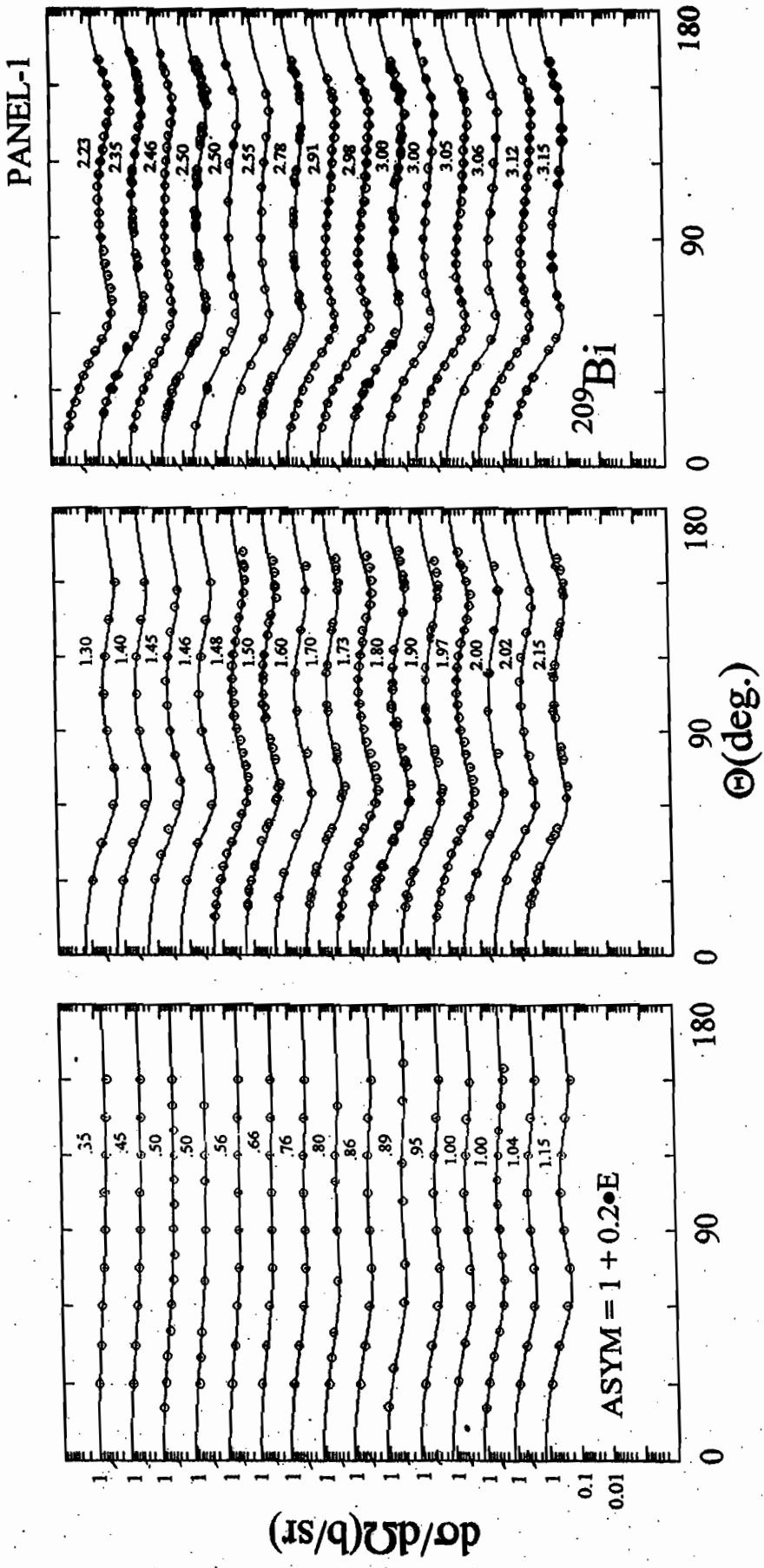
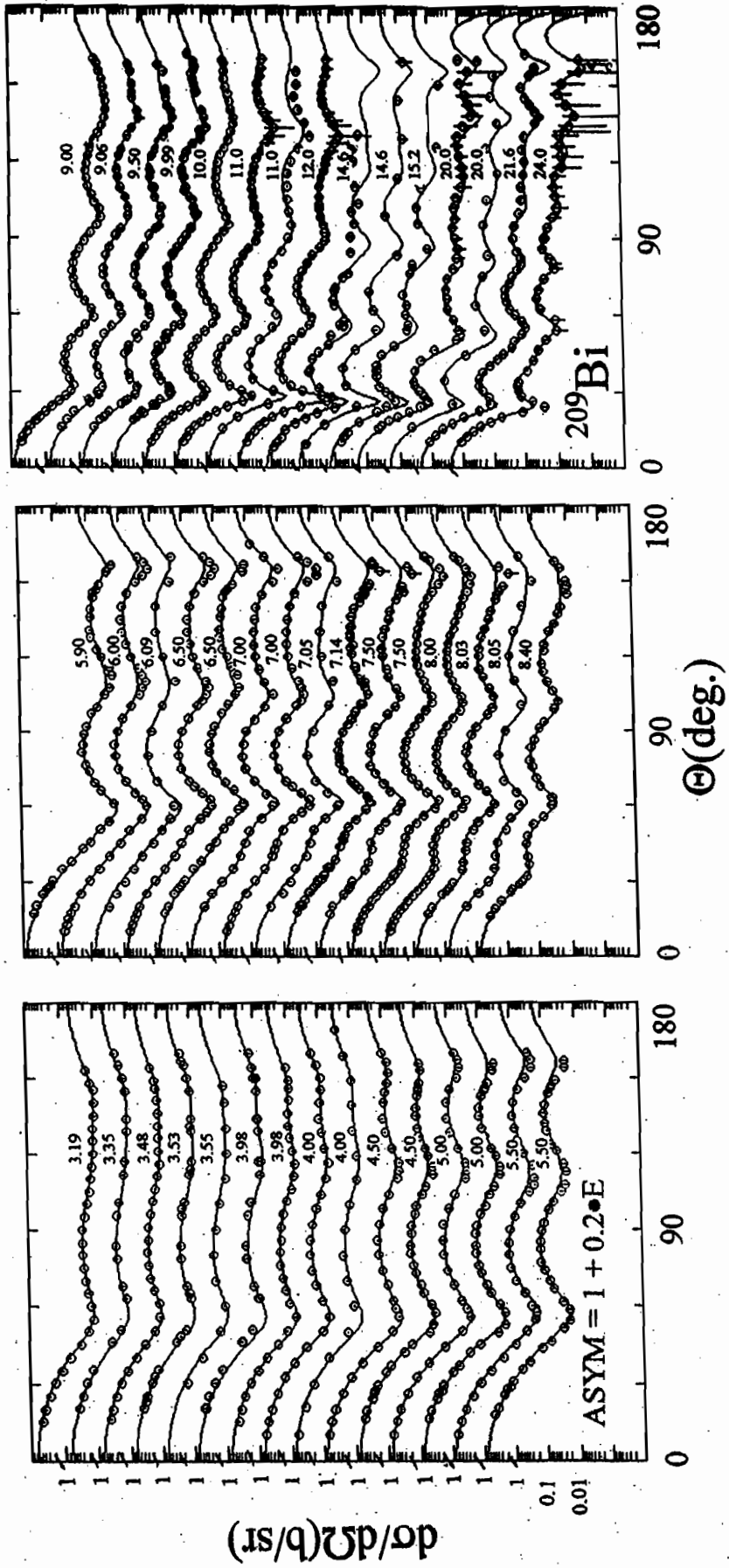


Fig. VI-16. Comparisons of measured (symbols) and calculated (curves) differential elastic scattering cross sections of ^{209}Bi . The calculations used the potential of Table VI-17 where ASYM = 1 + 0.20E. Otherwise the nomenclature is the same as that of Fig. 14.

PANEL-2



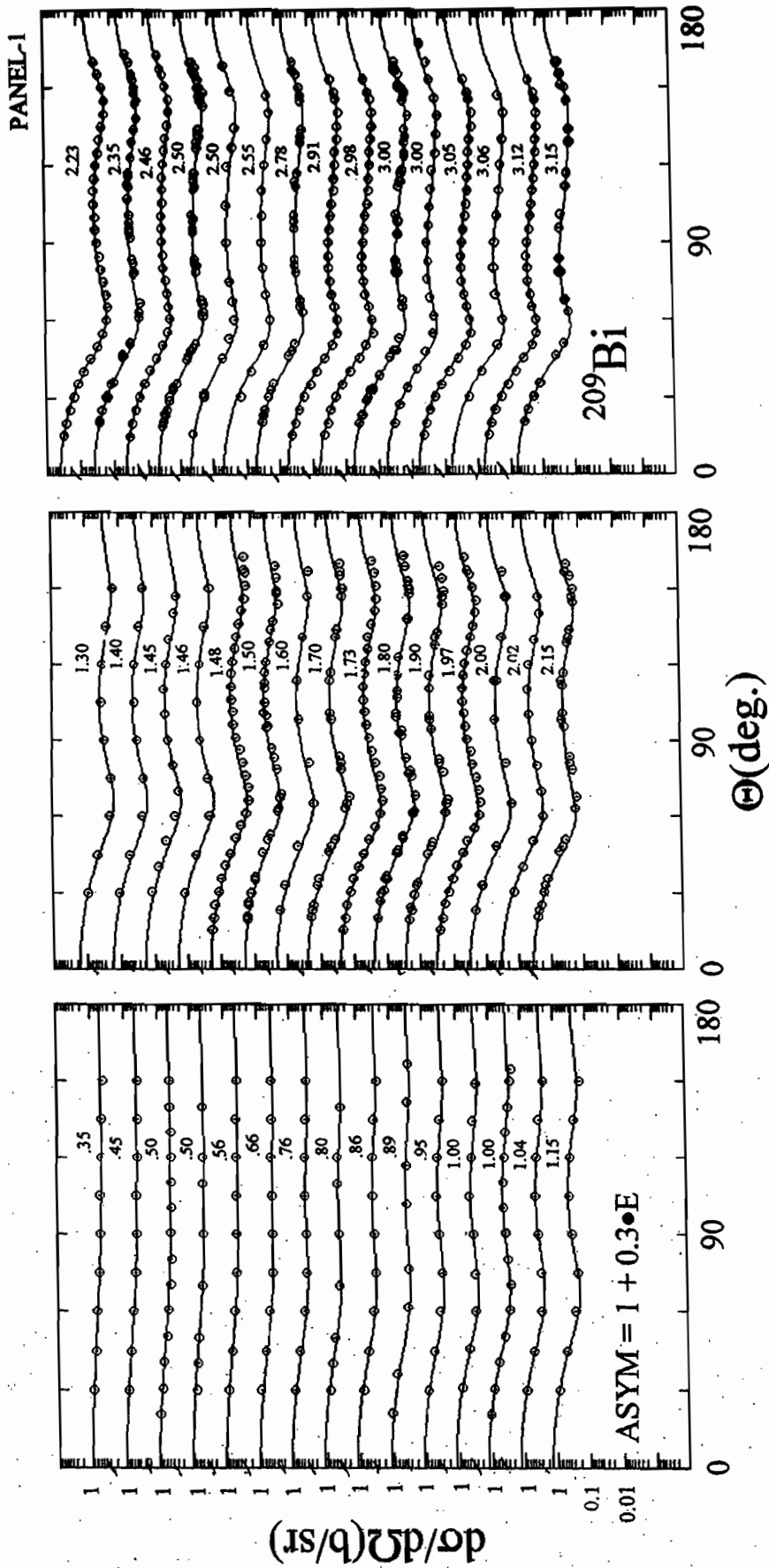
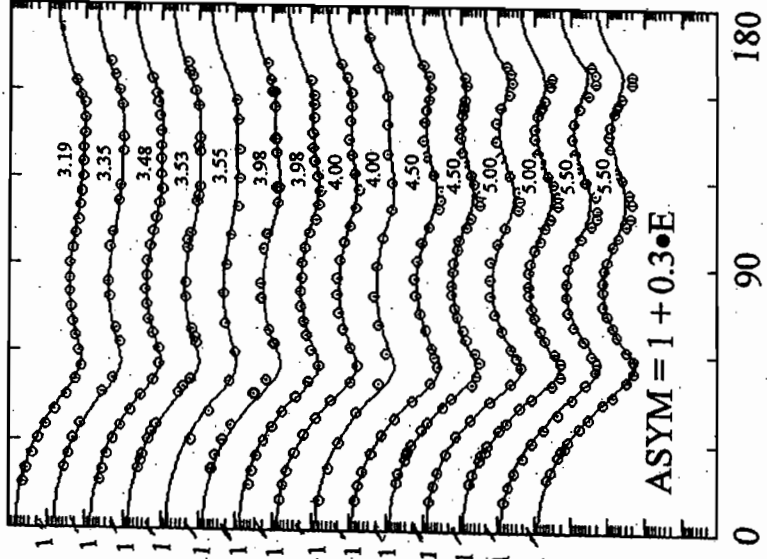
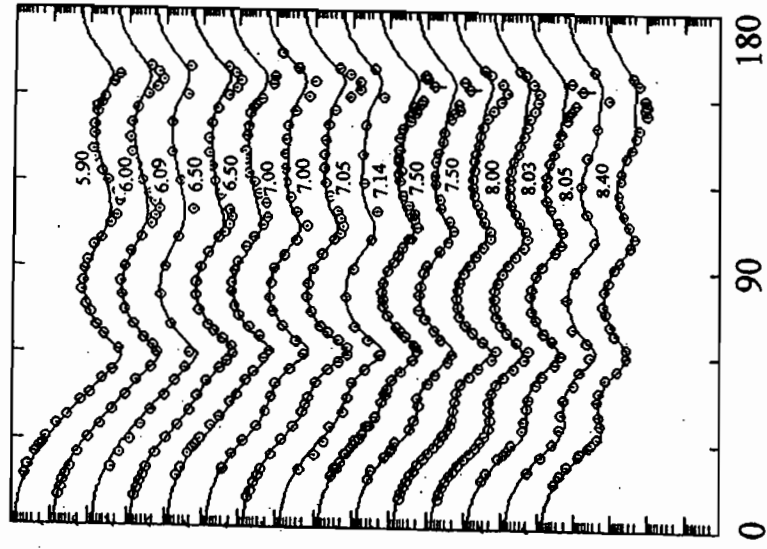
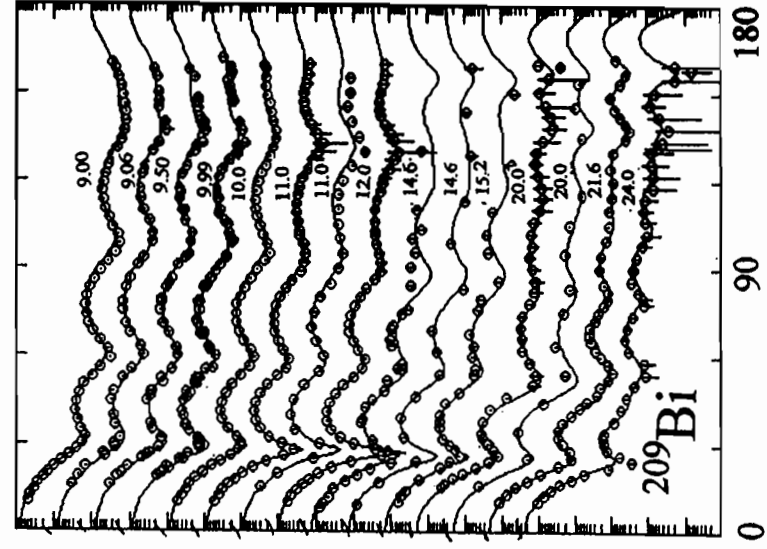


Fig. VI-17. Comparisons of measured (symbols) and calculated (curves) differential elastic scattering cross sections of ^{209}Bi . The calculations used the potential of Table VI-18 where ASYM = 1 + 0.30E. Otherwise the nomenclature is the same as that of Fig. VI-14.

PANEL-2



$d\sigma/d\Omega(\text{b/sr})$

$\Theta(\text{deg.})$

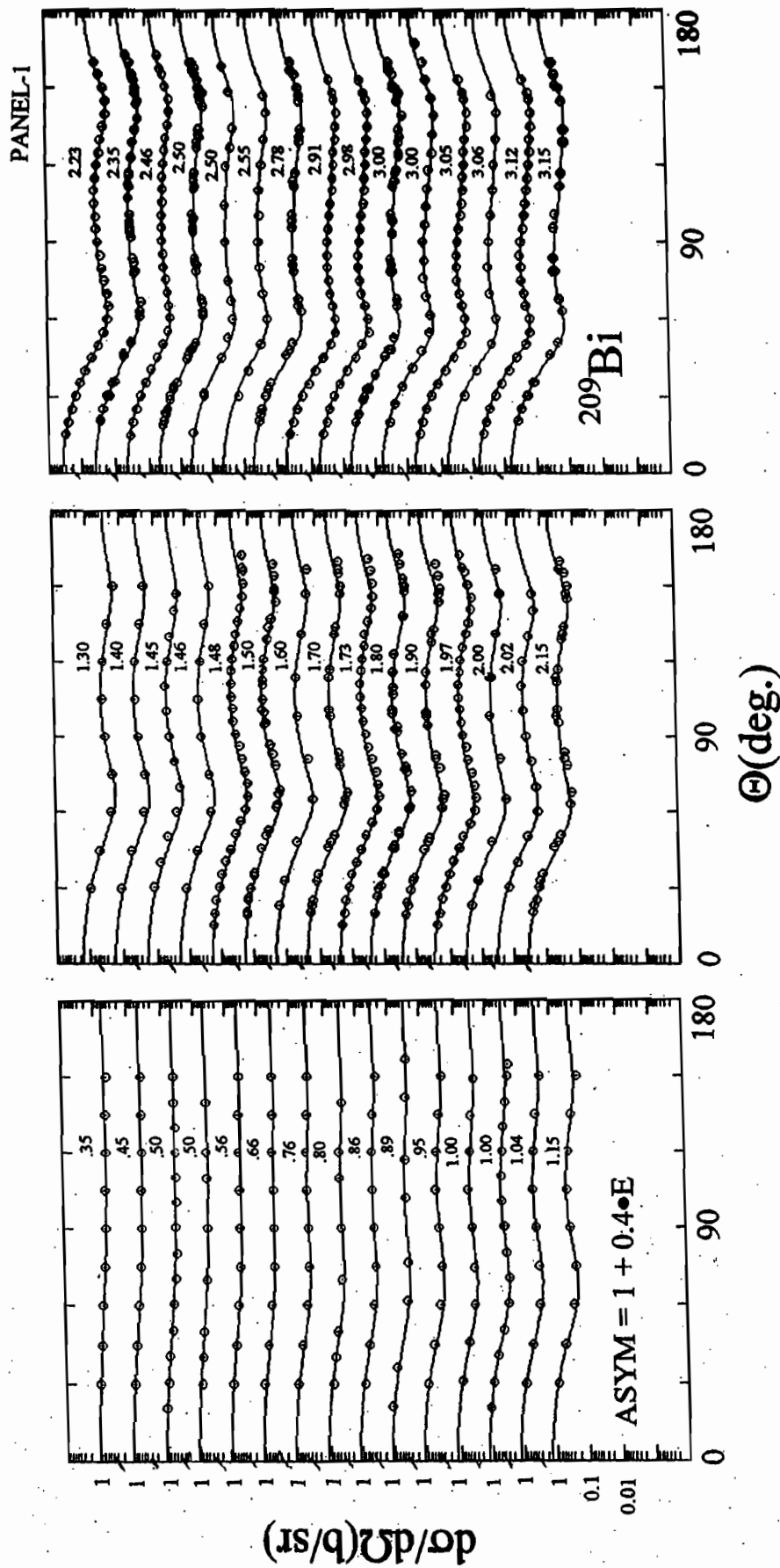
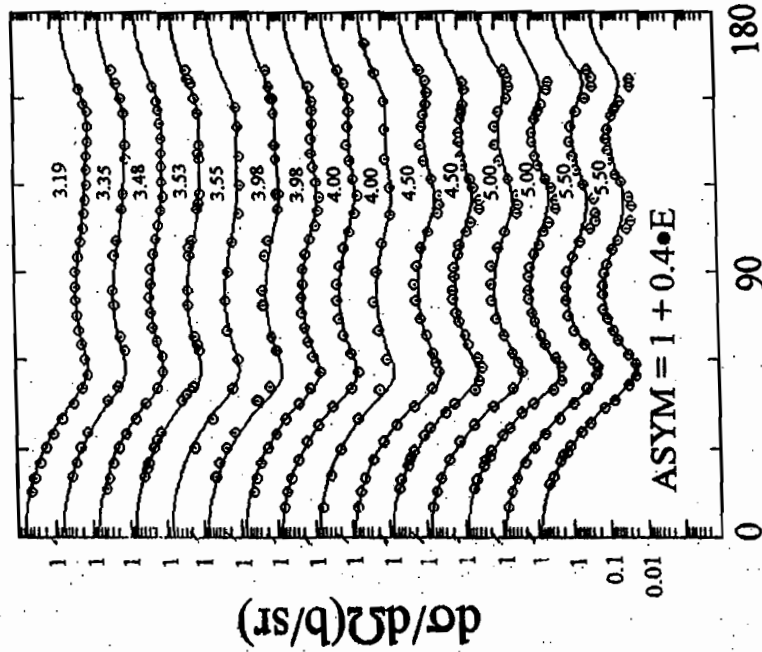
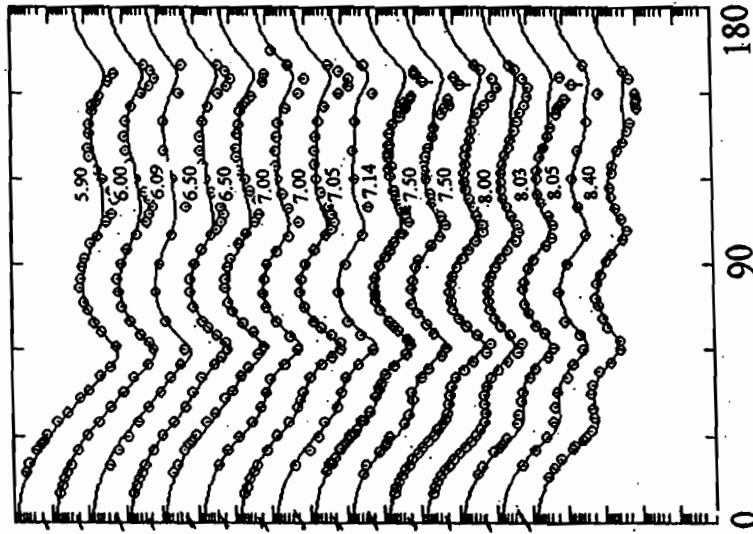
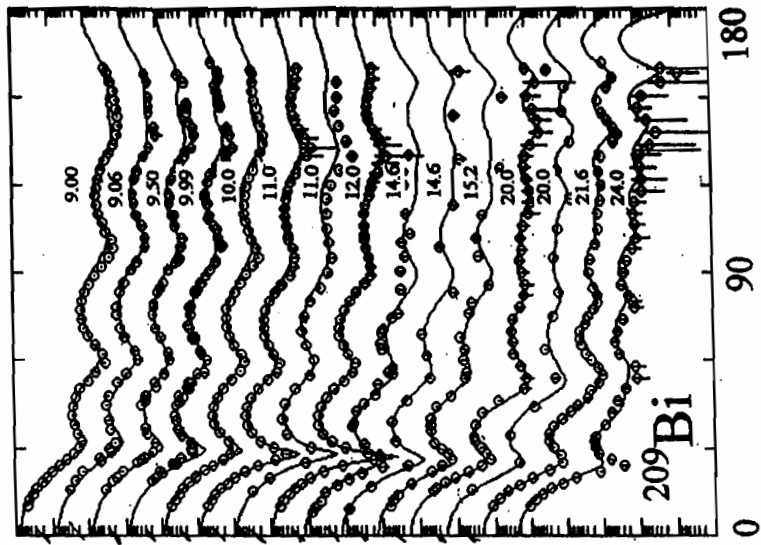


Fig. VI-18. Comparisons of measured (symbols) and calculated (curves) differential elastic scattering cross sections of ^{209}Bi . The calculations used the potential of Table VI-19 where ASYM = 1 + 0.40E. Otherwise the nomenclature is the same as that of Fig. VI-14.

PANEL-2



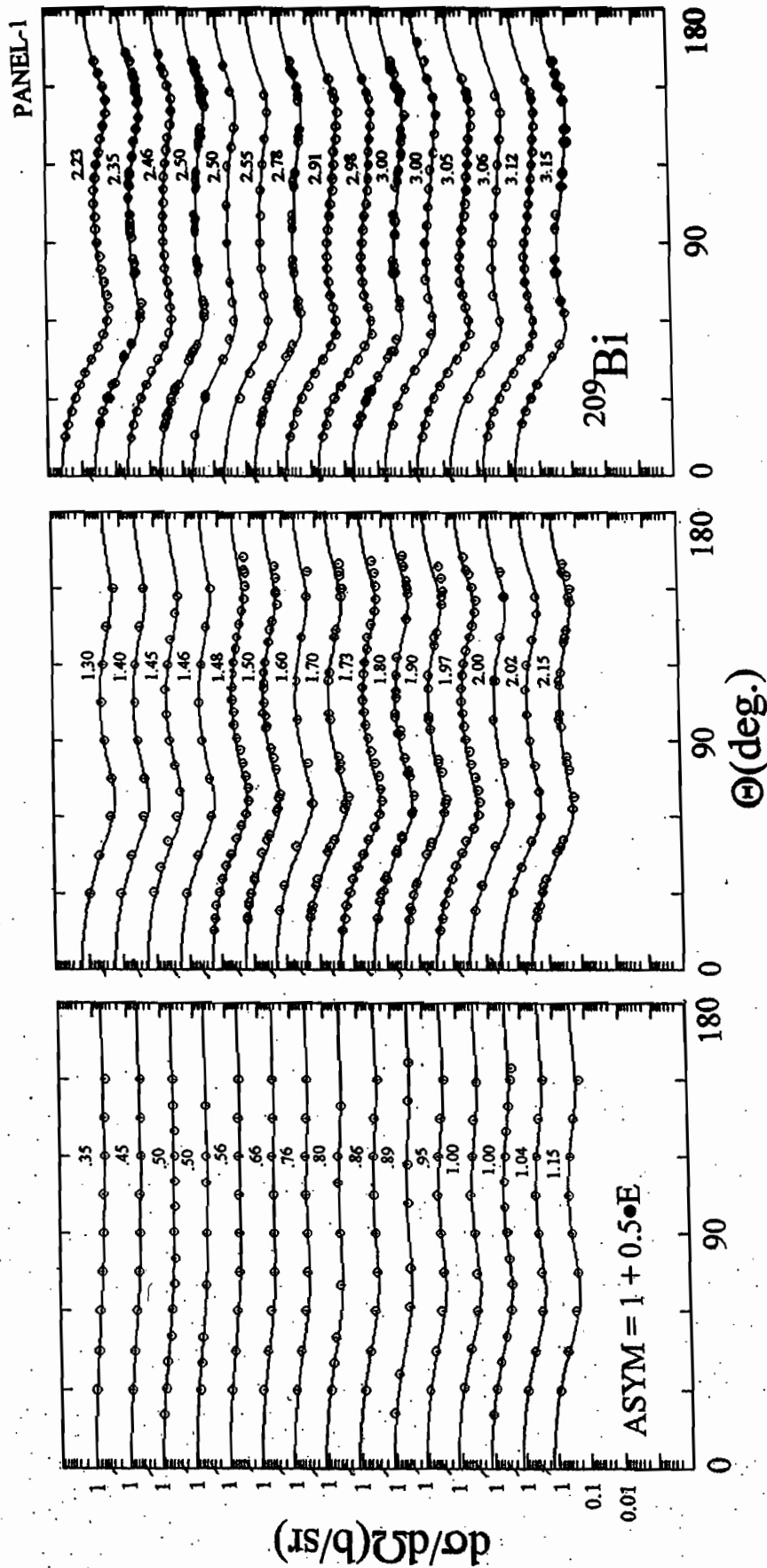


Fig. VI-19. Comparisons of measured (symbols) and calculated (curves) differential elastic scattering cross sections of ^{209}Bi . The calculations used the potential of Table VI-20 where ASYM = 1 + 0.50E. Otherwise the nomenclature is the same as that of Fig. VI-14.

PANEL-1

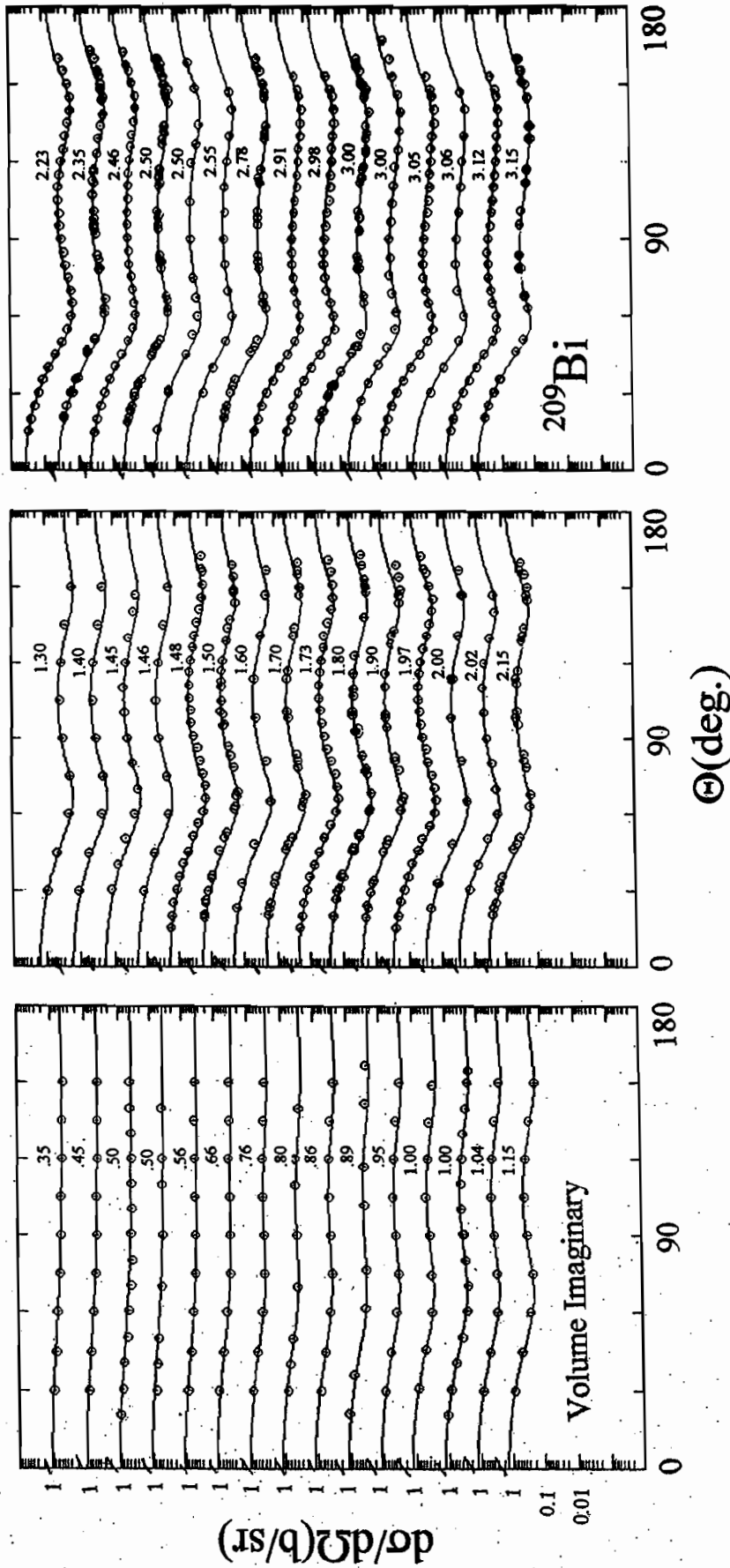
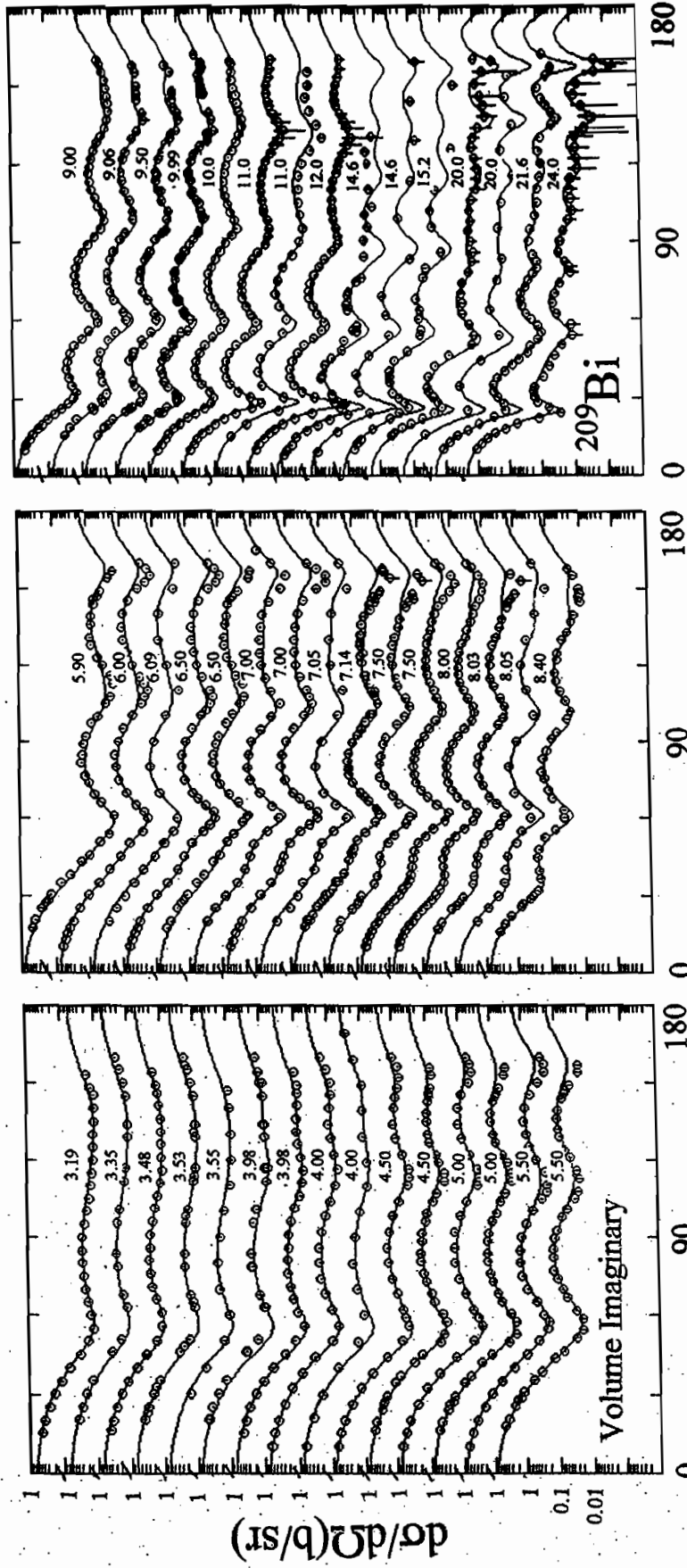


Fig. VI-20. Comparisons of measured (symbols) and calculated (curves) differential elastic scattering cross sections of ^{209}Bi . The calculations used the potential of Table VI-21 where the imaginary potential is entirely a volume contribution. Otherwise the notation is identical to that of Fig. VI-14.

PANEL-2



Θ (deg.)

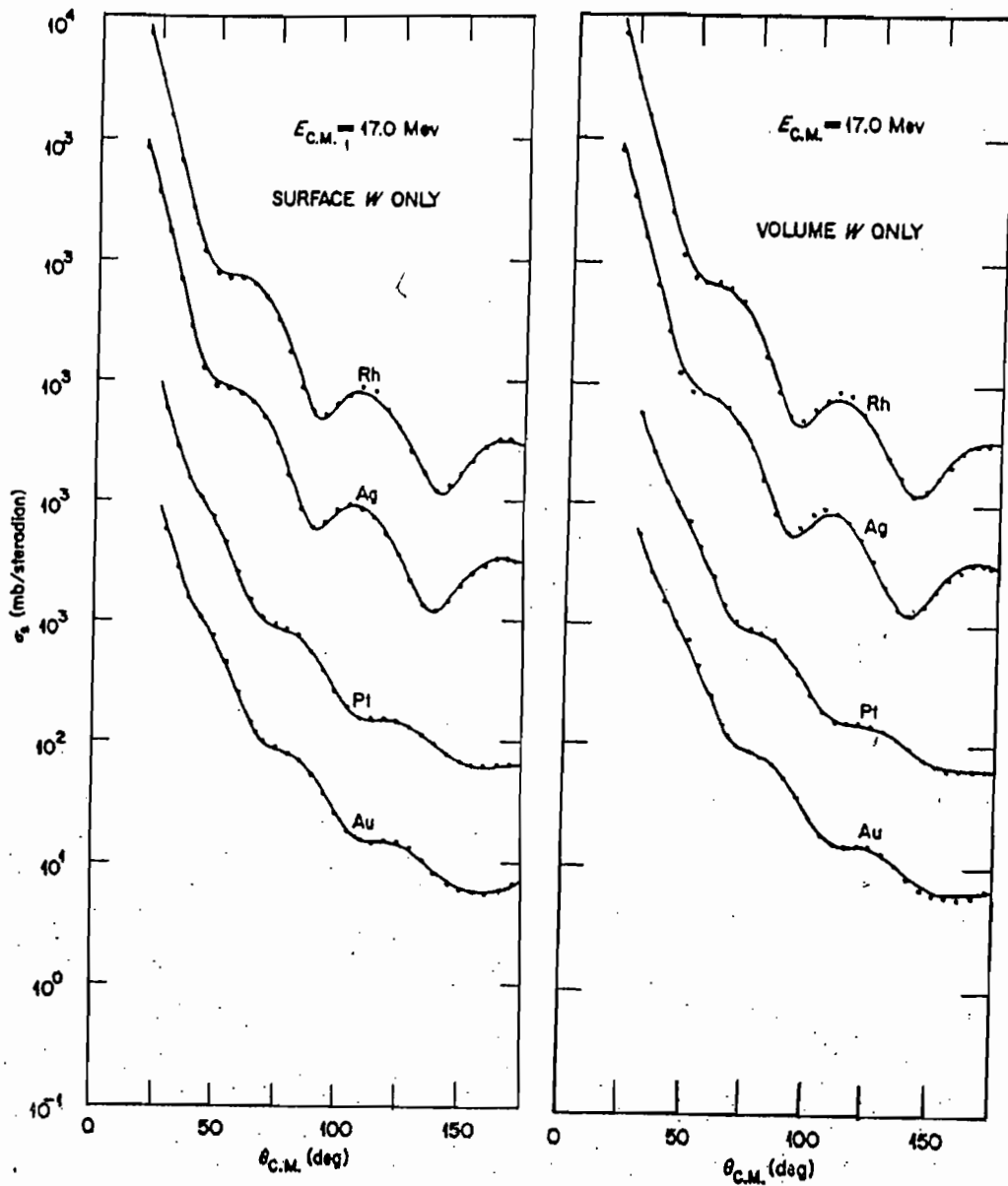


Fig. VI-21. Comparisons of measured and calculated 17 MeV proton scattering from some heavy targets. The left figure exclusively uses a Saxon-Woods derivative form of the imaginary potential while the right figure uses a simple Saxon-Woods volume absorption alone. These results are taken from the work of Perey (Per63).

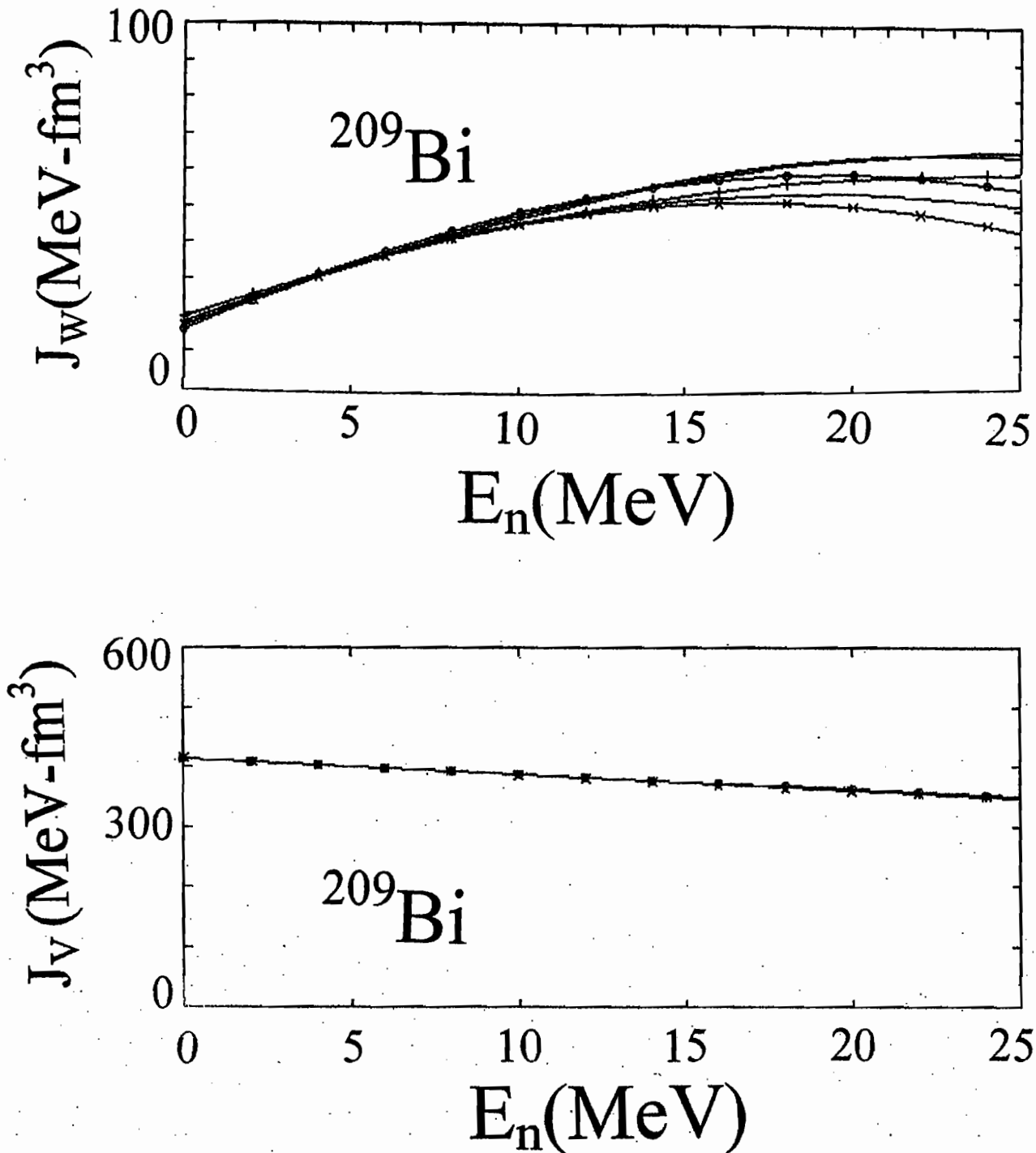


Fig. VI-22. The real (J_v) and imaginary (J_w) potential strengths as a function of energy as derived by 4-parameter fitting and numerically given in Tables VI-24 to VI-29. There are six curves in each panel of the figure corresponding to different asymmetries where the "O" symbols denote the $\text{ASYM} = 1 + 0.0 \cdot E$ results, the "+" symbols the $\text{ASYM} = 1 + 0.3 \cdot E$ results, and the "X" symbols the $\text{ASYM} = 1 + 0.5 \cdot E$ results. Intermediate curves interpolate between.

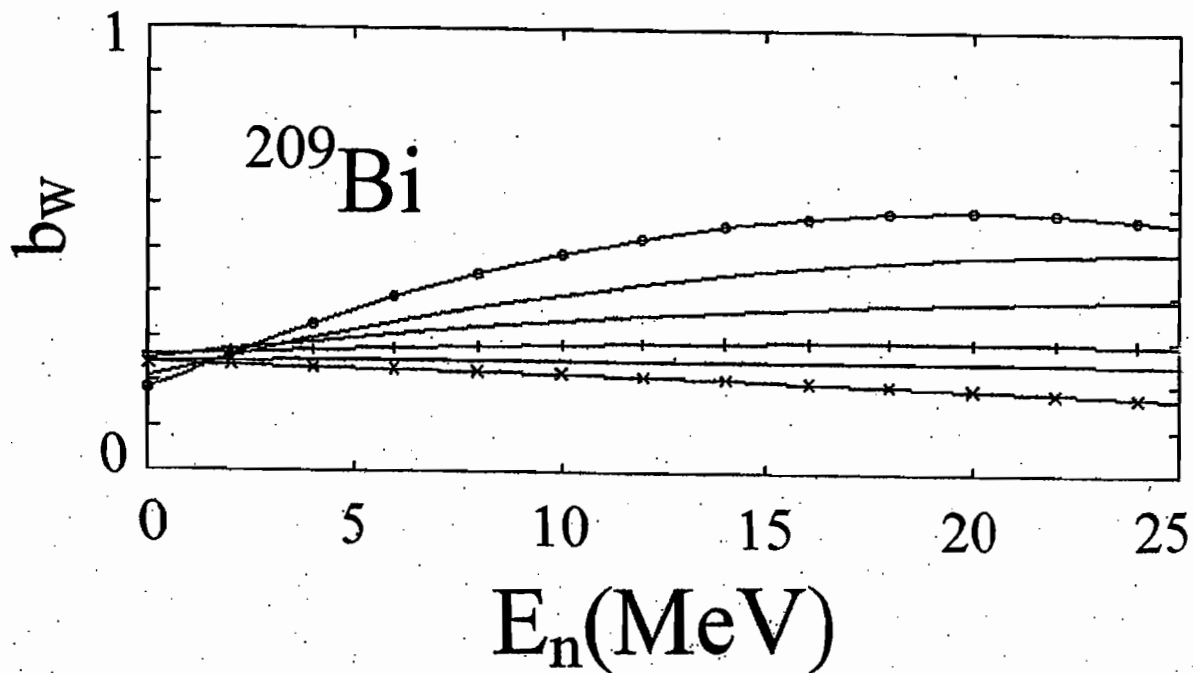
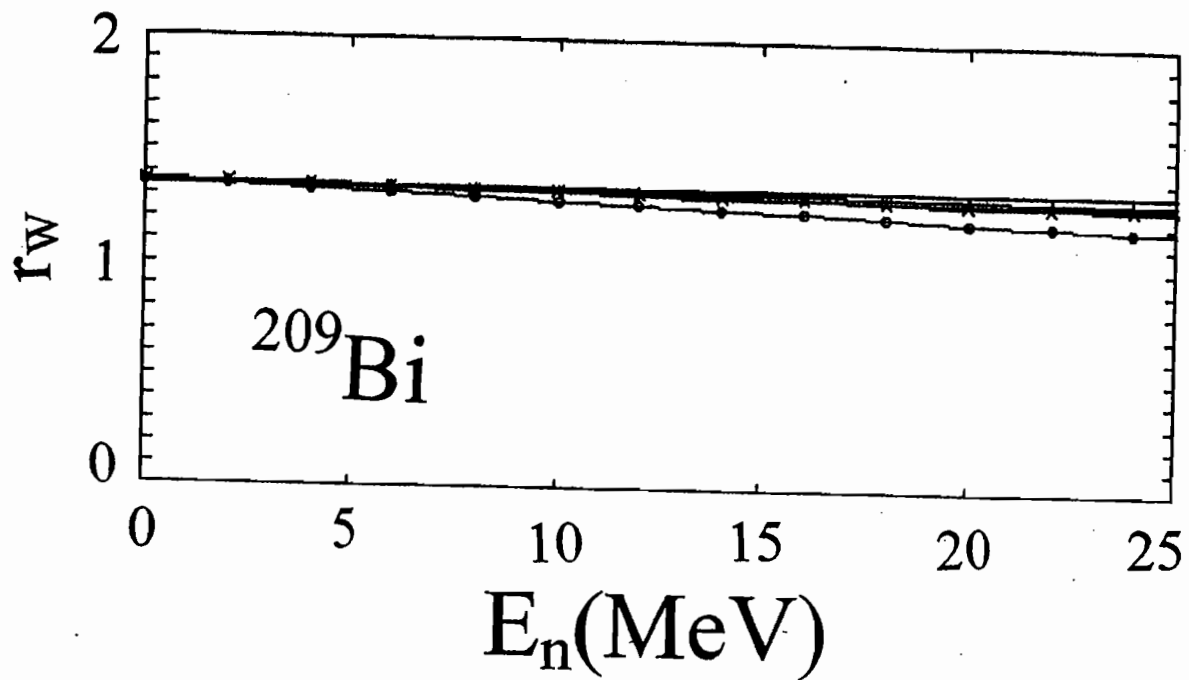


Fig. VI-23. ^{209}Bi imaginary potential radius, r_w (fms) and diffuseness a_w (fms) as function of energy as determined from 4-parameter fitting. Curves correspond to varying asymmetries with the same symbolic notation as in Fig. VI-22.

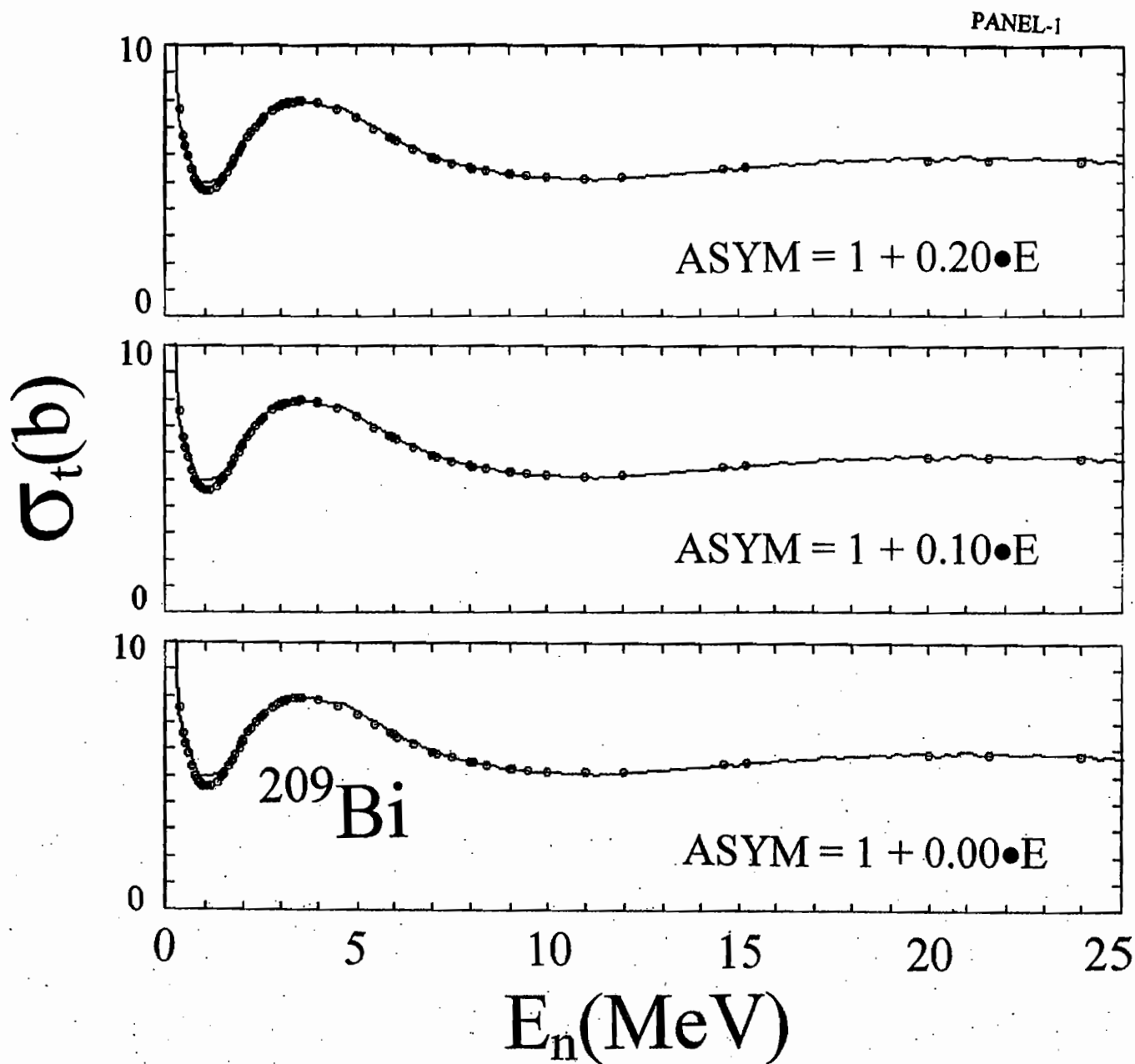
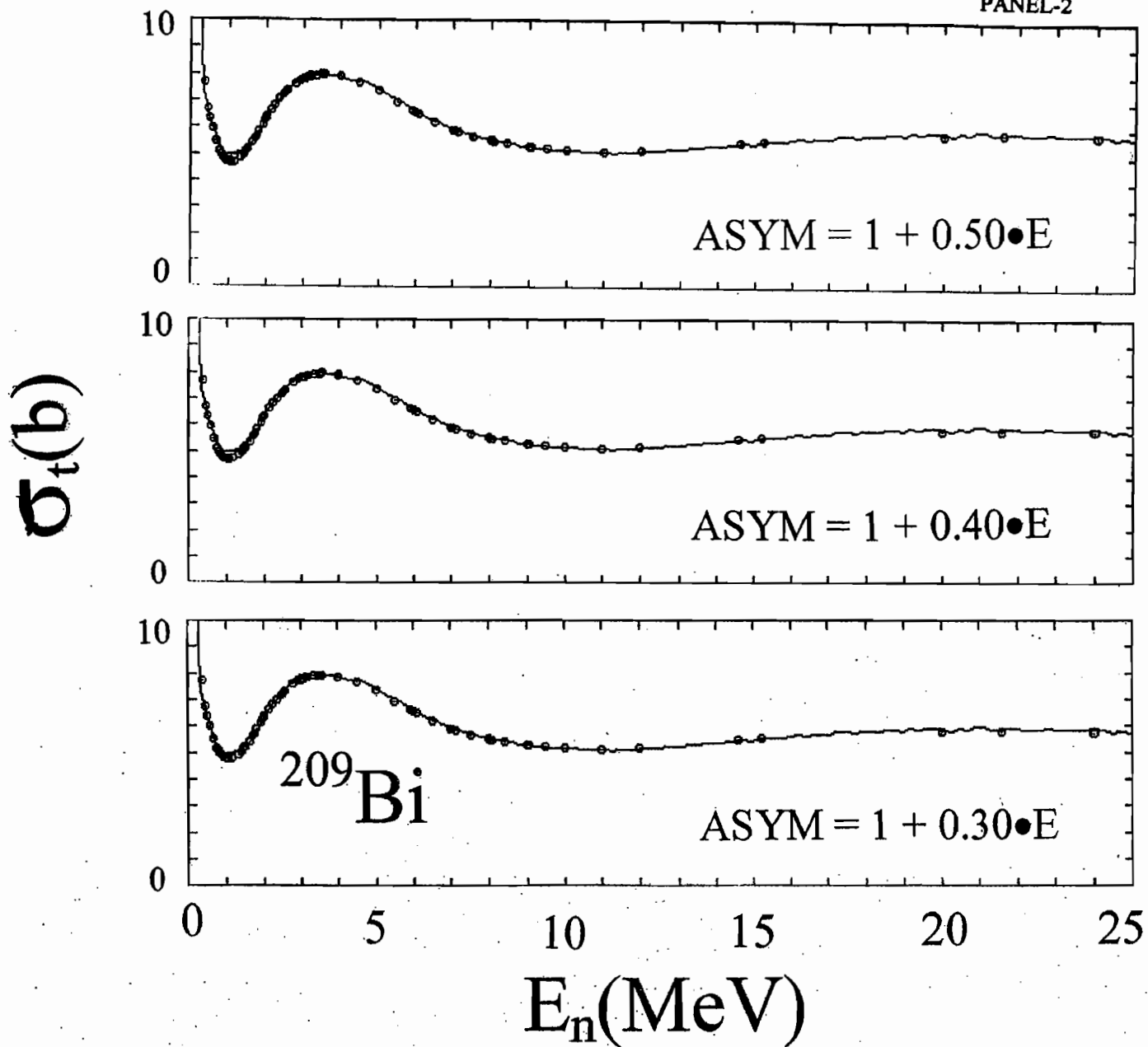


Fig. VI-24. Calculated (symbols) and experimental (curves) total cross sections of ^{209}Bi . Each panel corresponds to a different value of ASYM, as noted. The potentials were determined from four parameter fitting.

PANEL-2



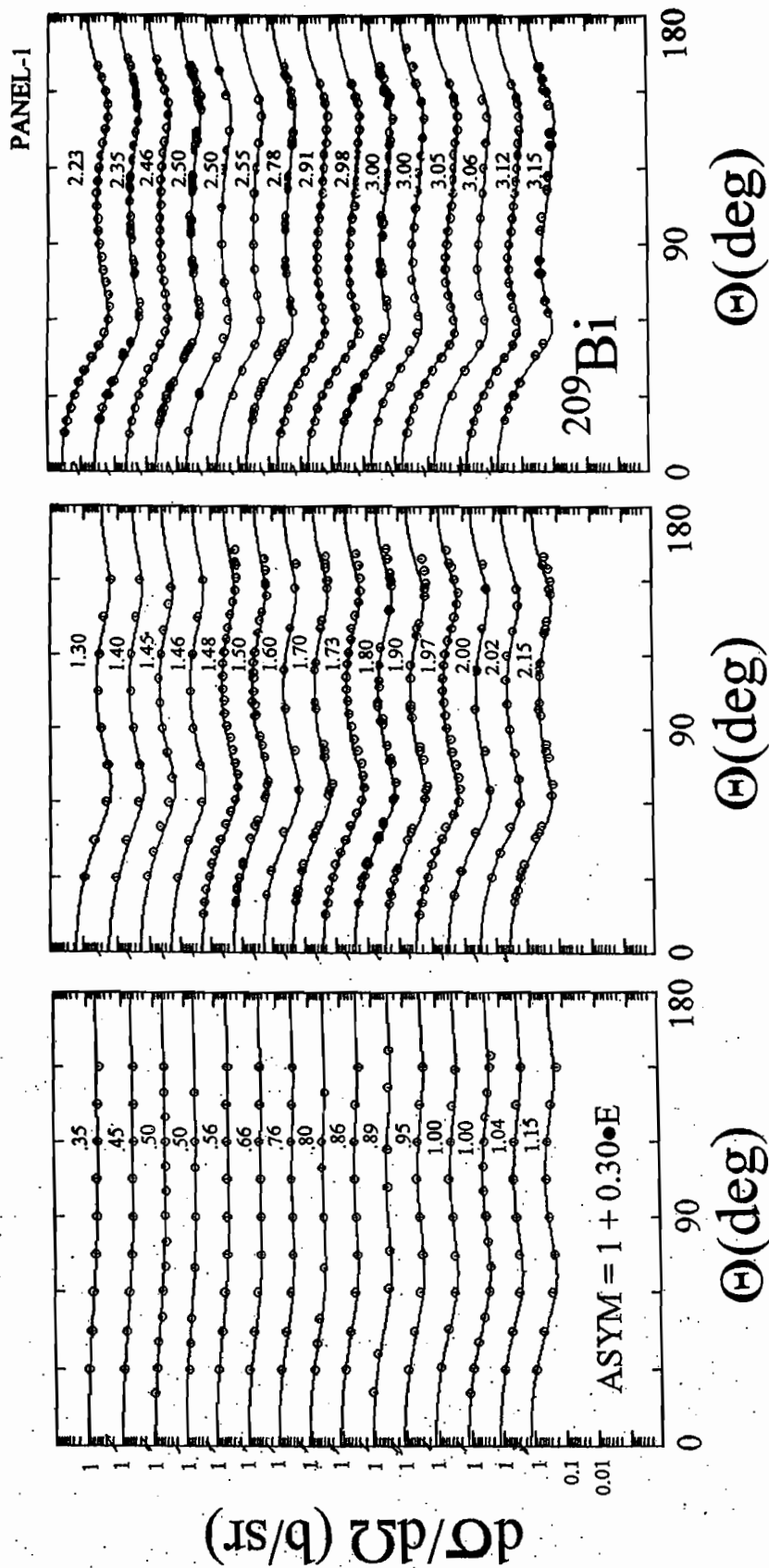
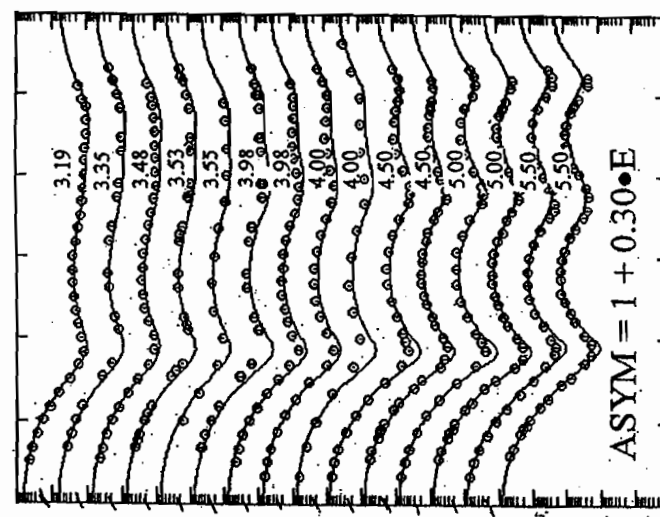
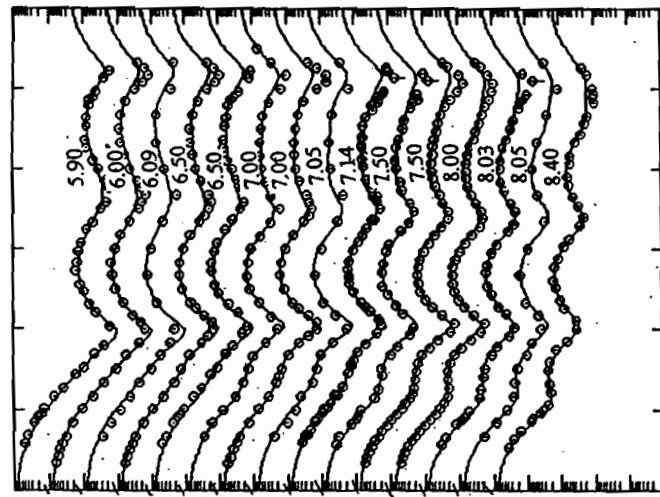
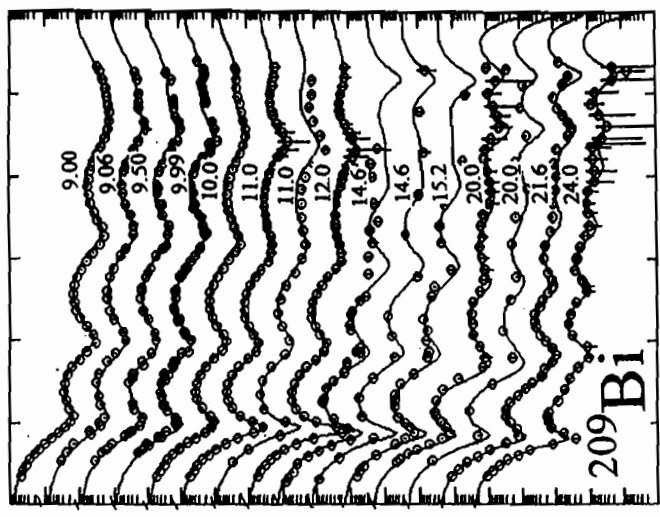


Fig. VI-25. Calculated (curves) and measured (symbols) differential elastic-scattering cross sections of ^{209}Bi . The calculations used the potential of Table VI-27 where ASYM = $1 + 0.30\bullet E$. The potential was determined by four-parameter fitting.

PANEL-2



$d\sigma/d\Omega$ (b/st)

Θ (deg)

Θ (deg)

Θ (deg)

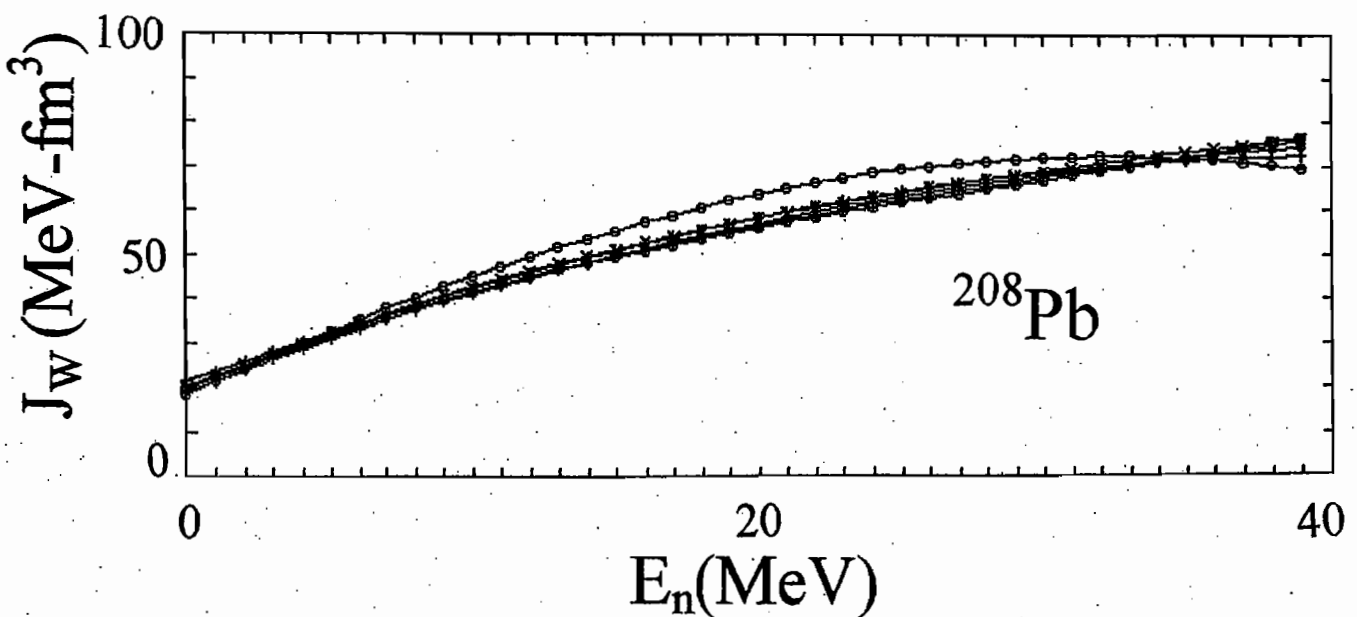
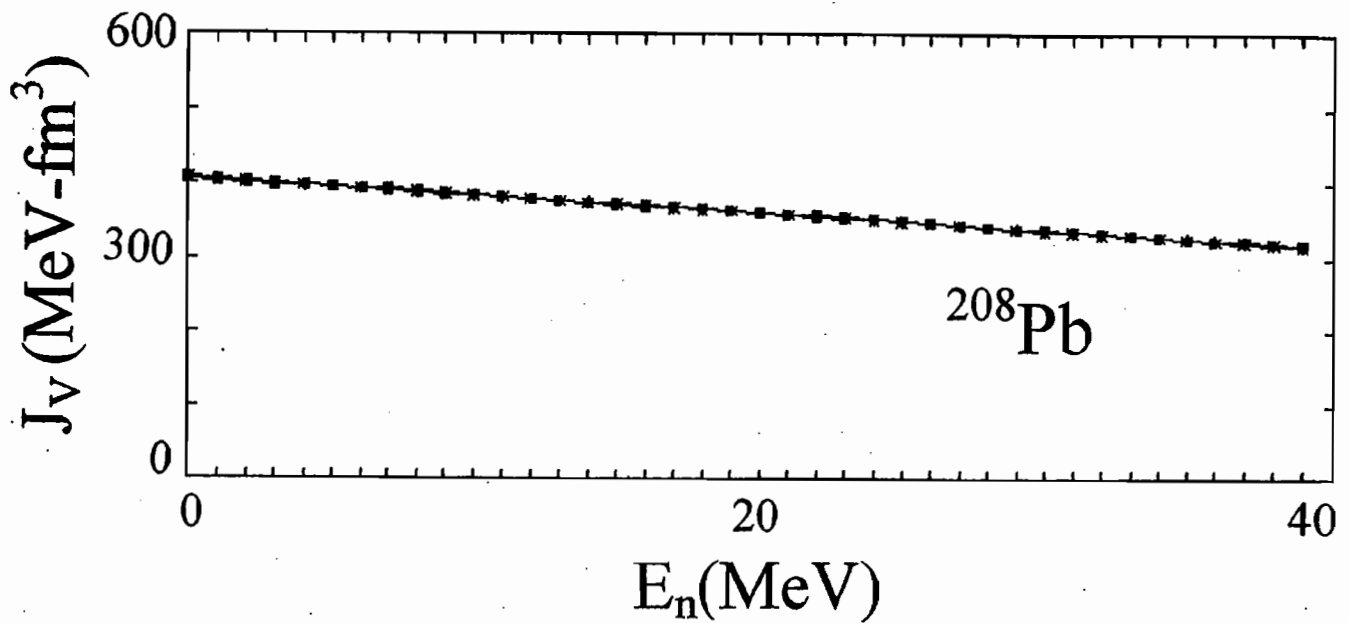


Fig. A - 1. Real (J_V) and Imaginary (J_W) potential strengths resulting from fitting with the energy referenced to the Fermi Energy. Each panel has six curves obtained with $K = 0.0, 0.1, 0.2, 0.3, 0.4,$ or 0.5 in Eq. A-1. The real potential curves are indistinguishable. For the imaginary potential only the $K = 0.0$ results differ significantly from the others. The figure is plotted in the laboratory energy scale.

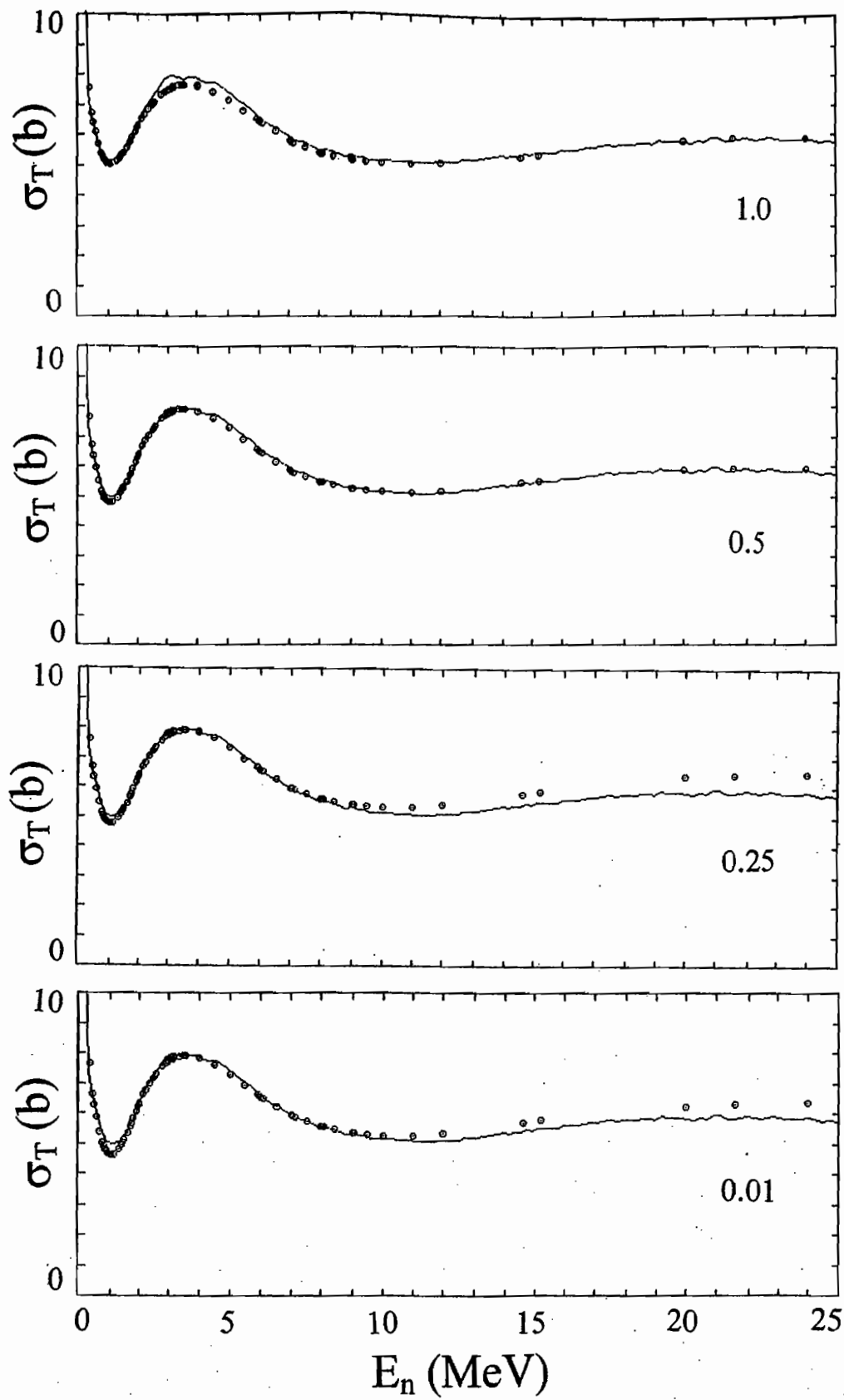


Fig. B-1. Comparison of calculated (symbols) and measured (curves) ^{209}Bi neutron total cross sections. The calculations employed various dispersive fractions as noted on each panel of the Figure and as defined in Tables B-1 to B-4. These Tables also defined the respective potential parameters.

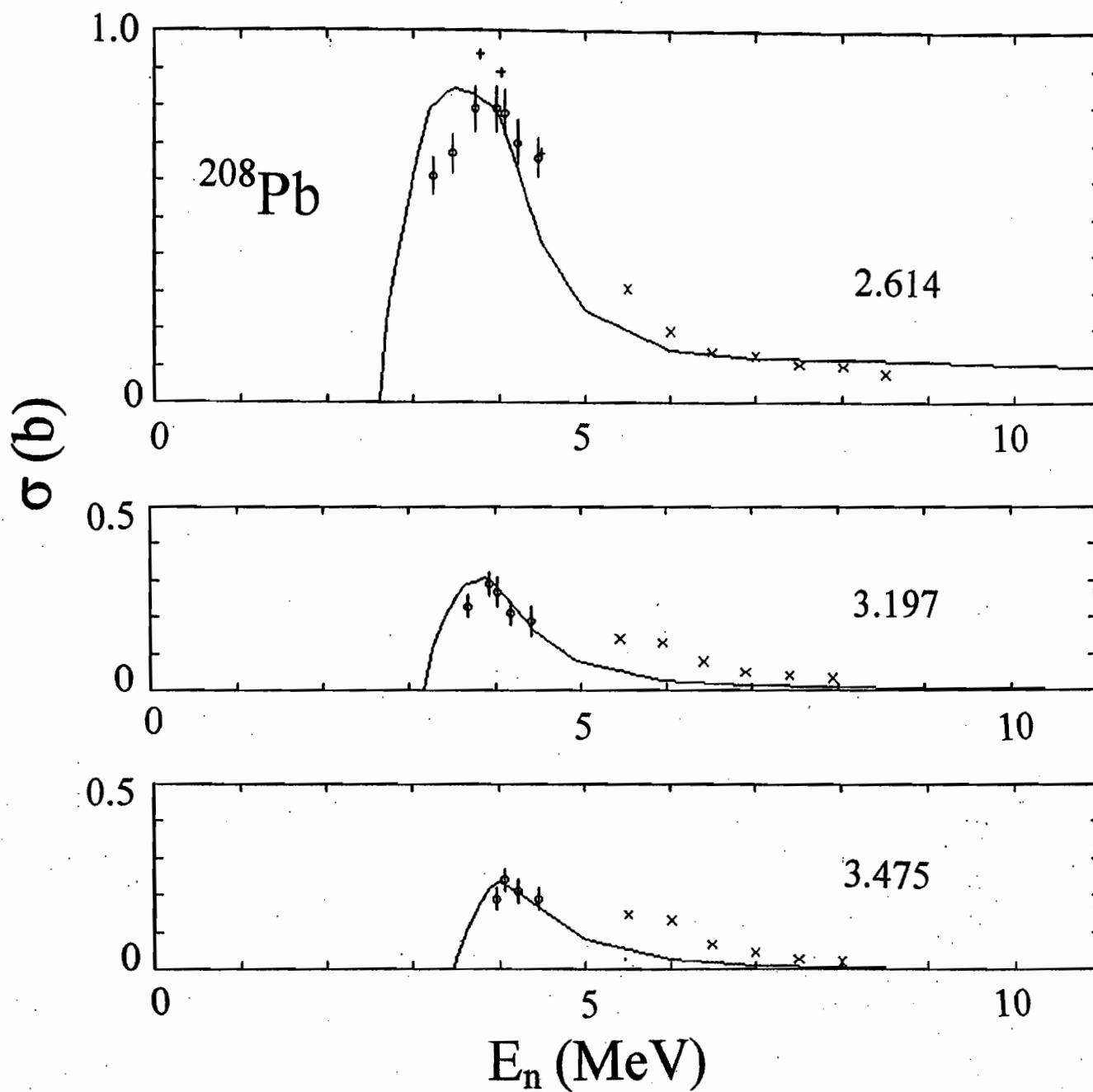


Fig. C-1. Measured and calculated excitation functions for the first three levels in ^{208}Pb at 2.61, 3.20 and 3.48 MeV. Selected experimental values are indicated by symbols and the results of calculations by curves, as described in the Appendix C.

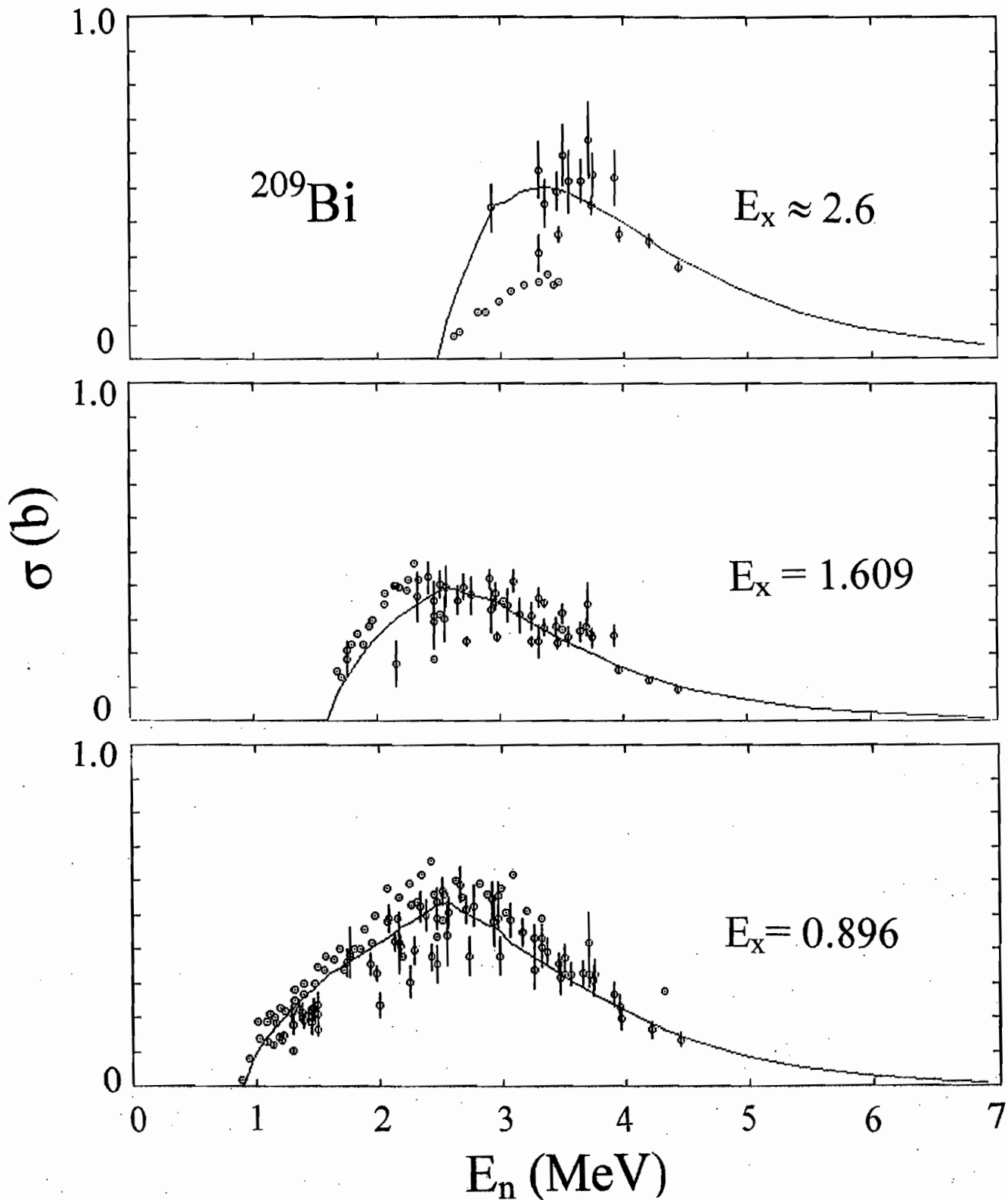


Fig. C-2. Measured and calculated excitation function for the first three excited levels in ^{209}Bi at 890 and 1600 keV. Selected experimental values are indicated by symbols and results calculated as discussed in the text by curves. The experimental values are limited to results of direct inelastic-neutron detection.

PANEL-1

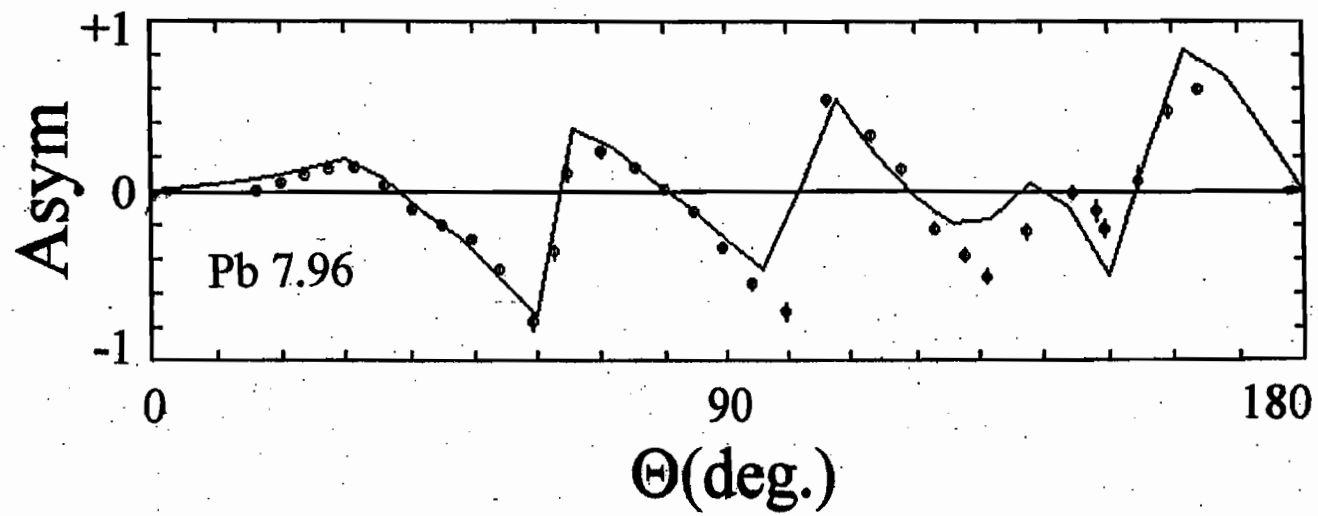
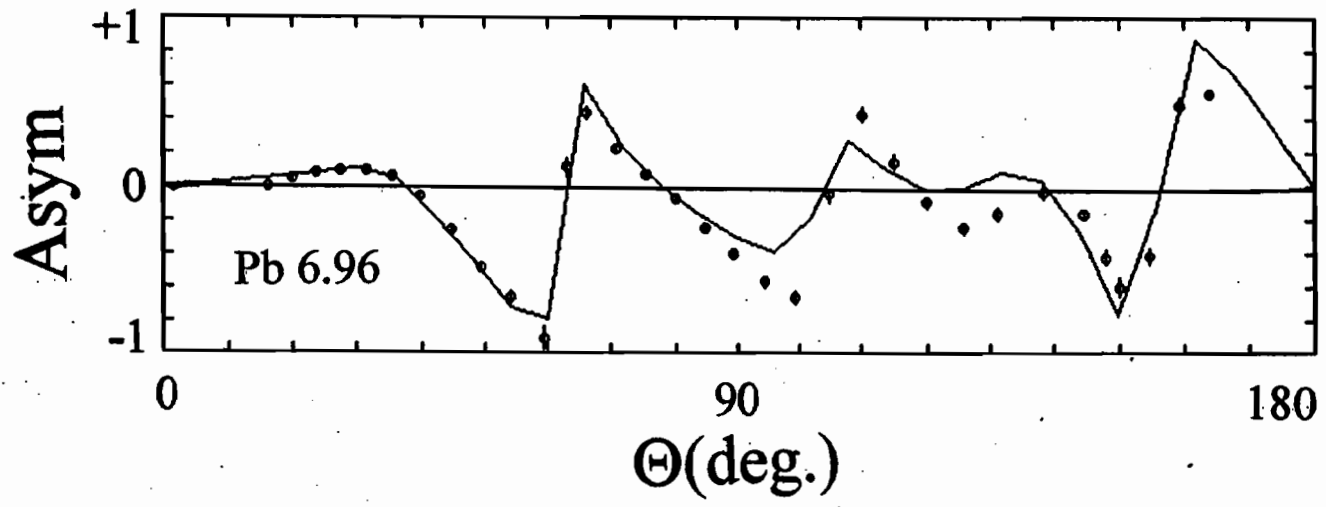
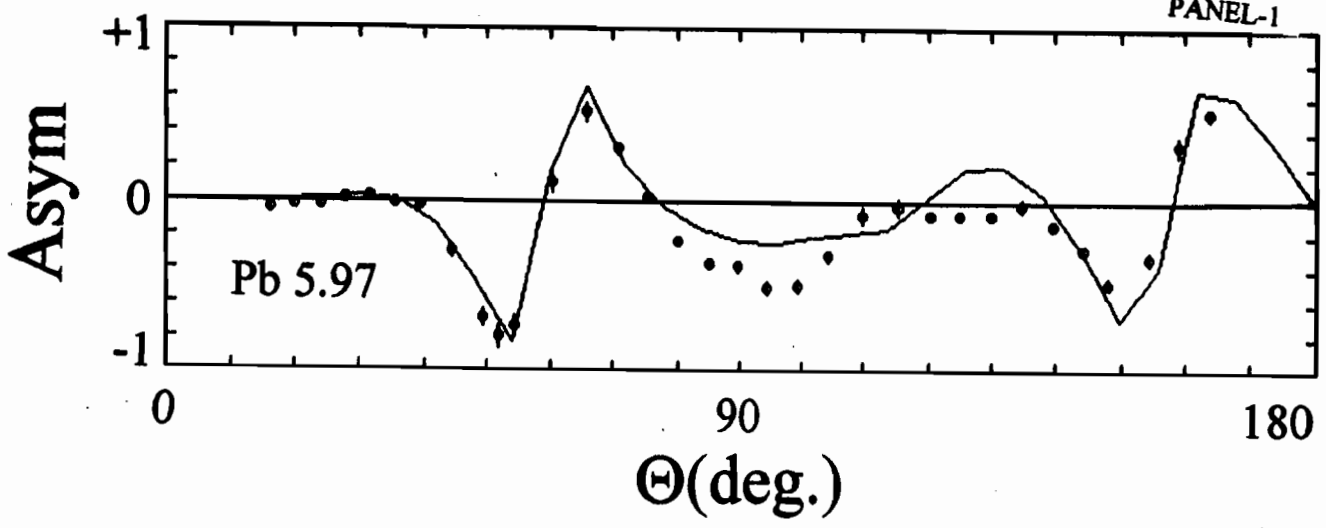
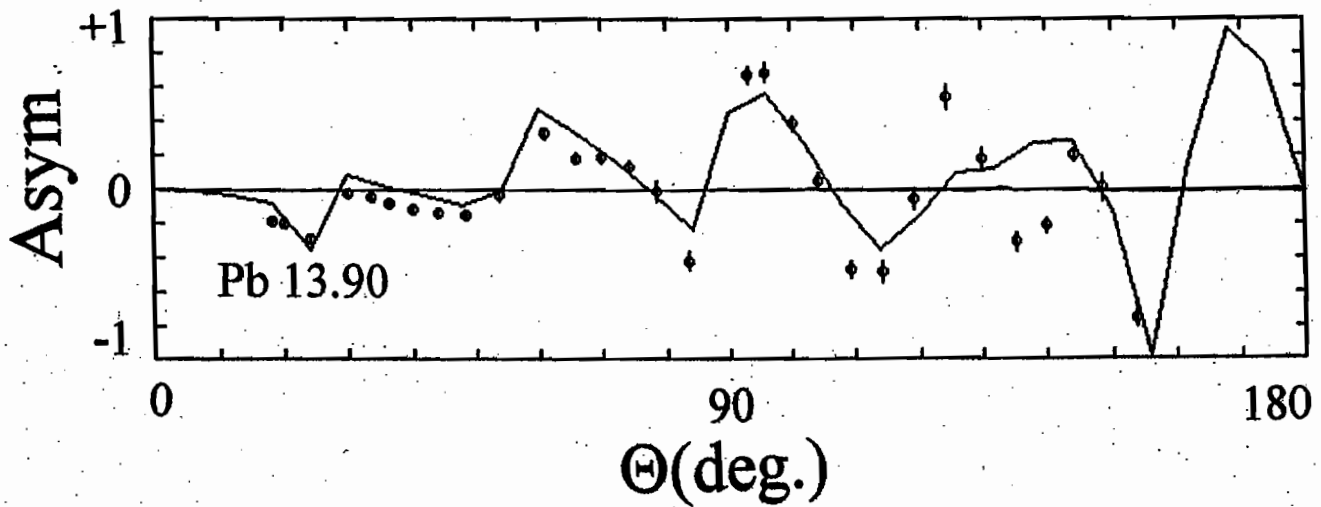
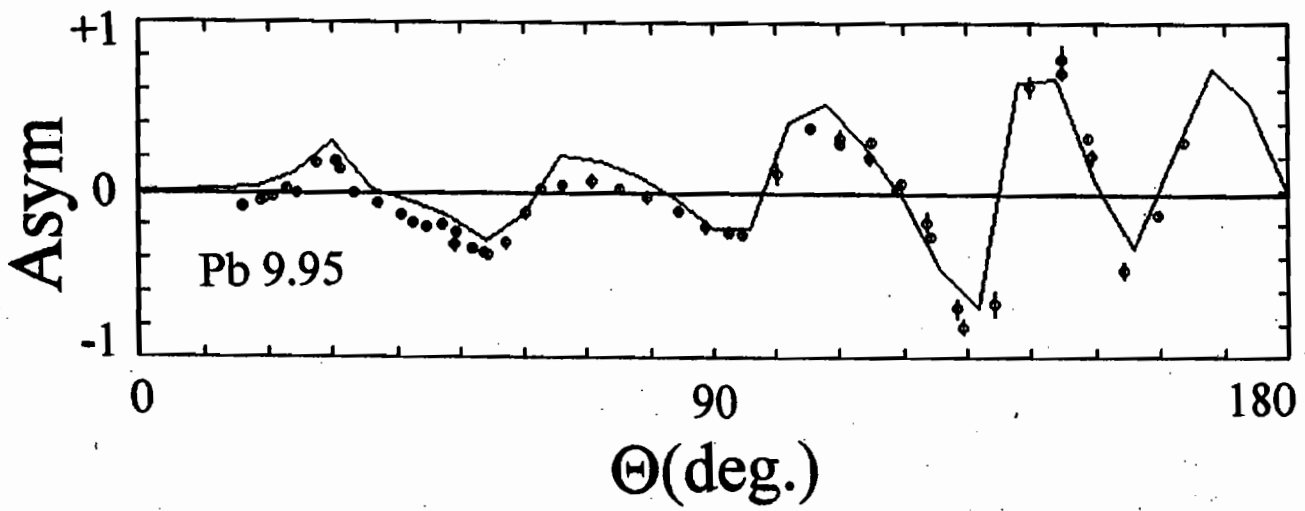
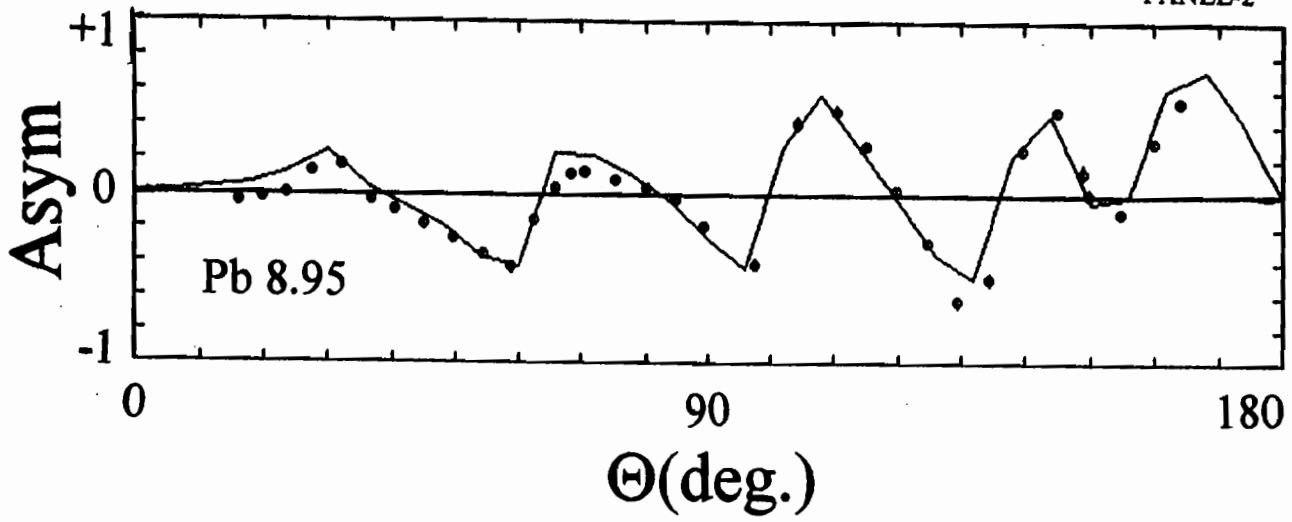


Fig. D-1. Comparisons of measured (symbols) and calculated (curves) polarization ("ASYM") of neutrons elastically scattered from ^{208}Pb at 5.97 to 13.90 MeV as marked on each panel of the figure. The calculations (curves) were generated on a 6-degree angular mesh using the SOM potential of Table IV-A-1. The data is referenced in the text.

PANEL-2



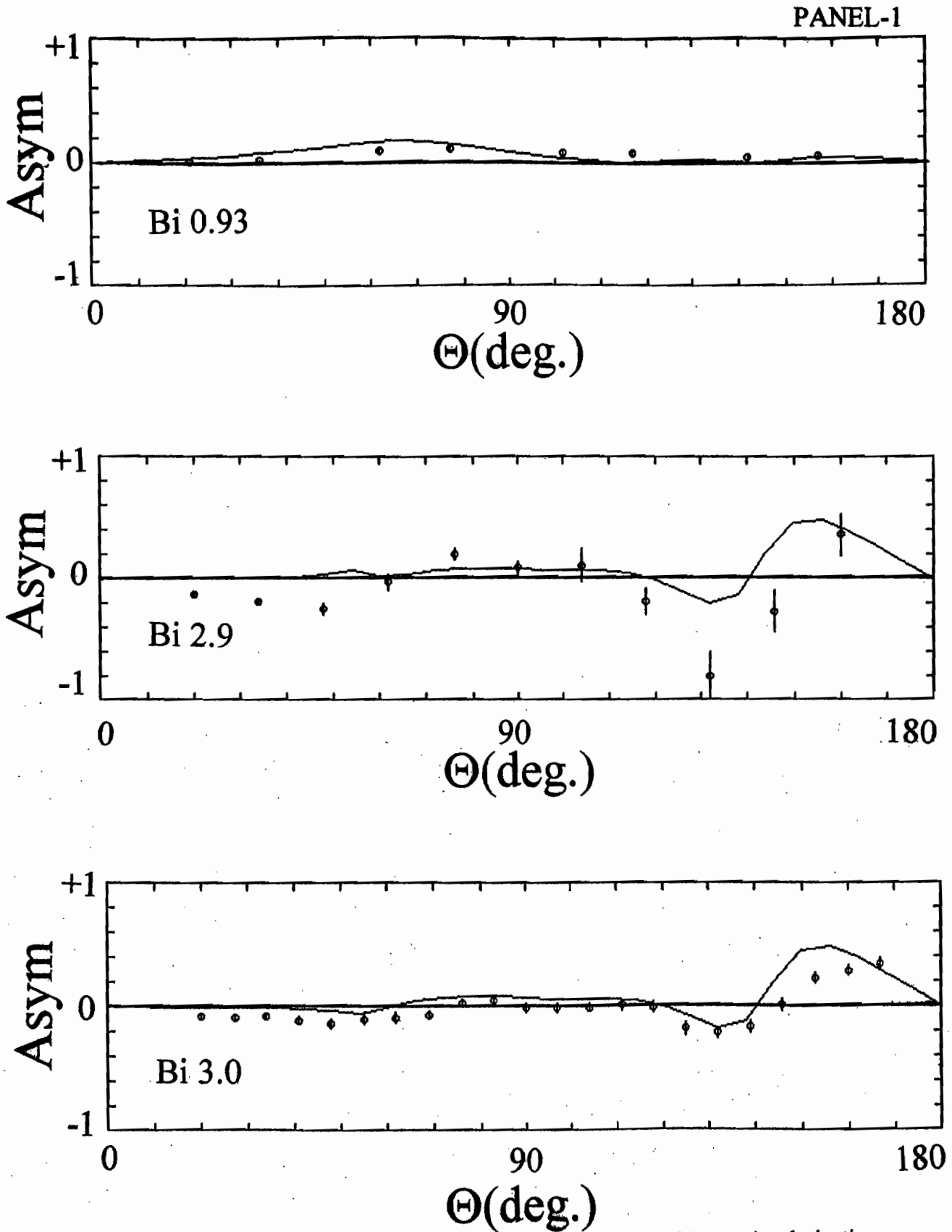
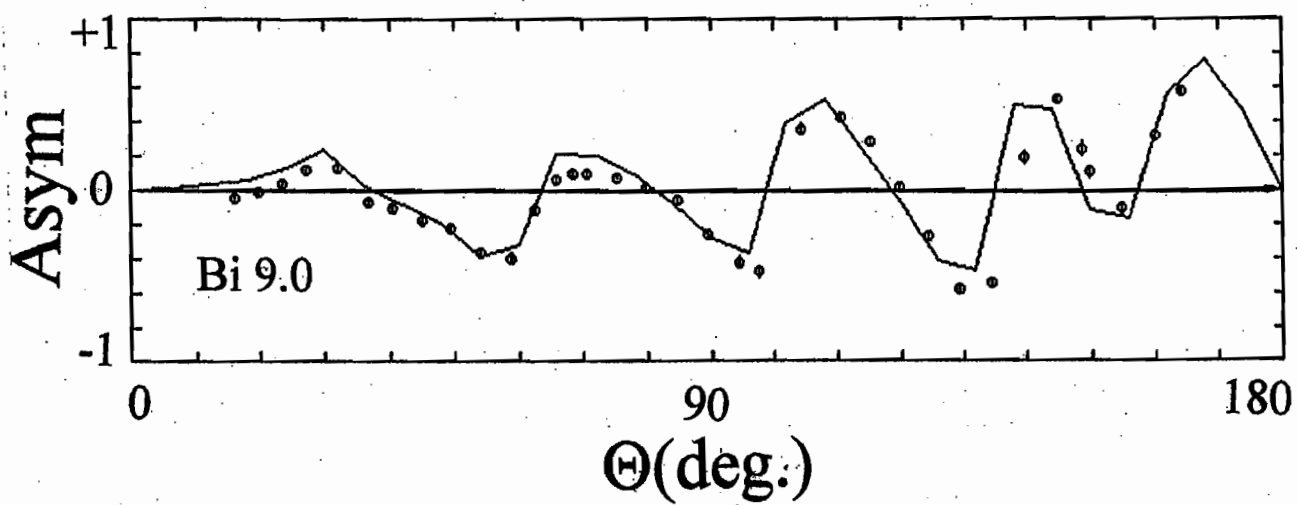
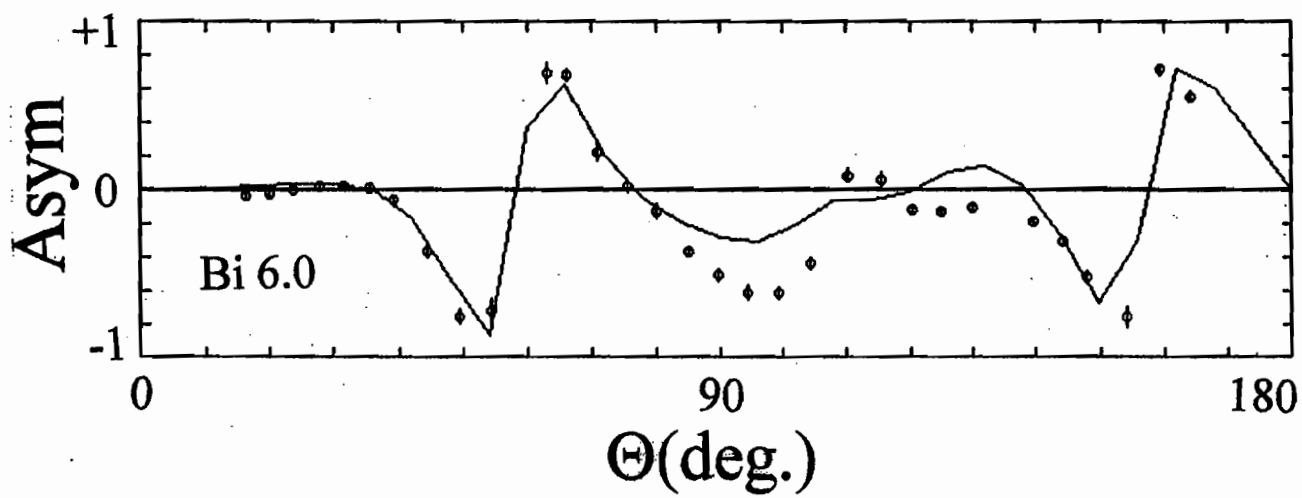
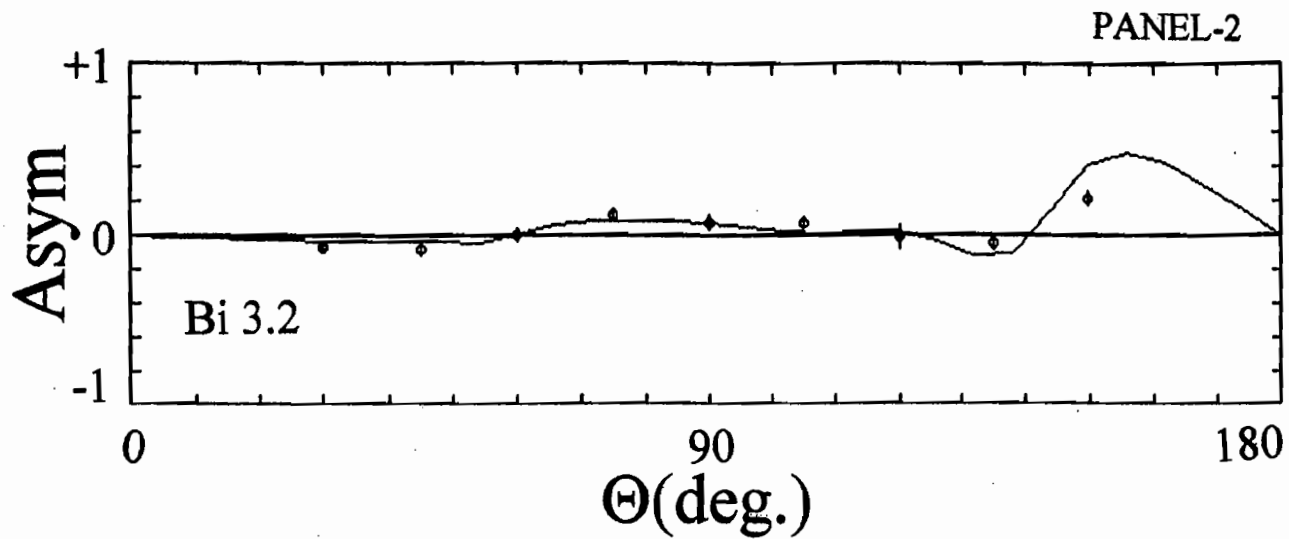


Fig. D-2. Comparisons of measured (symbols) and calculated (curves) polarization (ASYM) of neutrons elastically scattered from ^{209}Bi at 0.93 to 9.0 MeV as marked on each panel of the figure and as referenced in the text. The calculations were generated on a 6-degree angular mesh using the SOM potential of Table IV-A-2.



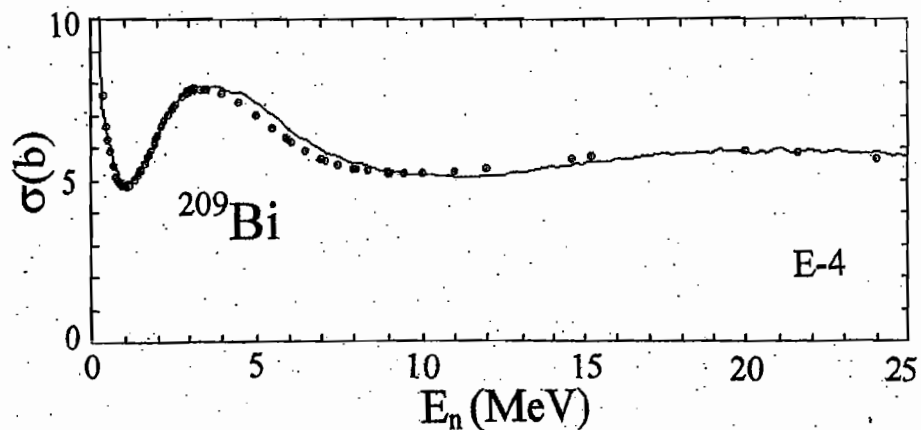
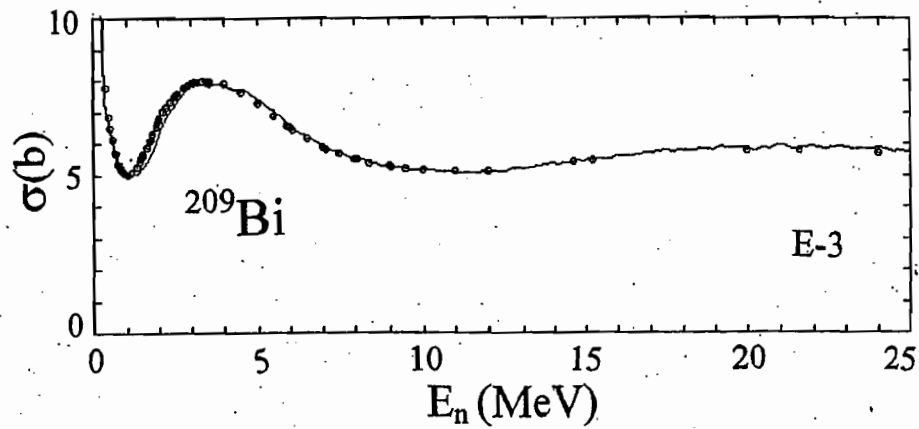
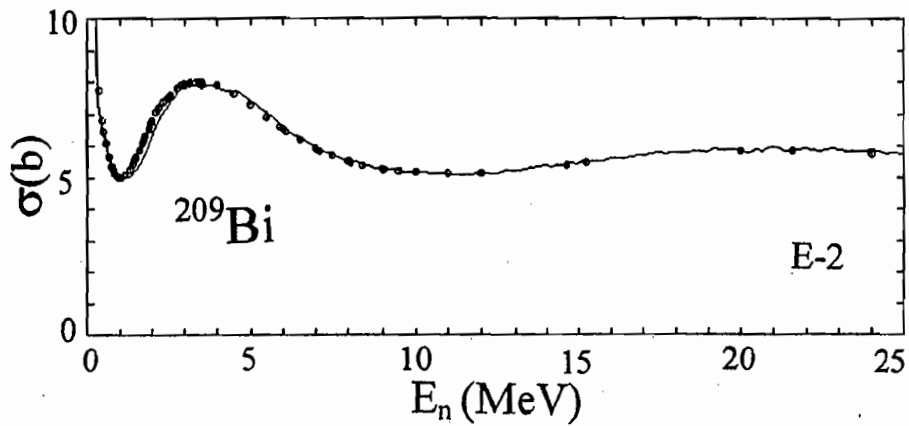
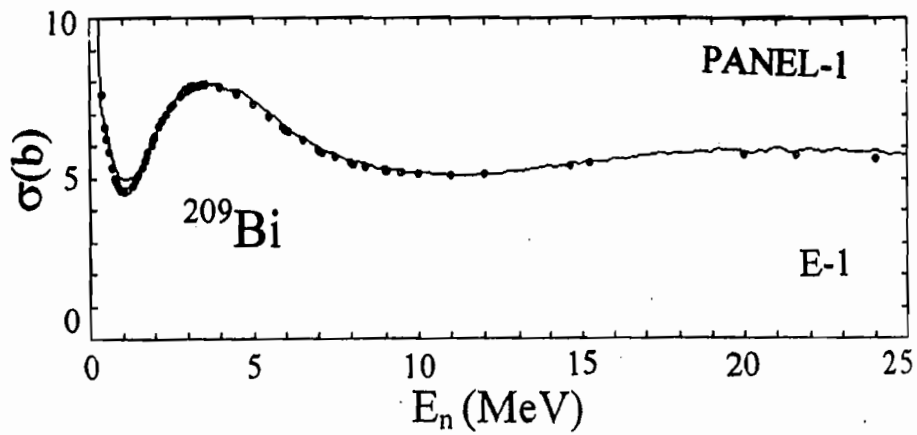
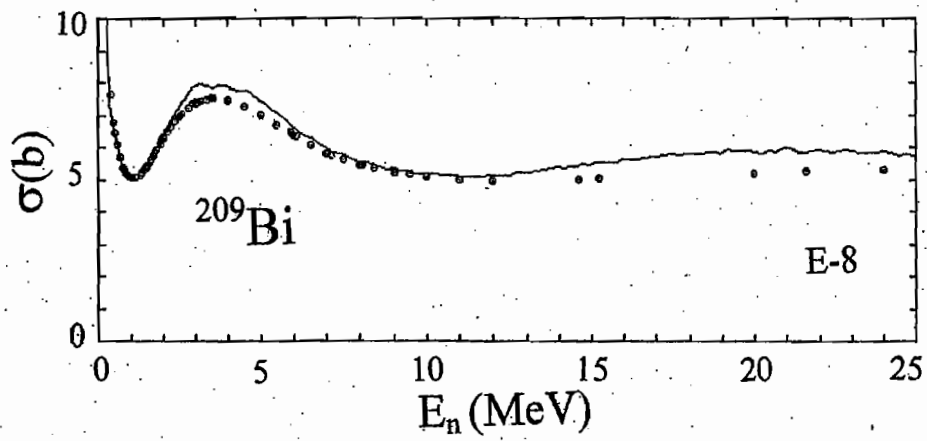
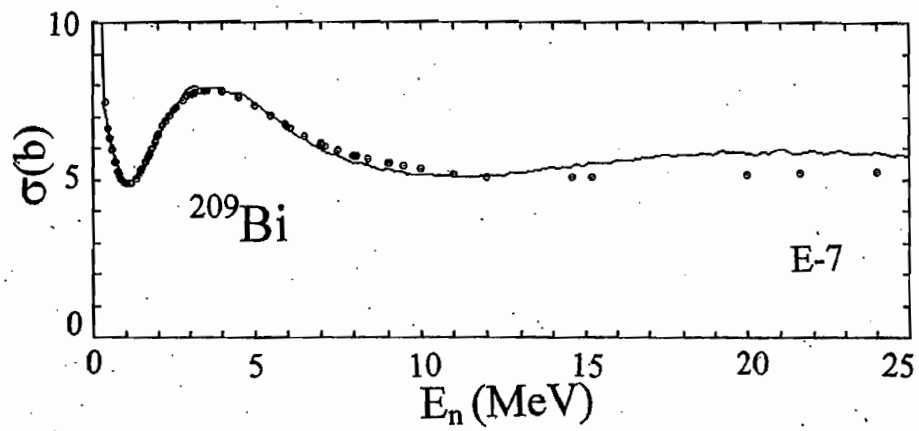
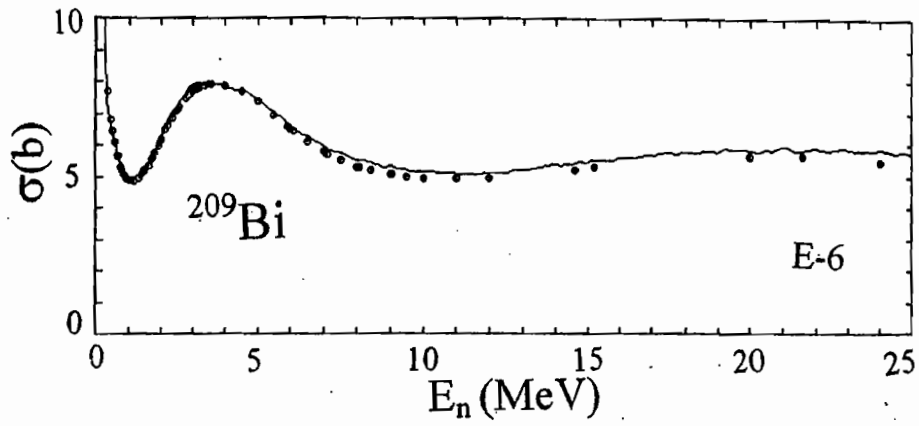
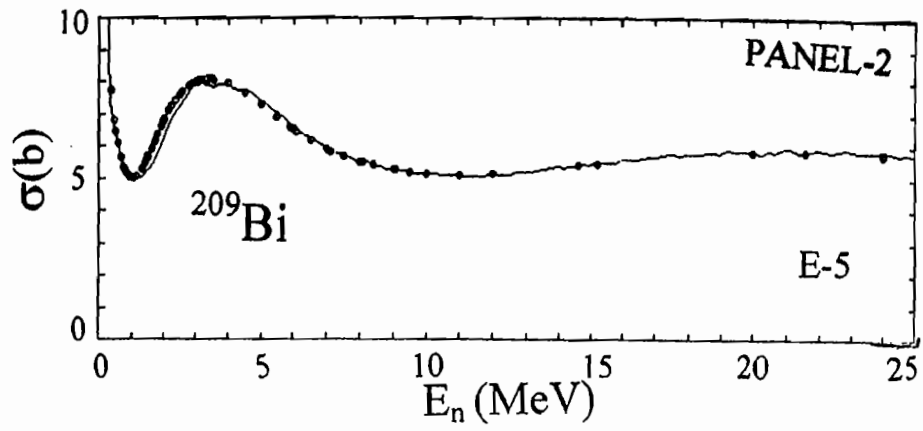


Fig. E-1. Comparison of measured (curves) and calculated (symbols) total cross sections of ^{209}Bi . The calculations used the potentials of Tables E-1 to E-8, as noted on each panel.



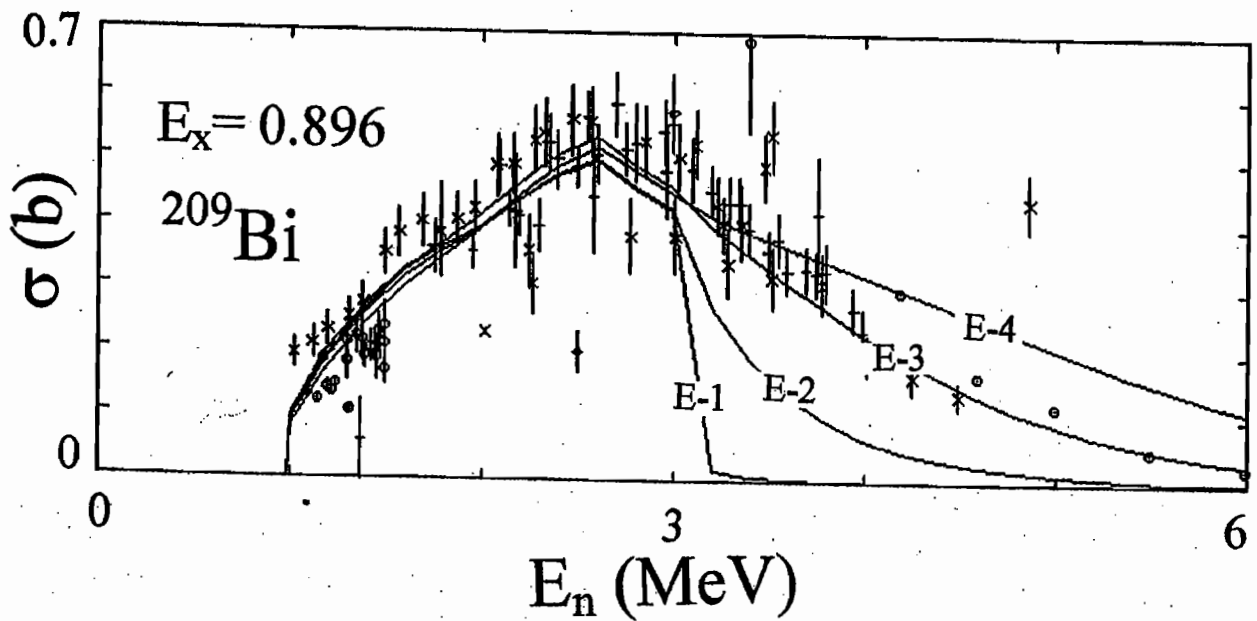
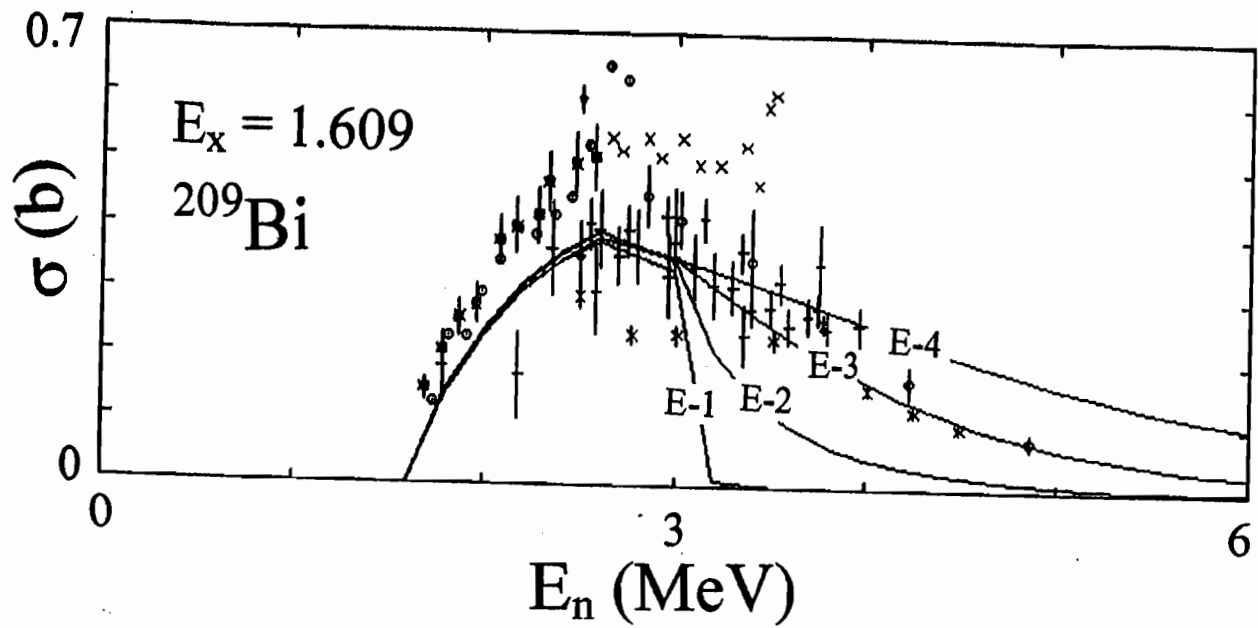


Fig. E-2. Comparisons of measured (symbols) and calculated (curves) cross sections for the excitation of the 0.896 MeV and 1.609 MeV states in ^{209}Bi . The experimental values are referenced in Appendix A and the curves correspond to the potentials of Table E-1 to E-4, as marked.

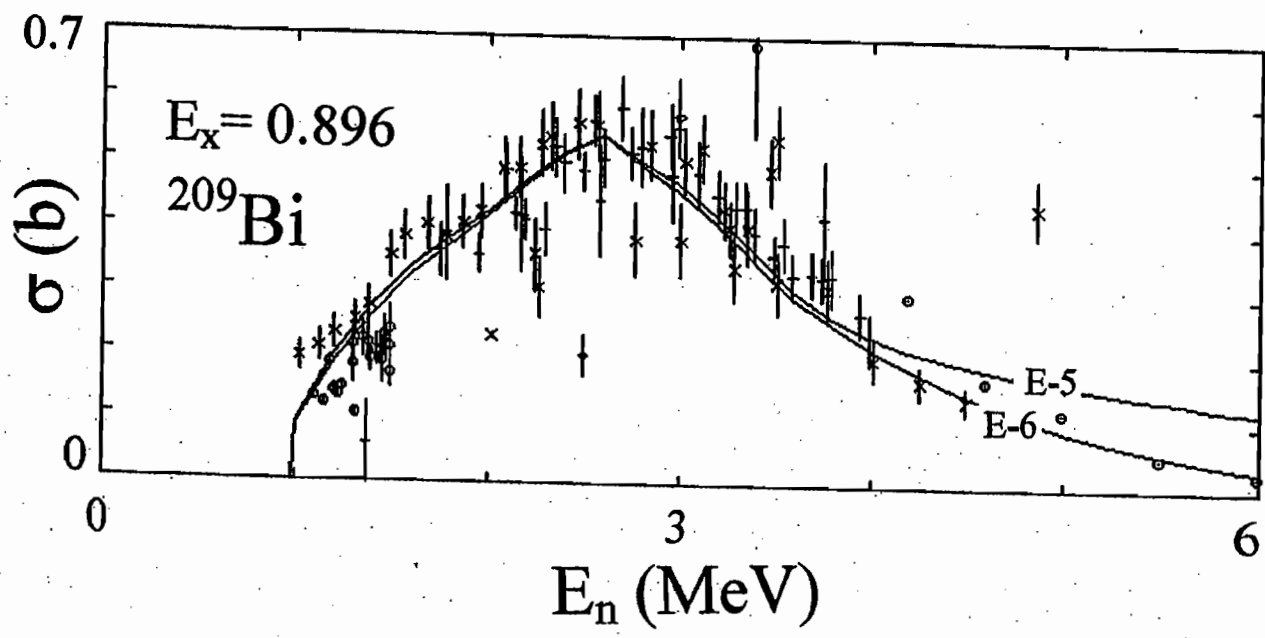
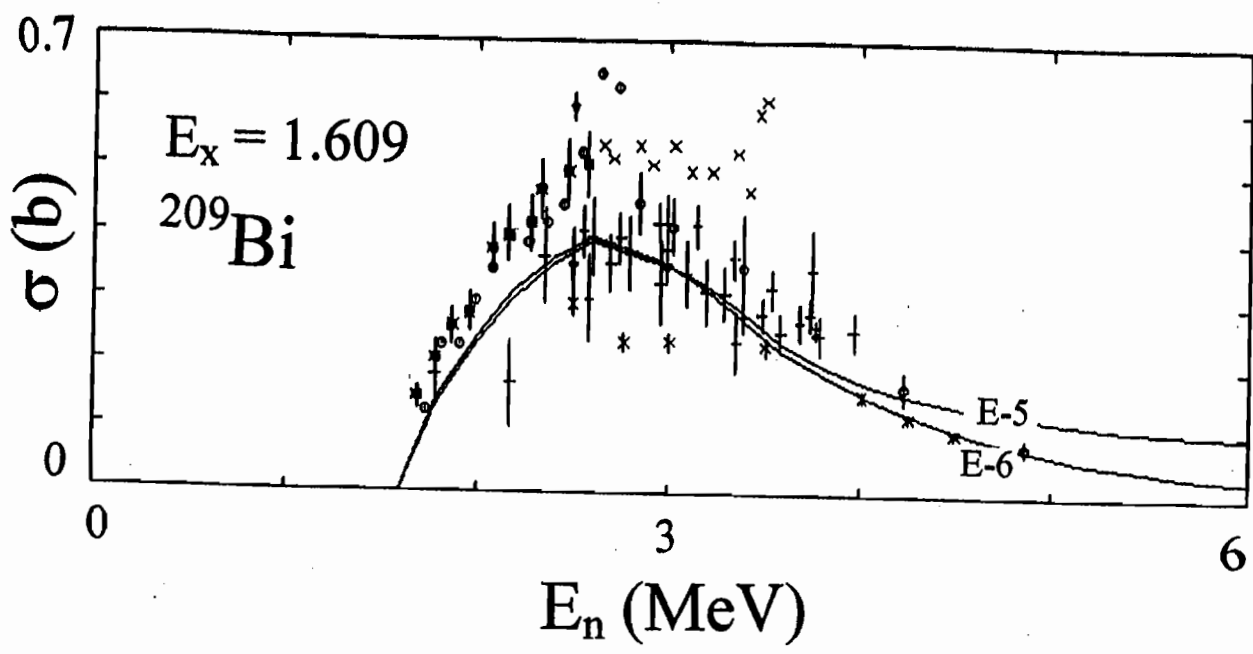


Fig. E-3. Comparisons of measured and calculated cross sections for the excitation of the 0.896 MeV and 1.609 MeV states in ^{209}Bi . The notation is the same as in Fig. E-2, except that the curves represent the results calculated with the potentials of Tables E-5 and E-6, as described in the text.

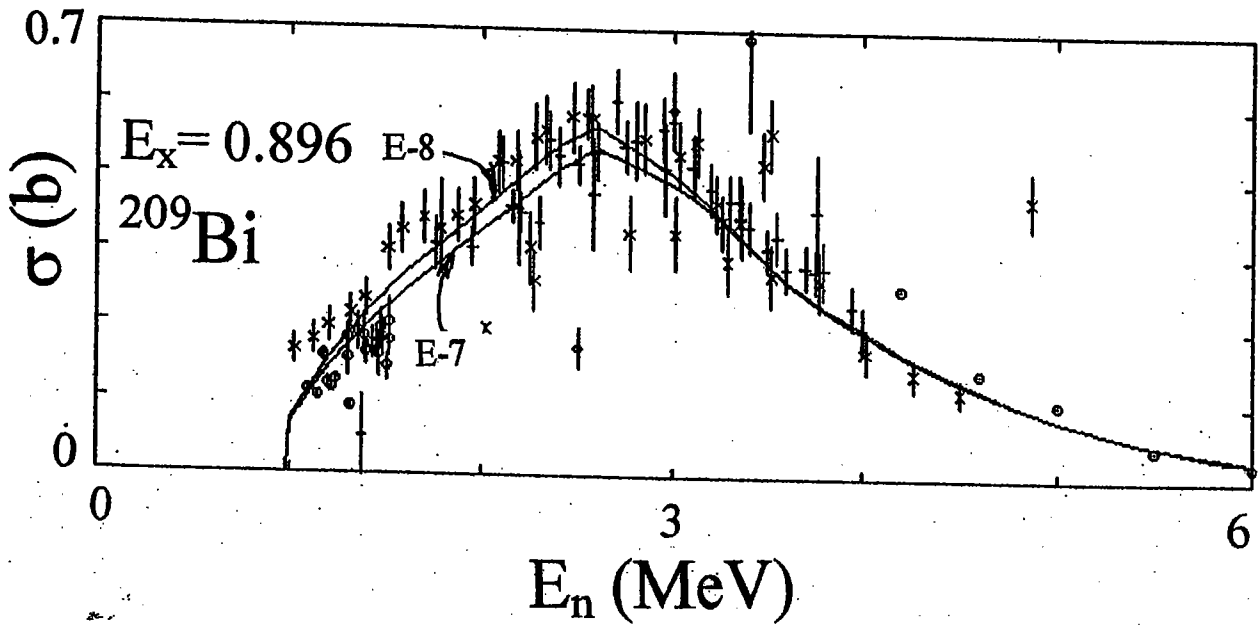
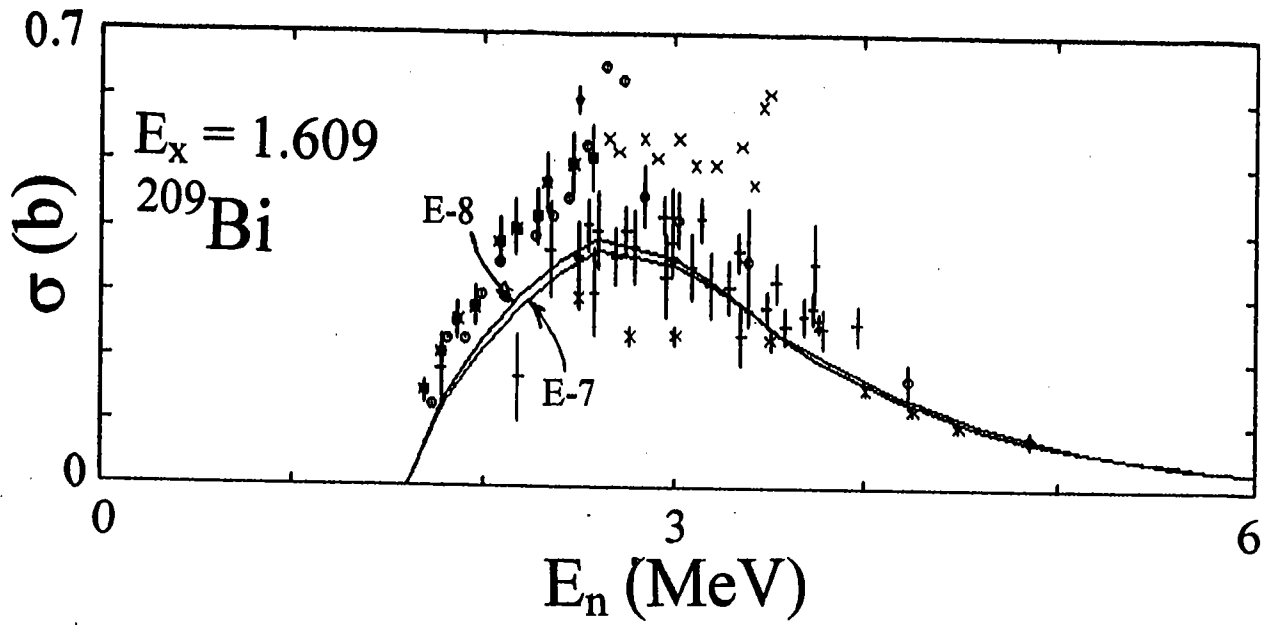


Fig. E-4. Comparisons of measured and calculated cross sections for the excitation of the 0.896 MeV and 1.609 MeV states in ^{209}Bi . The notation is the same as Fig. E-2, except the curves represent the calculations made with the potentials of Tables E-7 and E-8, as outlined in the text.



Nuclear Engineering Division

Argonne National Laboratory
9700 South Cass Avenue, Bldg. 208
Argonne, IL 60439-4842

www.anl.gov



UChicago ►
Argonne_{LLC}

A U.S. Department of Energy laboratory
managed by The University of Chicago